Titre: Title:	De la particule au procédé : modélisation de la production d'émulsions de Pickering
Auteur: Author:	Emir Tsabet
Date:	2014
Type:	Mémoire ou thèse / Dissertation or Thesis
Référence: Citation:	Tsabet, E. (2014). De la particule au procédé : modélisation de la production d'émulsions de Pickering [Thèse de doctorat, École Polytechnique de Montréal]. PolyPublie. https://publications.polymtl.ca/1615/

UNIVERSITÉ DE MONTRÉAL

DE LA PARTICULE AU PROCÉDÉ : MODÉLISATION DE LA PRODUCTION D'ÉMULSIONS DE PICKERING

EMIR TSABET

DÉPARTEMENT DE GÉNIE CHIMIQUE

ÉCOLE POLYTECHNIQUE DE MONTRÉAL

THÈSE PRÉSENTÉE EN VUE DE L'OBTENTION

DU DIPLÔME DE PHILOSOPHIÆ DOCTOR

(GÉNIE CHIMIQUE)

DÉCEMBRE 2014

UNIVERSITÉ DE MONTRÉAL

ÉCOLE POLYTECHNIQUE DE MONTRÉAL

Cette thèse intitulée:

DE LA PARTICULE AU PROCÉDÉ : MODÉLISATION DE LA PRODUCTION D'ÉMULSIONS DE PICKERING

présentée par : TSABET EMIR

en vue de l'obtention du diplôme de : Philosophiae Doctor

a été dûment acceptée par le jury d'examen constitué de :

M. CARREAU Pierre, Ph. D., président

M. FRADETTE Louis, Ph. D., membre et directeur de recherche

M. TAVARES Jason-Robert, Ph. D., membre

M. RODRIGUE Denis, Ph. D., membre

DÉDICACE

À Ilhem, Mouaad et Nour

À mes parents

REMERCIEMENTS

Je tiens tout d'abord à remercier mon directeur de thèse, le professeur Louis Fradette, pour m'avoir accordé sa confiance et m'avoir donné l'opportunité de réaliser ce projet. Grace à ses encouragements, sa disponibilité et ses précieux conseils qui allaient au-delà du domaine scientifique, j'ai pu accomplir ce travail.

Je remercie les membres du jury, les professeurs Pierre Carreau, Jason R. Tavares et Denis Rodrigue d'avoir accepté d'évaluer ce travail de thèse.

Je remercie l'ensemble des membres de l'URPEI, son directeur, le professeur François Bertrand, le professeur Mourad Heniche, les secrétaires successives, Diane, Damienne, Shirley et Kalonji, ainsi que l'ensemble des étudiants de m'avoir accueilli au sein du groupe et d'avoir fait en sorte que cette expérience soit si agréable et si enrichissante.

Je ne peux ne pas remercier les techniciens du département : Gino, Martine, Sylvie, Jean, Carol et Robert pour leur disponibilité, leur aide et leur constante bonne humeur.

Je remercie Patricia Moraille et Jacqueline Sanchez pour leur soutien et leurs conseils lors de mon passage au laboratoire d'AFM.

Je remercie mon épouse pour son soutien indéfectible et sa patience mais également mes chers parents sans qui la réalisation de cette thèse n'aurait jamais été possible.

À la fin je voudrais rendre grâce à dieu qui m'a inondé de ses bienfaits.

RÉSUMÉ

L'émulsification est un procédé largement répandu en industrie, il peut être rencontré dans les industries chimique, pétrochimique et pétrolière, les cosmétiques, l'agroalimentaire et l'agriculture ainsi que dans l'industrie pharmaceutique. Cette opération consistant à produire des dispersions stables liquide/liquide comporte deux principales étapes : la génération de gouttes et leur stabilisation. La génération de gouttes peut être réalisée en utilisant différents types d'équipements selon la taille de gouttes recherchée. Ainsi, des gouttes d'une taille allant de 30 à 300 microns peuvent être obtenue en utilisant des cuves agitées ou des mélangeurs statiques alors que des systèmes Rotor/Stator ou des moulins colloïdaux permettraient d'obtenir des tailles allant jusqu'au micron. De même, qu'il est possible d'atteindre une centaine de nanomètres en utilisant des systèmes à membranes ou des systèmes ultrasoniques. La stabilisation est, quant à elle, obtenue en réduisant la tension interfaciale phase dispersée/phase continue en utilisant des molécules tensio-actives ou bien en formant des barrières stériques autour des gouttes en utilisant des particules solides ou des chaines de polymère. Cela dit, la plupart des émulsions rencontrées en industrie sont stabilisées par des molécules tensio-actives dont la demande atteindra en quelques années 18 millions de tonnes ce qui équivaut à un marché annuel de 30 milliards de dollars (Transparency Market Research (2012-07-10)). À cette large demande vient s'ajouter le caractère toxique et néfaste pour l'environnement que présente l'utilisation de certains tensio-actifs notamment dans les industries chimique, pétrochimique, pétrolière et agricole. Ainsi, dans l'actuel contexte économique et environnemental, des solutions plus vertes et moins couteuses doivent être trouvées.

Dans cette optique, différentes possibilités ont été envisagées dont celle des particules solides qui présentent beaucoup de similarités avec les molécules tensio-actives. Il a été ainsi observé qu'il est possible de produire des émulsions extrêmement stables pour de longues durées : simples (huile/eau ou eau/huile) ou multiples (huile/eau/huile ou eau/huile/eau). Il a été également trouvé qu'une large variété de particules pouvait être utilisée. Cela dit, certaines différences doivent également être soulignées en raison de leur impact sur les mécanismes mis en jeu dans une opération d'émulsification. La génération d'interface est ainsi la première opération à être affectée par l'utilisation de particules vu que la tension interfaciale n'est pas réduite par l'utilisation de particules et que celles-ci modifient les propriétés de la phase continue. La

stabilisation est également affectée vu que les particules ne présentent pas de propriétés amphiphiliques et que leur taille est plus importante que l'échelle moléculaire. Le comportement de l'émulsion est également altéré par les propriétés des particules qui peuvent favoriser le crémage ou la sédimentation et également la floculation des gouttes. Ainsi, sur la base de ces considérations et s´inscrivant dans un contexte de développement de procédés d'émulsification, le présent projet a pour principal objectif d'étudier la possibilité d'utiliser des particules solides pour la stabilisation d'émulsion à l'échelle industrielle. L'idée directrice du projet est notamment d'identifier les mécanismes impliqués lors de la stabilisation et de déterminer l'effet des propriétés du système (propriétés des phases, formulation et conditions opératoires) sur ces mécanismes dans le but de définir les conditions optimales d'émulsification. Le travail a ainsi été réparti sur cinq articles :

L'article 1 consiste en une revue de littérature faisant le tour de la plupart des travaux consacrés à la caractérisation des émulsions de Pickering et à l'identification des paramètres affectant leurs propriétés. Cette partie a notamment permis de recenser les principales interactions mis en jeu entre une particule solide et une interface fluide à travers un milieu liquide mais également celles auxquelles sont soumises les particules lorsqu'elles sont adsorbées à une interface.

L'article 2 a été consacré à l'étude des interactions mis en jeu entre une particule sphérique et une goutte à travers un milieu aqueux pendant l'approche et l'adsorption. À travers l'utilisation de la technique de la sonde colloïdale, ce travail expérimental a notamment révélé que l'approche était caractérisée par une interaction répulsive associée au drainage du film séparant la particule et la goutte et que l'adsorption était caractérisée par une interaction attractive associée à un processus de montée capillaire.

L'article 3 a quant à lui été destiné à faire le lien entre les phénomènes mis en jeu à l'échelle particulaire et ceux impliqués à l'échelle de la goutte pendant une opération d'émulsification. Dans cette seconde approche expérimentale, il a été possible de faire la lumière sur l'effet des propriétés des éléments constituant le système (eau, huile et particules) sur la stabilisation et les performances de l'émulsification. Une meilleure compréhension des phénomènes mis en jeu lors de la stabilisation a ainsi été apportée.

L'article 4 a été consacré à l'étude expérimentale de l'effet des conditions opératoires (temps et énergie d'émulsification) sur les performances de l'opération d'émulsification. Les mesures de

distributions de taille ont ainsi révélé de fortes interactions entre les différents mécanismes impliqués pendant le processus. Il a été également observé que des conditions optimales doivent être considérées afin de promouvoir à la fois la génération d'interface et sa stabilisation.

Finalement, l'article 5 a consisté à définir une procédure permettant de déduire la taille moyenne des émulsions produites à partir des propriétés du système et des conditions opératoires. Des modifications ont ainsi été apportées à la corrélation développée par Calabrese et al. (1986) pour des émulsions diluées afin d'y inclure l'effet des particules sur les propriétés de la phase continue et l'impact de la coalescence vu que des émulsions concentrées ont été considérées.

Sur la base des résultats obtenus, il a été suggéré d'utiliser les minerais disponibles au niveau des sites d'extraction de bitume pour stabiliser des émulsions de pétrole lourd à des fins de transport par pipeline. L'idée étant de transporter le minerai d'intérêt et le bitume. Cette dernière partie a mis en évidence les problématiques associées à la conception d'un tel procédé à l'échelle industrielle et a permis donc des définir de nouveaux axes de recherche.

En conclusion, ce travail a permis d'identifier les principaux mécanismes contrôlant la stabilisation et les paramètres les affectant. Les résultats ont également fait ressortir la nécessité de faire des compromis en termes de conditions opératoires afin de favoriser la génération d'interface et la stabilisation. Enfin, une approche semi-empirique a permis de développer une méthodologie pouvant prédire la taille moyenne d'émulsions concentrées stabilisées par des particules à partir des conditions opératoires avec une précision très acceptable.

ABSTRACT

Emulsification is a common industrial process and emulsions can be seen in several fields like chemical industries, cosmetic, food, paints, oil and pharmacy. This operation aims to produce stable liquid/liquid dispersion. It involves two steps: droplet generation and droplet stabilization. Droplet generation can be performed using different equipment depending on the targeted droplet size. Therein, droplets between 30 and 300 microns can be obtained using stirred tanks or static mixers while rotor/stator systems and colloidal mills produce a few microns droplets. A hundred nanometers can be reached if membranes or ultrasonic systems are used. Besides, stabilization can be achieved by reducing interfacial tension using surfactants or by forming steric barrier around droplets using solid particles or polymers chains. Nevertheless, most of produced emulsions are stabilized using surfactants for which the global demand will reach 18 million tons in few years which is equivalent to 30 billion US dollars (Transparency Market Research (2012-07-10)). Thereby in the actual economic and ecological context, greener and less costly solutions should be considered.

An alternative to the use of surfactants can be solid particles. Indeed, it was observed that it is possible to produce different types of highly stable emulsions for long periods. It was also found that a wide variety of particles can be used with an eventually lower cost. However, in addition to these features, some particularities, notably affecting the emulsification operation itself, should also be regarded. By using particles, droplet generation is affected because solid particles don't reduce interfacial tension and modify the continuous phase properties. Stabilization step is affected because particles are not amphiphilic and their size is much larger than that of surfactant molecules. Emulsion behavior is also affected by particles properties and depending on these properties the produced emulsion could flocculate, cream or settle. Considering these features and being mainly interested in the development of new emulsification process using solid particles, the present project aims to study the possibility of using solid particles to stabilize emulsions at the industrial scale. The main idea is to identify the involved mechanisms during the stabilization step and to determine the impact of the system properties (properties of phases, formulation and operating conditions) on these mechanisms, the final goal being to define the optimal conditions for such a process. The work was divided in five papers:

The first paper is a literature review of the relevant findings on Pickering emulsions and parameters affecting their behavior. It notably highlights the main involved interactions between a solid particle and a liquid interface through a liquid media during approach and adsorption. Interactions between adsorbed particles at an interface are also regarded.

The second paper is dedicated to study the interaction between a spherical particle and a droplet in an aqueous media during approach and adsorption. The so-called colloidal probe technique was used and it was revealed that the approach step is controlled by a repulsive interaction associated to a film drainage process while the adsorption step is controlled by an attractive interaction related to a capillary rise process also characterised by an adsorption time.

The third paper aims to make a link between the involved mechanisms at the particle scale and those involved during emulsification. In this second experimental part, through the investigation of the effect of the system properties (water, oil and particles) on the stabilization step and the emulsification efficiency, a better understanding of stabilization mechanism was brought.

The fourth paper is dedicated to the investigation of the effect of operating conditions (emulsification time and energy) on the emulsification efficiency. Droplets size measurements revealed strong interactions between involved mechanisms. Therein, it was found that optimal conditions should be considered to promote both interface generation and interface stabilization.

Finally, the last paper focuses on the definition of a procedure allowing predicting droplet mean size from the system properties and the operating conditions. A modified version of the R.V. Calabrese et al. (1986) correlation is proposed. It notably includes the particles effect on the continuous phase properties in addition to a coalescence term since concentrated emulsions are considered.

Based on the obtained results, it was suggested to use Pickering emulsions properties for a heavy oil transportation application. The idea is to use available ores to stabilise bitumen emulsions and transport both bitumen and ores through pipelines. This part highlighted the associated issues to the design of such process at the industrial scale and new research axes were defined.

As a conclusion, it can be said that this work allowed the identification of involved mechanisms during the stabilization and highlighted the relevant parameters affecting this step. Results shed light on the importance of finding a compromise in terms of operating conditions to promote both

interface generation and interface stabilization. At the end, a semi-empirical approach was proposed to predict concentrated emulsion properties from operating conditions.

TABLE DES MATIÈRES

LISTE DES TABLEAUX

LISTE DES FIGURES

LISTE DES SIGLES ET ABRÉVIATIONS

Lettres latines

A_{cov}: Coverage potential.

$A_{cov/1p}$: Covered surface by 1 particle.

A_d: Droplet interfacial area.

A_{Eff}: Effectively covered interface.

A_f: Area of film (Assuming $h<<R_p$ and $h<<R_d$: $A_f = A_{fp} = A_{fd}$).

A_{gen}: Generated interface/Interface generation potential.

A_H: Hamaker constant.

A_p: Covered interface by 1 Particle.

A_{pp}: Particle Hamaker constant in the vacuum.

A_{pwp}: Effective particle Hamaker constant in water.

a_{seg}: Segment length.

A_{Th}: Theoretical covered interface.

A_σ: Average interfacial area occupied by a colloidal particles.

ΔA : Interfacial area variation.

B: Parameter describing interaction between particles at the interface.

B_{di}: Droplet birth rate of the droplet class i.

c: Salt concentration.

C_{emul}: A constant characterizing the emulsification system.

c_i: Concentration.

C_i: Adjustable constants.

CoV: Coefficient de variation.

c^0: Bulk concentration of salt.

C_0: Pre-exponential parameter.

c_m: Average concentration.

D: Separating distance.

D_i: Impeller diameter.

D_d: Droplet diameter.

D_{di}: Droplet death rate of the droplet class i.

D_{d_init} : Diamètre des gouttes avant l'adsorption des particules.

d_p : Diamètre des pores du mélangeur statique.

D_p: Particle diameter.

$D_{p/i}$: Distance between the particle center and the interface level.

D_{sm}: Static mixer diameter.

D_0: Characteristic decay length.

D_{32}: Sauter mean diameter.

e: Elementary charge [$1.602 \cdot 10^{-19}$ C].

E_{Att}: Particle attachment efficiency.

E_{Col}: Particle/droplet collision efficiency.

E_{Cov}: Droplet coverage efficiency.

E_{det}: Detachment energy.

$E_{d/with\ p}$: Interfacial energy of the drop with adsorbed particles.

$E_{d/without\ p}$: Interfacial energy of the drop without particles.

$E_{p/disp}$: Interfacial energy of the particle in the bulk.

$E_{p/interf}$: Interfacial energy of the particle at the interface.

E_{TPCL}: Three phase contact line formation efficiency.

$F_{B/o}$: Oil buoyancy force.

$F_{B/w}$: Aqueous buoyancy force.

F_{Col}: Collision force.

F_{Det}: Detachment force.

F^{el}: Electrodipping force acting on the particle.

F_g: Gravity force.

F_{Hyd}: Hydrodynamic force.

f_i: Immersion height fraction.

F_{Lap}: Laplace pressure associated force.

F_P: Hydrostatic pressure force.

f_{sm}: Static mixer friction factor.

$F_{\gamma/z}$: Capillary force.

$f_{\sigma\sigma}$, $f_{\varphi\sigma}$, $f_{\varphi\varphi}$: Force coefficients.

F_{12}: Interaction force between two dipoles (Particles).

g: Gravity acceleration.

ΔG : Gibbs energy variation.

h: Planck's constant [$6.626 \cdot 10^{34}$ J·s].

h_{ads}: Adsorbed height of the particle.

h_{cr}: Critical film thickness.

h_f: Final film thickness.

h_i: Initial film thickness.

HLB: Hydrophilic-Lipophilic Balance

H_{lw}: Thickness of the liquid layer near the wall.

k_B: Boltzmann's constant [$1.381 \cdot 10^{23}$ J/K].

k_c: Cantilever spring constant.

k_{HB}: Consistency.

L: Water height above the interface.

l_{circ}: Circulation length (Distance between the droplet interface and the zero velocity into the droplet).

L_m: Molecular characteristic length (≈ 0.1 nm).

L_{sm}: Static mixer length.

L_0^*: Equilibrium brush thickness.

Mol_i : Mole number of the component i.

m_p: Particles mass.

m_t: Total mass of the system (Water, Oil and particles).

m_w: Mass of water.

n: Power law index.

N_d : Droplets number density.

n_{di}: Number of droplets of the class i.

n_i: Refractive index.

N_i: Impeller speed.

N_p: Particles number.

N_{Po}: Power number (N_{Po}^{PBT} = 1.2).

$N_{p/d}$: Adsorbed particles number per droplet/Required particles number to cover one droplet.

$N_{p/Total}$: Total particles number density.

N_q: Flow number (≈ 0.85 for a PBT).

N_{seg}: The number of segments in a polymer chain.

N_θ: Dynamic contact angle steps number.

Δp: Excess pressure in the film (Assumed equal to Laplace pressure for small droplets).

Δp_{sm}: Pressure drop in the static mixer.

P: Power consumption.

p_d: Dipole moment.

PSD: Power spectral density.

P_1, P_2: Droplet internal and external pressure.

q_{oil}: Charge of the oil-immersed section of the particle.

Q_v : Global flow rate.

r: Distance between atoms or molecules.

r_c: Radius of the contact line.

r_{cr}: Critical radius of the drop (Ostwald ripening).

R_{cr}: Critical TPC line radius.

R_d: Droplet radius.

R_{dI}: Droplet radius before particles adsorption.

R_{dII}: Droplet radius after particles adsorption.

Re_c: Continuous phase Reynolds number.

R_{eq}: Characteristic size of the equipment.

Re_p: Reynolds based on the pores size of the static mixer.

R_f: Radius of the film.

R_g: Universal gas constant.

R_m: Macroscopic characteristic length (≈ particle radius).

R_p: Particle radius.

R_{sph}: Sphere radius.

R_{TPC}: TPC line radius.

R_1, R_2: Droplet internal and external curvature.

s: Average distance between grafting points on the surface.

S: Dispersed phase solubility.

s_f: Final surface area.

t: Characteristic time.

T: Temperature.

t_c: Contact time.

t_{circ}: Mean circulation time.

t_d: Drainage time.

t_{ret} : Temps caractéristique de rétention.

t_{sed} : Temps caractéristique de sédimentation des gouttes.

$\bar{U}$: Mean flow velocity.

V_{app}: Approaching velocity.

V_c: Continuous phase volume.

V_d: Dispersed phase volume.

V_{drop}: Droplet volume.

V_{eq}: Characteristic volume of the settling equipment.

V_f : Mean flow velocity.

V_{sed} : Settling velocity.

$V_{sed/cre}$: Droplet settling or creaming velocity.

V_{sm}: Fluid velocity in the static mixer.

V_{tank}: Tank volume.

v_i: Droplet volume.

We: Weber number.

We_p : Weber number based on the pores size of the static mixer.

Z: Cantilever deflection.

Lettres grecques

α: Electronic polarizability of the molecules.

α_{oil}: Degree of dissociation of the sulphate groups at the particle-oil surface.

α_{water}: Degree of dissociation of the sulphate groups at the particle-water surface.

γ: Interfacial tension.

γ_l: Line tension.

γ_{ow}: Oil/water interfacial tension.

γ_{ws}: Water/solid interfacial tension.

γ_{os}: Oil/solid interfacial tension.

$\Gamma(d, d')$: Coalescence frequency.

$\dot{\gamma}$: Shear rate.

ε: Dielectric constant.

ε_A: Dielectric constant of the aqueous media.

ε_{avr}: Average turbulent energy dissipation rate.

ε_n: Dielectric constant of the nonpolar fluid.

ε_{oil}: Dielectric constant of oil.

ε_{sm}: Static mixer porosity.

ε_t: Turbulent energy dissipation rate.

ε_{water}: Dielectric constant of water.

ε_0: Vacuum dielectric constant.

ζ: Distance between q_{oil} and the interface.

η: Dynamic viscosity.

η_c: Continuous phase dynamic viscosity.

η_d: Dispersed phase dynamic viscosity.

η_e: Emulsion apparent dynamic viscosity.

η_s: Dynamic viscosity of the liquid near the wall.

θ: Contact angle.

θ_e: Equilibrium contact angle.

$\theta(t)$: Dynamic contact angle.

θ_0: Initial Dynamic contact angle (t = 0).

λ: Kolmogorov length scale $((\nu^3/\varepsilon_t)^{1/4})$.

$\lambda(d, d')$: Coalescence efficiency.

$\xi(d, d')$: Collision frequency.

μ: Chemical potential.

ρ_c: Continuous phase density.

ρ_d: Dispersed phase density.

ρ_e: Emulsion apparent phase density.

ρ_p: Particle density.

ρ_w: Water density.

σ: Particle surface charge density corresponding to full dissociation.

σ_{pn}: Surface electric charge density at particle/nonpolar phase interface.

υ: Ionisation frequency.

υ_e: Mean absorption frequency.

$\Delta\varphi$: Potential difference between particle/water interface and nonpolar phase/water interface.

ϕ_{bulk}: Particles concentration in the bulk.

Φ_d: Dispersed phase volume fraction.

Φ_{Oil}: Oil volume fraction.

$\phi_{0,eq}$: Equilibrium particles concentration at the interface.

ψ: Electric potential.

τ_c: Constant degree of surface coverage.

τ_s: Shear stress.

τ_{sm}: Static mixer tortuosity.

τ_0: Apparent yield stress.

Ω : Rotational speed.

Acronymes

API: American Petroleum institute.

DLVO: Derjaguin, Landau, Verwey and Overbeek.

PDMS: Polydimethylsiloxane.

PBT: Pitched blade turbine.

RT: Rushton turbine.

SSE: Solid stabilized emulsion.

CHAPITRE 1. INTRODUCTION

1.1 Problématique du transport des pétroles non conventionnels

Malgré l'intérêt croissant pour les nouvelles énergies ou les énergies dites propres, celles-ci ne peuvent pour le moment être substituées aux énergies fossiles (pétrole, gaz et charbon) dont la demande ne cesse d'augmenter. La demande en pétrole aurait ainsi dépassé 92 millions de barils par jour au mois de décembre 2014 (Figure 1.1).

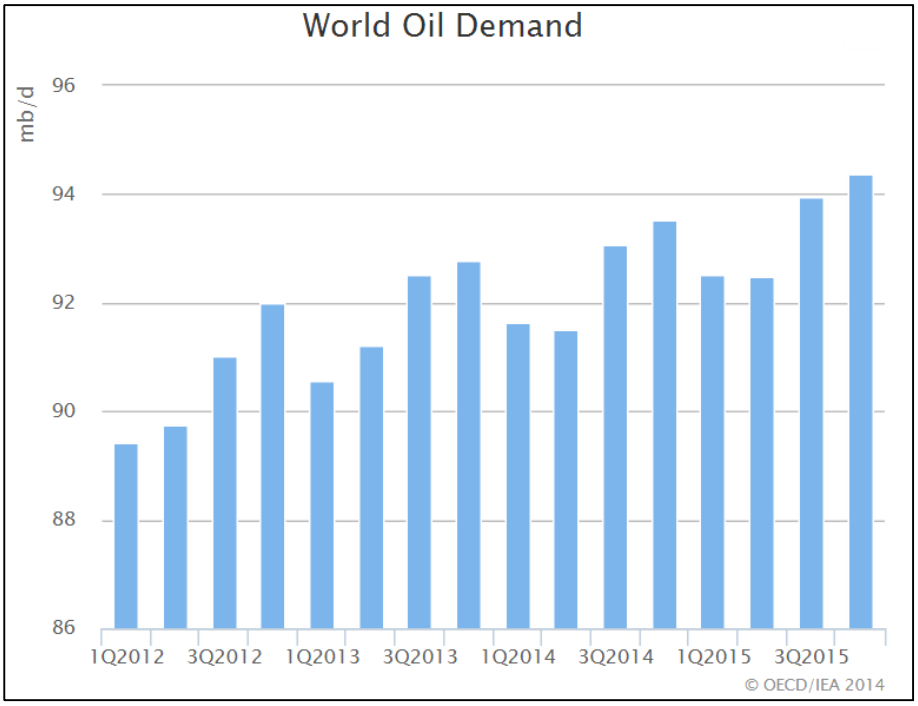

Figure 1.1 : Évolution de la demande mondiale en pétrole en millions de barils par jour

(Oil Market Report 2014 de l'Agence Internationale de l'Énergie)

Cette augmentation de la demande est cependant accompagnée par une diminution des réserves mondiales en brut léger ce qui fait que les regards se tournent actuellement vers un autre type de pétrole dit non conventionnel ou pétrole lourd. En effet, en raison des gigantesques réserves mondiales (environ 4700 milliards de barils), l´exploitation de cette matière semble être une alternative très intéressante. Ces réserves de pétrole lourd se trouvent essentiellement au Moyen-Orient, au Mexique, au Brésil, et en Russie. Cependant, en raison du fait que ces pays aient fait le

choix de concentrer leurs efforts sur des ressources plus faciles à exploiter leur production est relativement limitée. Les bruts extra-lourds se concentrent principalement au Venezuela, dans la "ceinture" qui borde le fleuve Orénoque. Les bitumes quant à eux se localisent au Canada dans la région de l'Athabasca de la province de l'Alberta (Figure 1.2).

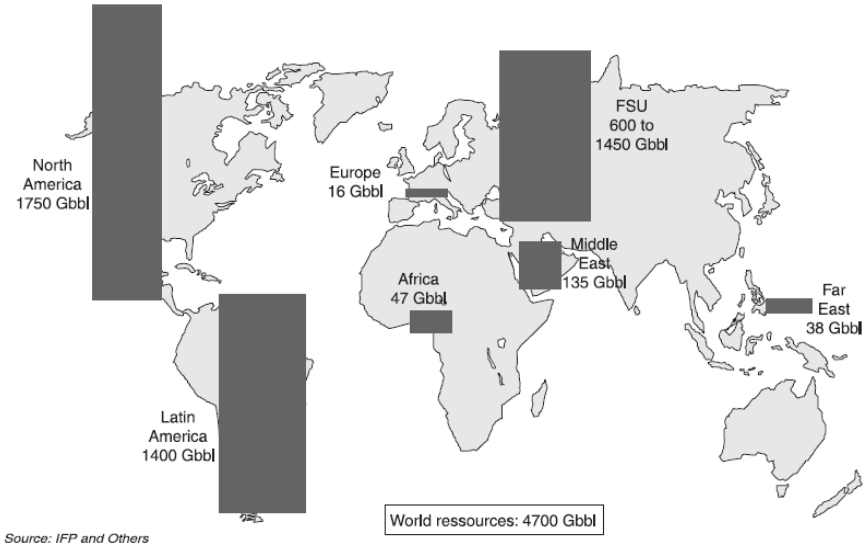

Figure 1.2 : Répartition géographique des réserves mondiales de pétrole non conventionnel (Saniere et al. (2004))

Nécessitant un traitement particulier, l´exploitation de ces pétroles requière d´énormes moyens technologiques et financiers que ce soit au niveau de l´extraction, du traitement ou du transport. Malgré cela, certains pays producteurs investissent de plus en plus dans ce secteur. Le Canada, produisant environ 2 millions de barils de pétroles bitumineux par jour, a notamment investi environ 116 G$ entre 2000 et 2010 dans des projets d´exploitation. Afin de limiter les coûts de l´exploitation et de rentabiliser ces projets, il est par conséquent devenu indispensable d´optimiser toutes les étapes de production dont le transport. En effet, en raison de leur viscosité élevée ces pétroles sont peu fluides et leur pompage nécessite beaucoup d'énergie (Figure 1.3). Cette problématique est particulièrement posée au Canada où le pétrole doit être acheminé des sites d'extraction en Alberta vers les sites de transformation et d'exploitation situé essentiellement sur la côte est canadienne ou aux États-Unis. Moins couteux et moins risqué que le transport ferroviaire (Accident du Lac Mégantic), l'utilisation de pipelines est actuellement le moyen de transport privilégié (projets Keystone XL, Northern Gateway et Énergie-Est).

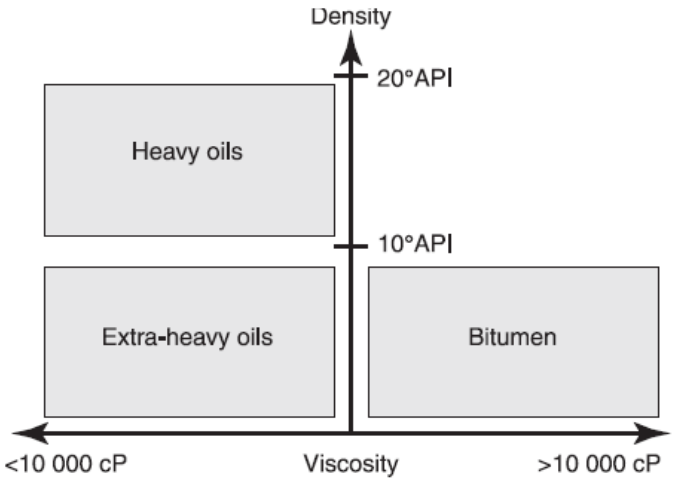

Figure 1.3 : Caractéristiques des pétroles lourds, extra-lourds et des bitumes

(Saniere et al. (2004))

Différentes techniques ont ainsi été mises au point pour transporter ce pétrole lourd et visqueux. Ces techniques résultent essentiellement de trois approches : 1) La réduction de la friction au niveau des parois des conduites en transportant le brut par écoulement annulaire; 2) La valorisation (upgrading) du brut en lui faisant subir un traitement partiel; 3) La réduction de la viscosité apparente du brut jusqu'à environ 200 cP (Messick (1982)) par augmentation de la température, par dilution ou par émulsification.

1.1.1 L´écoulement annulaire

Cette technique ne permet pas la réduction de la viscosité mais permet de réduire le frottement aux parois par le biais d´un film lubrifiant d´eau injecté aux parois (la fraction d´eau se situant typiquement entre 10 et 30%). Cette technique a fait l´objet de nombreuses études notamment celles réalisées par Bannwart (1999, 2001, 2004) et Rodriguez et al. (2009) qui ont démontré que la perte de charge pouvait être considérablement réduite. Les inconvénients de cette technique consistent en la possible formation d´émulsions stables, la rupture du film et l´adhésion de la phase huileuse aux parois notamment lors des arrêts, nécessitant ainsi d´importantes pressions lors des opérations de démarrages.

1.1.2 La valorisation partielle

Cette technique consiste à traiter partiellement le brut afin de produire un brut synthétique moins lourd et moins visqueux mais aussi contenant moins d´impuretés (Soufre). Ce traitement utilise en générale un procédé thermique de craquage à haute température (468 - 498°C) pour extraire le carbone des fractions lourdes produisant ainsi des fractions plus légères et du coke de pétrole. Un procédé d´hydrotraitement est également utilisé pour obtenir un pétrole de meilleure qualité et réduire les émissions de SO_2. Cela dit, il n´est pas toujours simples de construire de telles installations au niveau des sites de production, celles-ci sont en générale construites au niveau des raffineries. Ce qui fait que cette technique ne peut être réellement considérée comme une solution à la problématique du transport.

1.1.3 Le chauffage

Cette technique permet de diminuer la viscosité du brut moyennant une augmentation de sa température. Elle est notamment utilisée sur le pipeline d'Alyeska en Alaska qui transporte du brut à 50°C. Cependant, requérant d´importantes quantités d´énergie et imposant plusieurs contraintes (pertes thermiques, allongement des pipelines et corrosion interne), cette technique est très couteuse et peu flexible. D'autant plus que le chauffage pourrait altérer la structure colloïdale du brut ainsi que ces propriétés rhéologiques.

1.1.4 La dilution

Cette technique consiste à mélanger le brut lourd avec un autre hydrocarbure tel que le kérosène ou le naphta dont les viscosités sont très faibles par rapport à celle du brut. La difficulté de cette technique consiste en la limitation de la production en raison du taux de dilution requis (30% de diluant et de 70% de brut) mais aussi en la nécessité de disposer d´installations supplémentaires pour la séparation du brut et du diluant et du retour du diluant aux sites d´extraction.

1.1.5 L´émulsification

Cette dernière technique consiste à disperser les gouttelettes d´huile dans de l´eau. Ces émulsions sont généralement stabilisées par des surfactants (500 - 2000 ppm) et ont été utilisées au Venezuela sous le nom d´Orimulsion, elles peuvent contenir jusqu´à 70% de pétrole lourd avec une viscosité apparente en dessous de 400 cP (Langevin et al. (2004)). En plus de la présence

d’eau, l´inconvénient majeur de cette technique est la difficulté à détruire l´émulsion une fois le transport achevé mais aussi le coût élevé en tensio-actifs. Cela dit, il existe une alternative à l’utilisation des tensio-actifs qui est celle de l’utilisation de particules solides qui s´adsorbent aux interfaces eau / huile pour former une barrière stérique empêchant la coalescence des gouttes. Ces émulsions communément appelées émulsions de Pickering (Pickering (1907)) sont extrêmement stables mais peuvent être détruite par l’application d’une force extérieure (Centrifugation, champ magnétique…) ou par altération des propriétés de surface des particules (changement de mouillabilité).

S’inscrivant dans le cadre des sujets de recherche traités par la Chaire de recherche industrielle CRSNG-Total en modélisation hydrodynamique de procédés polyphasiques dans des conditions extrêmes, ce travail de thèse vise ainsi à étudier la possibilité de stabiliser des émulsions concentrées par des particules solides à l’échelle industrielle avec pour application la production d’émulsion de pétrole lourd à des fins de transport par pipeline.

La conception d’un tel procédé, mettant en jeu un système triphasique composé de deux liquides immiscibles et d’une phase solide, constitue un réel défi pour l’ingénieur chimiste. D’autant plus que cette opération implique des phénomènes complexes qui interagissent fortement. Il y est notamment question de génération d’interface, d’adsorption et de désorption de particules et de coalescence, le tout en régime turbulent. Il est ainsi essentiel d’identifier et de comprendre les mécanismes mis en jeu durant cette opération afin de pouvoir concevoir un procédé économiquement viable.

1.2 Physico-chimie des émulsions

La physico-chimie des émulsions est contrôlée par les phénomènes interfaciaux et plus précisément par la tension interfaciale entre les deux phases qui trouve son origine dans les interactions moléculaires notamment dominées par les forces de van der Waals qui elles-mêmes se décomposent en :

- **Forces de Keesom :** qui résultent d'une interaction moléculaire entre dipôles permanents.
- **Forces de Debye :** qui résultent de l'interaction entre un dipôle permanent et un dipôle induit.
- **Forces de London :** qui résultent de l´interaction entre des dipôles induits.

En effet, au sein d´un même liquide chaque molécule est soumise à l´attraction de toutes les molécules environnantes. La non-miscibilité des phases aqueuse et huileuse résulte du fait que la phase polaire ne peut établir de liaisons hydrogène (forces de Keesom) avec la phase huileuse dont les interactions attractives sont principalement composées par les forces de London. Ce phénomène a pour effet de créer une discontinuité qui se traduit par l´apparition d´une interface dont les propriétés diffèrent de celles des cœurs des deux phases. Contrairement aux molécules du cœur de la phase, les molécules en surface sont ainsi soumises à une action asymétrique qui les attire vers l´intérieur du liquide ce qui provoque une tendance de la surface à se restreindre, ce qui explique la forme sphérique des gouttes.

D'un autre côté, créer de l'interface nécessite un apport énergétique au système, énergie correspondant au travail qu'il faut effectuer pour étendre l´interface d'une unité d'aire, communément appelée tension de surface ou tension d´interface, elle s'exprime en milli joules par mètre carré ou en milli newton par mètre (la tension de surface eau / air est de l´ordre de 73 mJ/m^2). Elle est définie comme étant la variation de l´énergie libre du système à température et à composition constantes :

$$\gamma = \left(\frac{\Delta G}{\Delta A}\right)_{T,Mol_i} \cdots (1.1)$$

Cette tendance de la surface à se restreindre est limitée par la faible compressibilité du liquide et par la pression interne de la goutte. Celle-ci est notamment donnée par l´équation de Young-Laplace qui caractérise la différence de pression entre les deux côtés de l´interface :

$$P_1 - P_2 = \gamma_{12}\left(\frac{1}{R_1} + \frac{1}{R_2}\right) \cdots (1.2)$$

Par ailleurs, d'un point de vue thermodynamique, l'équilibre du système ne peut être atteint qu'en minimisant l'énergie libre de Gibbs ce qui se traduit par la réduction de l'interface (déstabilisation de l'émulsion) ou par la réduction de la tension interfaciale en utilisant des molécules tensio-actives ou en réduisant la température du système.

1.3 Caractérisation des émulsions

Différentes propriétés peuvent être utilisées pour la caractérisation des émulsions et leur niveau d'importance est étroitement lié à l'objectif du procédé et à l'utilisation de l'émulsion. Une

émulsion peut ainsi être caractérisée par son type, sa distribution de taille, sa stabilité ou sa durée de vie, son comportement rhéologique...etc.

1.3.1 Type d´émulsion

Une émulsion peut être simple (eau/huile ou huile/eau) ou bien multiple (eau/huile/eau ou huile/eau/huile). Cependant, sachant que l'objectif de la plupart des procédés d'émulsification est de produire des émulsions simples, les émulsions multiples sont souvent indésirables et obtenues en raison d'un disfonctionnement du procédé telle qu'une erreur au niveau de la formulation ou du protocole de préparation. En effet, le type d'émulsion est directement lié au type et aux propriétés de l'agent stabilisant ainsi qu'aux propriétés des deux phases et à leurs proportions. Ainsi, dans le cas d'un agent ayant une affinité relativement semblable avec les deux phases, le type d'émulsion produite dépendra de la phase dans laquelle sera initialement mélangé l'agent émulsifiant ainsi que des proportions des deux phases.

1.3.2 Fraction volumique de la phase dispersée

Tel que mentionné précédemment, les proportions des phases affectent fortement le type d'émulsion. Ces proportions sont souvent représentées par la fraction volumique de la phase dispersée donnée par :

$$\Phi = \frac{V_D}{V_D + V_C} \cdots (1.3)$$

Une émulsion est ainsi dite diluée quand $\Phi < 0.01$, moyennement concentrée pour $0.01 < \Phi < 0.2$ et concentrée quand $\Phi > 0.2$ et ce sont ces dernières émulsions qui sont les plus rencontrées en industrie. Cela dit, considérant l'émulsion comme un empilement de gouttelettes sphériques de même taille, la fraction volumique de la phase dispersée est limitée par le niveau d'encombrement à 0.74 mais il est possible de dépasser cette valeur en produisant des gouttes de différentes tailles.

1.3.3 Diamètre moyen et dispersion de taille

Une émulsion peut être également caractérisée par sa distribution de taille ou par un diamètre moyen des gouttes. Le diamètre moyen le plus fréquemment utilisé est le diamètre de Sauter donné par :

$$D_{32} = \frac{\sum_{i=1}^{i=m} n_i d_i^3}{\sum_{i=1}^{i=m} n_i d_i^2} = \frac{6\Phi_d}{A_{gen}} \cdots (1.4)$$

La distribution de taille des gouttes est généralement représentée par un histogramme en termes de fréquences de nombre de gouttes appartenant à la même classe :

$$f_n(d_i) = \frac{n_i}{\sum_{j=1}^{m} n_j} \cdots (1.5)$$

Ou bien en termes de fréquences de volume :

$$f_v(d_i) = \frac{n_i d_i^3}{\sum_{j=1}^{m} n_j d_j^3} \cdots (1.6)$$

La distribution de tailles des gouttes peut également se présentée sous une forme cumulative :

$$F_n(d_k) = \frac{\sum_{i=i}^{k} n_i d_i}{\sum_{j=1}^{m} n_j d_j} \cdots (1.7)$$

$$F_v(d_k) = \frac{\sum_{i=i}^{k} n_i d_i^3}{\sum_{j=1}^{m} n_j d_j^3} \cdots (1.8)$$

1.3.4 Stabilité des émulsions

En industrie, l'émulsification consiste essentiellement à produire une dispersion stable et homogène de deux liquides immiscibles. Cependant, ces systèmes sont souvent sujets à des mécanismes de déstabilisation pouvant être divisés en trois classes par (Figure 1.4) :

- Les mécanismes de migration de gouttes (floculation, crémage et sédimentation).
- Les mécanismes de variation de taille de gouttes (murissement d´Ostwald et coalescence).
- Les mécanismes d´inversion de phase.

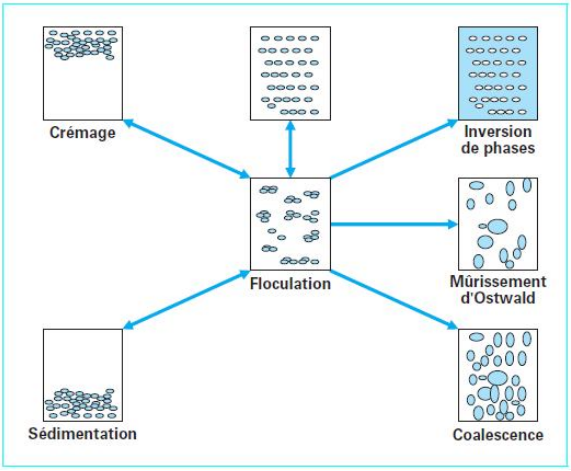

Figure 1.4 : Mécanismes de déstabilisation d'une émulsion (Abismail et al. (1999)).

1.3.4.1 La migration de gouttes

1.3.4.1.1 La floculation

La floculation consiste en l´agglomération des gouttes entre elles formant ainsi des paquets ou des grappes. Il précède en général le crémage ou la sédimentation. Cette interaction attractive peut avoir différentes origines :

a. Floculation par interaction de Lifshitz-Van der Waals

Différentes interactions sont mises en jeu entre des particules en approche dans un milieu liquide. Elles peuvent être classifiées selon leur nature (attractive ou répulsive), leur portée ou leur amplitude. Globalement on distingue les forces décrites par la théorie DLVO incluant les forces de van der Waals et les forces de la double couche électrique et les autres forces incluant les forces hydrophobiques, les forces d'hydratation, les forces stériques…etc. La floculation de particules étant le résultat de la domination des forces attractives, elle est souvent attribuée aux forces de van der Waals. Initialement définies à l'échelle atomique, il a été montré qu'il était possible de les considérer aux échelles microscopique ou macroscopique (Lifshitz (1956)). Ainsi, en considérant les deux gouttes comme étant deux sphères de rayons R_1 et R_2, les forces de Lifshitz-Van der Waals sont donnée par :

$$F = -\frac{A_H}{6D^2}\frac{R_1 R_2}{R_1 + R_2} \cdots (1.12)$$

b. Floculation par déplétion

Elle est provoquée par la présence de micelles ou de polymères dans la phase continue. Elle est plus précisément due au fait que lorsque deux gouttes se rapprochent, il arrive un moment où les objets (micelles, pelotes polymériques), initialement répartis dans tout le volume disponible de la phase continue, n'accèdent plus à l'espace séparant les deux gouttes, cette zone étant trop étroite, ce qui provoque un appauvrissement de ce film liquide en objets solvatés, donnant ainsi naissance à une différence de pression osmotique et favorisant le drainage de liquide de la zone séparant les gouttes vers le reste de la phase continue provoquant ainsi l'accolement des gouttes (Figure 1.5).

c. Floculation par pontage

Elle est provoquée par l'adsorption de polymères de haute masse moléculaire à la surface des gouttes ce qui a pour effet de produire des pontages entre celles-ci favorisant ainsi la floculation.

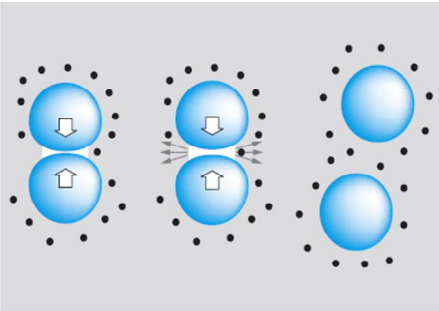

Figure 1.5 : Floculation par déplétion (TI traité J2150).

1.3.4.1.2 La sédimentation et le crémage

La sédimentation et le crémage sont dus à la différence de densité entre la phase continue et la phase dispersée. En effet, lorsque la phase dispersée est plus dense que la phase continue les gouttes ont tendance à migrer vers le bas sous l´effet de la pesanteur (la sédimentation) ou bien vers le haut dans le cas contraire (le crémage). La vitesse de migration des gouttes peut être obtenue par la loi de Stokes pour les dispersions diluées de particules sphériques :

$$V_{sed/cre} = \frac{g\mathrm{D}_d^2(\rho_c - \rho_d)}{18\eta_c} \cdots (1.9)$$

Pour tenir compte de la déformation des gouttes une autre forme dérivée de l'équation de Stokes a été proposée par Hadamard (1911) et Rybczynski (1911) :

$$V_{sed/cre} = \frac{g\mathrm{D}_d^2(\rho_c - \rho_d)}{6\eta_c}\left(\frac{\eta_\mathrm{d} + \eta_c}{3\eta_\mathrm{d} + 2\eta_c}\right) \cdots (1.10)$$

Pour les émulsions concentrées, les interactions entre les gouttes deviennent plus significatives et la vitesse de sédimentation (ou de crémage) est obtenue par (Mills et al (1994)) :

$$V_{sed/cre} = \frac{g\mathrm{D}_d^2(\rho_c - \rho_d)}{18\eta_c}\frac{\left[1 + \frac{4.6\Phi_d}{1 - \Phi_d^3}\right]}{(1 - \Phi_d)} \cdots (1.11)$$

1.3.4.2 L'augmentation de la taille de gouttes et la séparation des phases

1.3.4.2.1 Le Mûrissement d´Ostwald

Ce phénomène a été décrit pour la première fois par Wilhelm Ostwald en 1896. Dans le cas des émulsions, il consiste en un accroissement de la taille des gouttes d'une émulsion. Il résulte de la différence de pression de Laplace entre les gouttes de différentes tailles et dépend donc de la distribution de taille de l'émulsion ainsi que de la solubilité de la phase dispersée dans la phase continue. En effet, lorsqu'il s'agit d'émulsions polydispersées, une diffusion de matière peut se produire à partir des plus petites gouttes vers les plus grosses. Ce phénomène est dû au fait que la pression de Laplace est plus importante dans les plus petites gouttes. L'existence de cette surpression implique que le potentiel chimique dans les petites gouttes est plus élevé. Le retour vers l'équilibre thermodynamique s'accompagne donc d'un flux de matière des petites gouttes vers les plus grosses, à travers la phase continue ce qui provoque une augmentation de leur taille moyenne. L´évolution temporelle du rayon des gouttes peut être obtenu en considérant la théorie de Lifshitz-Slyozov-Wagner :

$$r_{cr}^3 = \left(\frac{8\gamma V_d S C_{Diff}}{9R_g T}\right)t \cdots (1.13)$$

1.3.4.2.2 La coalescence

C´est le principal mécanisme responsable de la déstabilisation des émulsions. Ce phénomène a été largement étudié et est même pris en compte pour les travaux de modélisation des opérations d'émulsification moyennant différentes approches (Yixiang Liao and Dirk Lucas (2009)) dont la

plus utilisée est celle considérant le mécanisme de drainage du film durant la collision des gouttes. Selon cette approche, le processus de coalescence se présente en trois étapes :

- La phase d´approche : Cette étape est contrôlée par l´hydrodynamique du système et est caractérisée par la fréquence de collision entre les gouttes.
- La phase de drainage du film : Cette étape est considérée lors de la collision et correspond à la l´amincissement du film jusqu'à la rupture. Elle est particulièrement affectée par la déformabilité des gouttes et la mobilité de leur interface.
- La phase de rupture du film : Cette étape se traduit par la fusion locale des interfaces lorsque le film atteint une épaisseur minimale et se rompt pour conduire à la formation d´une goutte de plus grande taille.

1.3.4.3 L´inversion de phase

Il existe deux types d´inversion de phase. Le premier étant l´inversion de phase transitionnelle qui peut être provoquée par la modification de la température ou de la concentration en électrolytes du système qui peuvent notamment influencer les propriétés des agents stabilisant l´émulsion. La seconde inversion est dite catastrophique, elle peut être obtenue par l´augmentation de la concentration de la phase dispersée. La limite d´inversion dépend de la forme et de la distribution de taille des gouttes, des propriétés du système et du type d´agent émulsifiant.

1.3.5 Rhéologie des émulsions

Le comportement rhéologique d'une émulsion dépend de différents paramètres tels que la rhéologie des phases, la distribution de taille, la déformabilité des gouttes et leur interaction. Cela dit, les émulsions sont souvent classifiées en termes de fraction volumique de la phase dispersée tel que cela ait été résumé par Derkach (2009). Différents comportements ont ainsi été mis en évidence. La Figure 1.6 résume l'effet de la fraction volumique de la phase dispersée sur le comportement rhéologique des émulsions en considérant la fraction volumique limite Φ^* (~75%) pour les émulsions monodispersées.

Un domaine newtonien est ainsi identifié avec les émulsions diluées (Domaine 1). À ce titre différentes expressions ont été proposées pour décrire la viscosité de ces systèmes dont celle

d'Einstein (1906) qui a été développée pour les dispersions diluées de solide sphériques ($\Phi < 0.05$) :

$$\eta_{émulsion} = \eta_c(1 + 2.5\Phi_d) \cdots (1.14)$$

Une expression tenant compte de la viscosité de la phase dispersée et de sa fraction volumique a été développée par la suite par Taylor (1932) :

$$\eta_{émulsion} = \eta_c \left(1 + 2.5\Phi_d \frac{0.4\eta_d + \eta_c}{\eta_d + \eta_c}\right) \cdots (1.15)$$

Pour les concentrations intermédiaires et les concentrations élevées (domaines II et III), des comportements non-newtoniens ont été observé. Des expressions plus complexes ont ainsi été développées telle que celle proposée par Phan-Thien et al. (1997) qui est une forme généralisée de celle de Taylor (1932) :

$$\left(\frac{\eta_{émulsion}}{\eta_c}\right)^{2/5} \left[\frac{2\eta_{émulsion} + 5\eta_d}{2(\eta_c + \eta_d)}\right]^{3/5} = (1 - \Phi_d)^{-1} \cdots (1.16)$$

Globalement, il a été trouvé que l'augmentation de la fraction volumique de la phase dispersée provoquait une augmentation de la viscosité de l'émulsion en raison de l´augmentation du nombre de gouttes et de l'éventuelle formation d'agrégats. Il a également été révélé que cette augmentation de la fraction volumique induisait une transition vers un comportement rhéofluidifiant tel que cela est illustré par la Figure 1.7 (Pal (2000)) avec éventuellement des effets thixotropiques ou viscoélastiques.

Le domaine IV concerne cependant les émulsions compressées hautement concentrées. Dans cette catégorie, des comportements viscoplastiques avec des contraintes seuils dans certains cas ont été observés.

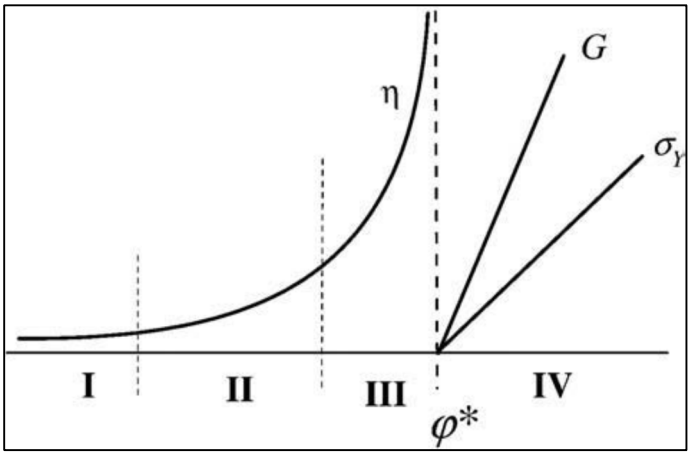

Figure 1.6: Effet de la fraction volumique de la phase dispersée sur le comportement rhéologique d'émulsions (Derkach (2009))

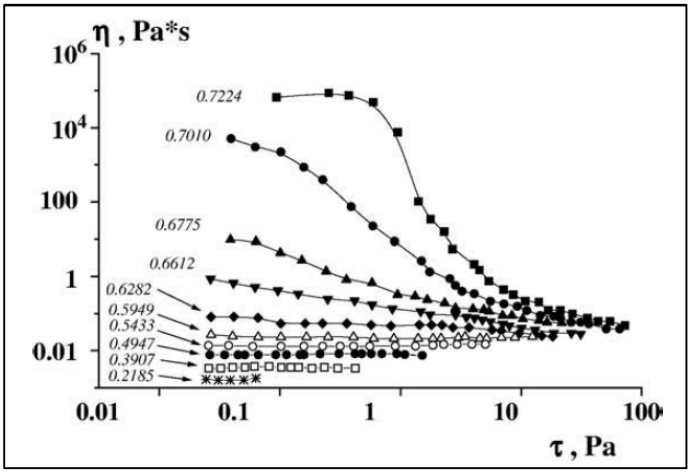

Figure 1.7: Effet de la fraction volumique de la phase dispersée sur les courbes d'écoulement d'émulsions H/E (Pal (2000))

L'effet de la taille des gouttes a également été considéré et il a été montré que la viscosité des émulsions augmentait lorsque la taille des gouttes est réduite tel que cela est illustré par la Figure 1.8 (Pal (1996)). De plus, Il est également montré que le comportement rhéofluidifiant est plus prononcé lorsque la taille des gouttes est réduite. Ce comportement est notamment attribué à l´augmentation de l´aire interfaciale induisant une augmentation des frictions et à la floculation des gouttes.

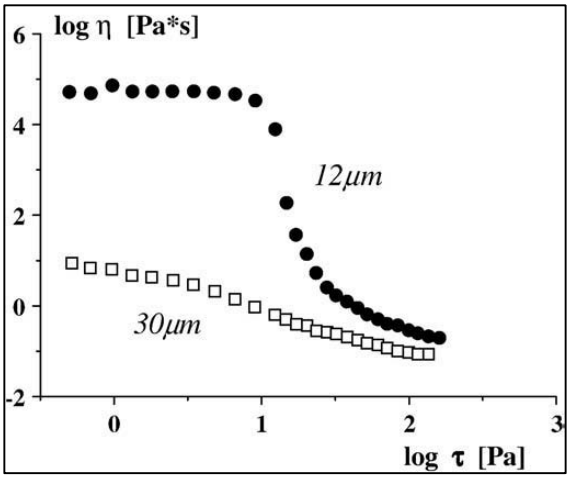

Figure 1.8: Effet de la taille moyenne de gouttes sur les courbes d'écoulement d'émulsions H/E (Pal (1996))

Les agents émulsifiant peuvent également contribuer à la modification des propriétés rhéologiques des émulsions en agissant sur celles de l´interface, notamment en lui conférant des propriétés élastiques ou bien en affectant l'état de floculation des gouttes à travers les interactions entre gouttes.

1.4 Les agents émulsifiant

1.4.1 Les tensioactifs (agents de surface)

Ce sont des molécules formées d´une chaîne à caractère hydrophobe ayant une affinité avec les phases huileuses et d´une tête hydrophile à caractère polaire ayant une affinité avec les phases aqueuses. Ces molécules, dites amphiphiles, tendent ainsi à s´accumuler aux interfaces (Figure 1.9) réduisant la tension interfaciale (Figure 1.10) et conférant à l´interface des propriétés élastiques permettant la stabilité de l´émulsion.

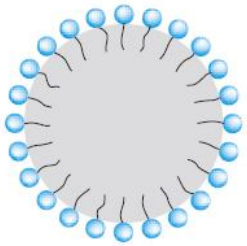

Figure 1.9: Molécules tensio-actives adsorbées à la surface d'une goutte (TI traité J2150)

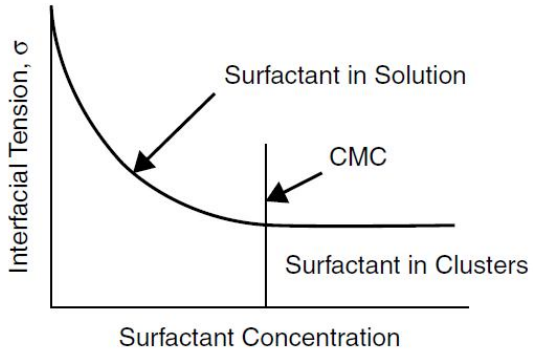

Figure 1.10: Évolution de la tension interfaciale en fonction de la concentration en tensio-actifs (Paul (2003))

Les propriétés tensio-actives d´une molécule dépendent de l´importance relative des parties hydrophiles et lipophiles de la molécule caractérisée par la HLB (Hydrophilic-Lipophilic Balance) introduite par Griffin en 1949. Elle varie de 0 à 20, 0 étant attribué à un produit totalement hydrophobe et 20 à un produit totalement hydrophile. Elle est donnée par :

$$HLB = 20 \times \frac{Masse\ moléculaire\ de\ la\ partie\ hydrophile}{Masse\ moléculaire\ totale} \cdots (1.17)$$

Il a été par ailleurs observé que les émulsions eau / huile étaient obtenues en utilisant des tensioactifs dont la HLB est inférieure à 8 (tensioactifs hydrophobes) tandis que les émulsions huile / eau étaient obtenues avec les tensioactifs hydrophiles.

La partie hydrophobe de la molécule est généralement constituée par une chaîne carbonée constituée de 6 à 18 carbones. Cela dit, il est à noter que les propriétés tensioactives les plus marquées sont obtenues avec des molécules dont la chaîne hydrophobe est constituée de 12 à 14 atomes de carbone.

1.4.2 Les particules solides (émulsions de Pickering)

Les particules solides constituent une alternative à l´utilisation de tensioactifs pour la stabilisation des émulsions. Elles s´adsorbent aux interfaces eau/huile pour former une barrière stérique empêchant la coalescence des gouttes (Figure 1.11). Ces émulsions communément appelées émulsions de Pickering sont beaucoup plus stables que celles stabilisées par des surfactants mais peuvent cependant être détruites par centrifugation. Cela dit, malgré le fait que ces émulsions

aient été découvertes au début du 20e siècle (Ramsden (1903) et Pickering (1907)), elles n´ont suscité l´intérêt des industriels et de la communauté scientifique que très récemment.

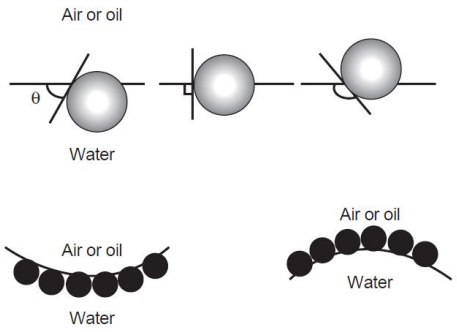

Figure 1.11: Représentation de particules solides adsorbées à l´interface

(Langevin et al. (2004))

1.4.3 Les polymères

Les polymères ont la capacité de s'absorber aux interfaces et à les stabiliser contre la coalescence en formant une barrière stérique qui empêche le rapprochement des gouttelettes. Il convient également de choisir des polymères possédant des portions hydrophiles et des portions lipophiles. Il est cependant recommandé d´éviter l´utilisation de polymères ayant des chaînes trop longues qui pourraient provoquer la floculation des gouttes par pontage et ensuite leur coalescence.

1.5 Objectif principal de la thèse

Dans une optique de développement d'un procédé d'émulsification par des particules, le présent travail a pour principal objectif d'identifier les mécanismes mis en jeu durant la stabilisation de l'émulsion et de définir les conditions opératoires optimales (formulation et paramètres procédés) d'un tel procédé avec comme application finale le transport du brut.

L'hypothèse de recherche associée à cet objectif stipule qu'il est tout à fait possible de remplacer les agents tensioactifs par des particules solides pour la stabilisation d'émulsion à l'échelle industrielle.

CHAPITRE 2. ARTICLE 1 : GENERATION OF PICKERING EMULSIONS: STATE OF THE ART

2.1 Présentation du premier article

Soumis dans : Advances in Colloid and Interface Science

Auteurs : Èmir Tsabet, Louis Fradette

Dans ce premier article ont été résumé les principaux travaux ayant été consacrée à l'adsorption de particules aux interfaces fluides et ceux traitant des émulsions de Pickering. La première partie a essentiellement porté sur les étapes d'adsorption et la condition d'équilibre des particules aux interfaces fluides. Les interactions mises en jeu ont ainsi été recensée et leurs contributions à la stabilité des particules ont été décrites. Les travaux consacrés aux émulsions de Pickering ont révélé l'importance des propriétés des particules et leurs effets sur celles des émulsions produites (type, stabilité, taille et comportement rhéologique). Les effets des propriétés des autres phases ont également été décrits. Finalement, une analyse du système a été proposée dans le but de modéliser le problème et pouvoir prédire les propriétés des émulsions produites à partir des conditions opératoires.

2.2 Generation of Pickering emulsions: State of the art

2.2.1 Summary

The most relevant findings concerning Pickering (solid-stabilized emulsions, SSE) emulsions are reviewed. The generation of SSEs (stabilization mechanism), their properties at rest (parameters affecting type and stability), and under flow (rheological behavior) are described and reviewed.

The stabilization mechanism can be visualized as three steps: (1) the particle first approaches and reaches the fluid/fluid interface, (2) the particle adsorbs and gets trapped, and (3) the adsorbed particles form a network that stabilizes the emulsion. The fundamental phenomena are described for each step, and the main interactions are emphasized (capillary forces, van der Waals forces, electrostatic double layer forces, hydration and hydrodynamic forces, hydrophobic and steric forces). The stability criteria of SSE are also explained.

Numerous articles have shown that Pickering emulsions are mainly sensitive to particle properties (wettability, concentration, size, shape, and flocculation state). Emulsion type depends on particle hydrophobicity: oil/water emulsions are obtained with hydrophilic particles and water/oil emulsions are obtained with hydrophobic particles. Moreover, the phase in which the particles are initially wetted becomes the continuous phase and obeys the Bancroft rule. The most stable emulsions are always obtained with particles of intermediate hydrophobicity. Stability can be further improved by increasing the concentration and aspect ratio of the particles, partially flocculating the particles, and reducing the size and size distribution of the particles. At a given energy input, smaller droplets can be obtained by increasing the particle concentration and/or decreasing the particle size.

Emulsion results are affected by aqueous and oil phase properties, mainly through their effects on particles. pH essentially influences particle wettability and/or size (swelling), while electrolytes affect particle flocculation through their impact on repulsive electrical double layer forces. Higher oil viscosities can hinder particle adsorption and, in some cases, prevent emulsion formation while polarity affects the contact angle and interfacial tension which is also sensitive to temperature. In addition, electrical or magnetic fields can be used to control emulsion stability when dielectric or paramagnetic particles are used. Rheological measurements have shown that Pickering emulsions exhibit yield stress and shear-thinning behavior and can be well described by the Herschel-Bulkeley viscosity model. Lastly, chemically stabilized emulsions exhibit both viscoelastic and thixotropic properties when the proper conditions are met.

Involved mechanisms during emulsification were analysed and the first bases of a model aiming to predict emulsion properties from operating conditions were defined. The modelling procedure considers firstly the interface generation and the coverage potentials to estimate the theoretical covered interface. The effectively covered interface was, then, deduced by defining four efficiencies associated to four stabilization conditions. At the particle scale, conditions are related to a film drainage process during approach and collision and to a capillary rise process during particle adsorption. At the droplet scale, the condition was associated to the particles network formation during emulsification.

2.2.2 Introduction

Emulsification is a common process used in many fields, including the food processing, cosmetics, pharmaceutical, paint, oil, and petrochemical industries. Given the current economic context and the strengthening of quality and environmental standards, emulsification processes, like many others, must be optimized to be economically viable.

Two approaches are generally used to develop better emulsification processes. The first is primarily aimed at improving existing processes and developing new ones, which has given rise to a wide variety of devices, systems, and techniques, including rotor/stator systems, colloidal mill systems, static mixers and phase inversion techniques. The second is aimed at optimizing formulations, mainly by evaluating different component fractions, improving the preparation protocol, and controlling physico-chemical properties. Stabilization agents, which are key to profitability since they define the type, stability, and rheology of emulsions, are largely limited to surfactants despite the fact that the pioneering work by Ramsden W. (1903) and Pickering S. U. (1907) over a century ago showed that solid particles can be used to generate emulsions that are more stable than surfactant-stabilized emulsions. No serious attempts were made to study SSEs until the 1980s.

The main goal of this review is to summarize the most relevant findings with respect to the design of solid-particle-based emulsification processes. It is divided into three sections:

- In the first section, we describe the fundamental phenomena involved in the generation of Pickering emulsions that are required to understand the stabilization mechanisms and their impact on the properties of emulsions (type, stability, and rheology).
- In the second section, we describe the effects of the relevant parameters described in the first section (particle, aqueous phase, and oil phase properties) on the stability, type, size, and rheology of Pickering emulsions.
- In the third part, we introduce the bases of a modelling procedure to predict the Pickering emulsions properties from operating conditions. The approach highlighted the main mechanisms involved during the emulsification operation.

2.2.3 Pickering emulsions stabilization

Over the past twenty years many studies have been carried out on Pickering emulsions, including those by N. Yan et al. (1994, 1995, 1996, 1997, 2001) on clay particle-, silica-, and polystyrene particle-stabilized emulsions, and B. P. Binks et al. (2000, 2001, 2002, 2003, 2005, 2007), T. S. Horozov et al. (2003, 2005), and S. Arditty et al. (2003, 2004, 2005) on silica- and PDMS particle-stabilized emulsions. The main finding of these studies, and many others like them, was that the stability of Pickering emulsions can be attributed to the formation of a steric particle barrier or network around the droplets. This clearly showed that emulsion formation and stabilization mechanisms are closely related to the formation of the particle network, which can be summarized in three steps:

a. Approach step: The particles first approach and reach the fluid/fluid interface.

b. Adsorption step: The particles adsorb to and get trapped at the interface.

c. Network formation step: The adsorbed particles form a network that stabilizes the emulsion.

The main interactions involved in each step are described below.

2.2.3.1 Particle/fluid interface approach and collision

Many studies have been devoted to investigating the particle/fluid interface approach and collision process, particularly in flotation processes that are used to separate mineral particles using air bubbles. Most have focused on a global approach based on film drainage flow analyses (A.F. Jones et al. (1978); R.H. Davis et al. (1989); A.K. Chester (1991); S. Abid et al. (1994); A. Saboni et al. (1995), S.A.K. Jeelani et al. (1994, 1998)). Film drainage been studied as a problem involving squeezed fluid flow into the gap between solid particles and fluid interfaces, with the complexity depending on fluid interface mobility and deformability (S. Hartland (1968, 1969); E. Riolo et al. (1974, 1975), A.D. Barber et al. (1976); H.J. Schultze et al. (1989)). However, the film drainage approach does not take several interactions into consideration, including van der Waals, and electrical double layer forces notably defined by the Derjaguin, Landau, Verwey, and Overbeek (DVLO) theory, and other forces such as hydration, hydrodynamic, hydrophobic, and steric forces.

2.2.3.1.1 DLVO Forces

DLVO forces include van der Waals and electrical double layer forces, which have been studied extensively and are relatively well understood. Van der Waals forces operate at the atomic and molecular levels and are composed of Keesom, Debye, and London forces, which are generally deduced from the following potential energy expressions developed by A.D. McLachlan (1963):

$$F = -\frac{dw_{vdW}(r)}{dr} \cdots (2.1)$$

$$w_{VDW}(r) = -\frac{3k_BT}{(4\pi\varepsilon_0)^2 r^6}\left(\frac{u_1^2}{3k_BT} + \alpha_{01}\right)\left(\frac{u_2^2}{3k_BT} + \alpha_{02}\right) - \frac{3}{2}\frac{\alpha_{01}\alpha_{02}}{(4\pi\varepsilon_0)^2 r^6}\frac{h\upsilon_1\upsilon_2}{\upsilon_1+\upsilon_2} \cdots (2.2)$$

where r is the distance between atoms or molecules [m], *1* and *2* are indexes of atoms or molecules, T is the temperature [K], h is Planck's constant [$6.626.10^{34}$ J.s], k_B is Boltzmann's constant [$1.381.10^{23}$ J/K], μ is the chemical potential [J/mol], α is the electronic polarizability of the molecules [C^2m^2/J], ε is the dielectric constant, and υ is the ionization frequency [Hz].

On the other hand, given that macroscopic bodies consist of a set of atoms or molecules and that the molecular van der Waals forces are additive, it is possible to define this interaction at the macroscopic level (Lifshitz theory) using the Hamaker constant (Table 2.1):

$$A_H \cong \frac{3}{4}k_BT\frac{\varepsilon_1-\varepsilon_3}{\varepsilon_1+\varepsilon_3}\frac{\varepsilon_2-\varepsilon_3}{\varepsilon_2+\varepsilon_3} + \frac{3h\upsilon_e}{8\sqrt{2}}\frac{(n_1^2-n_3^2)(n_2^2-n_3^2)}{\sqrt{|n_1^2-n_3^2|}\sqrt{|n_2^2-n_3^2|}\left[\sqrt{|n_1^2-n_3^2|}+\sqrt{|n_2^2-n_3^2|}\right]} \cdots (2.3)$$

where n is the refraction index; *1*, *2*, and *3* are the indexes of the first, second, and surrounding medium; and υ_e is the mean absorption frequency [Hz].

Tableau 2.1: Van der Waals forces expressions for different geometries (Butt H.-J. et al. (2005))

Geometry	Force
Two flat surfaces	$F = -\frac{A_H}{6\pi D^3}$ Per unit area
Two spheres	$F = -\frac{A_H}{6D^2}\frac{R_1 R_2}{R_1 + R_2}$
Sphere-flat surface	$F = -\frac{A_H R}{6D^2}$
Cone-flat surface	$F = -\frac{A_H \tan^2 \theta}{6D}$ (θ is the semi-aperture of the cone)
Paraboloid-flat surface	$F = -\frac{A_H}{12D^2}\frac{l_{xy}^2}{l_z}$ (l is the semi-axis of the paraboloid)
Cylinder-flat surface	$F = -\frac{A_H R^2}{6D^3}$

Given that van der Waals forces are often attractive, the Hamaker constant can also be deduced by analyzing the attractive part of the force-distance curves obtained by AFM (atomic force microscopy) measurements. Typical values for this constant for different systems are summarized in Table 2.2. It should, however, be noted that these forces may also be repulsive during interactions between two different systems. In such cases, the interaction is generally indicated by a negative value for the Hamaker constant.

Tableau 2.2: Typical Hamaker constant values obtained by AFM measurements (Butt H.-J. et al. (2005))

Material 1	Material 2	Medium	A_H ($\times 10^{-20}$ J)	Reference
Au	Au	Water	7-25	I. Larson et al. (1997)
Ag	Ag	Vacuum	38.5 ± 0.5	S. Eichenlaub et al. (2002)
Cu	Cu	Vacuum	27.5	S. Eichenlaub et al. (2002)
Ag	Cu	Vacuum	32.6-34	S. Eichenlaub et al. (2002)
Si_3N_4	Si_3N_4	Water	6.1	C.J. Drummond et al. (1994)
Si_3N_4	Mica	Water	3.4	C.J. Drummond et al. (1994)
SiO_2	SiO_2	Water	1	S. Biggs et al. (1997)
SiO_2	Au	Air	2.2-4.1	A.C. Hillier et al. (1996)
SiO_2	Au	Water	12-15	A.C. Hillier et al. (1996)
SiO_2	Ag	Vacuum	13	S. Eichenlaub et al. (2002)
SiO_2	Cu	Vacuum	14	S. Eichenlaub et al. (2002)
SiO_2	TiO_2	Water	1.4	I. Larson et al. (1995) and K. Hu et al. (1997)
SiO_2	Mica	Water	1.2	I.U. Vakarelski et al. (2000)
ZrO_2	ZrO_2	Water	6	S. Biggs (1996)
Al_2O_3	Al_2O_3	Water	5.3	M.E. Karaman et al. (1997)
Mica	Mica	Water	2.2	P. Kekicheff et al. (1999)
Teflon	Teflon	Air	3.9	C.J. Drummond et al. (1996)

The involvement of van der Waals forces in solid/solid interactions has received considerable attention, but far fewer studies have been devoted to solid/fluid interactions. This is mainly due to experimental problems related to interface deformability, which makes it difficult to evaluate

separation distances and to identify individual forces given the many forces involved at the same separation distance.

Some investigators have, however, succeeded in showing that these forces are attractive and in measuring their amplitude (P. Mulvaney et al. (1996); D.E. Aston (2001)). On the other hand, numerous other studies have shown that these forces can also be repulsive, notably in the case of dissimilar systems such as silica particles and air bubbles (W. A. Ducker et al. (1994); M. L. Fielden et al. (1996); M. Preuss et al. (1998, 1999)).

Much effort has also been devoted to studying electrostatic double layer forces, which have been show to occur between bodies in liquid media with a relatively high dielectric constants. They mainly arise due to the formation of charge layers at the interfaces through surface dissociation or from the adsorption of free charges in the aqueous medium (Y. Liang et al. (2007)). Their effect can be observed in colloidal dispersions where, at very low salt concentrations, a repulsive interaction occurs due to the formation of double layer charges. However, when the salt concentration is increased, particle coagulation occurs, indicating that the dominant interaction is attractive. This effect has been attributed to the screening of the electrostatic interaction by the free ions in the aqueous medium, which increases the effect of attractive interactions such van der Waals forces. At long range, these forces decay exponentially. The decay length (Debye length) for a monovalent salt can be deduced using the following expression (H.-J. Butt et al. (2005)):

$$\lambda_D = \sqrt{\frac{\varepsilon_r \varepsilon_0 k_B T}{2ce^2}} \cdots (2.4)$$

where T is the temperature [K], e is the elementary charge [1.602×10^{-19} J.s], k_B is the Boltzmann constant [1.381×10^{23} J/K], ε_r is the dielectric constant of the aqueous medium, ε_0 is the vacuum dielectric constant, and c is the salt concentration [Mol/L].

If there are many dissolved species with different valencies in the aqueous medium, the salt concentration (c) is replaced by $\sum c_i Z_i^2$, where Z_i is the valency. This force can also be deduced by resolving the Poisson-Boltzmann equation (W.R. Bowen et al. (1995)):

$$\frac{d^2\psi}{dr^2} + \frac{2}{r}\frac{d\psi}{dr} = \frac{2n^{\circ}ze}{\varepsilon_r \varepsilon_0} \sinh\left(\frac{ze\psi}{k_B T}\right) \cdots (2.5)$$

where ψ is the electric potential and n^0 is the bulk salt concentration [Mol/L].

Being a function of geometries, in the case of spherical bodies of the same size, these forces can be deduced using the following expression (Y. Liang et al. (2007)):

$$F_{el} = \frac{1}{3} S(D) n^{\circ} k_B T \left(\cosh\left(\frac{ze\psi(D)}{k_B T} \right) - 1 \right) \cdots (2.6)$$

Studies on electrostatic double layer forces in solid/solid systems (G. Toikka et al. (1998); J. Drelich et al. (2000); M. Giesbers et al. (2002)) have shown that the repulsive electrostatic double layer force decreases in parallel with an increase in salt concentration. While W.A. Ducker et al. (1994) reported that electrostatic double layers between silica particles and air bubbles can be repulsive or attractive in nature, other studies devoted to interactions between solid particles and fluid interfaces have shown that electrostatic double layer forces are solely repulsive in nature (P. Mulvaney et al. (1996); D.E. Aston (2001); M.L. Fielden et al. (1996); M. Preuss et al. (1998, 1999); G. Gillies et al. (2004, 2005)).

2.2.3.1.2 Non DLVO Forces

Non-DLVO forces, which include hydration, hydrodynamic, hydrophobic, and steric forces, arise at very short ranges (1-3 nm), and their amplitudes can be much greater than those of DLVO forces.

Hydration forces are usually repulsive but can oscillate between attractive and repulsive with extremely smooth surfaces and low salt concentrations (J.N. Israelachvili et al. (1984)). The origin and mechanism of hydration forces are not well known but have been attributed to the formation of aqueous molecular layers at interfaces that depend on physico-chemical properties. They are more relevant than DLVO forces in that they are associated with the energy required to remove the water molecular layer adsorbed at the interface. As with double layer forces, hydration forces decay exponentially with the separation distance (S. Leikin et al. (1993)):

$$F(D) = Ke^{-D/D_0} \cdots (2.7)$$

where D_0 is the characteristic decay length.

A number of studies have been devoted to hydration forces and their repulsive nature, especially during interactions between solid surfaces (H.-J. Butt (1991); S. Veeramasuneni et al. (1998)) and between solid particles and fluid interfaces ((W.A. Ducker et al. (1992, 1994); M. Preuss et al. (1998, 1999); G. Gillies et al. (2005)). These interactions have been attributed to the formation

of hydrogen bonds between water molecules, and between surface silanol groups (Si-OH) in the case of silica surfaces (J.J. Valle-Delgado et al. (2005)). The fact that adding alcohol to the aqueous phase reduces the hydration force provides support for this explanation (R.-H. Yoon et al. (1998); Y. Kanda et al. (1998)) since the adsorption of alcohol molecules to surfaces prevents the formation of hydrogen bonds between water molecules and between silanol groups (Si-OH).

In addition to hydration forces, which are related to aqueous continuous phase affinity with interfaces, hydrophobic forces arise between hydrophobic surfaces in aqueous media. The origin of these forces is unknown, but they may be associated with the migration of water molecules from the gap between two surfaces to the bulk water phase, mainly due to their lack of affinity with hydrophobic surfaces. Hydrophobic forces are attractive. They can be more significant than DLVO interactions and can arise at a relatively long range. The attractive nature of these forces has been studied using hydrophobic solid surfaces (J.W.G. et al. Tyrrell (2002); and K. Fa et al. (2005)) and particle/fluid interfaces between silica particles and bubbles (M.L. Fielden et al. (1996); M. Preuss et al. (1998); W.A. Ducker et al. (1994)). In addition, like hydration forces, exponential decay evolution with separation distance has been proposed to describe this interaction (J. Drelich et al. (2000)):

$$F/R = -C_0 e^{-H/D_0} \cdots (2.8)$$

where H is the separation distance, C_0 is the pre-exponential parameter, and D_0 is the decay length.

Hydrodynamic forces are repulsive and arises at very short range. They are associated with the friction induced by the drainage of the thin liquid film between surfaces. Like the drag force, hydrodynamic forces depend on the separation distance and can be described, in the case of the sphere with $D << R$ and a non-slippage condition, using the following expression (D.Y.C. Chan et al. (1985)):

$$F_{hyd} = 6\pi\eta v \frac{R^2}{D} \cdots (2.9)$$

where D is the separation distance, η is the dynamic viscosity of the liquid, v is the approach velocity, and R is the sphere radius.

This expression was later modified to take liquid slippage at boundaries into consideration by introducing a corrective factor (O.I. Vinogradova (1995)):

$$F_{hyd} = 6\pi\eta v \frac{R^2}{D} f^* \cdots (2.10)$$

$$f^* = \frac{D}{3b}\left[\left(1 + \frac{D}{6b}\right) ln\left(1 + \frac{6b}{D}\right) - 1\right] \cdots (2.11)$$

$$b = h\left(\frac{\eta}{\eta_s} - 1\right) \cdots (2.12)$$

where η_s is the dynamic viscosity of the liquid near the boundary, h is the thickness of the liquid layer near the boundary, and b is the effective slippage length.

This expression was confirmed by experimental results showing that the non-slippage condition cannot be met, at least in the case of interactions during the approach to solid surfaces (V.S.J. Craig et al. (2001); E. Bonaccurso et al. (2002)). While no recent studies have been devoted to investigating this force in solid/fluid interactions, in all likelihood the only differences that have to be taken into consideration are fluid interface mobility and deformability.

Lastly, steric forces arise when chain molecules or particles attach to surfaces and form an overlapping structure that prevents the approach of other surfaces through a repulsive interaction. Steric forces depend on the nature of the solvent, the properties of the adsorbed particles or macromolecules, and the adsorption time. However, since many parameters are involved in steric forces, modeling them is difficult. A few expressions have been proposed for special cases such as interactions between layers of Pluronic F108 (a triblock polymer) adsorbed on hydrophobic surfaces (brush configuration) and hydrophilic silica spheres (4-6 μm) in an electrolyte solution (S.C. McLean et al. (2005)):

$$F(D) = 4\pi R P_0 \left[\frac{2L_0^*}{D} + \left(\frac{D}{2L_0^*}\right)^2 - \left(\frac{D}{2L_0^*}\right)^5 - \frac{9}{5}\right] \cdots (2.13)$$

$$P_0 = \frac{k_B T N}{2}\left(\frac{\pi^2}{12}\right)^{1/3} \frac{a^{4/3}}{s^{10/3}} \cdots (2.14)$$

where R is the particle radius, L_0^* is the equilibrium brush thickness, D is the separation distance, k_B is the Boltzmann constant, T is the temperature, N is the number of segments in a polymer chain, a is the segment length, and s is the average distance between grafting points on the surface.

Steric forces arise at short range (20 nm) and increase monotonically until the surfaces reach a point where the polymer chains become incompressible. Short-range steric forces have also been observed for interactions between cellulose and silica surfaces in an electrolyte solution (J. Stiernstedt et al. (2006)) and for interactions between two gold surfaces with adsorbed poly(amidoamine) (PAMAM) dendrimers (D. Hiraiwa et al. (2006)). The amplitudes of steric forces increase in tandem with the concentration of polymer chains on the surface.

2.2.3.2 Particle adsorption dynamic and equilibrium conditions

Particle stability at the interface can be assessed using two approaches. The first is based on a free energy analysis, which considers that stability is attained when the system reaches its minimal free energy, whereas the second is based on a force analysis, which considers that stability is attained when the forces are balanced (B.P. Binks and T.S. Horozov (2006)).

2.2.3.2.1 Free energy approach

The free energy approach supposes that particles are adsorbed at the interface only if the interfacial energy of the particles and droplets is reduced after adsorption:

$$E_{p/interf} < E_{p/disp} \cdots (2.15)$$

$$E_{d/with\ p} < E_{d/without\ p} \cdots (2.16)$$

It also supposes that the equilibrium position of the particle at the interface corresponds to the minimal value of the interfacial energies:

$$\frac{dE_{p/interf}}{d\theta} = 0 \cdots (2.17)$$

$$\frac{dE_{d/with\ p}}{d\theta} = 0 \cdots (2.18)$$

where $E_{p/disp}$ is the interfacial energy of the particle in the bulk phase, $E_{p/interf}$ is the interfacial energy of the particle at the interface, $E_{d/with\ p}$ is the interfacial energy of the droplets with

adsorbed particles, $E_{d/without\ p}$ is the interfacial energy of the droplets without adsorbed particles, and θ is the contact angle.

This approach has been used to study the thermodynamic stability of these systems and to deduce the adsorption energy or work. Particle stability at the interface has been attributed to the presence of energetic wells at the interface where the particles are trapped (S. Levine et al. (1989a)). An expression has also been developed to describe the interfacial energy of the system for the adsorption of silica particles at a planar interface:

for $\theta < 90°$

$$E_\gamma = 4\pi r^2\gamma_{ws} - \pi r^2\gamma_{ow}(1-\cos\theta)^2 \cdots (2.19)$$

for $\theta > 90°$

$$E_\gamma = 4\pi r^2\gamma_{os} - \pi r^2\gamma_{ow}(1+\cos\theta)^2 \cdots (2.20)$$

where γ_{ow} is the oil/water interfacial tension, γ_{ws} is the water/solid interfacial tension, γ_{os} is the oil/solid interfacial tension, r is the particle radius, and θ is the contact angle.

The first two terms describe the interfacial energy of the particle when it is located in the bulk (oil or water) phase while the other terms describe variations of the particle interfacial energy when the particle is transported from the bulk phase to the interface. This led to the following expression for particle desorption energy:

$$E = \pi r^2\gamma_{ow}(1 \pm cos\theta)^2 \cdots (2.21)$$

By extending this reasoning to Np particles at the interface and by considering that capillary forces are the main interaction between particles at the interface, S. Levine et al. (1991) proposed the following expression to describe the variations in interfacial energy (before and after particle adsorption). It assumes a hexagonally close-packed monolayer configuration of particles around the drop, which stays spherical after adsorption:

$$\Delta(F_{II} - F_I)/N_p = -\pi r^2\gamma_{ow}(1-\cos\theta)^2\left[\frac{\pi}{18\sqrt{3}}\frac{r^2}{R_0^2D^2}(2+\cos\theta)^2(1-\cos\theta)^2\right] \cdots (2.22)$$

where R_0 is the drop radius before adsorption, r is the particle radius, θ is the contact angle, and D is the distance separating the centers of adsorbed particles.

R. Aveyard et al. (2003) proposed a similar expression that assumed a drop swelling effect after particle adsorption (Figure 2.1) and a line tension effect (Figure 2.2) to model the adsorption free energy variations of spherical particles on a spherically curved droplet interface:

$$\Delta E = 2\pi\gamma_{ow}\left[r^2(1 \pm cos\alpha)cos\theta_{ow}\left(1 - \frac{\tau cos\beta}{\gamma_{ow}x}\right) - R_{II}^2(1 - \cos\beta)\right] + 2\pi x\tau \cdots (2.23)$$

$$\alpha = \sin^{-1}(x/r) \cdots (2.24)$$

$$\beta = \sin^{-1}(x/R_{II}) \cdots (2.25)$$

$$(R_{II}/R)^3 = 1 + (r/4R)N_p(r/R)^2[(2 + \cos\theta_{ow})(1 - \cos\theta_{ow})^2 - (9\,r/4R)\sin^4\theta_{ow} + \cdots] \cdots (2.26)$$

where R is the droplet radius before particle adsorption, R_{II} is the droplet radius after particle adsorption, r is the particle radius, θ_{ow} is the contact angle, N_p is the number of particles, and τ is the line tension.

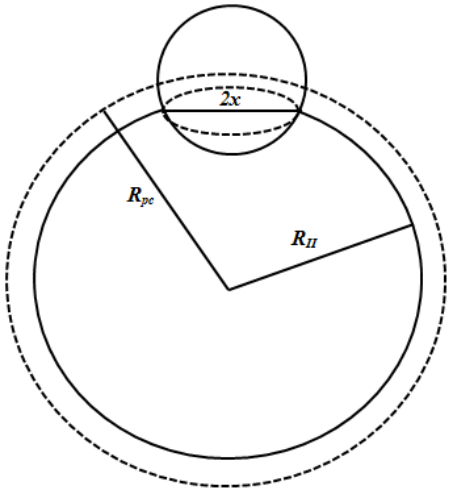

Figure 2.1: Particle adsorption at the interface

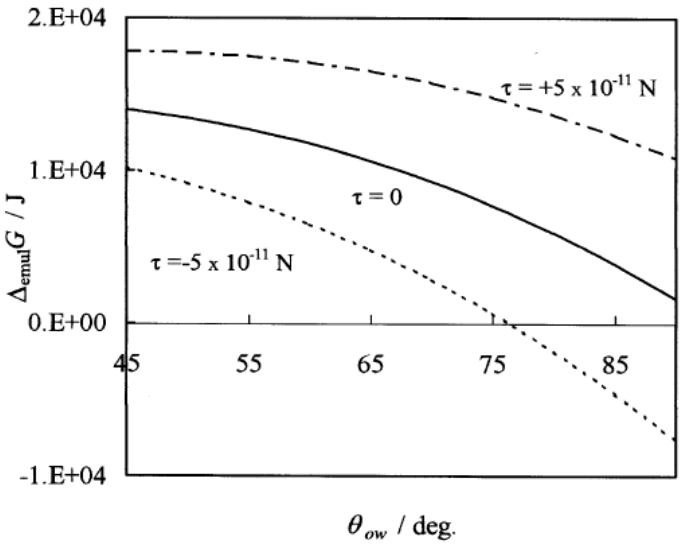

Figure 2.2: Tension line effect on free energy (R. Aveyard et al. (2003))

S. Sacanna et al. (2007) proposed the following expression that takes the line tension effect into consideration to explain the thermodynamic stability of Pickering emulsions. They defined the interfacial energy of emulsification using a free energy variation:

$$\Delta f = \frac{F_{II} - F_I}{2\pi r^2 N} = \Delta\gamma(1 - z) + \frac{\gamma_L}{r}\sqrt{(1 - z^2)} + \frac{\gamma_{ow}}{2}\left(\sigma - (1 - z^2)\right) \cdots (2.27)$$

$$\Delta\gamma = \gamma_{cw} - \gamma_{wc} \cdots (2.28)$$

$$z = \cos\theta \cdots (2.29)$$

where r is the particle radius, γ_L is the line tension, σ is the average interfacial area occupied by colloidal particles, and N is the number of particles.

On the other hand, M.J. Hey et al. (2006) proposed the following expression to deduce the particle equilibrium position from the contact angle of the particle:

$$\cos\theta = \frac{\left(1 - (1 + (b/a_0)^3)^{2/3}\right)}{(b/a_0)^2} \cdots (2.30)$$

where b is the particle radius and a_0 is the initial droplet radius.

Y. Hirose et al. (2008) proposed the following expression to estimate the equilibrium particle concentration at the interface by minimizing the interfacial energy:

$$\phi_{0,eq} = \frac{\phi_{bulk}}{\phi_{bulk} + exp\left[-\frac{\pi(r/2)^2\sigma_{12}}{k_B T}\left(1 + \left(\frac{\sigma_{1p} - \sigma_{2p}}{\sigma_{12}}\right)^2\right) - \frac{B}{k_B T}\phi_{0,eq}\right]} \cdots (2.31)$$

where $\phi_{0,eq}$ is the equilibrium particle concentration at the interface, k_B is the Boltzmann constant, T is the temperature, B is the parameter describing interaction between particles at the interface, σ is the interfacial tension, and r is the particle radius.

2.2.3.2.2 Force balance approach

With the force balance approach, the particle equilibrium position and the stability condition are deduced by assuming that the sum of external forces is zero at equilibrium. Adsorption is mainly related to capillary forces (Figure 2.3), as defined by the following expression (H.M. Princen (1969); A.V. Rapacchietta et al. (1977)):

$$F_{\gamma/z} = \gamma_{OW_z}(2\pi r_C) = 2\pi r \gamma_{OW} \sin\phi_c \sin(\theta + \phi_c) \cdots (2.32)$$

More recently, D.D. Joseph et al. (2003) and P. Singh et al. (2005) performed force balance analyses on the same system that took the gravity, capillary, buoyancy, and hydrostatic pressure forces, into consideration:

$$F_{B/w} = \rho_w V_{pw} g = \rho_w g \pi r^3 (2 - 3\cos\phi_c + \cos^2\phi_c)/3 \cdots (2.33)$$

$$F_{B/o} = \rho_o g(V_p - V_{pw}) = \rho_o g \pi r^3 [2 + 3\cos\phi_c - \cos^2\phi_c]/3 \cdots (2.34)$$

$$F_P = -(\rho_o - \rho_w) g z_c (r\sin\phi_c)^2 \cdots (2.35)$$

$$F_g = \rho_p g 4\pi r^3/3 \cdots (2.36)$$

where $F_{B/w}$ is the aqueous buoyancy force, $F_{B/o}$ is the oil buoyancy force, $F_{\gamma/z}$ is the capillary force, F_P is the hydrostatic pressure force, and F_g is the gravity force.

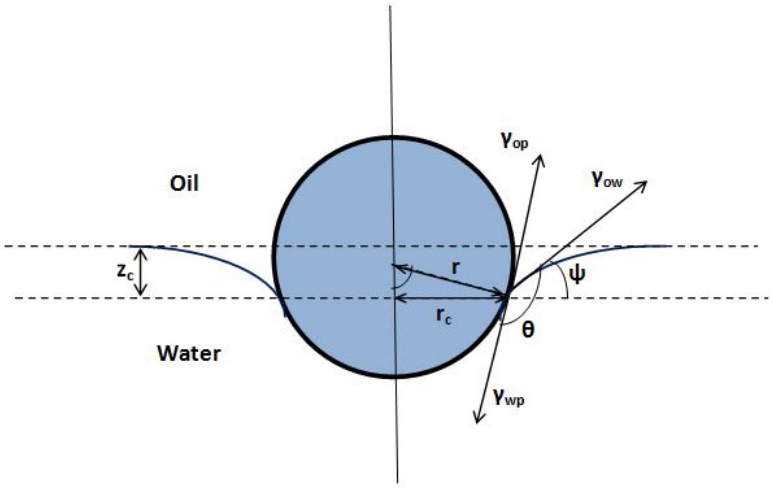

Figure 2.3: Representation of particle adsorption at an oil/water interface

The equilibrium position is thus deduced from the force balance using the following expression:

$$\sin\phi_c \sin(\theta + \phi_c) = \frac{gr^2(\rho_o - \rho_w)}{6\gamma_{OW}}\left[4\frac{\rho_p - \rho_o}{\rho_w - \rho_o} - (1 - \cos\phi_c)^2(2 - \cos\phi_c) + \frac{z_c}{r}\sin^2\phi_c\right] \cdots (2.37)$$

2.2.3.3 Particles Network Formation (Interactions at the interface)

The third and last stabilization step is the formation of the steric particle network, which prevents the destabilization of Pickering emulsions. Emulsion stability depends on particle compactness and the number of layers at the interface. Particles must form at least one layer to prevent emulsion destabilization (N. Yan et al. (1994, 1995a)). In addition, N. Yan et al. (1995b, 1996, 1997a) reported that an increase in particle compactness and layer number reduces the demulsification rate.

However, other studies have found that it is possible to stabilize Pickering emulsions without covering the entire interface with particles, especially if both polymers and particles are used. It has been shown that it is possible to stabilize emulsions by covering the interface with the equivalent of 29% close-packed silica spheres (B.R. Midmore (1998)). This was attributed to the use of a homopolymer that partially flocculated the particles, allowing the formation of a two-dimensional gel structure at the interface. However, more recently, R. Vignati et al. (2003) reported that emulsions can be stabilized with only 5% interface coverage and without using a homopolymer. This was attributed to particle dynamics at the interface, which was later

confirmed by particle motion at the droplet interface that depended on particle size and wettability, oil viscosity, and interface curvature (S. Tarimala et al. (2004, 2006) and L.L. Dai et al. (2008)). These findings indicated that there are many particle configurations that can stabilize emulsions. They can be divided into five categories based on particle interactions at the interface (R.J.G. Lopetinsky et al.; B.P. Binks and T.S. Horozov (2006)).

1. The droplets are entirely covered by close-packed hexagonal particles (Figure 2.4a).
2. The droplets are entirely covered, with a common layer between two droplets (Figure 2.4b).
3. The particles are partially flocculated and form a network at the interface (Figure 2.4c).
4. The particles are aggregated at the interface (Figure 2.4d).
5. The particles form a three-dimensional network (Figure 2.4e).

It is important to mention that, in terms of particle interactions at the interface, it is often assumed that there is no diagonal interaction between the particles (water side of particle 1 cannot interact with oil side of particle 2).

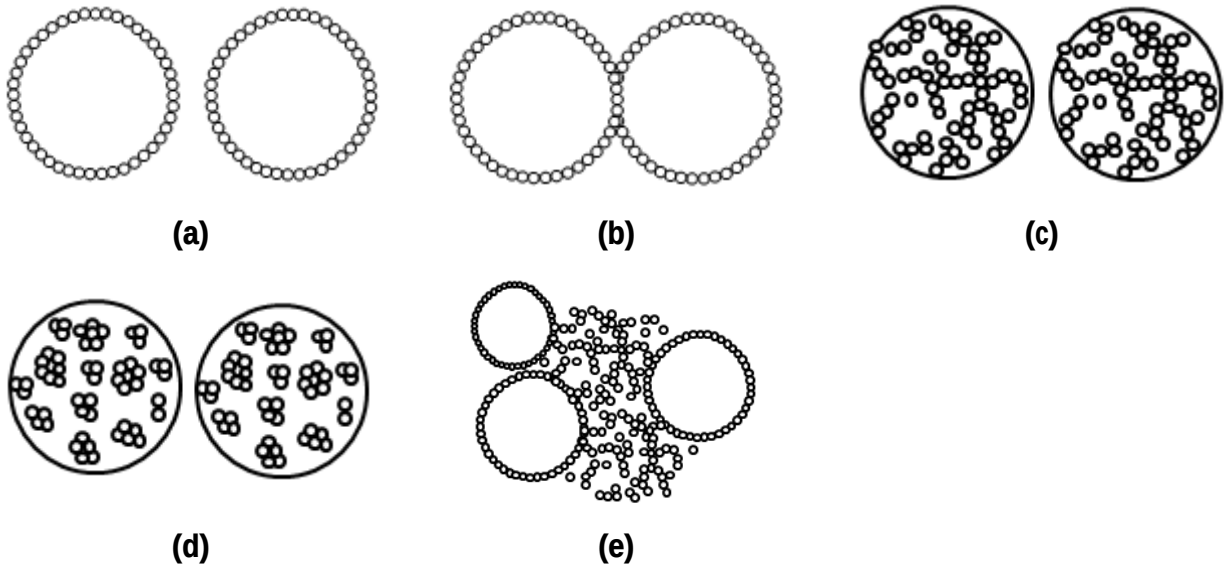

Figure 2.4: Particle configurations at Pickering emulsions interfaces

2.2.3.3.1 Repulsive dipolar interaction (Formation of the ordered hexagonal network)

Ordered hexagonal networks are one of the common particle configurations at fluid interfaces. Particles form a hexagonal network with a characteristic inter-particle distance (R. Aveyard et al.

(2000a, b, c)). Monolayer hexagonal structures have also been observed with charged latex particles at air/water, octane/water, and octane/surfactant interfaces. This behavior has been attributed to the presence of a repulsive electrostatic interaction between the adsorbed particles at the interface, which depends on particle size and adsorption level and electrolyte concentration. Based on these results and those of A. J. Hurd (1985), the interactions between the two phases can be deduced using the following expressions:

Aqueous phase:

$$f_{inter} \approx \frac{24\pi^2 R^2 \sin^2\theta\, \varepsilon_{oil}\sigma^2\alpha_{water}^2}{4\pi\varepsilon_0\varepsilon_{water}^2\kappa^4 L^4} \cdots (2.38)$$

Oil phase:

$$f_{inter} \approx \frac{q_{oil}^2}{4\pi\varepsilon_{oil}\varepsilon_0}\left[\frac{1}{L^2} - \frac{L}{(4\zeta + L^2)^{3/2}}\right] \cdots (2.39)$$

$$\zeta = R(3 + \cos\theta)/2 \cdots (2.40)$$

$$q_{oil} = 2\pi R^2\sigma(1 - \cos\theta)\alpha_{oil} \cdots (2.41)$$

where L is the distance between the centers of the particles, R is the particle radius, σ is the particle surface charge density corresponding to full dissociation, α_{oil} is the degree of dissociation of the sulfate groups at the particle-oil interface, α_{water} is the degree of dissociation of the sulfate groups at the particle-water interface, θ is the particle contact angle, q_{oil} is the charge of the oil-immersed portion of the particle, ζ is the distance between q and the interface, ε_0 is the vacuum permittivity, ε_{oil} is the dielectric constant of the oil, and ε_{water} is the dielectric constant of water.

S. Tarimala et al. (2004) observed ordered hexagonal structures with a characteristic separation distances using PDMS/water emulsions stabilized by monodispersed polystyrene particles (Figure 2.5). This behavior was attributed to dipolar repulsive interactions on the non-polar phase side (Figure 2.6).

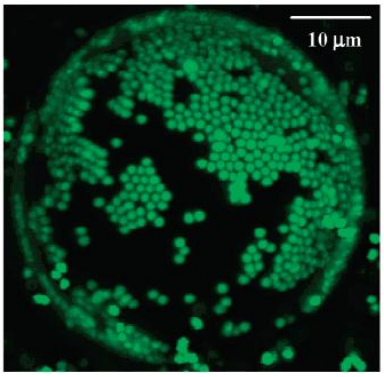

Figure 2.5: Polystyrene particle network on PDMS droplet surfaces

(Tarimala S. et al. et al. (2004))

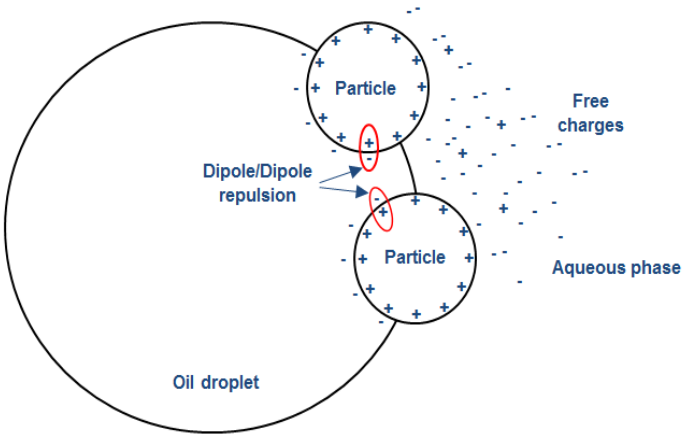

Figure 2.6: Illustration of dipolar repulsive interaction on the oil phase side

T.S. Horozov et al. (2003, 2005) investigated the wettability effect using silica particles adsorbed on an octane/oil interface. Their results showed that a decrease in the particle contact angle resulted in a decrease in the inter-particle distance, and thus a transition from ordered hexagonal network to a disordered structure with aggregated particles (Figure 2.7a: 70°, b: 115°, c: 129°, d: 150°).

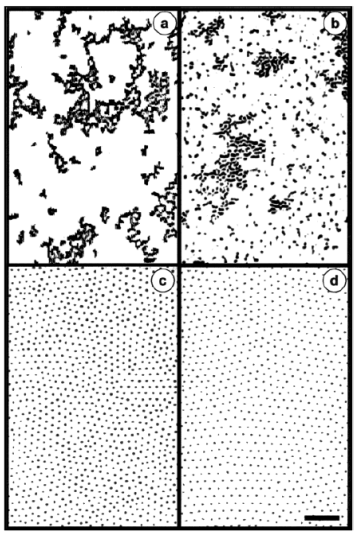

Figure 2.7: Effect of particle wettability on the configuration of the particle network

(Horozov T. S. et al. (2003))

2.2.3.3.2 Lateral capillary forces (Particle network cohesion)

As previously mentioned, particles at interfaces can form a close-packed hexagonal network with a characteristic separation distance between particles. We also discussed the role of the dipolar repulsive forces in the formation of the network. To maintain network cohesion, these repulsive forces are counterbalanced by attractive forces which, in some cases, cause particle aggregation distortion (T.S. Horozov et al. (2005); S. Tarimala et al. (2004 and 2006), L.L. Dai et al. (2008), B. Madivala et al. (2009)). Particle attraction at a fluid interface is usually attributed to capillary forces induced by the interface distortion which results from different causes.

Particle adsorption can cause interface deformation due to particle wettability and the resulting contact angle. Particle adsorption at the interface creates a meniscus around the particle due to the motion of the three contact line until the equilibrium position is reached. This phenomenon, which causes capillary interactions, has been observed with planar interfaces (H.M. Princen (1969); A.V. Rapacchietta et al. (1977); D.D. Joseph et al. (2003); P. Singh et al. (2005)) and with curved interfaces and emulsions. S. Levine et al. (1989, 1991, 1992, 1993) developed a number of models to evaluate the amplitudes of capillary forces and their impact on emulsion stability.

Particle irregularities, such as shape and roughness, which are also related to the particle wettability effect, can also deform the interface. Particle roughness affects emulsion stability through the reduction of the amplitudes of capillary forces (E. Vignati et al. (2003)). Irregularly shaped particles also increase the deformation of the interface and, as such, the amplitudes of attractive forces (D. Stamou et al. (2000)). For example, ellipsoidal particles, which increase the aspect ratio, cause more distortions at the interface (Figure 2.8) and thus an increase in capillary forces, resulting in the formation of aggregated structures (J.C. Loudet et al. (2005 and 2006)). This was confirmed using a theoretical approach (H. Lehle et al. (2008)) that showed that meniscus height is proportional to the particle aspect ratio (Figure 2.9).

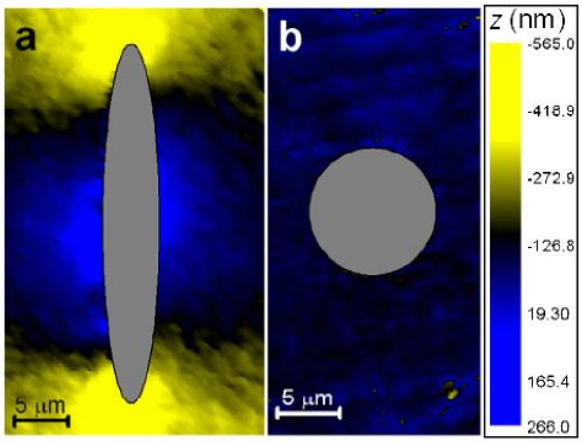

Figure 2.8: Effect of particle shape on interfacial distortions

(J.C. Loudet et al. (2006))

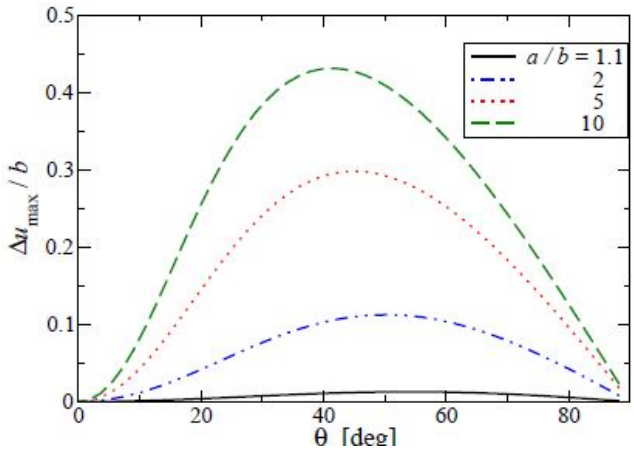

Figure 2.9: Effect of the aspect ratio on meniscus height

(H. Lehle et al. (2008))

Electrostatic stresses or pressures generated by dipolar electrical fields induced by charged particles on the interface are a third source of capillary forces (M.G. Nikolaides et al. (2002)). These pressures are caused by the asymmetry of the electrical field resulting from the difference in dielectric constants between the two liquids (Figure 2.10).

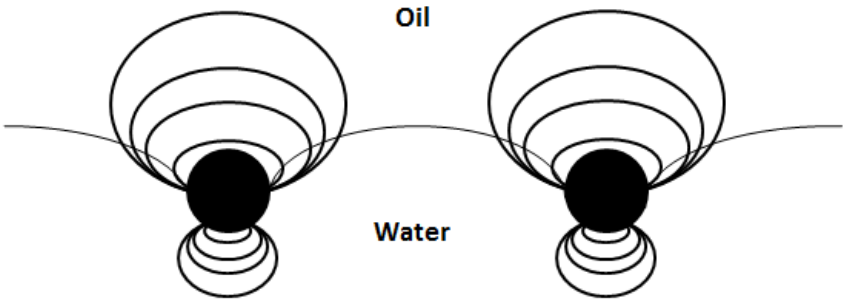

Figure 2.10: Illustration of electrical fields generated by particles at the interface

K.D. Danov et al. (2004) also reported similar interactions between glass beads at air/water and tetradecane/water interfaces. They reported that increasing the electrolyte concentration in the aqueous phase has no significant effect on the amplitude of capillary forces, which arises primarily from the non-polar phase, and that interface distortions result from particles being pushed toward the aqueous phase. Based on these findings, K.D. Danov et al. (2006) proposed the following expressions to describe the interactions between two particles (F_{12}) and the electrodipping force (f^{el}), which are responsible for interface distortion:

$$F_{12} = \frac{3p_{d1}p_{d2}}{2\varepsilon_n L^4} \cdots (2.42)$$

where F_{12} is the interaction force between two dipoles (particles), p_d is the dipole moment, ε_n is the dielectric constant of the nonpolar fluid, and L is the distance between two particles, and

$$F^{el} \approx \frac{4\pi}{\varepsilon_n} r_c^2 \sigma_{pn}^2 f_{\sigma\sigma} + 2r_c \sigma_{pn}(\Delta\varphi) f_{\varphi\sigma} + \frac{\varepsilon_n}{4\pi}(\Delta\varphi)^2 f_{\varphi\varphi} \cdots (2.43)$$

where F^{el} is the electrodipping force acting on the particle, σ_{pn} is the surface electric charge density at the particle/nonpolar phase interface, r_c is the radius of the contact line, $\Delta\varphi$ is the potential difference between the particle/water interface and the nonpolar phase/water interface, and $f_{\sigma\sigma}$, $f_{\varphi\sigma}$, and $f_{\varphi\varphi}$ are the force coefficients.

2.2.3.3.3 Van der Waals Forces

Given that particles can interact only through the same medium (oil or water or both), it is possible to use the classical approach describing particle interactions in the same medium in order to evaluate van der Waals forces. S. Levine et al. (1989) developed the following expression to describe the interaction energy based on the Hamaker constants of both phases:

$$V_s(H) = \frac{-A_w a}{24H}\left[1 + \frac{h}{(Ha + h^2)^{1/2}}\right] - \frac{A_o a}{24H}\left[1 - \frac{h}{(Ha + h^2)^{1/2}}\right] \cdots (2.44)$$

where A is the Hamaker constant, a is the particle radius, H is the shortest distance between the two particles, and h is the distance between the center of the particle and the interface.

D.F. Williams et al. (1992) used another approach to understand particles aggregation at water/air interfaces. They showed that van der Waals forces at the interface cannot be directly estimated from the Hamaker constant of each phase but had to be estimated from an effective Hamaker constant taking the particle immersion level into consideration:

$$A_{eff} = A_{pp} + f^2(3 - 2f)\left(A_{pwp} - A_{pp}\right) \cdots (2.45)$$

where f is the immersion height fraction, A_{pp} is the particle Hamaker constant in the vacuum, and A_{pwp} is the effective particle Hamaker constant in water.

Based on this result, S. Tarimala et al. (2006) and L.L. Dai et al. (2008) proposed a more adaptive expression of the Hamaker constant:

$$A_{eff} = A_{pp} + f_{water}^2(3 - 2f_{water})\left(A_{pwp} - A_{pp}\right) + f_{oil}^2(3 - 2f_{oil})\left(A_{pop} - A_{pp}\right) \cdots (2.46)$$

$$A_{121} = \sqrt{A_{11} - A_{22}} \cdots (2.47)$$

that showed that van der Waals forces have intermediate values ranging between those acting in the oil and the aqueous phases. They also discovered that van der Waals forces arise at short ranges and are less significant than repulsive dipolar and capillary forces. On the other hand, Ruiz-Garcia J. et al. (1997) reported that these forces are relatively important and lead to particle cluster formation in the case of latex particles at air/water interfaces.

2.2.3.3.4 Electrostatic double layer forces

Electrostatic double layer forces arise mainly in aqueous media and can be deduced from the Poisson-Boltzmann equation. Unfortunately, no relevant studies have been devoted to forces at fluid interfaces, but it is likely that electrolyte concentrations have a significant effect on these interactions.

2.2.3.3.5 Hydrophobic and hydration forces

Despite the relevance of hydrophobic and hydration forces in particle/interface and particle/particle interactions in aqueous media, no relevant studies have been devoted to investigating the forces between adsorbed particles at the interface.

2.2.3.3.6 Particle motion at the interface

Particle dynamics at the interface have been attributed to thermal agitation and, in some cases, to inter-particle forces. E. Vignati et al. (2003), who studied particle motion in partially covered isooctane or octanol droplets in an aqueous phase, reported that particles vibrated locally in densely packed layers and that gravity had an effect on particle motion. They deduced a particle diffusion coefficient at the interface (5×10^{-9} cm^2/s), which was the same order of magnitude as the bulk diffusion coefficient (5.9×10^{-9} cm^2/s). S. Tarimala et al. (2004) also deduced a diffusion coefficient and observed that it decreased considerably in parallel with an increase in oil viscosity. They also found that it increased with inter-particle distance and that particles oscillated around their equilibrium positions, especially at large inter-particle distances.

L.L. Dai et al. (2008) investigated other parameters and showed that an increase in oil viscosity reduces the diffusion coefficient to zero (no diffusion) beyond a characteristic viscosity threshold that depends on particle size. They also found that particle diffusion is hindered when the oil is somewhat elastic and that diffusion decreases with increases in particle size and contact angle, which can be attributed to the fact that hydrophobic particles are more immersed in the viscous oil phase than hydrophilic particles. They also reported that diffusion is reduced when the drop curvature is increased and that this parameter becomes less significant when oil viscosity is increased.

2.2.4 Pickering emulsions properties

Parameters such as stability, type, size, and rheology as well as, in some cases, appearance, formulation, and toxicity can be used to characterize emulsions in a general way, depending on the application for which the emulsions are intended.

2.2.4.1 Emulsion stability

Emulsion stability can be defined as the ability of the droplets to stay dispersed in the continuous phase over time. Emulsions can be destabilized by coalescence, Ostwald ripening, or inversion. Creaming and sedimentation can also cause destabilization since they promote droplet contact and thus increase the probability of coalescence, which is the main process leading to phase separation.

Given the importance of emulsion stability, especially in the case of SSE, which are much more stable than surfactant-stabilized emulsions, many studies have been devoted to investigating the roles of particle, water, and oil properties in emulsion stability.

In terms of particle wettability, it has been shown that highly hydrophobic and hydrophilic particles produce the least stable emulsions, whereas the most stable emulsions are obtained using particles of intermediate hydrophobicity (B.P. Binks et al. (2000a); N. Yan et al. (2001); S. Stiller et al. (2004); A. Ding et al. (2005)). N. Yan et al. (1995, part 2, 1997a) also reported that when fresh oil is added the demulsification rate reaches its minimal value when the contact angle is close to 90°. S. Levine et al. (1989) proposed the following expression to describe the energy required to remove a particle from the interface and thus the impact of the wettability effect on emulsion stability:

$$E = \pi R^2 \gamma_{ow} (1 \pm cos\theta)^2 \cdots (2.48)$$

where E is the detachment energy (J), R is the particle radius (m), γ_{ow} is the oil/water interfacial tension (J/m^2), and θ is the contact angle.

N. Yan et al. (1994) investigated the effect of wettability on the configuration of the particle network and thus on emulsion stability. They showed that particles with large contact angles form a compact layer at the interface whereas particles with small contact angles flocculate and form a less compact layer. T.S. Horozov et al. (2003, 2005) showed that there is a transition from

an ordered structure to a disordered and flocculated structure when the particle contact angle is reduced (Figure 7), confirming the impact of particle wettability on the structure of the particle network at the interface. B.P. Binks et al. (2000b) and B.P. Binks (2002) investigated the effect of particles with different wettabilities and showed that it is possible to produce transitional phase inversions using mixtures of hydrophilic and hydrophobic particles, while C.P. Whitby et al. (2010) reported that emulsions can be destabilized using mixtures of particles with different wettabilities, which is likely due to the inability of the particle network to prevent coalescence when such mixtures are used. On the other hand, B.P. Binks et al. (2001) reported that amphiphilic particles, or Janus particles, generate considerably more stable emulsions than SSEs.

N. Yan et al. (1994, 1995a) investigated the effect of particle concentration on emulsion stability and showed that droplets should be completely covered by at least one particle layer to ensure emulsion stability. This finding was supported by other results showing that the demulsification rate is reduced when the particle concentration is increased (N. Yan et al. (1995b, 1996, 1997a,b)). However, other investigators have reported that it is possible to stabilize emulsions without covering the entire droplet surface (S. Levine et al. (1989a); B.R. Midmore (1998), B.P. Binks et al. (2001); R. Vignati et al. (2003); S. Tarimala et al. (2004)) and attributed this to the fact that particles are partially flocculated at the interface or to particle dynamics at the interface. Emulsion stability can also be improved by decreasing the size of the particles (D.E. Tambe et al. (1994); B.P. Binks et al. (2001)) or by using monodispersed particles (S. Tarimala et al. (2004)), both of which result in the formation of a close-packed network. On the other hand, polydispersed particles (1 and 4 μm) decrease emulsion stability and, in some cases, even destabilize them due to network heterogeneity (Figure 2.11).

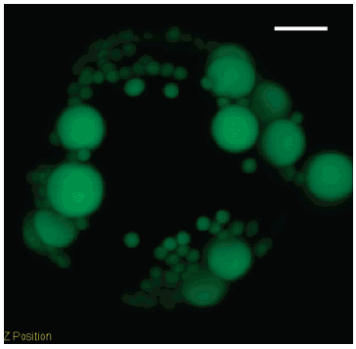

Figure 2.11: Effect of particle size distribution on particle disposition at the interface

(S. Tarimala et al. (2004))

The effect of particle shape on stability has also been investigated. B. Madivala et al. (2009) studied the aspect ratio effect of ellipsoidal particles (hydrophobic and hydrophilic) and reported that emulsion stability can be enhanced by increasing the aspect ratio. They attributed this effect to the formation of a denser packed-layer network at the interface with an elastic behavior resulting from the increase in the amplitude of the capillary forces induced by the shape of the particles.

On the other hand, the properties of the aqueous phase also have an effect on stability. Studies on the hydrogen potential (pH) have shown that the properties of emulsions are very sensitive to pH variations of the aqueous phase, mainly through the effect of pH on particle wettability. pH variations can also affect the surface charges of particles (zeta potential) and ionic species in the system, especially surfactants, which are amphiphilic molecules that contain both hydrophobic and hydrophilic groups. The presence of surfactants in the system can markedly influence the properties of emulsions by reducing the oil/water interfacial tension or/and by modifying the wettability of particles by adsorbing to their surfaces. Surfactants can be natural or synthetic and can be classified into four categories based on the structure of their hydrophilic group: non-ionic (uncharged functional groups), cationic (ionizable at acidic pHs), anionic (ionizable at basic pHs), and zwitterionic (both cationic and anionic groups). The sensitivity of surfactants to pH variations has been used to control the stability of SSEs with composite structures containing both solid particles and synthetic surfactant molecules (S. Fujii et al. (2006); B.P. Binks et al. (2006); B. Brugger et al. (2008)). For example, emulsions can be destabilized when the pH is decreased due to the swelling of nanocomposite particles (Figure 2.12).

Emulsion stability can also be controlled by natural surfactants such as asphaltene molecules, which behave like zwitterionic surfactants due to the presence of heteroatoms (O, N, and S) and charged groups (cationic and anionic). In this case, the particle adsorption rate at the interface decreases when the pH increases (N. Yan et al. (1996); G. Gu et al. (2003)). This has been attributed to the modification of particle wettability and interfacial tension by effect of the increase in pH on asphaltene chains (Figure 2.13). Increases in pH also lead to increases in the demulsification rate (N. Yan et al. (1997b)).

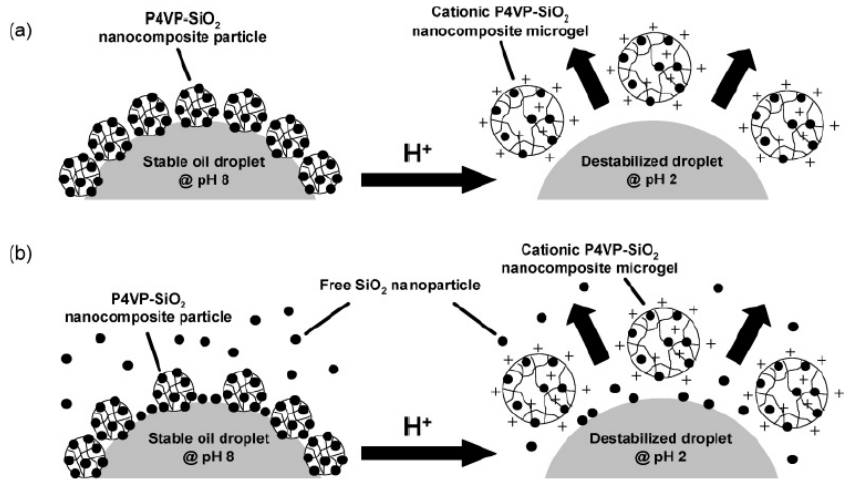

Figure 2.12: Effect of pH on microgel structures at the interface

(S. Fujii et al. (2006))

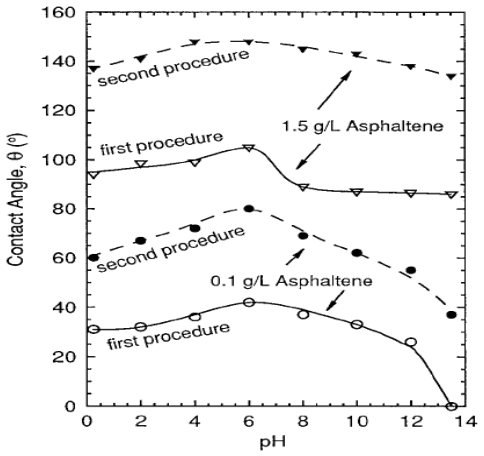

Figure 2.13: Effect of pH on the particle contact angle

(N. Yan and J.H. Masliyah (1996))

The effect of pH on particle and droplet surface charges has also been investigated using zeta potential measurements of bitumen emulsions (J. Liu et al. (2002)), crude oil emulsions (A. Hannisdal et al. (2006), X. Wang et al. (2008)), and vegetable oil emulsions (R. Pichot et al. (2009)). These studies showed that the stability of the emulsions depends on the surface properties of the particles and droplets (Figures 2.14 and 2.15). However, the main finding was that less stable emulsions are obtained at the isoelectric charge point where the particles flocculate. On the other hand, X. Wang et al. (2008) reported that particle–flocculation enhances the stability of emulsions.

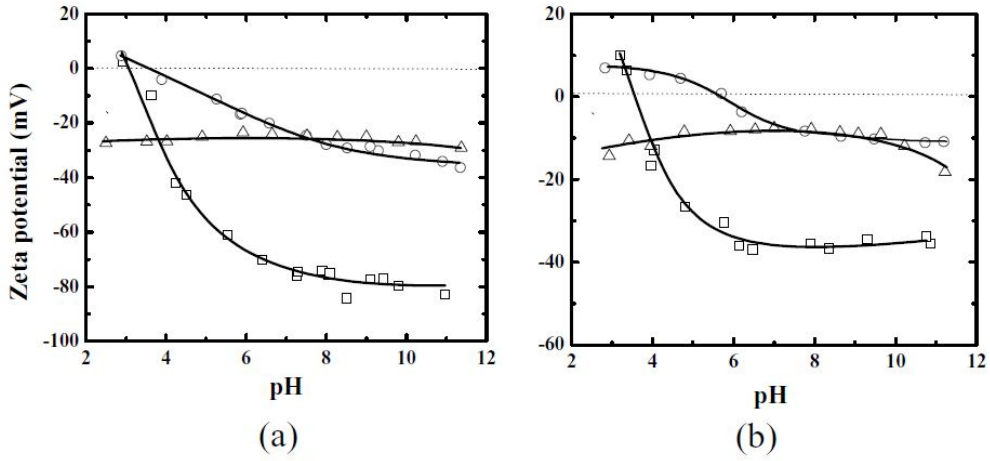

Figure 2.14: Effect of pH on the zeta potential of bitumen emulsions and clay dispersions

(Liu J. et al. (2002)) Squares: Bitumen; Triangles: Montmorillonite; Circles: Kaolinite

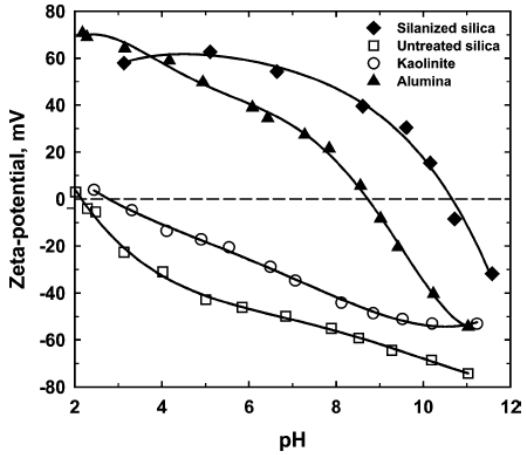

Figure 2.15: Effect of pH on the zeta potential

(W. Wang et al. (2004))

Particle flocculation has also been observed when electrolytes are added to the aqueous phase, likely due to particle interactions and DLVO forces. Force measurement experiments have shown that adding KCl or $CaCl_2$ to the aqueous solution decreases repulsive double layer forces between asphaltene surfaces (J. Liu et al. (2006)) due to an increase in the free ion concentration in the aqueous phase, which screens surface charges and reduces the effect of repulsive electrostatic double layer forces. In addition, it was found that, for the same concentration, the effect of $CaCl_2$ was more significant than that of KCl, indicating that ion valency plays a role in particle flocculation (Figure 2.16).

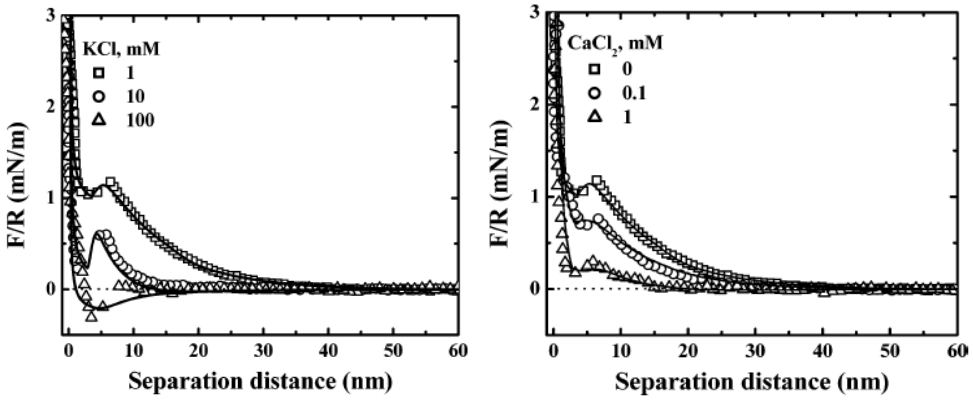

Figure 2.16: Effect of electrolyte concentration on colloidal interactions

(J. Liu et al. (2006))

Like the effect of particle flocculation on emulsion stability, It has also been shown that emulsion stability is enhanced when electrolytes are added and particles are partially flocculated, whereas emulsions are less stable when the particles are completely flocculated (B.P. Binks et al. (1999, 2005, 2006); F. Yang et al. (2006); T.S. Horozov et al. (2007)) as shown in Figure 2.17 for NaCl.

K. Golemanov et al. (2006) also studied the effect of electrolyte type and reported that an increase in ion valency (Na^{+}, Mg^{2+}, Al^{3+}) decreases the critical coagulation concentration described by the Schulze-Hardy rule, which assumes that this concentration is proportional to $1/Z^{6}$ (Z being the ion valency).

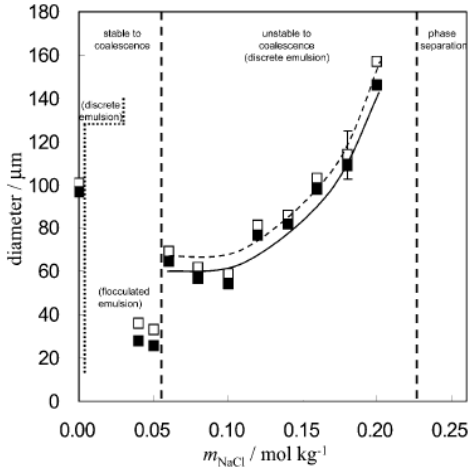

Figure 2.17: Effect of NaCl concentration on oil/water emulsion stability

(B.P. Binks et al. (2006))

Emulsion stability is also affected by the properties of the oil phase. An increase in oil viscosity ratio ($p = \eta_{oil}/\eta_{water}$) decreases the emulsified oil volume (Figure 2.18), mainly because particle attachment is hindered with viscous oils (K. Golemanov et al. (2006); C.-O. Fournier et al. (2009)). There is also a viscosity limit beyond which emulsification cannot occur for a given process condition (energy dissipation rate and mixing time).

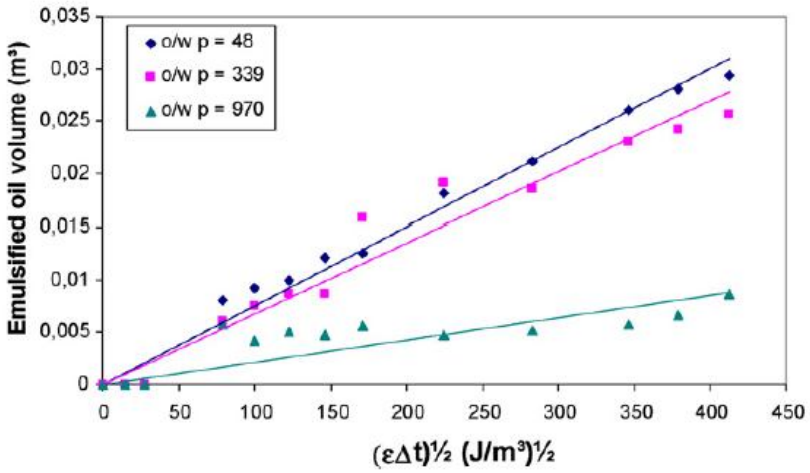

Figure 2.18: Effect of oil viscosity on the emulsified fraction

(C.-O. Fournier et al. (2009))

Other studies have shown that oil polarity can also affect emulsion stability. The polarity of a given oil depends on the presence of heteroatoms (O, N, and S), which confer electrical properties on the oil molecules, thus modifying their interactions with surrounding media (solid particles and aqueous solutions). In the case of Pickering emulsions, this property affects oil/particle affinity (B.P. Binks et al. (2000)) and interfacial tension (B.P. Binks et al. (2002); B.P. Binks et al. (2005); J. Zhou et al. (2011)). It was shown that an increase in oil polarity induced a decrease in interfacial tension and an increase in the contact angle (Table 2.3). On the other hand, if hydrophobic particles are used, the most stable water/oil emulsions are obtained with nonpolar oils, whereas the least stable are obtained with polar oils (K. Golemanov et al. (2006)). This is mainly due to an increase in particle/oil affinity that favors the passage of the particles into the oil phase rather than remaining at the interface. However, if hydrophilic particles are used, the most stable oil/water emulsions are obtained with the most polar oils (J. Frelichowska et al. (2009)).

Tableau 2.3: Effect of oil polarity on interfacial tension and silica particle wettability (B.P. Binks et al. (2000, 2002))

Huile	γ_{ow} (mN/m)	$\theta_{ow/exp}$ (°)	$\theta_{ow/theo}$ (°)
Perfluoroheptane	56.7	92	99
0.65 cS PDMS	38.7	105	112
Heptane	50.7	105	106
50 cS PDMS	38.0	123	119
Cyclohexane	50.9	110	109
Dodecane	52.5	122	110
Mystrate Isopropylique	28.6	155	142
Cineole	16.9	161	180
Undecanol	9.5	160	121
Toluene	36.0	125	129
Methyl Mystrate	25.3	164	157
Eugenol	9.0	144	180

Emulsion stability is also influenced by temperature through the effect on interfacial tension and oil viscosity, which decrease when the temperature increases. However, temperature can also affect emulsion stability when thermo-sensitive composite particles are used. These particles are obtained by grafting thermo-responsive polymer or copolymer chains such as poly[N-isopropylacrylamide] (PNIPAM) and poly[2-(dimethylamino)ethyl methacrylate-block-methyl methacrylate] (PDMA-b-PMMA) onto solid particles to produce polystyrene particles. Both PNIPAM and PDMA swell and are hydrophilic at low temperatures and contract and become hydrophobic when the temperature increases above the lower critical solution temperature. These properties have been used to control the wettability and size and hence emulsion behavior of microgel particles. It has also been shown that varying the temperature can cause emulsion inversion (B.P. Binks et al. (2005); B. Brugger et al. (2008)) or emulsion destabilization by coalescence (S. Tsuji et al. (2008)).

Paramagnetic and dielectric particles can also be used to stabilize emulsions through the application of a magnetic or electric field. For example, S. Melle et al. (2005) used a magnetic field to destabilize a paramagnetic iron particle-stabilized decane/water emulsion. This effect was only observed above a critical magnetic field value and was attributed to the movement of

particles away from the interface toward the high magnetic field region. However, the effect was reversible, making it possible to restore the emulsion by remixing. K. Hwang et al. (2010) and S. Nudurupati et al. (2010)) showed that dielectric microparticle-stablilized emulsions can be destabilized by applying an electric field. This effect was attributed to particle motion at the interface under the influence of electrophoretic forces induced by the electric field. The particles move to either the poles or the equator of the droplet (Figure 2.19), reducing their protection and leading to coalescence.

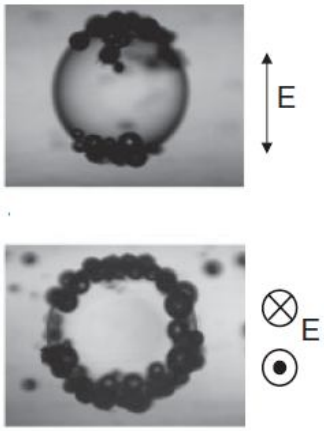

Figure 2.19: Effect of an electric field on the location of particles at the interface

(K. Hwang et al. (2010))

2.2.4.2 Emulsion type

Emulsions can be simple emulsions (oil/water or water/oil) or multiple emulsions (oil/water/oil or water/oil/water). Emulsion type is generally determined by direct visual observation, coloration, or conductivity measurements.

In terms of Pickering emulsions, most studies have focused on the effect of particle wettability on emulsion type and have shown that oil/water emulsions can be produced using hydrophilic particles and water/oil emulsions can be produced using hydrophobic particles (N. Yan et al. (2001); B. P. Binks et al. (2000a, 2005); S. Stiller et al. (2004); R. Aveyard et al. (2003)) (Table 2.4). This behavior is observed when the dispersed phase fraction is smaller or equal to the continuous phase fraction and when the particles are initially dispersed in the phase with which they have most affinity, which then becomes the continuous phase (Bancroft rule). It has also been shown that it is possible to produce multiple emulsions (B.P. Binks (2002)) and transitional

phase inversions (B.P. Binks et al. (2000b); B.P. Binks (2002); S. Simon et al. (2010)) using both hydrophilic and hydrophobic particles.

Tableau 2.4: Effect of particle wettability on Pickering emulsion type (R. Aveyard et al. (2003))

Solid particles	Oil	Contact angle	Emulsion type
Barium Sulphate	Dodecane	0	Oil/water
	Isopropyl Myristate	0	Oil/water
Calcium Carbonate	Dodecane	43	Oil/water
	Isopropyl Myristate	39	Oil/water
Hydrophilic Silica	Dodecane	38	Oil/water
	Cyclohexane	37	Oil/water
	PDMS 50 cS	81	Oil/water
	Isopropyl Myristate	32	Oil/water
	Undecanol	38	Oil/water
Partially hydrophobic silica	Dodecane	83	Oil/water
	Cyclohexane	87	Oil/water
	Isopropyl Myristate	101	Water/oil
	Undecanol	110	Water/oil
Hydrophobic Silica	Dodecane	135	Water/oil
	Cyclohexane	135	Water/oil
	PDMS 50 cSt	172	Water/oil
	Isopropyl Myristate	>175	Water/oil
	Undecanol	151	Water/oil
Bentonite for organic systems	Dodecane	81	Water/oil
	Isopropyl Myristate	96	Water/oil
Claytone HY (Hydrophobic Bentonite)	Dodecane	110	Water/oil
	Isopropyl Myristate	141	Water/oil
Polystyrene	Dodecane	152	Water/oil
	PDMS 50 cS	175	Water/oil
PTFE	Dodecane	147	Water/oil
	Isopropyl Myristate	175	Water/oil
	Undecanol	130	Water/oil

These results illustrate the similarities between surfactant-stabilized emulsions and SSEs, notably with respect to the Bancroft rule, the relationship between wettability and emulsion type, and transitional phase inversions. Based on these similarities, P.M. Kruglyakov et al. (2004) proposed an expression to define a particle HLB based on the contact angle:

$$HLB_{particle} = \left(\frac{1 + cos\theta}{1 - cos\theta}\right)^2 \cdots (2.49)$$

Like the effect of pH on emulsion stability, emulsion type can be extremely sensitive to pH variations through the effect on particle wettability. Water/oil and oil/water emulsions can be stabilized using the appropriate pH and type of particle (G. Gu et al. (2003); S. Fujii et al. (2006); B.P. Binks et al. (2006); B. Brugger et al. (2008); Y. He et al. (2013)). Other studies have shown that temperature can be used to control emulsion type if thermo-responsive particles are used, and emulsion inversion can be induced by varying the temperature (B.P. Binks et al. (2005)).

B.P. Binks et al. (2000) showed that oil polarity controls oil/particle affinity and thus particle wettability and that emulsion type depends on oil polarity (Figure 2.20). Particles become more hydrophobic with polar oils, resulting in water/oil emulsions (low conductivity: the oil is the continuous phase), whereas particles become more hydrophilic with nonpolar oils, resulting in oil/water emulsions (high conductivity: the water is the continuous phase).

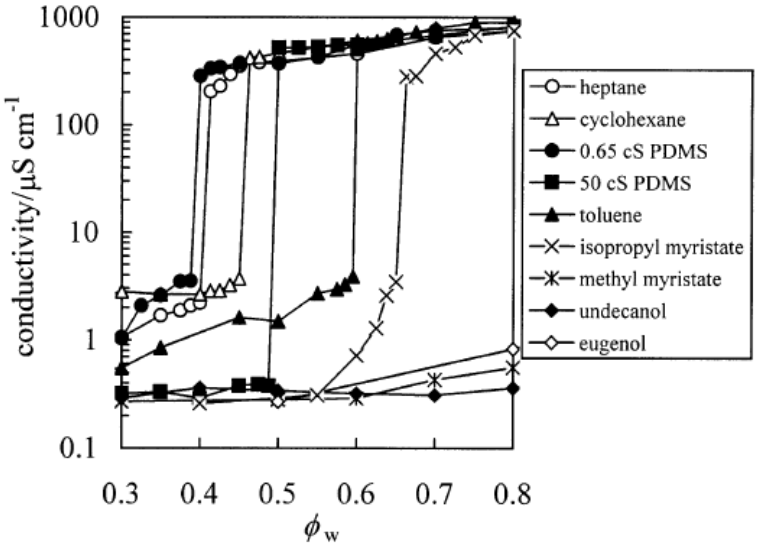

Figure 2.20: Effect of oil polarity on the emulsion apparent conductivity

(B.P. Binks et al. (2000))

2.2.4.3 Emulsion size distribution

Emulsion size distribution, which is an indication of emulsification process efficiency and emulsion stability over time, is mainly affected by particle concentration. An increase in particle concentration leads to a decrease in the size of oil droplet size (B.P. Binks et al. (2003, 2004, 2005)). The decrease in droplet size has been quantified (Figure 2.21) and modeled based on the "limited coalescence phenomena," which assumes that for a given particle concentration the emulsion will coalesce until it is completely covered in droplets. S. Arditty et al. (2003) proposed the following expression to deduce droplet size from a given particle concentration:

$$\frac{1}{\overline{D(t)}} = \frac{s_f}{\tau}\frac{m_p}{6V_d} \cdots (2.50)$$

where, s_f is the final surface area, m_p is the particle mass, V_d is the dispersed phase volume, and τ is the constant related to the degree of surface coverage.

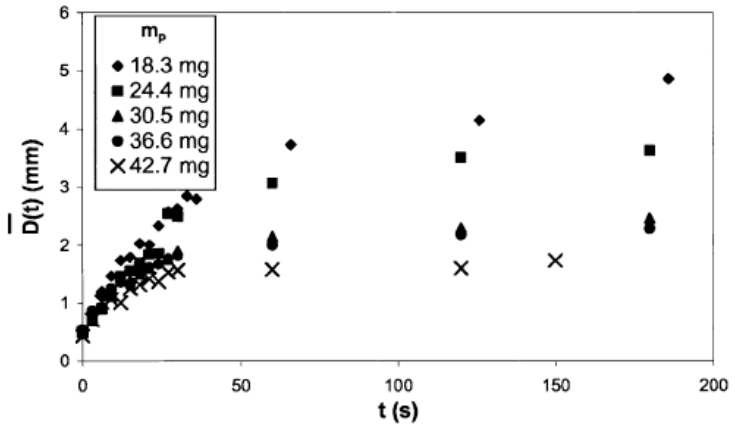

Figure 2.21: Effect of particle concentration on droplet size (S. Arditty et al. (2003))

D.E. Tambe et al. (1994) and B.P. Binks et al. (2001) reported that emulsion size is also affected by particle size whereby an increase in particle size results in an increase in emulsion size (Figure 22). In addition, B. Madivala et al. (2009) used ellipsoidal particles to generate polydispersed emulsions containing some spheroidal droplets.

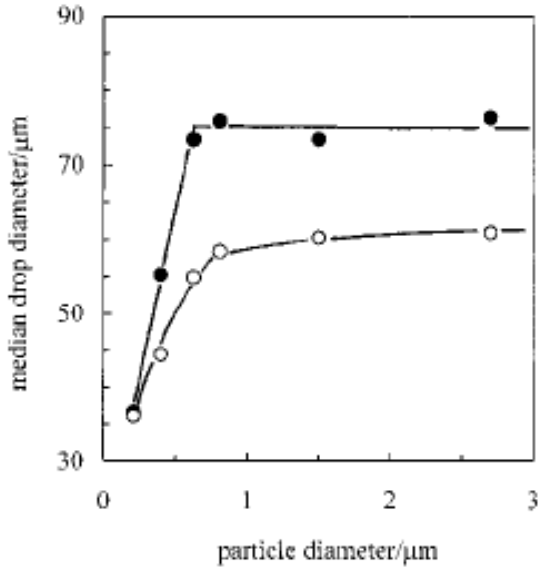

Figure 2.22: Effect of particle size on water/cyclohexane emulsion size

(B.P. Binks et al. (2001))

In terms of wettability, the smallest droplets can be obtained using particles displaying intermediate hydrophobicity. This is mainly due to the effect of wettability on emulsion stability and to the fact that the most stable emulsions are obtained with particles displaying intermediate hydrophobicity (B.P. Binks et al. (2000a); N. Yan et al. (2001); S. Stiller et al. (2004)). In addition, particle wettability is affected by the pH of the aqueous phase. pH has an effect on the particle adsorption rate and thus on stabilization and droplet size (N. Yan et al. (1996)) as well as on particle flocculation (S. Fujii et al. (2006); B.P. Binks et al. (2006)) which is also affected by salinity (B.P. Binks et al. (1999, 2005, 2006)). The size of the droplets is reduced if the particles are partially flocculated due to the pH (Figure 2.23) or the concentration of ionic species (Figure 2.24). Similarly, since particle wettability is also affected by oil polarity (B.P. Binks et al. (2000, 2002, 2005); J. Zhou et al. (2011)), droplet size is very sensitive to oil polarity (J. Frelichowska et al. (2009)). On the other hand, if thermo-responsive particles are used, temperature variations affect both emulsion stability and droplet size through the effect on particle wettability and size. Droplet size increases when the temperature increases, thus destabilizing the emulsion (S. Tsuji et al. (2008); B. Brugger et al. (2008)).

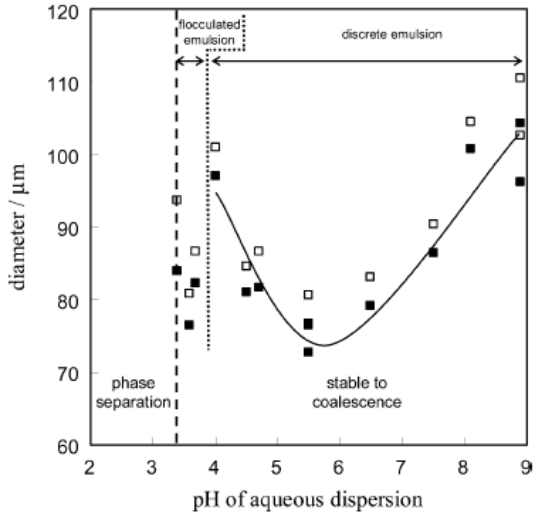

Figure 2.23: Effect of pH on oil droplet size and emulsion stability

(B.P. Binks et al. (2006))

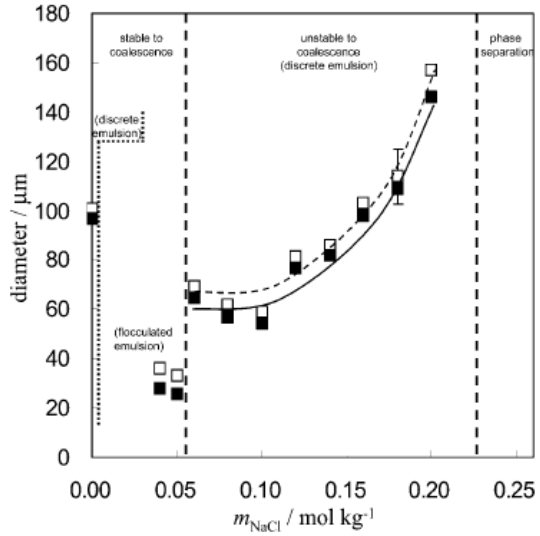

Figure 2.24: Effect of NaCl concentration on oil/water emulsion stability

(B.P. Binks t al. (2006))

2.2.4.4 Emulsion rheology

Along with emulsion stability, type, and size, emulsion rheology must also be taken into consideration when designing emulsification processes. Most studies on emulsion rheology have shown that Pickering emulsions exhibit yield stress, shear-thinning behavior, viscoelasticity, and thixotropy. Rheological measurements have been used to study yield stresses, shear-thinning

behavior, and viscoelasticity with concentrated carnation oil/water (75%) emulsions stabilized with partially flocculated silica particles (B.R. Midmore (1998)), with hexane/water emulsions stabilized with silica, bentonite, or kaolin (L.G. Torres et al. (2007)), with concentrated corn oil/water emulsions stabilized with silica nanoparticles (B. Braisch et al. (2009)), and with water/decane or decane/water emulsions stabilized by hydrophobic or hydrophilic silica particles, respectively (S. Simon et al. (2010)). Further, the results from these emulsions agreed remarkably with the Herschel-Bulkeley model (B.R. Midmore (1998); L.G. Torres et al. (2007); S. Simon et al. (2010)):

$$\tau = \tau_0 + k_{HB}\dot{\gamma}^{\alpha} \cdots (2.51)$$

where, τ is the shear stress, τ_0 is the apparent yield stress, k_{HB} is the consistency, α is the power law index, and $\dot{\gamma}$ is the shear rate.

It was also shown by L.G. Torres et al. (2007) that the model parameters were very sensitive to particles concentration (Table 2.5).

Tableau 2.5: Effect of bentonite concentration on Herschel–Bulkeley parameters (L.G. Torres et al. (2007))

Bentonite concentration (%w/w)	Yield stress (Pa)	k_{HB}	α
5	8.06	0.004	1.40
3	2.84	0.082	0.80
2	1.73	0.017	0.97
1	0.48	0.24	0.2

The Thixotropic effect was attributed to the particle aggregation state (Braisch B, et al. (2009) and Simon S. et al. (2010)) which was taken into consideration by S. Simon et al. (2010) in the Herschel-Bulkeley model. Oscillatory rheology measurements (Figure 2.25) have shown that the elastic modulus is much higher than the loss modulus (L.G. Torres et al. (2007)).

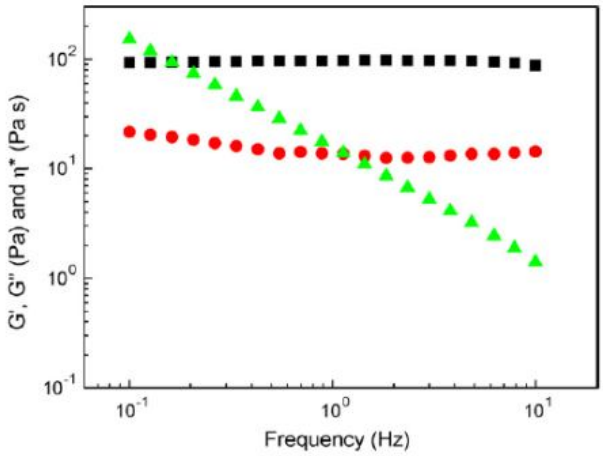

Figure 2.25: Elastic response to shear thinning of emulsions

(black squares: G', red circles: G'', green triangles: η*)

(L.G. Torres et al. (2007))

Studies on the effects of particle concentration, oil viscosity, CTAB, and NaCl concentration on emulsion rheology (L.G. Torres et al. (2007); S. Simon et al. (2010)) have shown that the consistency, shear thinning, and elastic modulus of emulsions increase with particle concentration and oil viscosity, whereas the elastic modulus decreases with increasing NaCl concentrations, indicating that particle coagulation plays a role in emulsion behavior. In addition, the consistency, shear thinning, and elastic modulus of emulsions are highest at an optimal concentration of CTAB, which affects both particle wettability and oil/water interfacial tension. On the other hand, relatively dilute emulsions (20%) exhibit Newtonian behavior. In addition, emulsion time dependency is more pronounced at pH 10 and 0.003 M $AlCl_3$, which cause particle aggregation (B. Braisch et al. (2009)).

The rheological properties of mixtures of hydrophilic and hydrophobic particles are similar to those of hydrophilic particles alone. This is likely due to the fact that hydrophilic particles flocculate at the interface when they interact with droplets, whereas hydrophobic particles are preferentially dispersed in the oil phase (Figure 2.26).

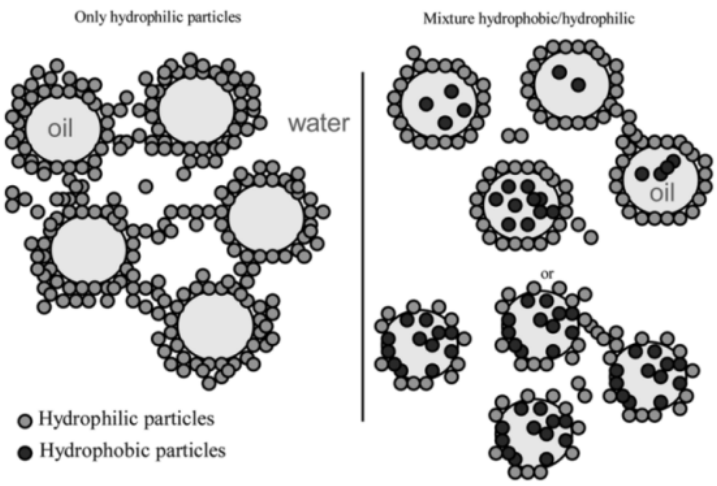

Figure 2.26: Sketch of the structure of oil/water emulsions stabilized by hydrophilic particles and by mixtures of hydrophilic and hydrophobic particles

(S. Simon et al. (2010))

2.2.5 Process-based analysis of the generation of Pickering emulsions

Emulsification involves three different mechanisms: Droplet generation, droplet stabilization and droplet coalescence. With standard emulsions, only breakage and coalescence are generally considered because the stabilization step, achieved by reducing the interfacial tension using surfactant, is much faster. However, all the emulsification operation is affected if solid particles are used as a stabilizer. Droplet generation and coalescence are affected through particle effect on the system hydrodynamic and because particles do not reduce interfacial tension, while the stabilization step is affected because solid particles are not amphiphilic and their size is much higher than surfactant molecules size meaning that the stabilization characteristic time is much larger. Emulsion behavior is affected by particles properties and depending on these properties the emulsion could flocculate, cream or settle. On the other hand, similarly to surfactant stabilized emulsion, a strong interaction between the involved mechanisms and the system hydrodynamic should be considered making the system analysis more complicated. A global approach is presented hereafter to evaluate emulsification performances from operating conditions in a given emulsification system.

Droplets are firstly generated then stabilized by particles. During the droplet generation step, it is assumed that only droplet breakage and coalescence are involved and the particles affect the

system through their effect on the continuous phase properties. The resulting droplet size can be obtained by solving a population balance equation or by using correlations. An interface generation potential can thus be defined from the Sauter mean diameter to characterize the system capacity to produce droplets:

$$A_{gen} = \frac{V_d}{D_{32}} \cdots (2.52)$$

where, A_{gen} is the interface generation potential, V_d is the dispersed phase volume, and D_{32} is the Sauter mean diameter.

On the other hand, a coverage potential of the system can also be defined. If N_p particles are considered, the coverage potential can be obtained by:

$$A_{cov} = N_p \cdot A_{cov/1p} \cdots (2.53)$$

where, A_{cov} is the coverage potential and, $A_{cov/1p}$ is the covered surface by one particle.

A theoretical mean diameter of stabilized droplets can be deduced by comparing the interface generation potential to the coverage potential. Two cases can be considered. In the first case, if produced interface is higher than coverage capacity of the system, resulting droplets will be partially covered and will coalesce until reaching the coverage capacity of the system (Limited coalescence process), the final mean diameter will therefore depend on this coverage capacity. However, if there is enough particles to cover the produced interface, the final mean diameter will depend on the system capacity to generate interface. The theoretical stabilized interface can be given by:

$$A_{Theo} = Min(A_{gen}, A_{cov}) \cdots (2.54)$$

Pickering emulsions are stabilized by covering the droplets with particles. As such, the generation of Pickering emulsions can be analyzed in terms of particles and droplets. For particles, the goal is to promote particle/droplet contact and maximize the adsorption force, while for droplets; the goal is to promote droplet generation and coverage (Figure 2.27).

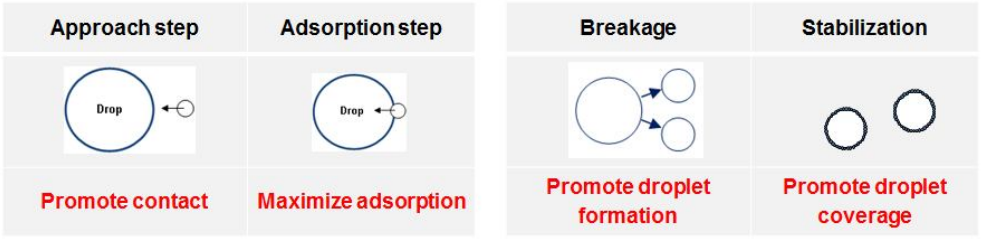

Figure 2.27: Illustration of stabilization conditions

In terms of droplets, stabilization can be defined as follows:

$$\text{Coverage rate} > \text{Coalescence rate} \cdots (2.55)$$

By assuming that the system produces a droplet size distribution with a mean diameter d and that N particles are required to cover each droplet, stabilization can be formulated as follows:

$$\text{Attachment rate of N particles} > \text{Coalescence rate} \cdots (2.56)$$

Attachment rate of N particles is related to collision frequency between particles and droplets and to the attachment efficiency of each particle. Particle attachment includes the approach step related to a film drainage process and the adsorption step related to a capillary rise process. From these two steps, three particle attachment conditions can be defined:

1) Film drainage has to be achieved to allow particle/droplet contact.

2) Three phase contact line has to be formed to initiate the capillary rise process.

3) Particle detachment has to be prevented.

Three efficiencies can be associated to these three conditions to characterize the particle attachment at the droplet interface: The Collision efficiency, the TPC line formation efficiency, and the attachment efficiency. Collision efficiency evaluates the probability of contact between the particle and the droplet. It depends on film flow conditions and involved interactions during approach and collision. TPC line formation efficiency is associated to the probability of formation of a stable meniscus around the particle after collision. Particle attachment efficiency is generally estimated by comparing forces promoting the particle attachment at the interface and those inducing particles detachment. From these efficiencies and considering the particle/droplet collision frequency, global efficiency can be defined:

$$E_{Glob} = E_{Col} \cdot E_{TPCL} \cdot E_{Att} \cdot E_{Cov} \cdots (2.57)$$

where, E_{Col} is the particle/droplet collision efficiency, E_{TPCL} is the three phase contact line formation efficiency, E_{Att} is the particle attachment efficiency, and E_{Cov} is the droplet coverage efficiency.

The effectively covered interface can be obtained by:

$$A_{Eff} = E_{Glob} \cdot A_{Theo} \cdots (2.58)$$

Once the effectively covered interface is deduced for a given emulsification system, it is possible to determine emulsion properties. The overall approach is described below.

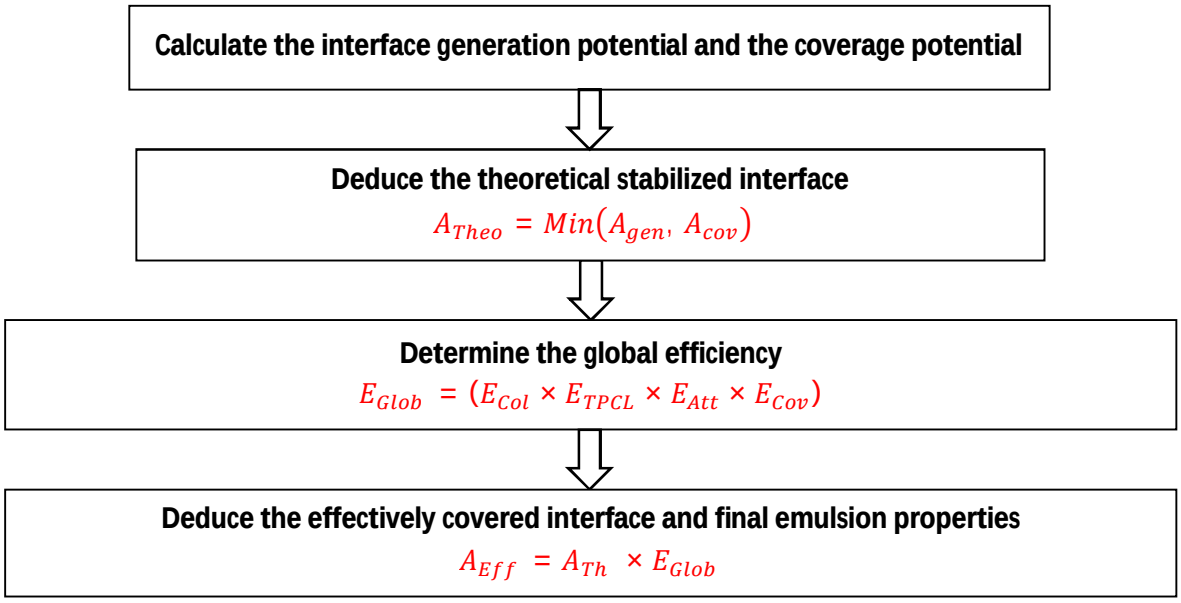

Figure 2.28: Calculation procedure of the effectively covered interface

2.2.6 Conclusions

The replacement of traditional molecular surfactants by nano- or micrometer-sized solid particles in emulsification processes offers many advantages and new opportunities in the process industry. A great deal of research has been carried out on these processes since the 1980s. We have reviewed the most relevant results, including emulsion stabilization mechanisms, the parameters affecting emulsion properties, and the rheological behavior of emulsions.

The first part of this review describes the fundamental phenomena involved in the generation of Pickering emulsions and highlighted the fact that particle/drop interactions, particle stability at the interface, and particle network formation must be taken into consideration. We then showed

that capillary, van der Waals, electrostatic double layer, hydration and hydrodynamic, hydrophobic, and steric forces are the main interactions involved during emulsion stabilization.

The second part deals with the effects of the relevant parameters on the stability, type, size distribution, and rheological behavior of Pickering emulsions (particle, aqueous phase, and oil phase properties). We showed that Pickering emulsions are mainly sensitive to particle properties (wettability, concentration, size, shape, and flocculation state) and that oil-in-water emulsions are obtained with hydrophilic particles while water-in-oil emulsions are obtained with hydrophobic particles. We also showed that the Bancroft rule is satisfied. The most stable emulsions are obtained with particles displaying intermediate hydrophobicity, and stability can be improved by increasing the particle concentration and aspect ratio, partially flocculating the particles, reducing the particle size and size distribution. Droplet size can be reduced by increasing the particle concentration or reducing the particle size. Particle properties are affected by aqueous phase properties. The pH of the aqueous phase influences particle wettability or/and size (swelling) while electrolytes affect particle flocculation by acting on repulsive electrical double layer forces. Using high viscosity oils can hinder particle adsorption and, in some cases, prevent emulsion formation, while oil polarity and temperature affect the interfacial tension and contact angle. In addition, electrical or magnetic fields can be used to control the stability of emulsions when paramagnetic or dielectric particles are used. Lastly, the rheological properties of Pickering emulsions were reviewed. Pickering emulsions exhibit yield stress and shear-thinning behavior and their viscosity can be described using the Herschel-Bulkeley model. Moreover, they exhibit viscoelastic and thixotropic properties, like more conventional emulsions, when the required conditions are met.

While numerous features of SSEs have been described in the literature and have been summarized here, others have to be investigated in greater detail, including many aspects of emulsion stabilization and emulsion properties. In addition, most of the currently available information is essentially qualitative and based on observations from which many hypotheses have been formulated to explain the behavior of SSEs.

Most studies on stabilization mechanisms have focused on identifying the interactions involved and have only partially investigated the effects of particle, water, and oil properties on those interactions. This also holds true for the formation of the particle network. Very few studies have

investigated the relationships between the configuration of the particle network and emulsion properties. In addition, the dynamic aspects of the adsorption step have been generally ignored despite their important for process design.

There has been a greater emphasis on studying certain parameters (particle wettability and concentration, aqueous phase pH and ionic strength) that affect the properties of emulsions, while other parameters have received much less attention. In addition, most rheological studies have focused on rheological behavior after emulsification, without investigating the effects during processing.

The current state of knowledge is insufficient to design or optimize emulsification processes for SSEs. It is thus essential to determine the stabilization conditions required for emulsification processes and to relate emulsion formulations and operating conditions to the properties of the emulsions during and after processing.

In the last part, a global procedure is proposed to predict emulsion properties from operating conditions. The first step is to estimate a theoretical stabilized interface by comparing the interface generation potential and the coverage potential of the system. The second step is to define stabilization efficiencies from stabilization conditions. The first efficiency is related to the film drainage mechanism characterizing the particle/droplet collision while the second efficiency describes the three phase contact line formation and its expansion. The third efficiency is related to the ability of the particle to remain attached at the interface while the last efficiency describes the capacity of the system to cover the entire generated interface and prevent coalescence. Finally, the third step is to determine the effectively covered interface and emulsion properties.

2.2.7 Acknowledgments

The authors gratefully acknowledge financial support from the Natural Sciences and Engineering Research Council of Canada and TOTAL.

CHAPITRE 3. ORGANISATION DE LA THESE

3.1 Objectifs spécifiques

La revue de littérature présentée au chapitre précédent a clairement mis en évidence le potentiel des particules solides pour la stabilisation d'émulsion. Il a ainsi été observé qu'il est possible de produire différents types d'émulsions avec une très grande stabilité en utilisant différents types de particules. Il a été également trouvé que ces systèmes peuvent être déstabilisés dans plusieurs cas par centrifugation, en appliquant un champ magnétique ou électrique, ou bien en modifiant la mouillabilité des particules. Cependant, la grande majorité des travaux réalisés sur ces systèmes ont négligé l'opération d'émulsification et ne se sont intéressés qu'aux aspects qualitatifs ce qui est insuffisant pour la conception d'un tel procédé à l'échelle industrielle.

Afin de dimensionner un procédé d'émulsification par des particules, il est nécessaire de considérer l'effet qu'aurait l'utilisation de particules sur les mécanismes mis en jeu lors de l'émulsification c'est-à-dire la rupture, la stabilisation et la coalescence. En remplaçant les tensio-actifs par des particules, la rupture et la coalescence sont affectées parce que les particules ne réduisent pas la tension interfaciale et que les propriétés de la phase continue sont affectées par la présence de particules. La stabilisation est également affectée par le fait que les particules ne soient pas amphiphiliques et que leur taille est beaucoup plus grande que celle des tensio-actifs. Dans cette étude nous nous sommes concentrés sur la stabilisation vu que c'est l'étape clé d'une opération d'émulsification.

Sachant que la stabilisation par des particules est assurée par la formation d'une barrière stérique autour des gouttes, barrière qui résulte de l'adsorption de chaque particule, le système a été analysé en considérant deux échelles. Nous avons donc considéré deux échelles dans notre analyse. L'échelle de la particule ou l'objectif est de favoriser le contact entre la particule et la goutte et ensuite son attachement à l'interface et l'échelle de la goutte ou l'objectif est de favoriser la génération d'interface et sa couverture par des particules. À partir de cette analyse trois objectifs spécifiques ont ainsi été définis.

1) **Identification des interactions mises en jeu lors de l'approche et de l'adsorption d'une particule solide à une interface liquide/liquide.**

Cette première partie est consacrée à l´identification et à la quantification des interactions mises en jeu lors de l´adsorption de particules à une interface liquide/liquide. La technique de la sonde colloïdale a ainsi été utilisée et a permis de définir les mécanismes contrôlant l'étape de l'approche et celle de l'adsorption. Les paramètres affectant ces deux étapes ont également été identifiés et leur impact quantifié (Article 2).

2) **Étude de l'effet des paramètres contrôlant l'adsorption de la particule à l'échelle d'une opération d'émulsification.**

Cette seconde partie a pour objectif de quantifier l'effet des paramètres identifiés à l'échelle d'une particule sur le comportement des émulsions produites. Ces émulsions ont notamment été obtenues en utilisant une configuration standard en cuve agitée. Les émulsions ont été caractérisées par des mesures de distribution de taille, des techniques de visualisation et des mesures de temps de mélange et de circulation. Considérant à la fois les paramètres caractérisant les phases mises en jeu (Article 3) et les conditions opératoires (Article 4), de fortes interactions entre les différents processus ont été révélées.

3) **Définition d'une méthodologie permettant de prédire les propriétés des émulsions produites.**

Dans une optique de développement d'un nouveau procédé d'émulsification par des particules, cette dernière partie a pour objectif de mettre en place une procédure permettant de prédire les propriétés des émulsions produites à partir des conditions opératoires. Une approche semi-empirique a été considérée et a permis d'obtenir des tailles moyennes d'émulsions très proches des résultats expérimentaux validant ainsi l'analyse proposée pour décrire l'évolution de l'opération d'émulsification par des particules (Article 5).

CHAPITRE 4. ARTICLE 2: STUDY OF THE PROPERTIES OF OIL, PARTICLES, AND WATER ON PARTICLE ADSORPTION DYNAMICS AT AN OIL/WATER INTERFACE USING THE COLLOIDAL PROBE TECHNIQUE

4.1 Présentation du second article

Soumis dans : Colloids and Surfaces: A Physicochemical and Engineering Aspects

Auteurs : Èmir Tsabet, Louis Fradette

Dans ce second article la technique de la sonde colloïdale a été utilisée pour mesurer les forces mises en jeu lors de l'approche et de l'adsorption d'une microbille de verre et d'une particule sphérique de polyéthylène à une interface huile silicone/eau. L'approche et le contact, l'adsorption ainsi que le détachement des particules ont été observés à travers la quantification de trois forces. Les courbes de forces ont révélé une force de nature répulsive lors de l'approche et ensuite une force attractive lors de l'adsorption de la particule à l'interface. Les résultats ont montré que l'étape de l'approche pouvait être associée à un processus de drainage de film tandis que l'adsorption était reliée à un processus de montée capillaire, les deux étapes étant essentiellement contrôlées par les propriétés des particules. Il a également été observé que la viscosité de l'huile affectait considérablement la force répulsive de contact et le temps nécessaire à l'adsorption. De plus, il a été trouvé que les propriétés de la phase aqueuse affectaient beaucoup plus l'approche et le contact à travers l'altération de l'affinité de la particule.

4.2 Study of the properties of oil, particles, and water on particle adsorption dynamics at an oil/water interface using the colloidal probe technique

4.2.1 Summary

The replacement of traditional molecular surfactants by nano- or micrometer-sized solid particles in emulsification processes offers many advantages and new opportunities for process industries. The solid-stabilization of emulsions occurs in three steps: (1) the particles first approach and contact the fluid/fluid interface, (2) the particles adsorb to and are trapped at the interface, and (3) the adsorbed particles form a network that stabilizes the emulsion. The current state of knowledge

makes process design impossible or impracticable, mainly because of the lack of information on the overall stabilization mechanism. A colloidal probe technique (atomic force microscopy) was used to measure the adsorption force and time of model glass and polyethylene microspheres to a planar silicone oil/water interface. Particle approach, contact, adsorption, and detachment as well as adsorption time were studied. Force curves revealed that a repulsive force is involved during approach and contact and an attractive force is involved during adsorption. Particle properties governed the approach, contact, adsorption, and detachment steps, and oil viscosity had a significant impact on the contact force and adsorption time. Aqueous phase pH and salinity had no significant effect on the detachment force and adsorption time but were involved during the approach and initial adsorption steps through their effect on particle affinity and aqueous film drainage.

4.2.2 Introduction

Conventional emulsions are used in numerous industrial fields. Since the pioneering work of W. Ramsden (1903) and S. U. Pickering (1907) over a hundred years ago, it has been shown that fine solid particles can be used as emulsifiers and that appropriately selected particles produce emulsions that are more stable than emulsions stabilized with chemical surfactants (Binks B. P., 2002). This enhanced stability has been attributed to the formation of a steric particle barrier around the droplets that prevents coalescence. S. Levine et al. (1991, 1992, 1993) also reported that droplet stability depends on particle interactions at the interface, which are dominated by capillary forces, and that the most stable emulsions are obtained when particles form a close-packed network. Particle adsorption at the interface can be assessed using two approaches. The first is based on a free energy analysis whereas the second is based on a force analysis (Binks B. P. and Horozov T. S., 2006). In the first case, equilibrium is considered to be attained when the system reaches its minimal free energy while, in the second case, equilibrium is considered to be attained when the forces are balanced.

The first approach has been studied by many researchers, including S. Levine et al. (1989), who defined the energy required to detach particles from an interface using the following equation:

$$E = \pi R^2 \gamma_{ow} (1 \pm cos\theta)^2 \cdots (4.1)$$

A similar approach has also been used to calculate particle adsorption energy in order to analyze the stability of emulsions (Aveyard R. et al., 2003; Sacanna S. et al., 2007), which has been attributed to the line tension effect. Other researchers have deduced the equilibrium position of particles at the interface (Komura S. et al., 2006; Hey M. J. et al., 2006) by taking the interface curvature effect into consideration (Hey M. J. et al., 2006) or by determining the equilibrium particle concentration at the interface (Hirose Y. et al., 2008).

On the other hand, the force analysis approach considers that particle equilibrium and stability can be deduced by assuming that the sum of the external forces at equilibrium is zero. This type of analysis was initially used by H. M. Princen (1969) and A. V. Rapacchietta et al. (1977) and, more recently, by D. D. Joseph et al. (2003) and P. Singh et al. (2005). However, much less effort has been devoted to studying the force analysis approach than the free energy approach. Nonetheless, this approach has been used to identify the main steps involved in emulsion stabilization:

a. Approach step: Particles first approach and contact the fluid/fluid interface.
b. Adsorption step: Particles adsorb to and are trapped at the interface.
c. Network formation step: Adsorbed particles form a network that stabilizes the emulsion.

Based on these three steps as well as the results of studies on microscopic interactions, it has become clear that DLVO forces (Ducker W. A. et al., 1994; Mulvaney P. et al., 1996; Aston D. E., 2001; Fielden M. L. et al., 1996; Preuss M. et al., 1998, 1999; Gillies G. et al., 2004, 2005), hydration forces (Ducker W. A. et al., 1992, 1994; Preuss M. et al., 1998, 1999; Gillies G. et al., 2005), hydrophobic forces (Ducker W. A. et al., 1994; Fielden M. L. et al., 1996; Preuss M. et al., 1998), and steric forces are involved the first step, whereas viscous, capillary, and dipolar forces are involved in the second step (Tarimala S. et al., 2004a; Horozov T. S. et al., 2003, 2005), and lateral capillary forces (Horozov T. S. et al.; 2005; Tarimala S. et al., 2004a, 2006; Dai L. L. et al., 2008; Madivala B. et al., 2009) and DLVO forces (Ruiz-Garcia J. et al., 1997; Midmore B. R., 1998; Tarimala S. et al., 2006; Dai L. L. et al., 2008) are involved in the third step. Other authors have observed particle motion at the interface (Vignati E. et al., 2003; Tarimala S. et al., 2004a, 2006; Dai L. L. et al., 2008).

The force analysis approach has also made it possible to identify the main parameters that affect the stabilization steps and, as such, that are associated with the properties of the final emulsion.

These parameters have also been described by many investigators who have characterized the macroscopic properties of Pickering emulsions and have led to the conclusion that Pickering emulsions are mainly sensitive to oil viscosity and particle properties (wettability, concentration, size, shape, and flocculation).

In terms of particle wettability, oil/water emulsions can be produced using hydrophilic particles while water/oil emulsions can be produced using hydrophobic particles (Yan N. et al., 2001; Binks B. P. et al., 2000, 2005; Stiller S., et al., 2004). This type of behavior is mainly observed when the dispersed phase fraction is smaller or equal to the continuous phase fraction and when the particles are initially dispersed in the phase with which they have most affinity, which then becomes the continuous phase (Bancroft rule). It has also been shown that highly hydrophobic and highly hydrophilic particles produce the least stable emulsions, whereas particles with intermediate hydrophobic properties produce the most stable emulsions (Yan N. et al., 1995b, 1997a; Binks B. P. et al., 2000; Yan N. et al., 2001; Stiller S. et al., 2004; Ding A. et al., 2005).

Much effort has also been devoted to studying the effect of particle concentration on emulsion behavior. Increasing the concentration of particles has been shown to improve stability (Yan N. et al., 1994, 1995a, 1995b, 1996b, 1997a, 1997b) and reduce droplet size (Binks B. P. at al., 2003, 2004, 2005). The reduction in droplet size reduction has notably been studied by S. Arditty et al. (2003), who defined the so-called “limited coalescence phenomena,” which assumes that, for a given particle concentration, the emulsion will coalesce until the droplets reach the coverage limit. This makes it possible to determine the size of the droplets based on the concentration of the particles. A decrease in particle size (Binks B. P. et al., 2001; Tambe D. E. et al., 1994) and the use of monodispersed particles (Tarimala S. et al., 2004b) and ellipsoidal particles (Madivala B. et al., 2009) also improves emulsion stability.

Emulsions are also affected by the properties of the aqueous and oil phases, mainly through the effects of these parameters on particles. Aqueous phase pH essentially influences particle wettability (Yan N. et al., 1996a, 1996b, 1997b; Gu G. et al., 2003) and/or size (Fujii S. et al., 2006; Binks B. P. et al., 2006; Brugger B. et al., 2008) while electrolytes influence particle flocculation through their impact on the repulsive electrical double layer force (Binks B. P. et al., 1999, 2005, 2006; Yang F. et al., 2006; Horozov T. S. et al., 2007; Golemanov K. et al., 2006). It has been shown that oil polarity affects interfacial tension and the particle contact angle (Binks B.

P., et al., 2000, 2002, 2005; Golemanov K. et al., 2006; Frelichowska J. et al., 2009; Zhou J. et al., 2011) and that high viscosities can hinder particle adsorption and, in some cases, prevent the formation of emulsions (Golemanov K. et al., 2006; Fournier C.-O. et al., 2009).

While many parameters affecting emulsion behavior have been identified, their effects on the various emulsification steps are not well known. The adsorption step, which is central to the solid-stabilized emulsification process, has to be studied in greater detail and defined so that it can be coupled to two other phenomena involved in emulsification, that is, droplet breakage and droplet coalescence, which can be quantitatively expressed as the breakage and coalescence rates. This will lead to an emulsification condition stating that a stable Pickering emulsion with a given size distribution can be obtained if a given interface surface is created by breakage and is stabilized before coalescence occurs. This condition can be formulated as follows:

Stabilization rate > Coalescence rate

In addition, since stable emulsions result from the formation of a steric particle barrier around the droplets, the stabilization rate is closely related to the formation of a close-packed particle network and thus to the particle adsorption rate. Efficient emulsion stabilization thus relies on three conditions:

- Particle/droplet contact should be enhanced.
- The initial adsorption force should be maximized to overcome destabilization forces (hydrodynamic forces).
- Particle adsorption time and network formation time should be less than coalescence time.

The main objective of the present work was to quantify the interactions involved during approach and adsorption and to identify the main parameters affecting each step.

4.2.3 Materials and methods

4.2.3.1 Materials

Three sizes (65, 35, and 25 μm) of glass (Potters Industry) and polyethylene (Cospheric) microspheres were used as model solid particles. Particle contact angles were measured on planar surfaces of each material using an NRL-100 goniometer (Ramé-Hart). The contact angles were 48° ± 4° for the glass microspheres and 94° ± 2° for the polyethylene microspheres.

Deionized water (72.6 mJ/m^2 at 20°C) was prepared using a Milli-Q reagent water system (Fisher Scientific). Aqueous phase pH and salinity were controlled using NaOH/HCl (analytical grade, Fisher Scientific) and NaCl (commercial grade), respectively. Three pHs (2, 6.5, and 10) and four salinities (0.0125 M, 0.05 M, 0.1 M, and 0.25 M) were studied.

Four silicone oils with different viscosities (Dow Corning Corporation) were used (Table 4.1). The rheological properties of the oils were determined using a Bohlin Visco88-BV viscometer with the Couette configuration (Malvern). All the viscosities exhibited Newtonian behavior. The de Noüy ring technique was used to measure silicone oil/water interfacial tension, which was 42 mJ/m^2 at 25°C.

Tableau 4.1: Physical properties of silicone oils

	1	**2**	**3**	**4**
Dynamic viscosity (Pa·s)	29.10	12.13	8.13	4.85
Density (g/cm^3)	0.97	0.97	0.97	0.97
Surface tension (mJ/m^2)	21.3	21.3	21.3	21.3

4.2.3.2 Experimental methods

4.2.3.2.1 Experimental setup

We used a colloidal probe technique (atomic force microscopy) to measure the forces involved and the time required to reach final equilibrium. Briefly, a Dimension 3100 SFM microscope equipped with a Nanoscope V controller (VEECO) was used to measure the forces (deflection of the cantilever according to Hooke's law $[= Kz \cdots]$) at water/air, water/oil, and oil/air interfaces during the approach and adsorption steps (Figure 4.1).

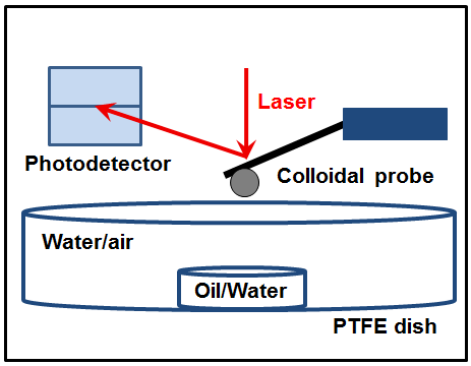

Figure 4.1: Simplified representation of the colloidal probe setup

By analyzing the amplitudes of the forces involved in adsorption (Figure 4.2), we deduced that capillary forces predominates (Table 4.2). As such, the force balance at equilibrium allows the capillary force to be determined from the cantilever spring force.

However, during the approach step, many forces of equivalent amplitude can be involved, especially at small separation distances (< 1 µm). These include DLVO forces such as attractive van der Waals forces and repulsive electrostatic double layer forces, and non-DLVO forces such as repulsive hydration forces and attractive hydrophobic forces (Figure 4.2). Cantilever deflection measurements make it possible to deduce the overall force and to identify the dominant force by analyzing the experimental conditions (pH, ionic strength, particle wettability, interfacial tension). Adsorption time was measured between the first contact and the final equilibrium cantilever position.

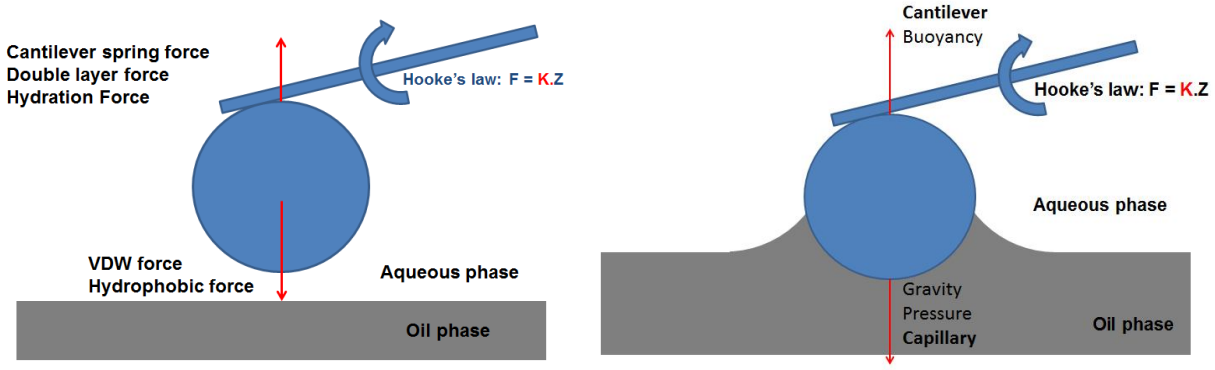

Figure 4.2: Force balance during approach and adsorption

Tableau 4.2: Force analysis during adsorption

Force	Nature	General Expression	Order of Magnitude
Viscous	Repulsive	$6\pi\eta V_p R_p$	~ 10 nN
Buoyancy	Repulsive	$4\pi R_p^3 \rho_w g/3$	~ 1 nN
Gravity	Attractive	$4\pi R_p^3 \rho_p g/3$	~ 3 nN
Hydrostatic pressure	Attractive	$\pi R_p^2 L\, \rho_w g$	~ 50 nN
Capillary	Attractive	$2\pi R_p \gamma$	~ 10,000 nN

4.2.3.2.2 Colloidal probe preparation

Colloidal probes were prepared using a micromanipulator and two-component epoxy glue under an optical microscope. The cantilever tip (Vistaprobes; Nanoscience Instruments) (Table 4.3) was first plunged into the glue and the particle was captured (Figure 4.3 and 4.4).

Tableau 4.3: Properties of Vistaprobe cantilever probes (Nanoscience instruments)

Technical Data	Typical Value	Range
Force Constant	3.0 N/m	1.2 – 6.4 N/m
Resonance Frequency	62 kHz	47 - 76 kHz
Length	225 µm	215 - 235 µm
Mean Width	30 µm	25 - 35 µm
Thickness	3.0 µm	2.5 – 3.5 µm
Coating	None	
Shape / Cross-section	Rectangular / Trapezoidal	

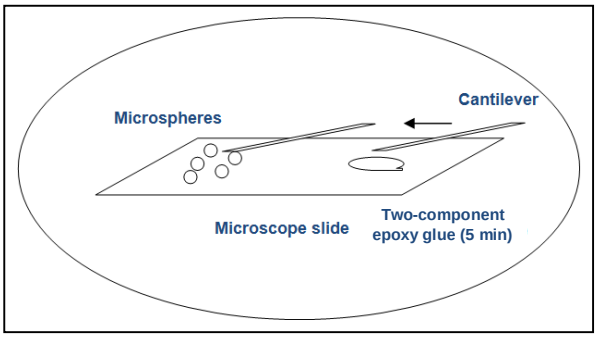

Figure 4.3: Schematic representation of colloidal probe preparation

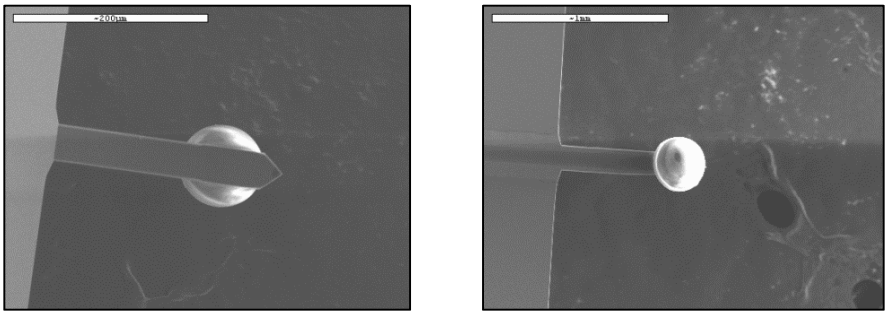

Figure 4.4: Colloidal probe prepared with 65 µm glass beads (SEM images)

4.2.3.2.3 Colloidal probe calibration

The exact properties of the cantilever probes were not provided by Nanoscience Instruments. Since the cantilever spring and resonance frequency had to be taken into consideration, we calibrated these parameters using the Nanoscope V controller before taking the force measurements using the thermal tune method (Hutter J. L. et al., 1993). This technique is based on measuring the thermal noise intensity. When the cantilever is modeled as a harmonic oscillator, the spring constant can be expressed as a function of the mean square deflection $<z^2>$:

$$k_c = \frac{k_b T}{\langle z^2 \rangle} = \frac{k_b T}{PSD} \cdots (4.2)$$

where k_c is the cantilever spring constant, k_b is the Boltzmann constant, T is room temperature, and PSD is the power spectral density.

A standard deviation of ± 8% from the mean was observed with the free cantilever (without a particle) and ± 22% with the colloidal probe (Figure 4.5). The increase in the standard deviation may have been due to particle size, the amount of glue, and/or the location of the particle on the cantilever. It is, however, important to note that all the colloidal probes were calibrated before each measurement to ensure that their properties remained in an acceptable range. In addition, measurements of all the parameters were taken using fifteen probes. The distributions are shown in Figure 4.5.

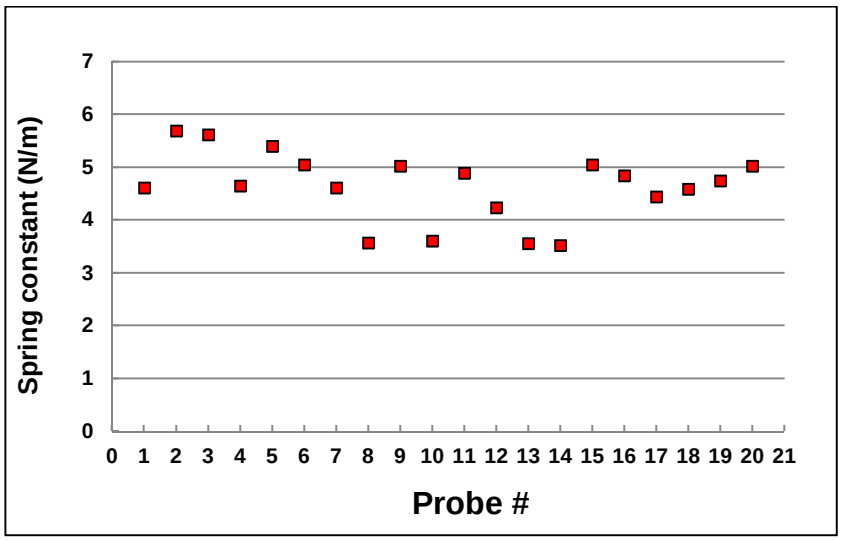

Figure 4.5: Spring constant calibration

4.2.4 Results and discussion

4.2.4.1 Results validation

Once the colloidal probes were prepared and calibrated, a second calibration step was performed to ensure that the particle surface was not contaminated with epoxy glue (Figure 4.6). The adsorption force and time were first measured on a simple air/water interface. The water adsorption force (4.1 ± 0.7 µN) showed good agreement with the theoretical value calculating using the following equation:

$$F_{Theor} = \gamma_w 2\pi R sin\theta = (72.6\, mJ.m^{-2}) \cdot \pi \cdot (65\, \mu m) \cdot \sin(48° \pm 4°) \cdot 10^6$$
$$\approx 11 \pm 0.7\, \mu N \cdots (4.3)$$

In addition, the adsorption times of the various probes were very similar (t = 440 ± 140 s).

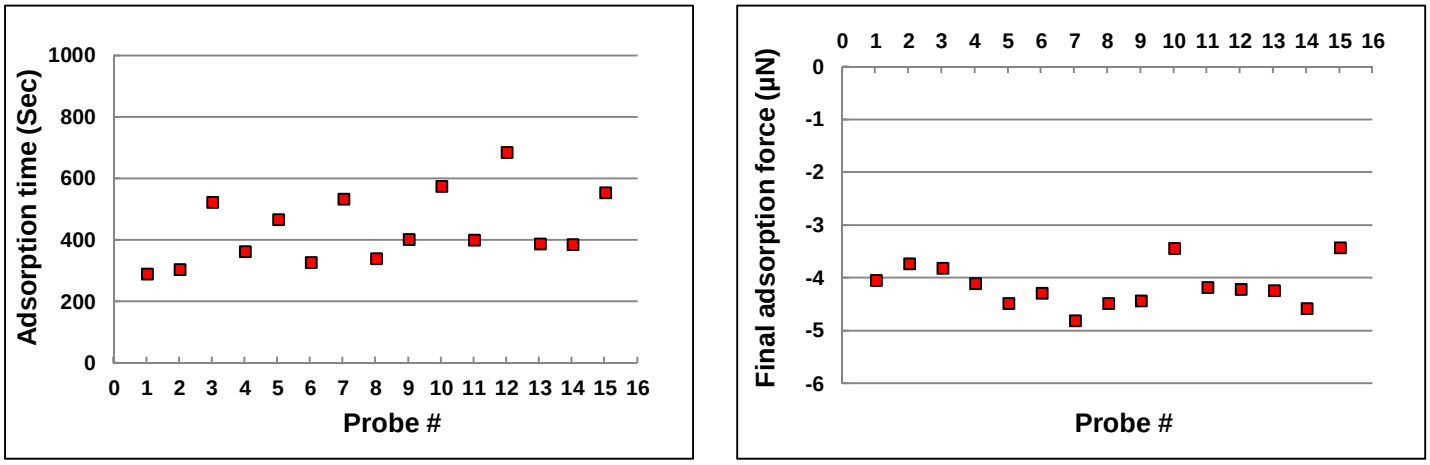

(a) **(b)**

Figure 4.6: Fifteen colloidal probes were calibrated at the surface of the deionized water by measuring the adsorption force and time of a 65-µm glass microsphere

4.2.4.2 Force evolution during adsorption

Figure 4.7 shows the evolution of the force amplitude during the adsorption of a 65-µm glass microsphere at a water/silicone oil (4.85 Pa·s) interface. Based on this evolution, three forces were identified: contact force, initial adsorption force, and final adsorption force. The contact force is a repulsive interaction that occurs during the approach/contact step and is composed of hydration, double layer, and viscous forces. The initial adsorption force is an attractive

interaction that occurs very soon after contact (~0.1 s) and is essentially composed of capillary forces. The final adsorption interaction takes place over a much longer period of time (~480 s). Two behaviors were, however, observed for the final adsorption force. First, the particle stayed at it final position for a given time and was then sheared off from the interface. This behavior was especially evident with viscous oil. Secondly, the particle detached immediately after reaching its final position. These two behaviors indicated that the final adsorption force is related to the detachment force.

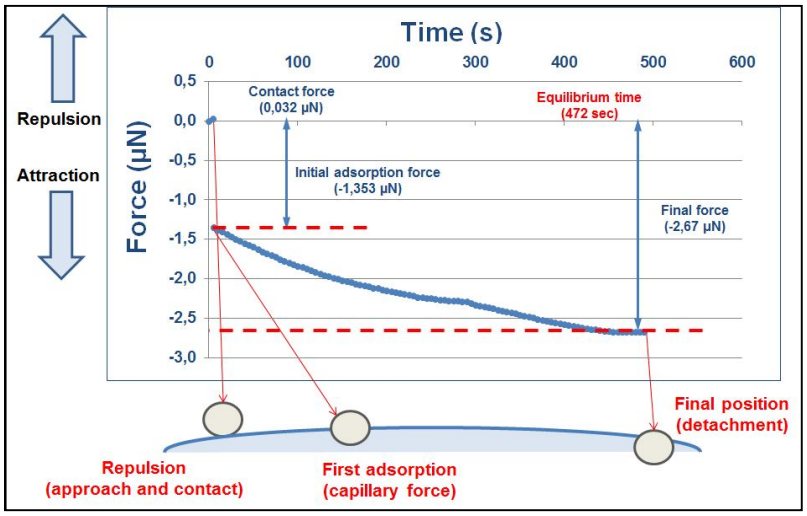

Figure 4.7: Force evolution during the adsorption of a 65-µm glass microsphere at a water/silicone oil interface (4.85 Pa·s)

4.2.4.3 Parameters affecting particle adsorption at the interface

Repulsive contact force, initial and final adsorption forces and adsorption time were measured for different conditions. Each point on the graphs was obtained by averaging several measurements represented by error bars.

4.2.4.3.1 Repulsive contact force

A repulsive contact force was observed just before initial adsorption occurred. To identify the origin of this repulsive force, several parameters were investigated (oil viscosity, particle size, pH, ionic strength, and particle wettability). The combined effect of particle size and oil viscosity was studied first. Figure 3.8 shows that the repulsive contact force increased with oil viscosity

and particle size. This behavior can be attributed to the viscous force defined by Stokes law and expressed by the following equation (sphere flowing through a viscous oil phase):

$$F_{hyd} = 6\pi\eta v_p r_p \quad \cdots (4.4)$$

where v_p is the approach velocity (0.972 µm/s).

As expected, the theoretical viscous force (dashed lines) increased with particle size and oil viscosity (Figure 4.8). On the other hand, the experimental contact force was much higher than the theoretical viscous force, which confirms that other forces are involved. Indeed, as the droplet coalescence studies by A. K. Chesters et al. (1991) showed, increasing the oil viscosity reduces surface mobility and inhibits particle/droplet contact by making film drainage more difficult. In addition, by increasing the particle size more fluid is trapped between the particle and the oil droplet, delaying film rupture and particle/droplet contact.

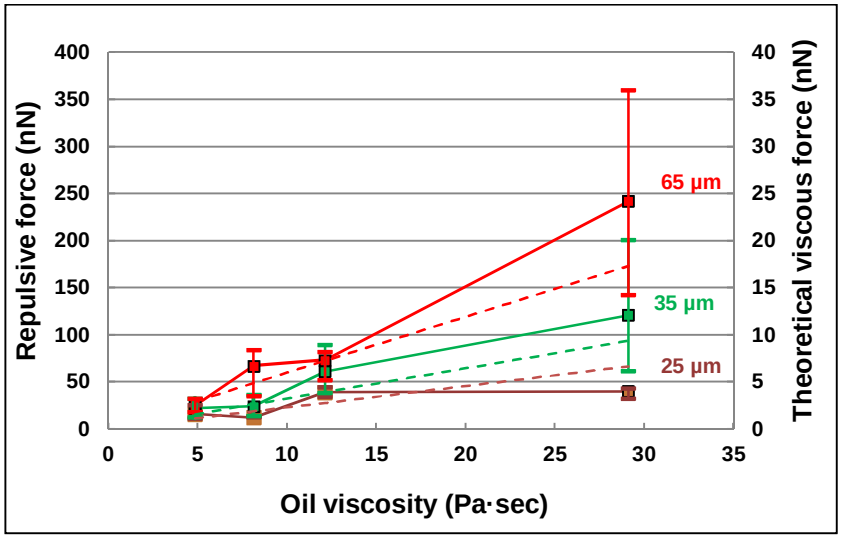

Figure 4.8: The effect of oil viscosity and particle size on the experimental repulsive contact forces (solid lines) and theoretical viscous forces (dashed lines)

(pH 6.5/0 M NaCl)

The properties of the aqueous phase were also studied in order to identify the forces involved in the first step. The effect of increasing salinity was studied using 65-µm glass microspheres at a water/oil interface (12.1 Pa·sec/pH 6.5). The contact force decreased significantly from 73 nN at 0 M NaCl to 31 nN at 0.25 M NaCl (Figure 4.9). In addition, when the pH of the aqueous phase (65-µm glass microsphere/12.1 Pa·sec/0 M NaCl) was changed from neutral to acidic or basic,

the repulsive force decreased (Figure 4.10). This was caused by the electrostatic double layer force between bodies in a liquid media with a relatively high dielectric constant ($\varepsilon_{water} \approx 78.5$ PF/m, $\varepsilon_{air} \approx 1$ PF/m). This effect can also be observed in colloidal dispersions where, at very low salt concentrations, a repulsive interaction occurs due to the formation of double layer charges. On the other hand, at high salt concentrations, particle coagulation occurs, indicating that the dominant interaction is attractive. This effect is notably caused by the screening of electrostatic interactions by free ions in the aqueous phase, which increases attractive forces effect such as van der Waals forces (Figure 4.11). This result, combined with the results from studies of emulsion behavior, showed that the presence of ionic species in the aqueous phase, depending on their concentration, can enhance the stability of Pickering emulsions through the partial flocculation of particles (Binks B. P. et al., 1999, 2005, 2006). Our findings also showed that adsorption can be promoted by adding ionic species, which minimize the repulsive electrostatic double layer force.

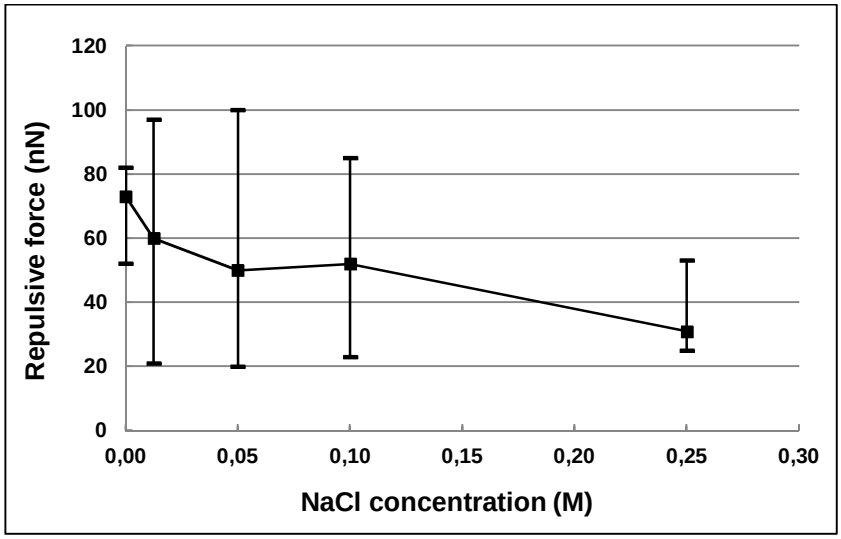

Figure 4.9: The effect of the ionic strength of the aqueous phase on the repulsive contact force (65-μm glass microsphere/12.1 Pa·sec/pH 6.5)

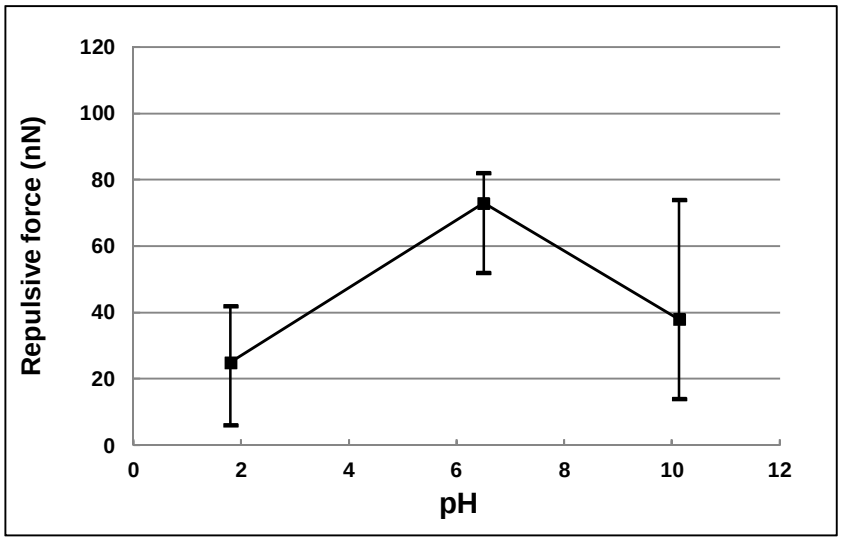

Figure 4.10: Effect of the pH of the aqueous phase on the repulsive contact force (65-µm glass microsphere/12.1 Pa·sec/0 M NaCl)

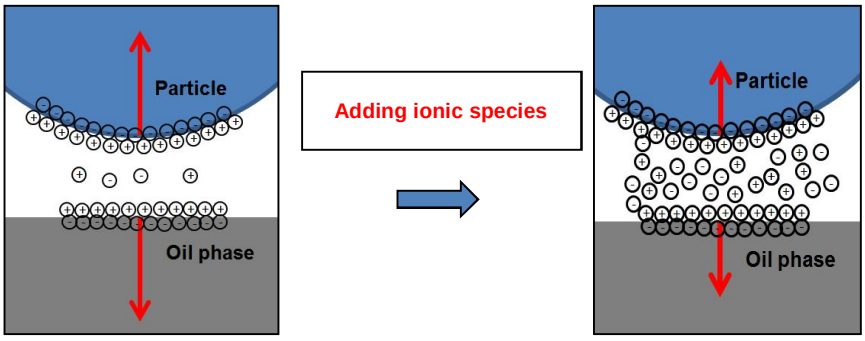

Figure 4.11: Simplified representation of electrostatic double layer force screening

The particle wettability effect was also studied using glass and polyethylene microspheres (65 µm/12.1 Pa·sec/0 M NaCl) (Figure 4.12). Our results showed that increasing particle/oil affinity decreases the repulsive force due to the reduction of the repulsive hydration force and the increase in the attractive hydrophobic force. Increasing oil/particle affinity, decreases particle/water affinity, causing water molecules to migrate from the gap separating the particle and the oil phase (Figure 4.13). These findings illustrated the importance of the effect of the approach step and the film drainage effect on the contact step.

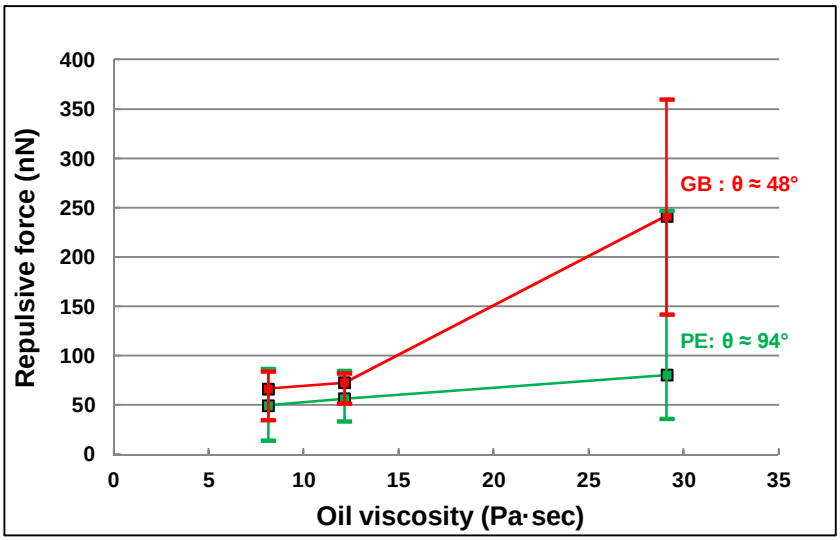

Figure 4.12: The effect of oil viscosity and particle wettability on the repulsive contact force (65-µm glass microsphere/pH 6.5/0 M NaCl)

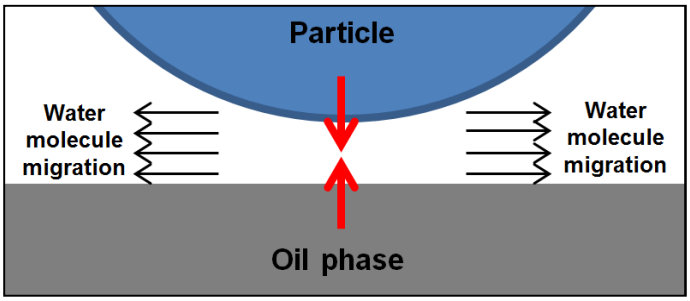

Figure 4.13: Water molecule migration from the gap (film drainage)

4.2.4.3.2 Initial adsorption force

The initial adsorption force was observed immediately after the repulsive contact force. Since it is related to the attractive capillary force, it can be theoretically calculated from the interfacial tension and the oil wetted perimeter using the following equation:

$$F_\gamma \approx \gamma_{OW}(2\pi r_c) \approx \gamma_{OW}(2\pi R_p sin\theta) \cdots (4.5)$$

where R_p is the particle radius, r_c is the oil wetted radius, γ_{ow} is the oil/water interfacial tension, and θ is the particle contact angle.

The oil viscosity/particle size effect was also studied. Our results showed that the initial adsorption force is more sensitive to particle size than oil viscosity (Figure 4.14), which is likely due to the fact that the capillary force is a function of the oil/water interfacial tension, which was

approximately the same for all the viscosities studied, as well as of the wetted radius, which increases with particle size and depends on particle wettability. On the other hand, we also found that increasing oil/particle affinity (contact angle) increases the amplitude of the initial adsorption force (Figure 4.15).

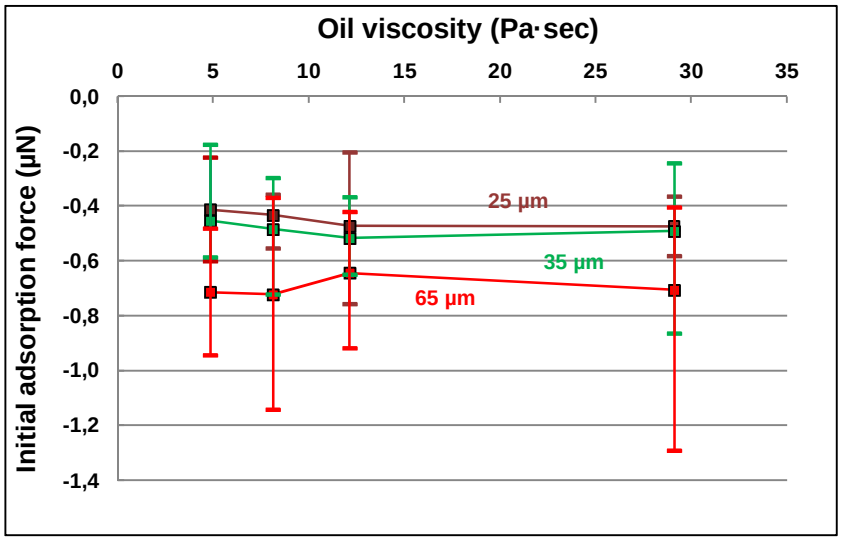

Figure 4.14: The effect of oil viscosity and particle size on the initial adsorption force (pH 6.5/0 M)

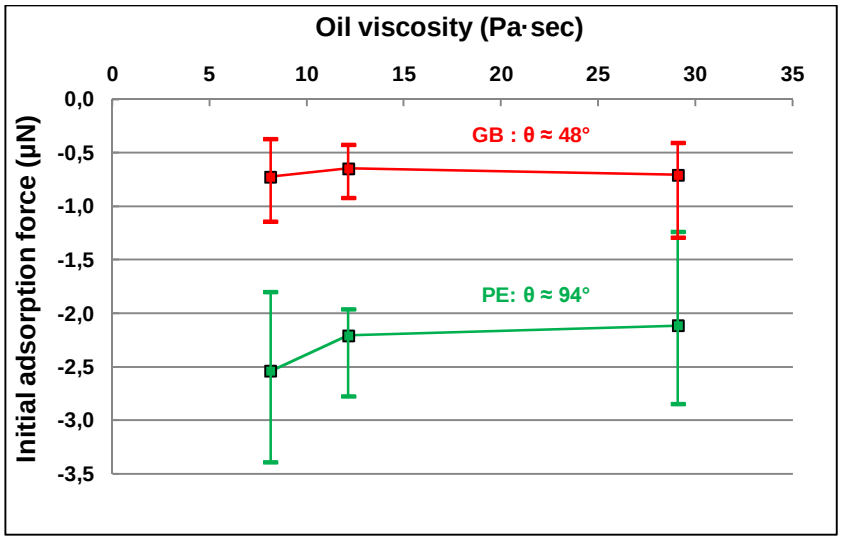

Figure 4.15: Effect of oil viscosity and particle wettability on the initial adsorption force (pH 6.5/0 M)

The initial adsorption force was reduced by adding NaCl (Figure 4.16) and by shifting the pH from neutral to acidic or basic (Figure 4.17). This reduction can be attributed to the hydration effect. Indeed, by adding ionic species, the charge density at the particle and oil surfaces increases when ionic species are added, which enhances the affinity of water molecules for both surfaces, hindering film drainage during adsorption and delaying particle entrapment (Figure 4.18).

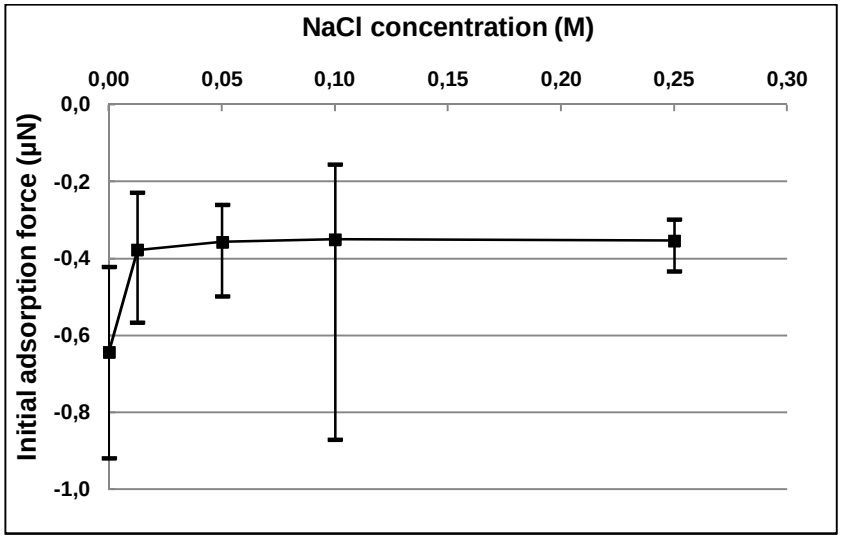

Figure 4.16: Effect of salinity on the initial adsorption force

(65-µm glass microsphere/12.1 Pa·sec/pH 6.5)

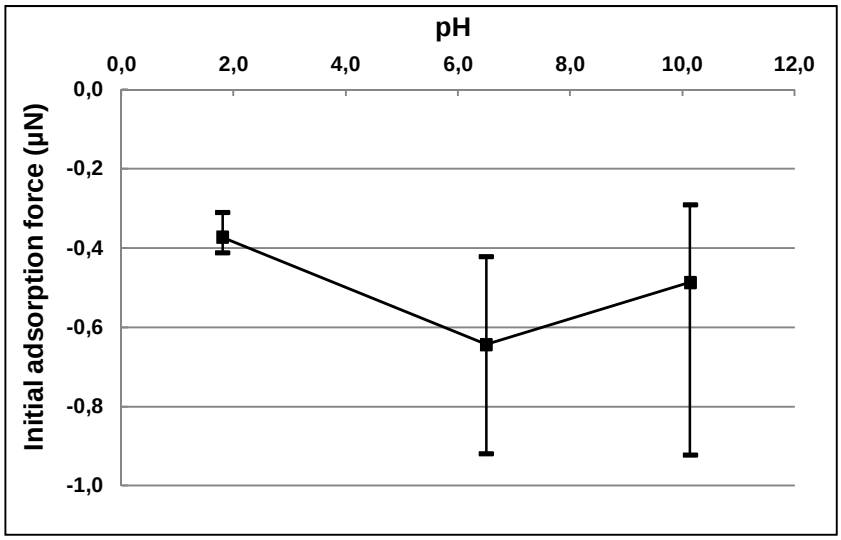

Figure 4.17: Effect of pH on the initial adsorption force

(65-µm glass microsphere/12.1 Pa·sec/0 M NaCl)

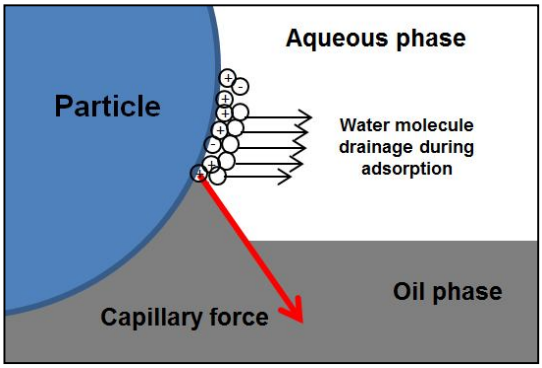

Figure 4.18: Schematic representation of water molecule drainage during adsorption

4.2.4.3.3 Final adsorption force

As can be seen in Figure 4.7, following initial adsorption, slow adsorption occurred until the final position was reached, at which point two behaviors were observed. In the first case, the probe immediately detached from the interface and, in the second case, the probe detached after a given time. The second type of behavior was mainly observed with viscous oils, indicating that oil viscosity may play a role in the detachment and destabilization process.

We also found that, of all the parameters investigated (oil viscosity, pH, salinity, and particle size and wettability), only particle size and wettability significantly affected the final adsorption force, which increased slightly with particle size, while oil viscosity had no significant effect given that all the oils had a similar interfacial tension (Figure 4.19). However, it was possible to increase the final adsorption force by increasing particle/oil affinity, indicating that particle wettability is the most important parameter (Figure 4.20).

The detachment force was evaluated using the following equation proposed by S. Levine et al. (1989) for calculating the detachment energy:

$$E = \pi R^2 \gamma_{ow} (1 \pm cos\theta)^2 = F \cdot wetted\ depth$$

The theoretical values showed good agreement with the experimental values, especially in the case of the polyethylene microspheres (Table 4.4).

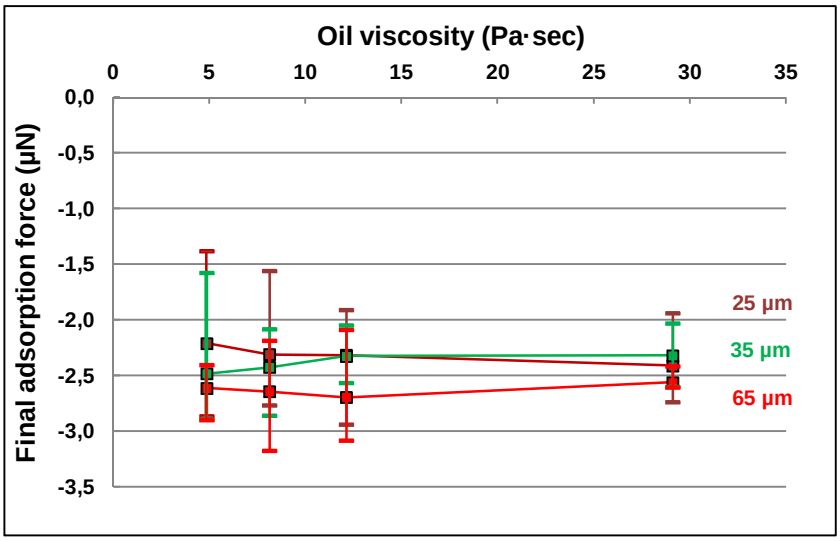

Figure 4.19: Effect of oil viscosity and particle size on the final adsorption force

(pH 6.5/0 M NaCl)

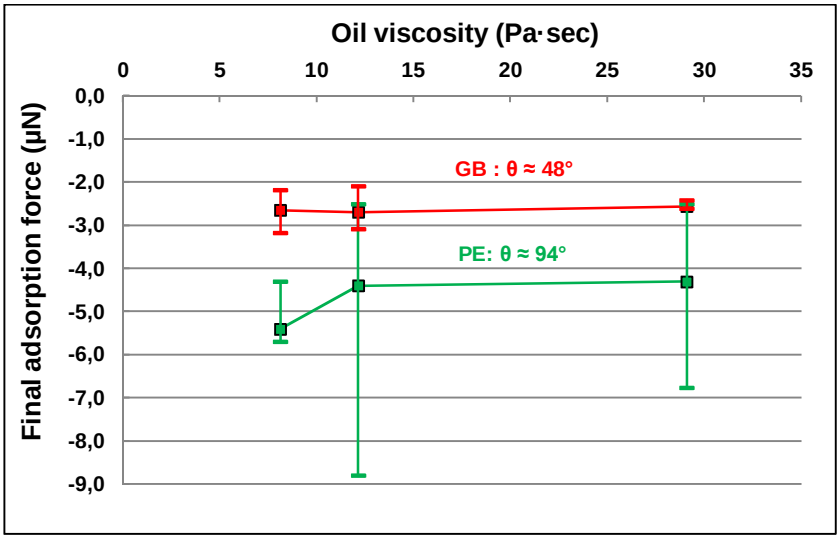

Figure 4.20: Effect of oil viscosity and particle wettability on the final adsorption force

(pH 6.5/0 M NaCl)

Tableau 4.4: Theoretical and experimental final adsorption forces

Particle Type	Particle Size	Theoretical Force	Experimental Force
Polyethylene microspheres	65 µm	-4.4 µN	-4.7 µN
Glass microspheres	65 µm	-1.4 µN	-2.6 µN

Changes in aqueous phase pH and salinity (Figure 4.21 and Figure 4.22, respectively) had no effect on the final adsorption force, which is likely due to the fact that the wettability of the glass microspheres was not sensitive to these parameters.

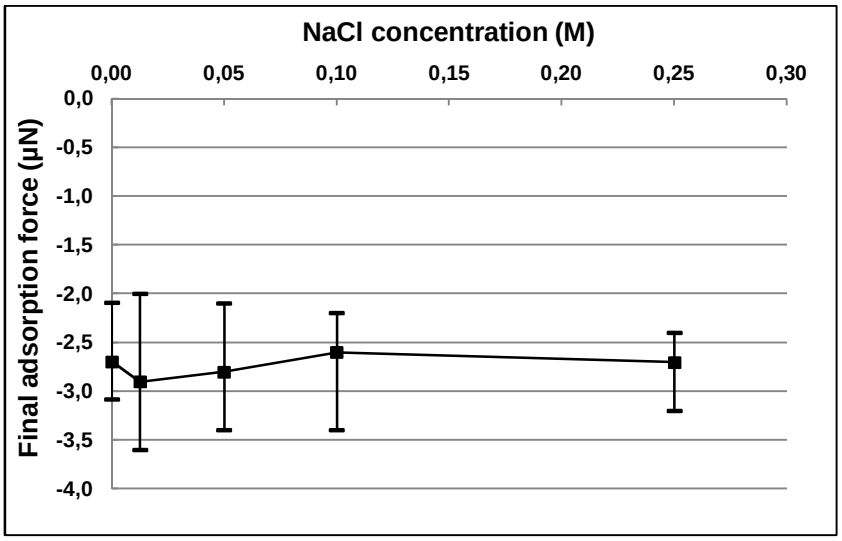

Figure 4.21: Effect of salinity on the final adsorption force

(65-µm glass microsphere/12.1 Pa·sec/pH 6.5)

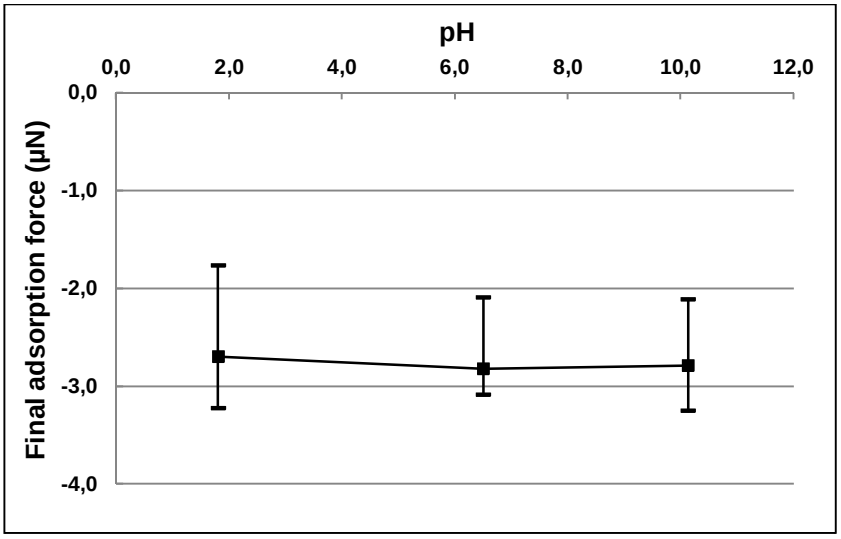

Figure 4.22: Effect of pH on the final adsorption force

(65-µm glass microsphere/12.1 Pa·sec/0 M NaCl)

4.2.4.3.4 Adsorption time

Adsorption time increased with oil viscosity (Figure 4.23), mainly because adsorption is associated with capillary rise, which is a function of fluid viscosity. Adsorption time also increased with particle size given that adsorption is a function of particle/oil affinity, which is determined by the particle contact angle. Since the particle surface was the same for the 35-µm and 65-µm glass microspheres, the wetted depth would be greater for the largest particle for the same contact angle.

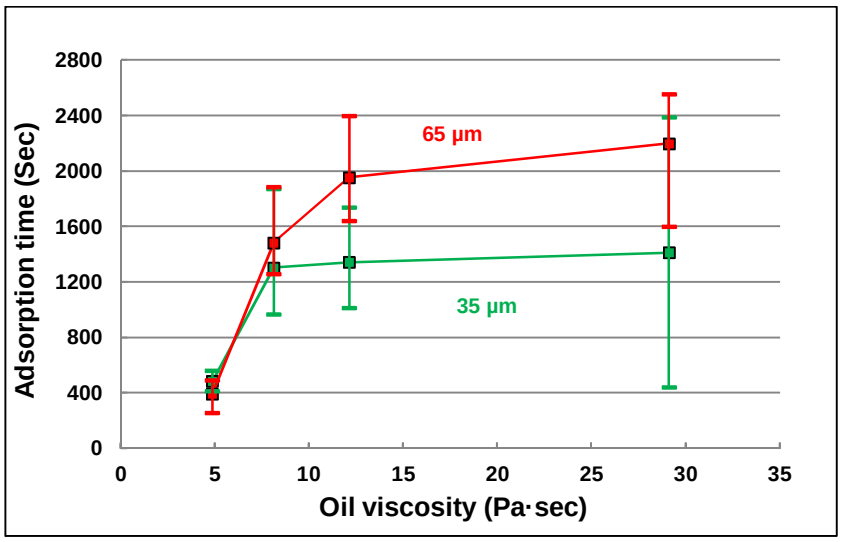

Figure 4.23: Effect of oil viscosity and particle size on the final adsorption time

(pH 6.5/0 M NaCl)

An increase in particle/oil affinity also resulted in an increase in adsorption time (Figure 4.24). This can be explained by the fact that an increase in particle/oil affinity leads to an increase in wetted depth and thus adsorption time.

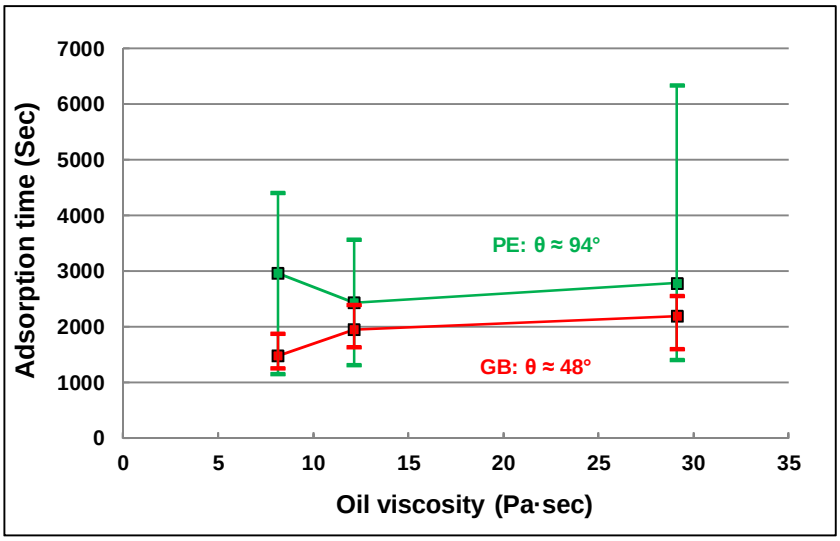

Figure 4.24: Effect of oil viscosity and particle wettability on the final adsorption time (pH 6.5/0 M NaCl)

Aqueous phase pH (Figure 4.25) and salinity (Figure 4.26) had no significant effect on the final adsorption time. However, it is important to note that adsorption times can be as long as 2,000 to 3,000 s for viscous oils, indicating that the initial repulsive force and the initial adsorption force may play significant roles in controlling emulsion stabilization.

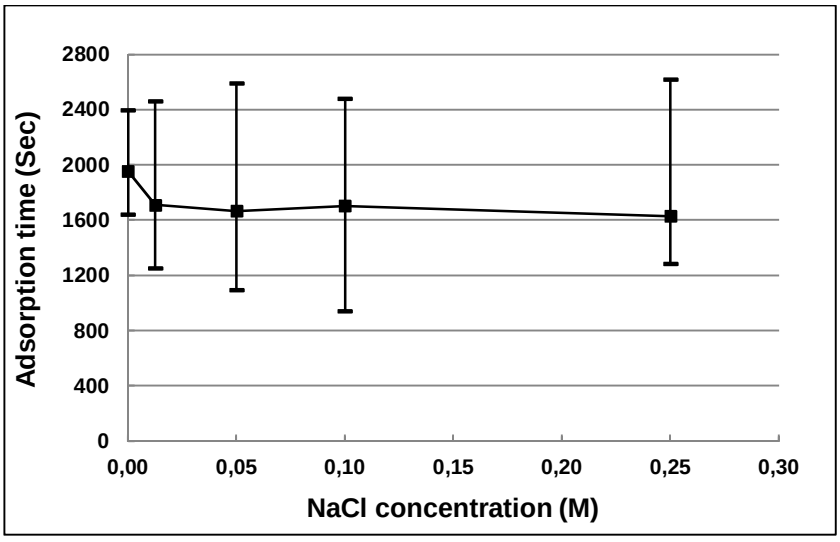

Figure 4.25: Effect of salinity on the final adsorption time (65-μm glass microsphere/12.1 Pa·sec/pH 6.5)

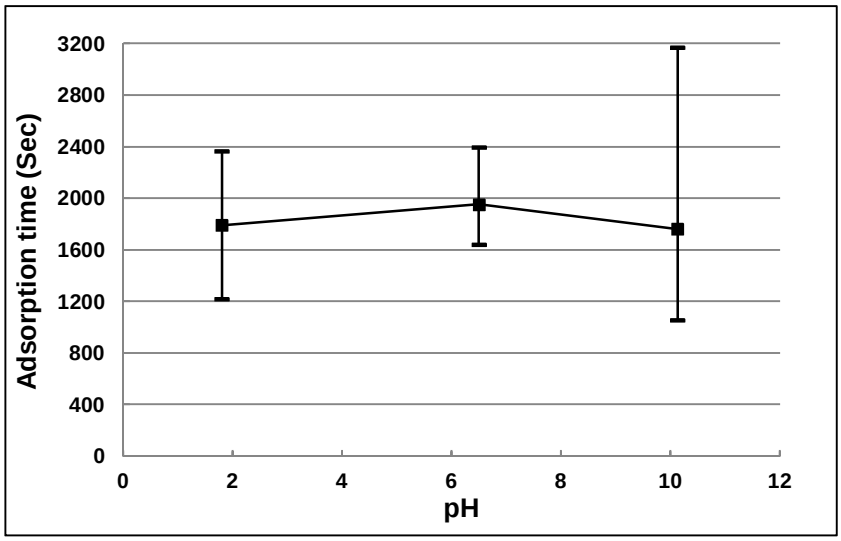

Figure 4.26: Effect of pH on the final adsorption time

(65-μm glass microsphere/12.1 Pa·sec/0 M NaCl)

4.2.5 Conclusions

Since we are interested in the development of solid-stabilized emulsions, we investigated the parameters affecting solid particle adsorption at oil/water interfaces. Our results showed that the stabilization mechanism involves three steps: (1) the particle first approaches and contacts the fluid/fluid interface, (2) the particle adsorbs to and is trapped at the interface, and (3) the adsorbed particles form a network that stabilizes the emulsion.

Particle size and wettability were the most important parameters affecting particle approach, adsorption, and detachment, while aqueous phase pH and salinity had an impact on the approach/contact and adsorption steps through their effect on particle affinity with both phases and on aqueous film drainage. However, we observed no significant effects by these parameters on the detachment force, which is mainly related to interfacial tension and particle wettability.

On the other hand, oil viscosity had a significant effect on approach/contact and adsorption time but less so on adsorption and detachment forces, which are essentially driven by interfacial tension, particle size, and particle wettability. Nonetheless, we showed that adsorption time, which is of the order of one hour, was sensitive to different degrees to all the parameters we studied.

In summary, the time required to reach the final particle position at the interface was much higher than the droplet formation and coalescence times, indicating that emulsion stabilization is mainly controlled by the approach, contact, and initial adsorption steps, which largely depend on particle/oil affinity and aqueous phase properties. On the other hand, the destabilization process mainly depended on particle properties and interfacial tension through their effect on detachment energy.

4.2.6 Acknowledgments

The authors gratefully acknowledge financial support from the Natural Sciences and Engineering Research Council of Canada and TOTAL.

CHAPITRE 5. ARTICLE 3: EFFECT OF THE PROPERTIES OF OIL, PARTICLES, AND WATER ON THE PRODUCTION OF PICKERING EMULSIONS

5.1 Présentation du troisième article

Soumis dans : Chemical Engineering Research and Design Aspects

Auteurs : Èmir Tsabet, Louis Fradette

Dans ce troisième article les effets des propriétés des phases sur les performances d'émulsification ont été étudié. Pour cela, un dispositif d'emulsification en cuve agitée a été utilisé, il comportait une cuve d'un litre sans chicanes dans laquelle a été disposée une turbine à pales inclinées qui a été décentrée pour éviter l'apparition de vortex. Des microbilles de verre standard et hydrophobisées ont été utilisées pour stabiliser des émulsions concentrées d'huile silicone dans de l'eau. L'effet de la taille des particules, de leur concentration et de leur mouillabilité a été étudié, de même que l'effet de la viscosité de l'huile et des propriétés de la phase aqueuse (pH et salinité). Les résultats obtenus ont mis en évidence l'importance du mécanisme de stabilisation par des particules. Les performances d'émulsification ont été quantifiées par la mesure de la distribution de taille des émulsions produites en utilisant le Mastersizer 3000 de Malvern. Les résultats ont montré que la stabilisation des gouttes était essentiellement liée à l'approche, le contact et l'adsorption initiale des particules. Il a été également démontré que ces étapes étaient affectées par la viscosité de l'huile, la taille et la mouillabilité des particules. D'un autre côté, il a été observé que les propriétés de la phase aqueuse affectaient la stabilisation à travers leurs effets sur l'état de floculation des particules. Il a par ailleurs été trouvé que les plus petites tailles de gouttes avec les distributions les plus étroites étaient obtenues en réduisant la taille des particules ou la viscosité de l'huile ou bien en augmentant l'affinité des particules avec l'huile. Finalement, il a été révélé que l'efficacité de stabilisation était étroitement liée à la concentration en particules.

5.2 Effect of the properties of oil, particles, and water on the production of Pickering emulsions

5.2.1 Summary

Oil-in-water Pickering emulsions were prepared using a standard mixing configuration. Emulsification experiments were performed in an unbaffled tank using an off-centered pitched-blade turbine. Regular and modified glass beads were used as a stabilizer, and their size, concentration, and wettability effects were investigated as were oil viscosity and the properties of the aqueous phase (pH and salinity). Our findings highlighted the importance of the stabilization mechanism in the emulsification process, which is different from that of surfactant-based systems. The stabilization mechanism can be divided into four steps: (1) droplet formation by breakage, (2) particle/droplet approach and collision, (3) particle adsorption, and (4) formation of the particle network. Emulsification efficiency was mainly quantified by size distribution measurements using a Mastersizer 3000 (Malvern). Our results showed that droplet stabilization is closely related to particle/droplet approach, collision, and initial adsorption and that it is highly sensitive to oil viscosity and particle size and wettability, while the properties of the aqueous phase influence stabilization mainly through their effect on particle interactions (flocculation). The smallest droplets with the narrowest distribution were obtained with small particles, low oil viscosities, and good oil/particle affinity. It was possible to mitigate the effects of particle size and oil viscosity by increasing oil/particle affinity. We also showed that stabilization efficiency was dependent on the particle fraction.

5.2.2 Introduction

Fine particles have been used as emulsifiers since the beginning of the 20th century when solid-stabilized emulsions were first described by W. Ramsden (1903) and S. U. Pickering (1907). Following in the footsteps of this pioneering work, it was (Binks, 2002) later showed that particles displayed much greater potential for producing highly stable emulsions than surfactant-stabilized emulsions. Other studies showed that the highly stable emulsions result from the formation of a steric particle barrier around the droplets that prevents coalescence. It has also been shown that the most stable emulsions are obtained when particles form a close-packed network due to capillary forces and to particle interactions at the interface (Levine S. et al., 1991,

1992, 1993). This led to the realization that stability at the interface must be taken into consideration in order to analyze the stability of emulsions. Based on this realization, two approaches were developed (Binks B. P. and Horozov T. S., 2006). The first is a thermodynamic approach based on a free energy analysis that considers that stability is achieved when the system reaches its minimal free energy. The second is a mechanical approach based on a force analysis that considers that stability is reached when the sum of the forces is zero.

Based on the first approach, the energy of particle detachment from the interface can be calculated using the following formula (Levine S. et al., 1989):

$$E = \pi R^2 \gamma_{ow} (1 \pm cos\theta)^2 \cdots (5.1)$$

A similar approach has been used to define particle adsorption energy in order to analyze the stability of Pickering emulsions based on the line tension effect (Aveyard R. et al., 2003; Sacanna S. et al., 2007). The same approach has also been used to deduce the equilibrium position of the particles at the interface (Komura S. et al., 2006; Hey M. J. et al., 2006) as well as the equilibrium particle concentration at the interface (Hirose Y. et al., 2008).

The force analysis approach was also used by H. M. Princen (1969) and A. V. Rapacchietta et al. (1977) and, more recently, by D. D. Joseph et al. (2003) and P. Singh et al. (2005). Based on the results reported in the literature and standard emulsification operation mechanisms (breakage and coalescence), the stabilization of emulsions by particles in a non-coalescent system occurs in four steps:

1. Droplet formation by breakage
2. Particle/droplet approach and collision
3. Particle adsorption
4. Network formation and droplet stabilization

Process-scale studies of emulsion stability have shown that less stable emulsions are obtained when highly hydrophobic or hydrophilic particles are used and that the most stable emulsions are obtained when particles with intermediate wettability are used (Yan N. et al., 1995b, 1997a; Binks B. P. et al., 2000; Yan N. et al., 2001; Stiller S. et al., 2004; Ding A. et al., 2005). Emulsion stability can also be improved by increasing particle concentrations (Yan N. et al. (1994, 1995a, 1995b, 1996b, 1997a, 1997b), reducing particle size (Binks B. P. et al., 2001;

Tambe D. E. et al., 1994), using monodispersed particles (Tarimala S. et al., 2004), using ellipsoidal particles (Madivala B. et al., 2009), and slightly increasing water salinity, all of which mainly act on particle flocculation through their impact on the repulsive electrical double layer force (Binks B. P. et al., 1999, 2005, 2006; Yang F. et al., 2007; Horozov T. S. et al., 2007; Golemanov K. et al., 2006). Increasing oil viscosity prevents stabilization by hindering particle adsorption and/or by hampering emulsion formation (Golemanov K. et al., 2006; Fournier C.-O. et al., 2009).

In addition to emulsion stability, studies on emulsion size have shown that droplet size can be reduced by decreasing particle size (Binks B. P. et al., 2001; Tambe D. E. et al., 1994) or by increasing particle concentrations (Binks B. P. at al., 2003, 2004, 2005). The effect of particle concentration on droplet size was notably studied by S. Arditty et al. (2003), who defined the so-called "limited coalescence phenomenon," which assumes that the droplets produced will coalesce until the reach the coverage limit, which in turn is defined by the particles available in the system. This makes it possible to predict droplet size based on particle concentration.

On the other hand, many other studies have investigated emulsion types, and the authors have concluded that this aspect is mainly controlled by particle affinity with the two phases. For example, hydrophilic particles produce oil/water emulsions while hydrophobic particles produce water/oil emulsions (Yan N. et al., 2001; Binks B. P. et al., 2000, 2005; Stiller S. et al., 2004). This behavior is observed when the dispersed phase fraction is smaller or equal to the continuous phase fraction and when the particles are initially dispersed in the phase with which they have most affinity, which then becomes the continuous phase (Bancroft rule). Emulsion type can be affected by oil polarity (Binks B. P. et al., 2000, 2002, 2005; Golemanov K. et al., 2006; Frelichowska J. et al., 2009; Zhou J. et al., 2011) and water pH (Yan N. et al., 1996a, 1996b, 1997b); Gu G. et al., 2003) due to the effect of these two parameters on particle wettability.

In summary, the effects of the formulation on the final properties of Pickering emulsions (Table 5.1 presents the parameters affecting the properties of Pickering emulsions) have received much attention while the emulsification process itself has been largely neglected. The goals of the present study were to analyze the emulsification process in order to determine the parameters with the most impact on the properties of the final emulsion and to understand the effect these parameters have on the various stabilization steps.

Tableau 5.1: Relevant parameters affecting Pickering emulsions properties

Emulsion Property	Parameter	References
Emulsion type Controlled by particle affinity to oil and water	**Particle wettability** Hydrophilic: O/W, Hydrophobic: W/O Hydrophilic + hydrophobic: O/W/O or W/O/W	**N. Yan et al. (2001)** **B. P. Binks et al. (2000, 2005)** **R. Aveyard et al. (2003)**
	Oil polarity Oil/particle affinity	**B. P. Binks et al. (2002, 2005)** **K. Golemanov et al. (2006)** **J. Frelichowska et al. (2009)**
	Aqueous phase pH Particle wettability is affected by the mean surface charges and/or surfactants	**N. Yan et al. (1996, 1997)** **B. P. Binks et al. (2006)**
Emulsion size Droplet size is reduced by	**Particle size** Decreasing particle size	**B. P. Binks et al. (2001)** **S. Tarimala et al. (2004)**
	Particle concentration Increasing particle concentration	**S. Arditty et al. (2003)**
Emulsion stability Emulsion stability is improved by	**Particle wettability** Contact angle ~90°	**B. P. Binks et al. (2000, 2005)** **R. Aveyard et al. (2003)**
	Particle size distribution Using small monodispersed particles	**S. Tarimala et al. (2004)**
	Particle concentration Increasing particle concentration	**S. Arditty et al. (2003)** **B. P. Binks et al. (2003, 2004, 2005)**
	Salt concentration Increasing the salt concentration to promote partial particle flocculation	**B. P. Binks et al. (2005, 2006)** **T. S. Horozov et al. (2007)**
	Oil viscosity Decreasing oil viscosity	**K. Golemanov et al. (2006)** **C.-O. Fournier et al. (2009)**
	Particle shape Increasing the particle aspect ratio	**B. Madivala et al. (2009)**

We produced Pickering emulsions using a system that mimics industrial conditions in order to study the effects of particle size and wettability, oil viscosity, and continuous phase pH and salinity on the properties of emulsions. Emulsions were notably characterized by determining the droplet size distribution using a Mastersizer 3000 (Malvern) to make accurate size measurements.

5.2.3 Materials and methods

5.2.3.1 Materials

Glass microspheres (Potters Industry and Cospheric) were used as solid particles (Table 5.2). Deionized water (72.6 mJ/m^2 at 20°C) was used as the continuous phase. Silicone oils (CLEARCO Inc.) were used as dispersed phases (Table 5.3). The salinity and pH of the continuous phase were controlled using NaCl (commercial grade, Fisher Scientific) and NaOH/HCl (analytical grade, Fisher Scientific).

Tableau 5.2: Physical properties of the particles

Particles	**Type**	**Density (kg/m^3)**	**D_{32} (µm)**
Spheriglass 3000	Regular glass beads	2520	27.6
Spheriglass 5000	Regular glass beads	2520	5.9
P2011SL	Regular glass beads	2520	2.9
Spheriglass 3000E	Silanized glass beads	2520	22.4
P2011SL – F1	Silanized glass beads	2520	3.5

Tableau 5.3: Physical properties of silicone oils

Silicone Oils	**Density (kg/m^3)**	**Dynamic Viscosity (mPa·sec)**	**Surface Tension (N/m)**
S10	935	9.35	2.01E-02
S20	950	19.00	2.06E-02
S50	960	48.00	2.08E-02
S100	966	96.60	2.09E-02
S200	968	193.60	2.10E-02
S500	971	485.50	2.11E-02
S1000	971	971.00	2.12E-02
S5000	975	4875.00	2.13E-02

5.2.4 Experimental methods

5.2.4.1 Emulsification setup

Emulsification experiments were performed with a standard configuration using an unbaffled 1 L beaker to ensure a simple flow field and to generate controlled turbulence. An off-centered pitched-blade turbine was used to avoid vortex formation (Figure 5.1). In terms of mixing performances, this system is equivalent to a centered impeller with baffles for the considered regimes (Nishikawa M. K. et al., 1979; Novak V. P. et al., 1982; King R. et al., 1985; Karcz J. et al., 2004, 2005; Montante G. A. et al., 2006). The oil-to-water volume ratio was 53%v (concentrated emulsions). The particle-to-oil weight ratio was between 45%w and 120%w. The water was stirred at an impeller speed of 260 rpm. The particles were added to the water and were stirred for 10 min to homogenize the dispersion and break up aggregates. Oil was then added, and the mixture was stirred for a further 24 h to ensure that the emulsion was homogenous and that the minimal droplet size was reached before collecting samples (Figure 5.2).

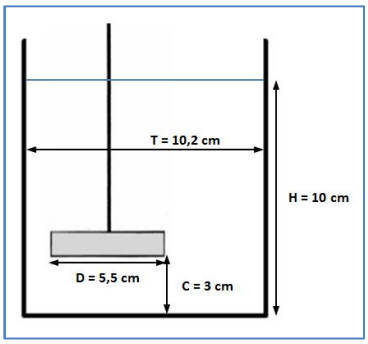

Figure 5.1: Emulsification setup

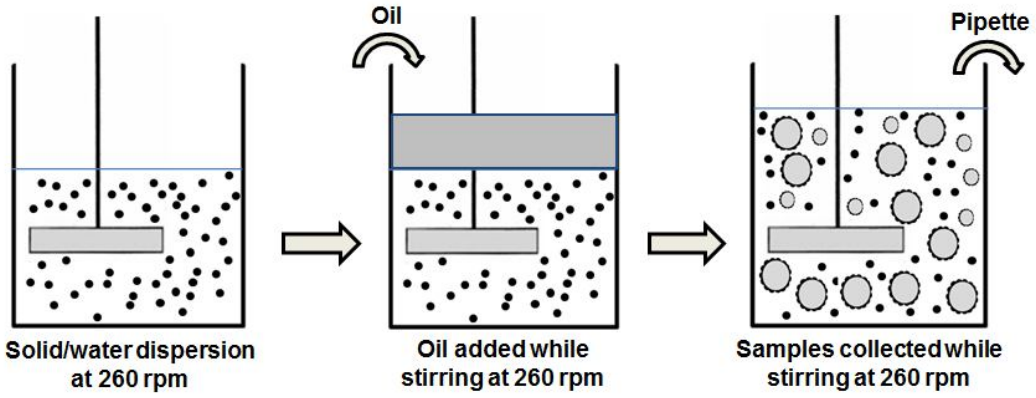

Figure 5.2: Emulsification procedure

5.2.4.2 Contact angle measurements

A goniometer was used to evaluate particles contact angle, regular flat glass plates and silanized ones were thus considered. Results are shown on Table 5.4.

Tableau 5.4: Particles contact angle

Type	Contact angle
Regular glass beads	48° ± 4°
Silanized glass beads	93° ± 3°

5.2.4.3 Interfacial tension measurements

A Nouy ring technique was used to determine interfacial tensions. Measurements show almost the same value for the considered silicone oils (γ_{ow} = (42 ± 2) E-02 N/m).

5.2.4.4 Size distribution measurements

5.2.4.4.1 Size distribution measurements

A Mastersizer 3000 (Malvern) was used to deduce the size distributions of the particles and droplets. Three diameters were used to analyze the system: D_{v10} and D_{v90}, which respectively define the diameter below which 10% and 90% of the overall droplet volume is located, and the Sauter mean diameter which is associated with the overall dispersed phase volume and the interface.

In most of emulsion cases a bimodal distribution was obtained (Figure 5.3). Being very close to solid particles size distribution, the smallest distribution was considered as the size distribution of free particles in the emulsion and, consequently, wasn't regarded in emulsion size analysis.

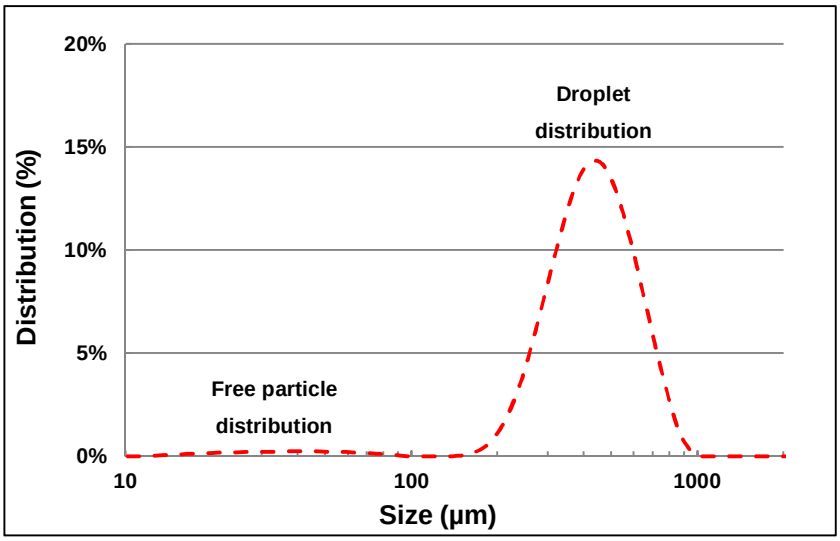

Figure 5.3: Typical emulsion size distribution

Considering that stabilization is achieved by covering the generated interface, emulsions were also characterized by deducing the effectively covered interface and the coverage potential.

The coverage potential defines the capacity of the system to cover the produced droplets. It is obtained from the properties of the particles (size, wettability, and amount) according the following formula:

$$A_{cov} = A_{cov/1p} \cdot (N_p)_{total} = \pi(R_p \sin\theta_{ow})^2 \cdot (N_p)_{total} \cdots (5.2)$$

where A_{cov} is the coverage potential, $A_{cov/1p}$ is the coverage potential of one particle, $(N_p)_{total}$ is the total number of particles, R_p is the particle radius, and θ_{ow} is the contact angle.

The effectively covered interface is estimated from the measured Sauter mean diameter. The effect of particle adsorption on apparent droplet size was taken into consideration in order to correct for and interpret the size distributions given that particle adsorption causes a swelling effect (Levine S. et al., 1991). The non-adsorbed particles parts were also taken into consideration since they also contribute to the final apparent droplet size, as shown in Figure 5.4.

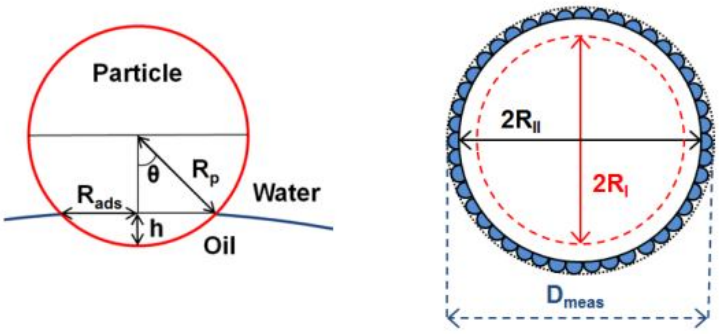

Figure 5.4: Droplet diameters before and after adsorption as well as particle dimensions

Following a geometrical analysis and using a Taylor development, S. Levine et al. (1991) obtained the following formula to describe the droplet swelling effect:

$$\left(\frac{R_{dII}}{R_{dI}}\right)^3 = 1 + N_{p/d}\left(R_p/4R_{dI}\right)\cdot\left(R_p/R_{dI}\right)^2 \cdot\left[(2+\cos\theta_{ow})\cdot(1-\cos\theta_{ow})^2 - \left(9R_p/4R_{dI}\right)\sin^2\theta_{ow} + \cdots\right] \cdots (5.3)$$

where R_{dI} is the droplet radius before particle adsorption, R_{dII} is the droplet radius after particle adsorption, R_p is the particle radius, θ_{ow} is the contact angle, and $N_{p/d}$ is the number of adsorbed particles per droplet.

In addition, the following formula was proposed to include the contribution of the non-adsorbed part of adsorbed particles in the apparent droplet diameter:

$$D_{apparent} = 2R_{dII} + \left(2R_p - h\right) \cdots (5.4)$$

where h is the adsorbed height of the particle.

Knowing the overall oil volume V_{oil}, the droplet coverage rate $\%p$ (obtained from the number of particles covering a single droplet), and the coverage potential of a single particle $A_{1particle}$, the effectively covered interface is obtained from the measured Sauter diameter according the procedure described on Figure 5.5.

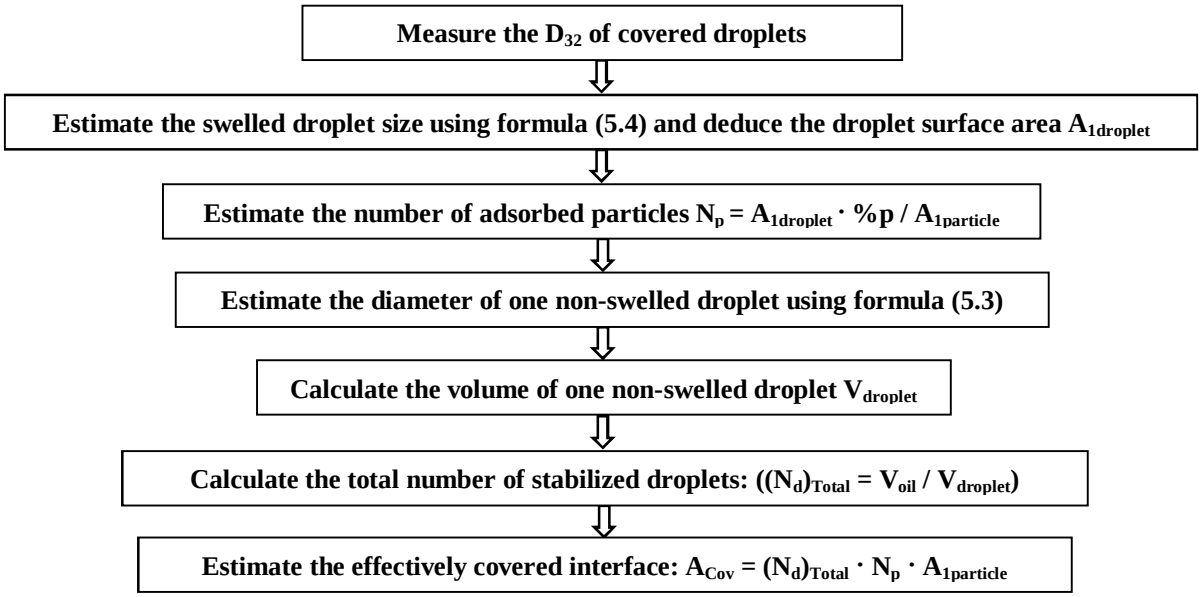

Figure 5.5: Calculation procedure of the effectively covered interface

The coverage rate was estimated by considering the solution of the Fejes problem (L. Fejes Toth, 1953). L. Fejes Toth studied the arrangements of N equal sized spheres on a spherical surface and found that the coverage rate can reach $\pi/(2\sqrt{3})=0.9069$ with a hexagonal close-packed configuration for an infinite radius of the covered sphere. We thus used this rate since the droplet radius was more than ten times larger than the particle radius (Figure 5.6).

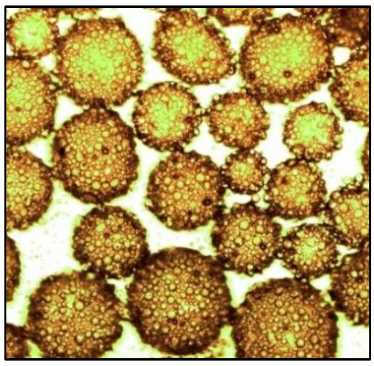

Figure 5.6: S200 silicone oil droplets stabilized by modified glass beads (22.4 µm)

5.2.5 Results and discussion

5.2.5.1 Final droplet size

We assumed that droplets are first produced in proximity to the impeller (breakage in the high shear zone). The particles then start to adsorb to the interface at a given adsorption rate. The final droplet size distribution thus depends on the stirring intensity, stirring time, and coverage potential, which in turn depends on the concentration, size, and wettability of the particles. Two theoretical mean diameters can then be defined, that is, the diameter associated with the capacity of the system to create an interface by breakage and the diameter associated with the coverage capacity. In the first case, if the interface produced by breakage is greater than the coverage capacity of the system, the resulting droplets will be partially covered and will coalesce until reaching the coverage capacity of the system (limited coalescence process). The final mean diameter will thus depend on the coverage capacity, which can be defined as the mean diameter of adsorption. In the second case, there are enough particles to cover the interface produced. The final mean diameter will thus depend on the breakage capacity of the system, which can be defined as the mean diameter of emulsification (Figure 5.7). However, it is important to take stabilization efficiency into consideration, notably particle adsorption efficiency, to determine the coverage capacity of the system. The particle adsorption process is composed of the following three steps:

a. The particle first approaches and collides with the fluid/fluid interface.
b. The particle is adsorbed at an initial position.
c. The final position of particle at the interface is reached after a given time.

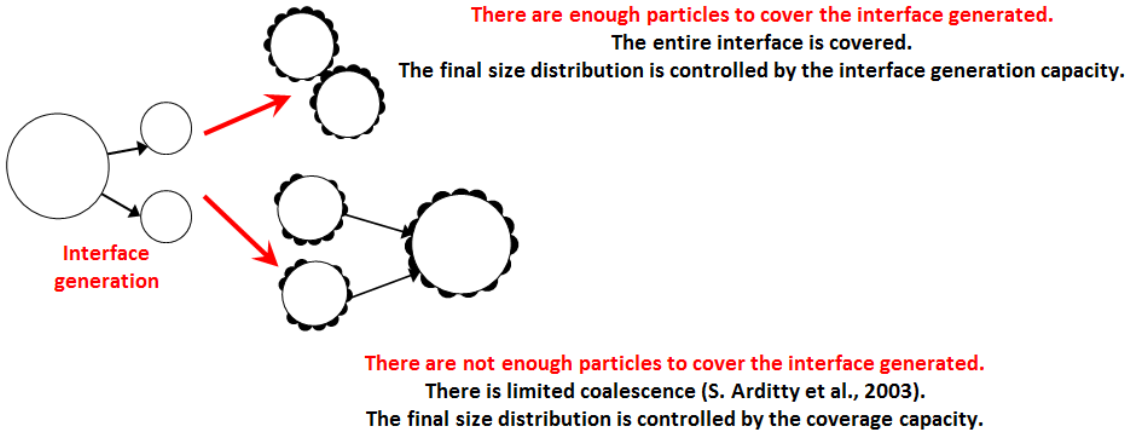

Figure 5.7: Typical representation of the mechanism controlling the solid stabilized emulsion size

5.2.5.2 Oil viscosity effect

Figure 5.8 illustrates the oil viscosity effect on droplet size for the same emulsification conditions (coverage potential, emulsification time, and mixing intensity). The results showed a power law increase in droplet size with the same exponents for all the diameters measured. The droplet diameters and distribution widths were constant until 485.5 mPa·s, beyond which both parameters began to increase. Based on this finding, two emulsification zones or regimes can be defined. In the first case, below 485.5 mPa·s, the plateau evolution of droplet size revealed that the stabilization process is controlled by the coverage potential where smaller droplets are produced. However, the oil viscosity effect is more marked above this level. When oil viscosity is increased, the entire emulsification process is affected, including the interface generation capacity, which is reduced as reported by R. V. Calabrese et al. (1986) for free particle systems. A correlation coefficient illustrating this effect has, for example, been proposed for the Sauter mean diameter:

$$\frac{d_{32}}{D} = 0{,}053 \cdot We^{-0{,}6} \cdot (1 + 0{,}97 \cdot Vi^{0{,}79})^{0{,}6} \cdots (5.5)$$

$$We = \frac{\rho_c N^2 D^3}{\sigma}, Vi = \frac{\mu_d N D}{\sigma}\left(\frac{\rho_c}{\rho_d}\right)^{0{,}5} \cdots (5.6)$$

where We is the Weber number, N the impeller speed, D the impeller diameter, σ the interfacial tension, μ_d the dispersed phase dynamic viscosity, ρ_c the continuous phase density, and ρ_d the dispersed phase density.

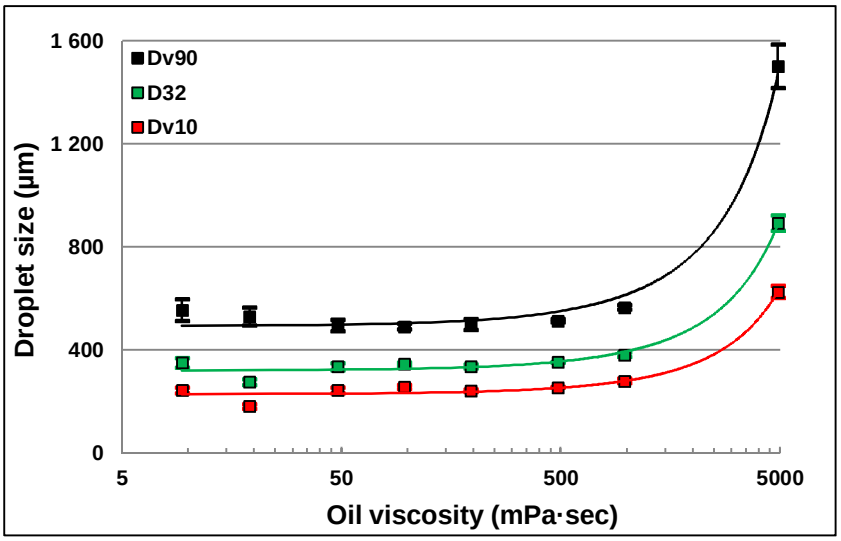

Figure 5.8: Effect of silicone oil viscosity on droplet size

(W: 56.4%v, O: 30.2%v, P: 13.4%v, modified GB 22.4 µm, Re = 11400)

On the other hand, oil viscosity is also involved in the dynamics of particle adsorption. Indeed, during particle/droplet collision, the continuous phase film between the particle and the droplet should be drained to allow contact and adsorption. For example, A. K. Chesters (1991) reported that increasing oil viscosity reduces droplet surface mobility, hindering film drainage and preventing particle contact and adsorption. Moreover, particle adsorption is slower at high oil viscosities, which has a significant effect on the stabilization process if the initial attachment force is lower than the breakage force. When particle/droplet collision occurs, the particle is adsorbed at a given level, which can be different from the final level depending on the properties of the system. In addition, since the level of adsorption corresponds to a given capillary force, the particle will detach from the interface and the droplet will be less stable to coalescence if the initial adsorption force is lower than the shearing off forces. Furthermore, since shearing off forces are larger in proximity to the impeller, the time required to reach this zone, which is defined as the droplet circulation time, should also be taken into consideration in the stabilization process.

5.2.5.3 Particles size effect

Figure 5.9 illustrates the particle size effect on droplet size distribution using regular glass beads. As can be seen, droplets mean diameter and distribution width both increase with particle size. This effect is mainly related to the stabilization process since the same emulsification conditions

were used. As was mentioned previously, the solid particle emulsion stabilization mechanism can be divided into three steps: (1) the particle first approaches and reaches the fluid/fluid interface, (2) the particle adsorbs to and is trapped at the interface, and (3) the adsorbed particles form a network that stabilizes the emulsion.

For the first step, by increasing the particle size, the contact surface between the particle and the trapped continuous phase film increases and the repulsive forces associated with the film drainage process (hydrodynamic and hydration forces) become more significant as does the electrostatic double layer force if charges are involved in the system. In addition, for the same emulsification conditions, the collision force increases with particle size, which does not necessarily promote film drainage since it can also deform the droplet interface and thus increase the surface area of contact.

For the second step, increasing the particle size increases the adsorption time. This effect is related to the fact that adsorption is a function of particle/oil affinity, which is defined by the particle contact angle. As such, for the same contact angle, the wetted depth should be higher for larger particles.

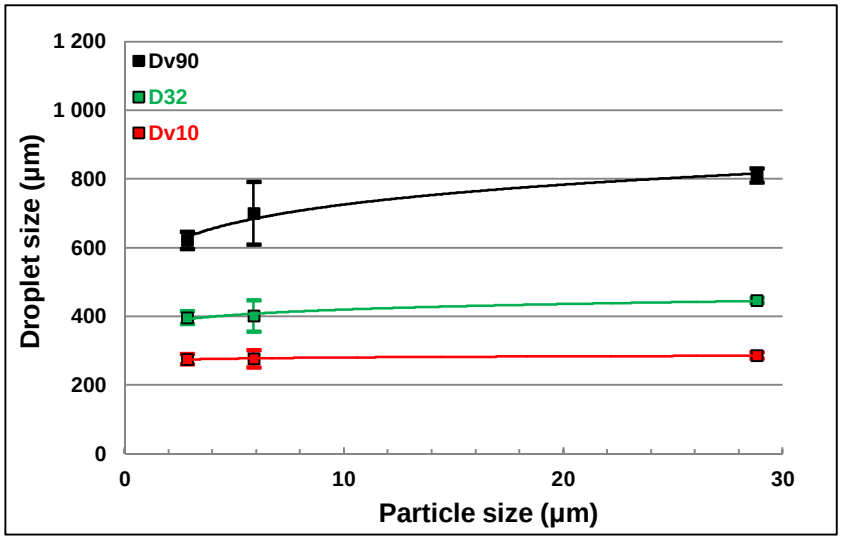

Figure 5.9: Effect of particle size on droplet size

(O/W: 53%v, regular GB, coverage potential: 3.55 m^2 at 48°, μ_{S10}: 9.35 mPa·s, Re = 11400)

To better understand the effect of various particle sizes, covered surfaces resulting from measured d_{32} were plotted for different oil viscosities. Figure 5.8 shows that the real covered surfaces are below the coverage potential of the system for all the particle sizes studied, which

confirms the concept of stabilization efficiency. Figure 5.10 also shows that the covered surface decreases when oil viscosity or particle size increases. This effect is related to the initial repulsion force. However, this decrease is less significant for the smallest particles (for different oil viscosities) or the lowest viscosities (for different particle sizes), which indicates that it is possible to compensate for the oil viscosity effect by reducing the particle size or for the particle size effect by reducing oil viscosity.

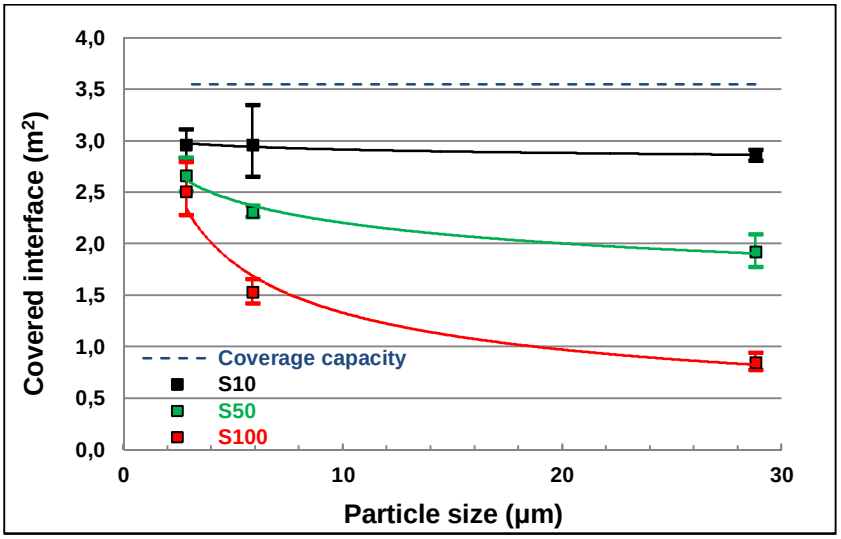

Figure 5.10: Effect of particle size/oil viscosity on the covered interface

(O/W: 53%v, regular GB, coverage potential: 3.55 m^2 at 48°, Re = 11400)

5.2.5.4 Particles wettability effect

Figure 5.11 illustrates the effect of particle wettability on droplet size distribution for the same coverage potential and shows that both droplet size and distribution width decrease if the contact angle is increased to 90°. The effect of oil viscosity and particle size is related to the stabilization process, notably to the initial repulsive force and initial adsorption force. By enhancing particle/oil affinity, the initial repulsion force decreases due to the decrease in the repulsive hydration force and, in some cases, the increase in the attractive hydrophobic force, which favors film drainage and particle/droplet contact. On the other hand, increasing particle/oil affinity promotes attachment through the capillary force, which increases with the increasing hydrophobicity of the particles.

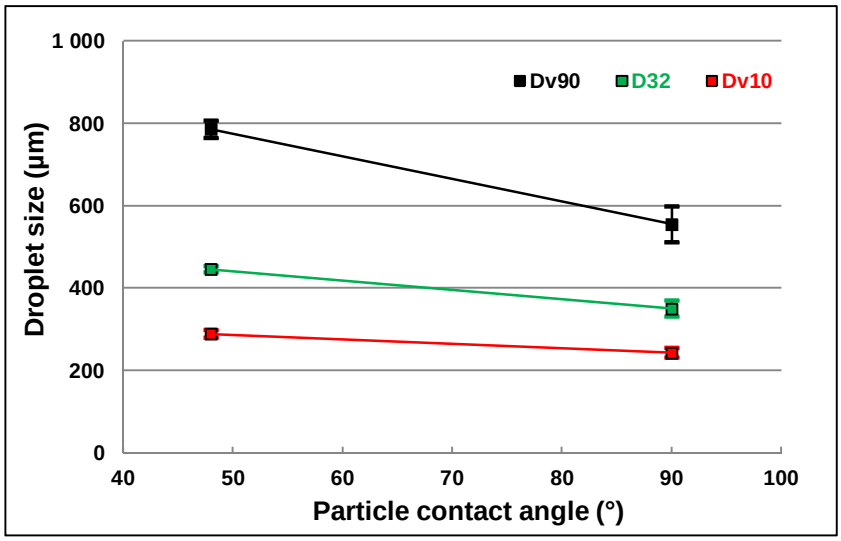

Figure 5.11: Effect of particle wettability on droplet size

(O/W: 53%v, D_p = 26 µm, coverage potential: 6.44 m^2 at 90°, μ_{S10}: 9.35 mPa·s, Re = 11400)

When covered surface areas are compared, it can be seen that the coverage capacity increases with the particle contact angle for different particle sizes (Figure 5.12) and oil viscosities (Figure 5.13). However, Figure 5.12 and Figure 5.13 show, respectively, that the particle size and oil viscosity effects (Figure 5.8 and Figure 5.9, respectively) are less significant for less hydrophilic particles (90°). This behavior highlights the importance of particle wettability in the stabilization process. Indeed, we observed that increasing particle size or oil viscosity results in reduced attachment efficiency by increasing the initial repulsive force and adsorption time. However, less hydrophilic particles (modified glass beads), reduced the initial repulsive force and increased the adsorption force and time compared to hydrophilic particles (regular glass beads). These finding suggested that the stabilization process is mainly driven by the contact and initial adsorption step. Moreover, at a process scale, the particle size effect and oil viscosity effect can be compensated by the wettability effect, thus improving stabilization efficiency.

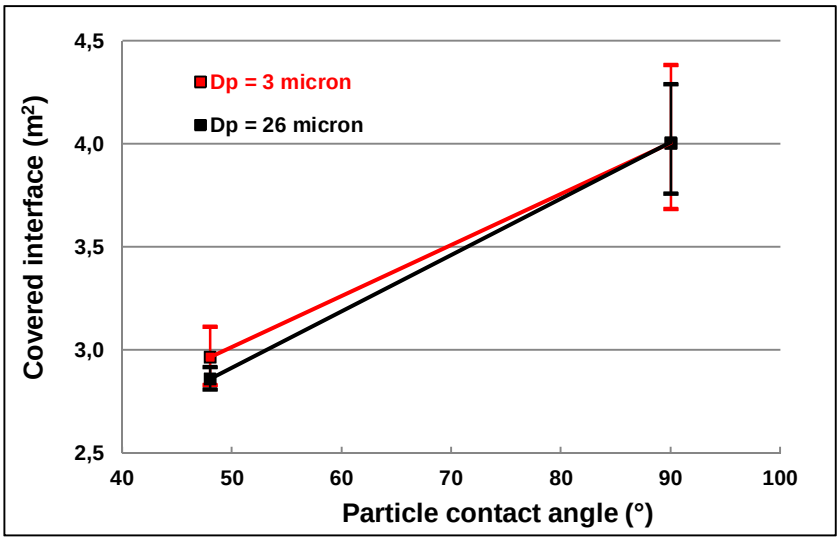

Figure 5.12: Effect of particle size/wettability on the covered interface

(O/W: 53%v, coverage potential: 6.44 m^2 at 90°, μ_{S10}: 9.35 mPa·s, Re = 11400)

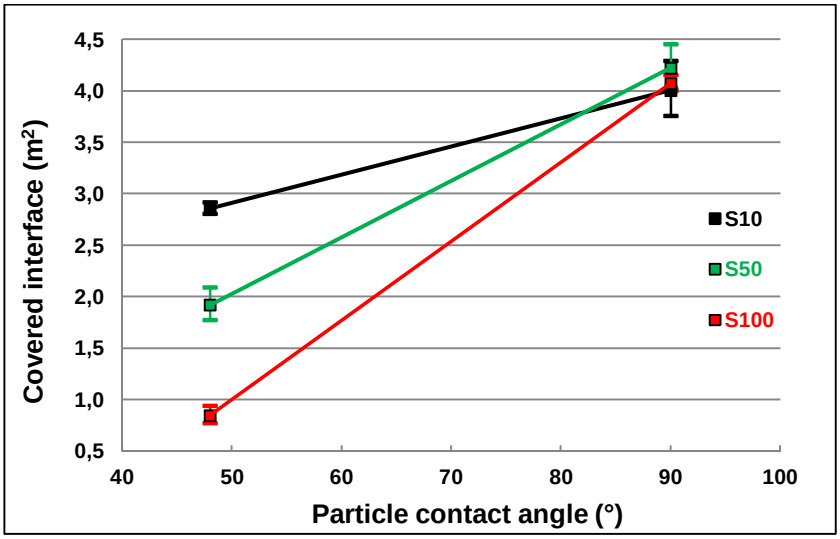

Figure 5.13: Effect of particle wettability/oil viscosity on the covered interface

(O/W: 53%v, coverage potential: 6.44 m^2 at 90°, μ_{S10}: 9.35 mPa·s, Re = 11400)

5.2.5.5 Coverage potential effect

The coverage potential effect on droplet size distribution is plotted on Figures 5.14 and 5.15. Our results showed that increasing the particle content results in a linear decrease in droplet size and distribution width, which was predictable given that using more particles resulted in a higher breakage capacity (higher continuous phase density), more particle/droplet collisions, and more

coverage capacity. However, if changes in the covered surface area are taken into consideration, it can be seen that, even if the change is linear, the effectively covered surface/coverage potential ratio decreases with the particle fraction, which was not expected (Figure 5.16). Indeed, by adding more particles, the collision frequency should increase, leading in turn to an increase in contact and attachment efficiency. This behavior may be due to the effect of particle concentration on the energy dissipation rate. For the same impeller speed, adding more particles reduces the energy dissipation rate and, as such, the particle/droplet collision force, which is proportional to the energy dissipation rate. Reducing the collision force would thus result in an increase in the effect of repulsive forces, which in turn would decrease particle attachment and stabilization.

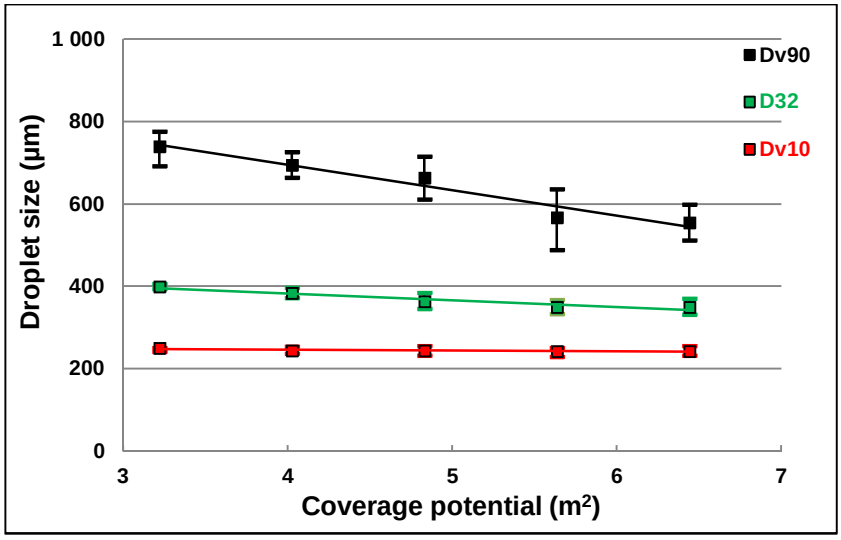

Figure 5.14: Effect of the coverage potential on droplet size

(O/W: 53%v, modified GB: 22.4 µm, μ_{S10}: 9.35 mPa·s, Re = 11400)

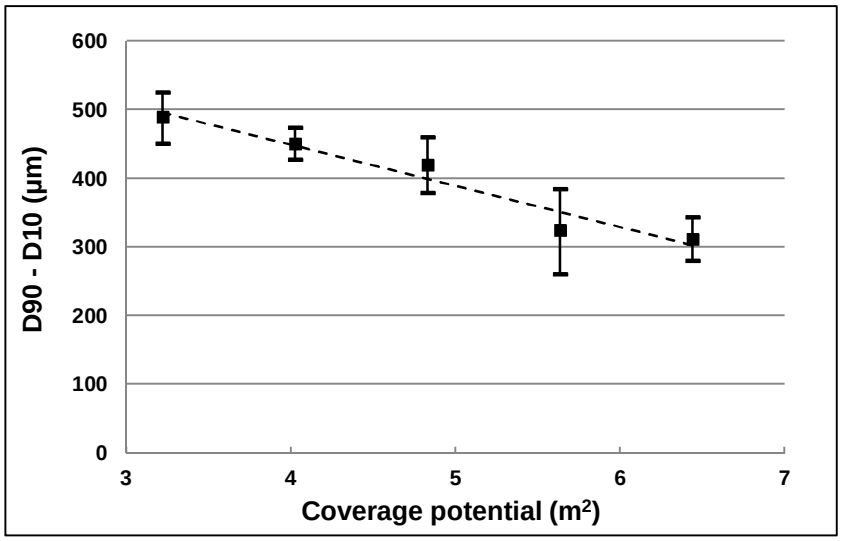

Figure 5.15: Effect of the coverage potential on droplet size distribution width

(O/W: 53%v, modified GB: 22.4 µm, μ_{S10}: 9.35 mPa·s, Re = 11400)

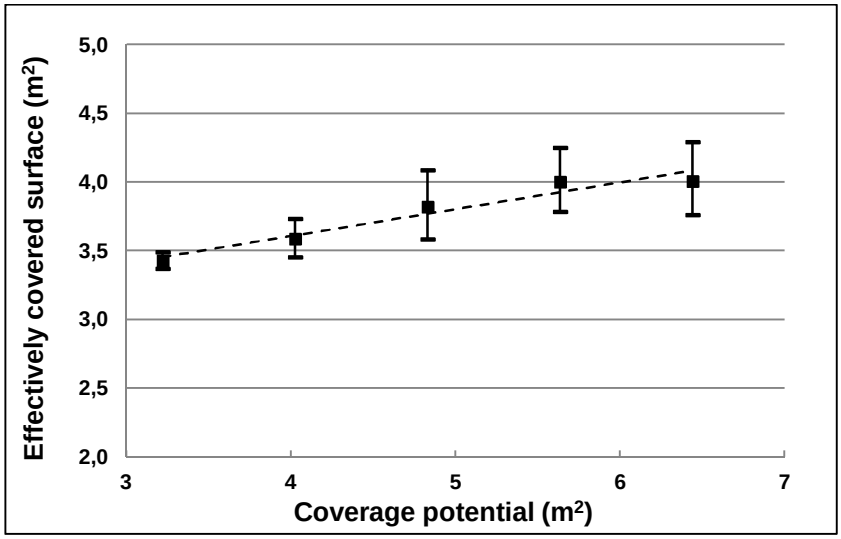

Figure 5.16: Effectively covered surface vs. Coverage potential

(O/W: 53%v, modified GB: 22.4 µm, μ_{S10}: 9,35 mPa·s, Re = 11400)

5.2.5.6 Aqueous phase properties (Ionic strength and pH)

The results plotted on Figures 5.17 and 5.18 show that droplet size and distribution width increase when ionic species are added (NaOH, HCl, or NaCl). This can be explained by the effect of ionic species on particle interactions. It is well known that the addition of ionic species to dispersions causes particle flocculation. This effect was notably observed when we added NaCl

to the same particles used as a stabilizer, as illustrated in Figures 5.17 and 5.18. The results plotted on Figure 5.19 clearly show that the particles flocculate, resulting in apparent larger particles. The ionic species effect is thus similar to the particle size effect by which droplet size increases in a linear fashion with increases in particle size.

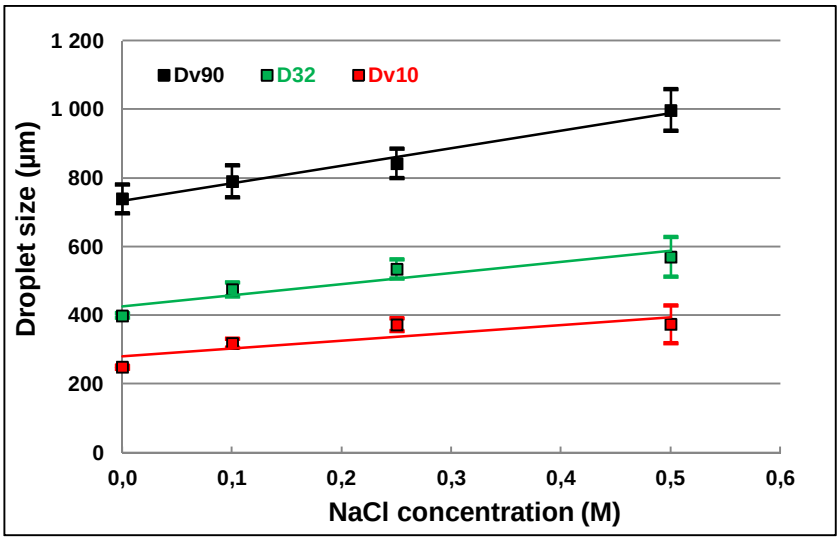

Figure 5.17: Effect of NaCl concentration on droplet size

(O/W: 53%v, modified GB: 22.4 µm, μ_{S10}: 9.35 mPa·s, Re = 11400)

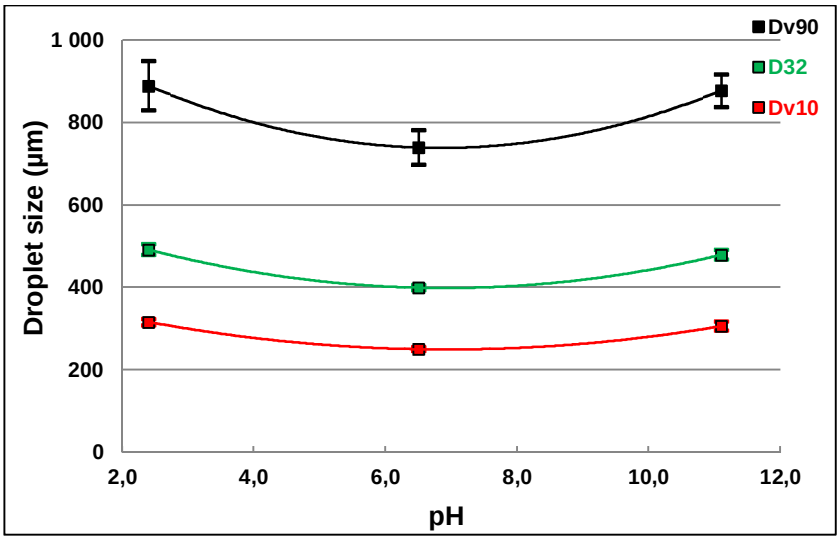

Figure 5.18: Effect of pH on droplet size

(O/W: 53%v, modified GB: 22.4 µm, μ_{S10}: 9.35 mPa·s, Re = 11400)

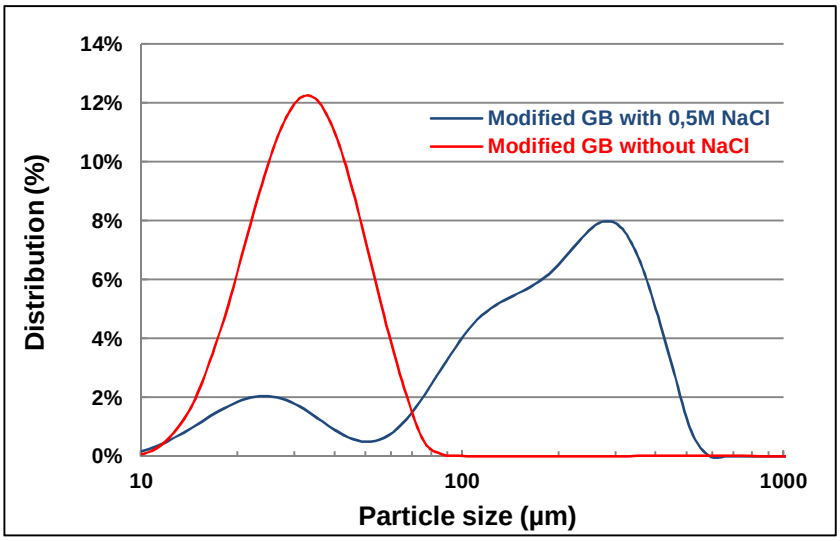

Figure 5.19: Effect of NaCl on particle size distribution

5.2.6 Conclusions

Since we are mainly interested in the development of new emulsification processes, we investigated the effects of the properties of oil, particles, and water on Pickering emulsion stabilization using a conventional mixing system (unbaffled tank with an off-centered pitched-blade turbine). Regular and modified glass beads were used as stabilizers. The beads were all over 2 µm in diameter in order to reduce the impact of colloidal forces (van der Waals and electrostatic double layer forces). The behavior of the emulsification process highlighted the importance of the particle attachment process, notably the approach, collision, and initial adsorption steps.

The approach and collision steps were very sensitive to oil viscosity and particle size and wettability, which all affect the continuous phase film drainage mechanism. Adding ionic species to the aqueous phase did not improve stabilization and resulted in the production of larger droplets. This behavior was related to the effect of particle size on stabilization. The smallest droplets with the narrowest distribution were obtained with small particles. The effects of changes in water pH and salinity were similar to those observed with the particle size effect. Stabilization was improved by lowering oil viscosity and increasing oil/particle affinity, which have an effect on collision and initial adsorption. In addition, increasing oil/particle affinity significantly reduced the impact of increasing oil viscosity and/or particle size.

The particle fraction effect displayed good agreement with previously published results since we observed that smaller and more stable droplets are obtained by increasing the number of particles. However, we also showed that stabilization efficiency, which is defined as the ratio of the real covered surface and the coverage potential of the system, decreases in parallel with an increase in particle concentration.

5.2.7 Acknowledgments

The authors gratefully acknowledge financial support from the Natural Sciences and Engineering Research Council of Canada and TOTAL.

CHAPITRE 6. ARTICLE 4: EFFECT OF PROCESSING PARAMETERS ON THE PRODUCTION OF PICKERING EMULSIONS

6.1 Présentation du quatrième article

Soumis dans : Industrial & Engineering Chemistry Research
Auteurs : Èmir Tsabet, Louis Fradette

Dans cet article des expériences d'émulsification ont été réalisées dans un dispositif de mélange en cuve agitée a été utilisé, incluant une turbine à pales inclinées décentrée dans un bécher d'un litre sans chicanes. Les effets du temps de mélange, de la concentration en particules, de la vitesse de l'agitateur et de la viscosité de l'huile sur les performances d'émulsification par des particules solides ont été étudiés. Les émulsions produites ont été caractérisées par des mesures de distribution de taille en utilisant un Mastersizer 3000 (Malvern). Les temps de mélange et de circulation ont été mesurés en utilisant la technique de la décoloration pour évaluer l'effet de la vitesse d'agitation sur la stabilisation.

Les résultats ont révélé une forte interaction entre les paramètres affectant l'hydrodynamique du système soulignant ainsi la nécessité de définir des conditions optimales pour obtenir la plus petite taille de gouttes avec la plus étroite distribution possible. Cette interaction est notamment due à la présence de deux différents processus durant l'émulsification, la génération de gouttes et leur couverture ou stabilisation ce qui diffère de l'émulsification par des tensio-actifs ou la stabilisation est beaucoup plus rapide que la génération de gouttes qui est également favorisée par la réduction de la tension interfaciale. Il a ainsi été montré que les conditions optimales d'émulsification dépendaient du niveau de cisaillement, du taux de dissipation de l'énergie cinétique turbulente et du temps de circulation. L'effet de la concentration de particules sur la production d'interface et la stabilisation a été également mis en évidence.

6.2 Effect of processing parameters on the production of Pickering emulsions

6.2.1 Summary

Emulsification experiments were performed in an unbaffled tank using an off-centered pitched-blade turbine. The effects of mixing time, particle concentration, impeller speed, and oil viscosity on the production of Pickering emulsions were investigated. Emulsification efficiency was quantified by size distribution measurements using a Mastersizer 3000 (Malvern). Mixing and circulation times were measured using a decolorization technique to investigate the effect of impeller speed on the stabilization process.

There was a strong interaction among all the parameters affecting mixing tank hydrodynamics. Optimal conditions were determined in order to produce the smallest droplets with the narrowest distribution. Droplet production and coverage were involved simultaneously in the interaction, which is very different from surfactant-based systems where the stabilization step is much faster than the droplet production step and where droplet breakage is promoted by reducing the interfacial tension. The impeller speed and emulsification time results indicated that the shear level in the impeller zone, the energy dissipation rate, and the fluid circulation time are important drivers of the stabilization mechanism. The particle concentration results showed that the particle effect played a role in the production of an interface and in stabilization efficiency.

6.2.2 Introduction

Emulsification processes are used in numerous fields, including the cosmetics, food processing, paint, petroleum, and pharmaceutical industries. Most emulsions are stabilized by surfactants. Global demand for surfactants is expected to total 18 million tons in 2017, or the equivalent of $30 billion in sales (Transparency Market Research, July 10, 2012). In this context, increasing efforts are being devoted to developing less costly and greener alternatives such as solid particles. Since the pioneering work of W. Ramsden (1903) and S. U. Pickering (1907) over a century ago, solid particles have been used to produce highly stable emulsions. In the past 20 years especially, many studies on emulsion stability, type, and size and, more recently, on the rheological behavior of emulsions, have been conducted.

It has been shown that it is possible to produce solid-stabilized emulsions that are much more stable than emulsions produced with surfactants (Binks B. P., 2002). This enhanced stability has been attributed to the formation of a steric particle barrier around the droplets that prevents coalescence and to particle packing at the interface and, as such, to particle interactions, notably capillary forces (Levine S. et al., 1991, 1992, 1993). These findings highlighted the importance of particle stability at the interface and led to two approaches for studying this aspect (Binks B. P. and Horozov T. S., 2006). The first approach is based on a free energy analysis, which considers that stability is attained when the system reaches its minimal free energy, whereas the second approach is based on a force analysis, which considers that stability is attained when the sum of the forces involved is zero.

In the first approach, the energy required to detach particles from the interface is expressed using the following equation developed by S. Levine et al. (1989):

$$E = \pi R^2 \gamma_{ow} (1 \pm cos\theta)^2 \cdots (6.1)$$

A similar approach has also been used to calculate particle adsorption energy, which is related to the line tension effect (Aveyard R. et al., 2003; Sacanna S. et al., 2007). The equilibrium position of particles at the interface (Komura S. et al., 2006; Hey M. J. et al., 2006) and the equilibrium particle concentration at the interface (Hirose Y. et al., 2008) have also been determined. On the other hand, the force analysis approach has revealed the importance of capillary forces (Princen H. M., 1969; Rapacchietta A. V. et al., 1977; Joseph D. D. et al., 2003; Singh P. et al., 2005).

The most stable emulsions are obtained using particles with intermediate hydrophobic properties whereas the least stable emulsions are obtained with highly hydrophobic and highly hydrophilic particles (Yan N. et al., 1995b, 1997a; Binks B. P. et al., 2000, Yan N. et al., 2001; Stiller S. et al., 2004; Ding A. et al., 2005). Emulsion stability can also be improved by increasing the particle concentration (Yan N. et al., 1994, 1995a, 1995b, 1996b, 1997a, 1997b), reducing particle size (Binks B. P. et al., 2001; Tambe D. E. et al., 1994), using monodispersed (Tarimala S. et al., 2004) and ellipsoidal particles (Madivala B. et al., 2009), or slightly increasing water salinity, which mainly acts on particle flocculation through its impact on the repulsive electrical double layer force (Binks B. P. et al., 1999, 2005, 2006; Yang F. et al., 2007; Horozov T. S. et al., 2007; Golemanov K. et al., 2006). It has also been shown that high oil viscosities prevent stabilization

by hindering particle adsorption and/or by hampering emulsion formation (Golemanov K. et al., 2006; Fournier C.-O. et al., 2009).

Droplet size can be reduced by decreasing particle size (Binks B. P. et al., 2001; Tambe D. E. et al., 1994) or by increasing particle concentration (Binks B. P. at al., 2003, 2004, 2005). The effect of particle concentration on droplet size was notably studied by S. Arditty et al. (2003), who defined the so-called "limited coalescence phenomenon," which assumes that the droplets produced will coalesce until they reach the coverage limit, which is defined by the particle concentration.

Emulsion type has been shown to be mainly controlled by particle affinity with both phases. For example, oil/water emulsions are obtained with hydrophilic particles while water/oil emulsions are obtained with hydrophobic particles (Yan N. et al., 2001; Binks B. P. et al., 2000, 2005; Stiller S. et al., 2004). However, this behavior only occurs when the dispersed phase is smaller than or equal to the continuous phase and when the particles are initially dispersed in the phase with which they have the most affinity, which then becomes the continuous phase (Bancroft rule). Emulsion type can also be affected by oil polarity (Binks B. P. et al., 2000, 2002, 2005; Golemanov K. et al., 2006; Frelichowska J. et al., 2009; Zhou J. et al., 2011) and water pH (Yan N. et al., 1996a, 1996b, 1997; Gu G. et al., 2003) through their effects on particle wettability.

In summary, the qualitative effects of oil, water, and particle properties have been studied extensively. However, from a process design perspective, more quantitative data are required at the particle scale and at the droplet scale. At the particle scale, the goal being to find ways to promote particle/droplet contact and particle adsorption at the interface while the goal at the droplet scale is to find ways to promote droplet production and droplet coverage.

Particle adsorption can be enhanced by facilitating drainage of the film between the particle and the droplet during approach and contact in order to reduce particle adsorption time, increase the adsorption force, and reduce the detachment force. These parameters all involve the properties of particles, oil, and water (particle size, particle wettability, oil/water interfacial tension, oil viscosity, and water pH and salinity) as well as the properties of the emulsification system that control the contact and detachment forces. On the other hand, droplet generation is promoted by increasing the energy level in order to produce a larger interface and by increasing particle concentration in order to cover and stabilize the interface. However, increasing the energy level

to promote interface generation necessarily affects the stabilization process, which is controlled by the contact and detachment forces as well as the circulation time, which is controlled by the type and speed of the impeller.

Based on the results reported in the literature, the properties of the components of the emulsion (oil, water, and particles) have a marked impact on the final emulsion. However, it is also clear that not enough information is available to enable process engineers to design and build the appropriate processing units. Our goal was to quantify the effects of process conditions on the properties of the final emulsion by varying emulsification times and energy levels while monitoring droplet size to evaluate processing efficiency versus drop stabilization.

6.2.3 Materials and methods

6.2.3.1 Materials

The physical properties of the glass microspheres (Potters industry and Cospheric) used as model solid particles are listed in Table 6.1. Deionized water (72.6 mJ/m^2 at 20°C) was used as the continuous phase in all the experiments. Silicone oils (Clearco) covering a range of viscosities were used as the dispersed phase. Their viscosity and surface tension are listed in Table 6.2. The salinity and pH of the continuous phase were controlled using NaCl (commercial grade, Fisher Scientific) and NaOH/HCl (analytical grade, Fisher Scientific), respectively.

Tableau 6.1: Physical properties of the particles

Particles	Type	Density (kg/m^3)	D_{32} (µm)
Spheriglass 3000E	Silanized glass beads	2520	22.4

Tableau 6.2: Physical properties of silicone oils

Silicone oils	Density (kg/m^3)	Dynamic Viscosity (mPa·sec)	Surface Tension (N/m)
S20	950	19.00	2.06E-02
S100	966	96.60	2.09E-02
S200	968	193.60	2.10E-02
S500	971	485.50	2.11E-02
S1000	971	971.00	2.12E-02
S5000	975	4875.00	2.13E-02

6.2.3.2 Experimental methods

6.2.3.2.1 Emulsification setup

Emulsification experiments were performed with a standard configuration using an unbaffled 1-L beaker to ensure a simple flow field. An off-centered pitched-blade turbine was used to avoid vortex formation (Figure 6.1). In terms of mixing performances, this system is equivalent to a centered impeller with baffles for the considered regimes (Nishikawa M. K. et al., 1979; Novak V. P. et al., 1982; King R. et al., 1985; Karcz J. et al., 2004, 2005; Montante G. A. et al., 2006). The oil-to-water volume ratio was 53%v (concentrated emulsions). The particle-to-oil weight ratio was between 100% and 300% w/w.

The emulsification procedure was as follows:

a) Start water-only agitation at a given impeller speed.
b) Add particles. Mix for 10 min to homogenize the dispersion and break up aggregates.
c) Gently add oil and continue mixing.
d) Collect samples at different times to determine the effect of emulsification time.

Figure 6.2 illustrates the emulsification procedure.

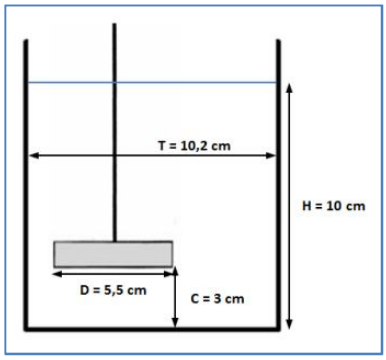

Figure 6.1: Emulsification setup

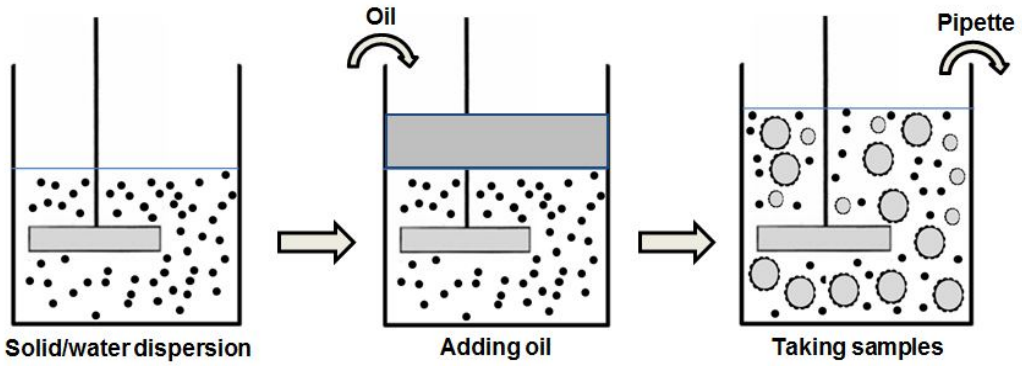

Figure 6.2: Emulsification procedure

Rupture-coalescence-stabilization events were represented by assuming that droplets are first produced in proximity to the impeller (breakage in the high shear zone). The particles then start to adsorb to the interface at a given adsorption rate. The resulting droplets can be stable or unstable, depending on droplet size and particle coverage. If the droplets are uncovered or partially covered and thus unstable, coalescence and/or breakage can occur again. This can happen during the next passage through the impeller zone. If the droplets are sufficiently covered to be considered stable, two cases have to be taken into consideration. In the first case, the covered droplets are small enough and can be assumed to be unbreakable at a given emulsification energy level. In the second case, the droplets are larger than the defined unbreakable threshold and can thus be broken during the next passage through the impeller region. These cases are illustrated in Figure 6.3. Based on the mechanism described above, the generation of the final stabilized interface is a function of mixing intensity, circulation time, and coverage capacity (particles amount). It should also be noted that if the interface produced by breakage is larger than the coverage capacity of the particles, the resulting droplets will be partially covered and will only coalesce until the coverage capacity of the system is reached. This can be considered as the equivalent of the limited coalescence phenomenon applied to the mixing configuration used here. On the other hand, if there are enough particles to cover the interface produced, the stabilized interface will depend on the interface generation capacity of the system. It is important to keep in mind that the stabilization efficiency of the system depends on its particle adsorption capacity.

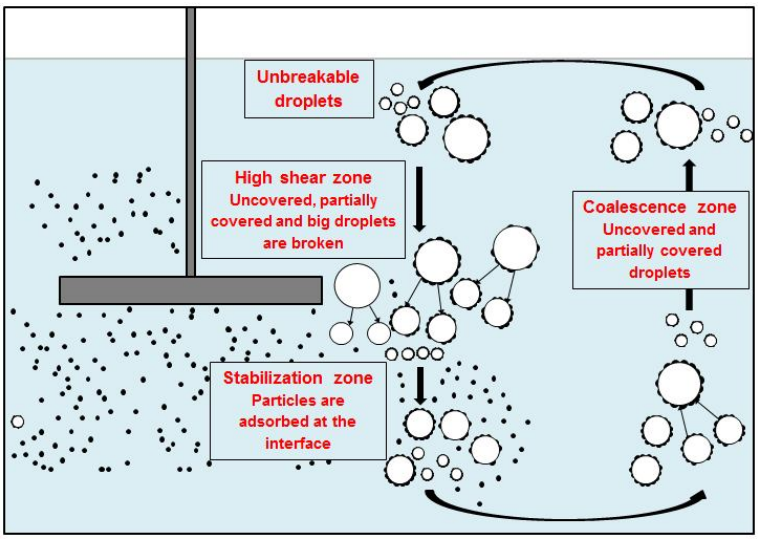

Figure 6.3: Typical representation of a solid-stabilized emulsification system

6.2.3.2.2 Contact angle measurements

A goniometer was used to evaluate particles contact angle, regular flat glass plates and salinized ones were considered. Results are shown on Table 6.3.

Tableau 6.3: Particles contact angle

Type	Contact angle
Silanized glass beads	93° ± 3°

6.2.3.2.3 Interfacial tension measurements

A Nouy ring technique was used to determine interfacial tensions. Measurements show almost the same value for the considered silicone oils (γ_{ow} = (42 ± 2) E-02 N/m).

6.2.3.2.4 Size distribution measurements

A Mastersizer 3000 (Malvern) was used to deduce the size distributions of the particles and droplets. Three diameters were used to analyze the system: D_{v10} and D_{v90}, which respectively define the diameter below which 10% and 90% of the overall droplet volume is located, and the Sauter mean diameter which is associated with the overall dispersed phase volume and the interface.

In most of emulsion cases a bimodal distribution was obtained (Figure 6.4). Being very close to solid particles size distribution, the smallest distribution was considered as the size distribution of free particles in the emulsion and, consequently, wasn't regarded in emulsion size analysis.

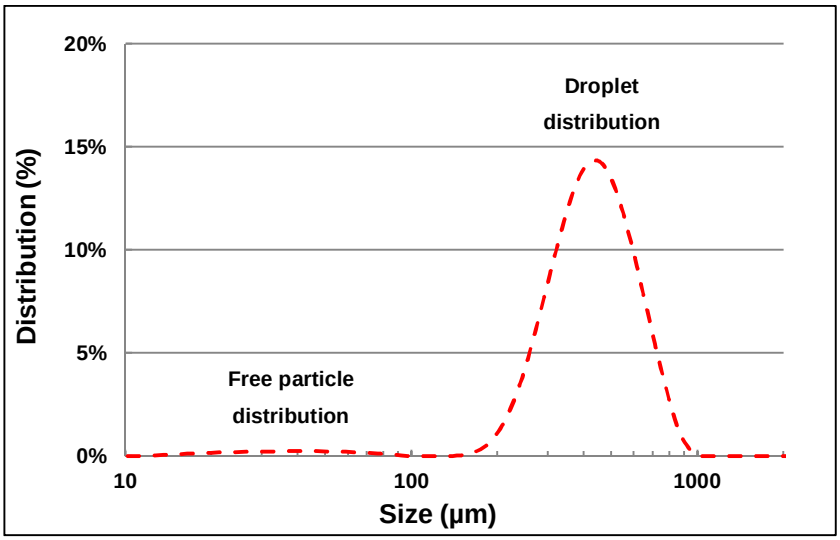

Figure 6.4: Typical emulsion size distribution

Considering that stabilization is achieved by covering the generated interface, emulsions were also characterized by deducing the effectively covered interface and the coverage potential.

The coverage potential defines the capacity of the system to cover the produced droplets. It is obtained from the properties of the particles (size, wettability, and amount) according the following formula:

$$A_{cov} = A_{cov/1p} \cdot (N_p)_{total} = \pi(R_p \sin\theta_{ow})^2 \cdot (N_p)_{total} \cdots (6.2)$$

where A_{cov} is the coverage potential, $A_{cov/1p}$ is the coverage potential of one particle, $(N_p)_{total}$ is the total number of particles in the system, R_p is the particle mean radius, and θ_{ow} is the contact angle.

The effectively covered interface is estimated from the measured Sauter mean diameter. The effect of particle adsorption on apparent droplet size was taken into consideration in order to correct for and interpret the size distributions given that particle adsorption causes a swelling effect (Levine S. et al., 1991). The non-adsorbed particles parts were also taken into consideration since they also contribute to the final apparent droplet size, as shown in Figure 6.5.

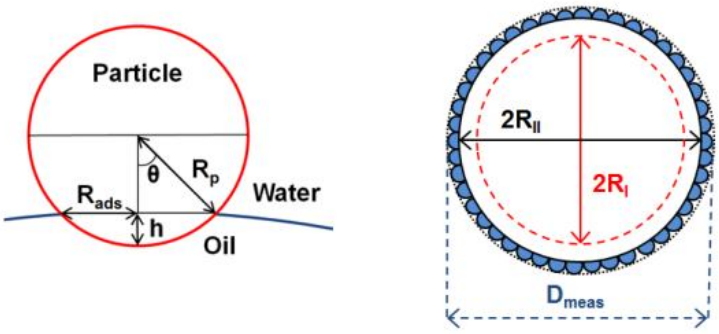

Figure 6.5: Droplet diameters before and after adsorption as well as particle dimensions

Following a geometrical analysis and using a Taylor development, S. Levine et al. (1991) obtained the following formula to describe the droplet swelling effect:

$$\left(\frac{R_{dII}}{R_{dI}}\right)^3 = 1 + N_{p/d}\left(R_p/4R_{dI}\right)\cdot\left(R_p/R_{dI}\right)^2 \cdot\left[(2+\cos\theta_{ow})\cdot(1-\cos\theta_{ow})^2 - \left(9R_p/4R_{dI}\right)\sin^2\theta_{ow} + \cdots\right] \cdots (6.3)$$

where R_{dI} is the droplet radius before particle adsorption, R_{dII} is the droplet radius after particle adsorption, R_p is the particle radius, θ_{ow} is the contact angle, and $N_{p/d}$ is the number of adsorbed particles per droplet.

In addition, the following formula was proposed to include the contribution of the non-adsorbed part of adsorbed particles in the apparent droplet diameter:

$$D_{apparent} = 2R_{dII} + \left(2R_p - h_{ads}\right) \cdots (6.4)$$

where h is the adsorbed height of the particle.

Knowing the overall oil volume V_{oil}, the droplet coverage rate $\%p$ (obtained from the number of particles covering a single droplet), and the coverage potential of a single particle $A_{1particle}$, the effectively covered interface is obtained from the measured Sauter diameter according the procedure described on Figure 6.6.

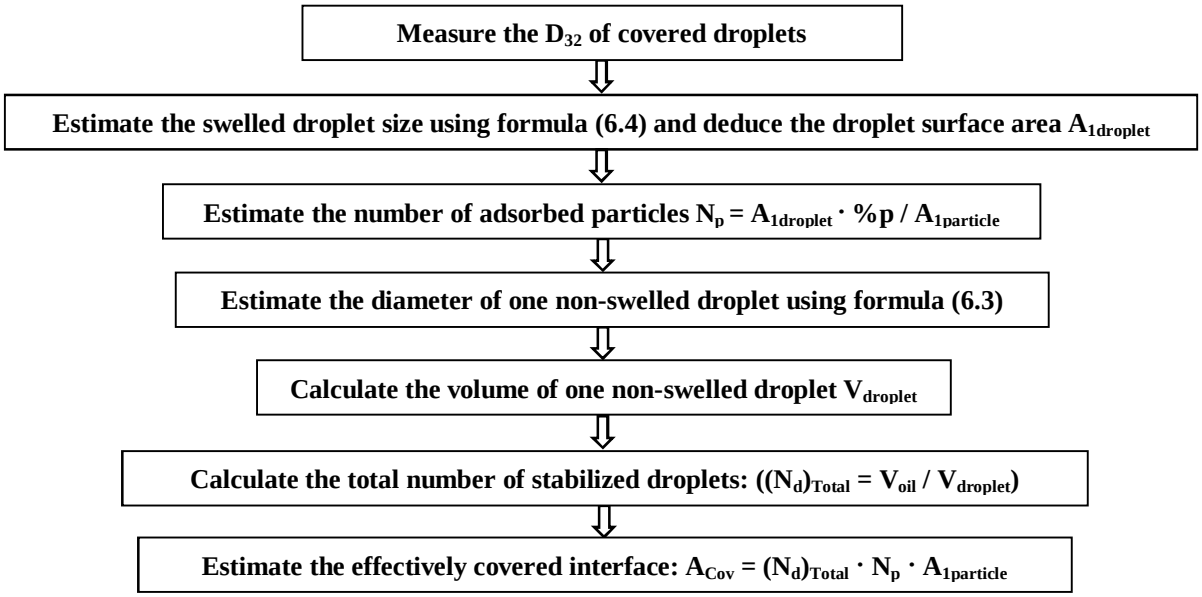

Figure 6.6: Calculation procedure of the effectively covered interface

The coverage rate was estimated by considering the solution of the Fejes problem (L. Fejes Toth, 1953). L. Fejes Toth studied the arrangements of N equal sized spheres on a spherical surface and found that the coverage rate can reach $\pi/(2\sqrt{3})=0.9069$ with a hexagonal close-packed configuration for an infinite radius of the covered sphere. We thus used this rate since the droplet radius was more than ten times larger than the particle radius (Figure 6.7).

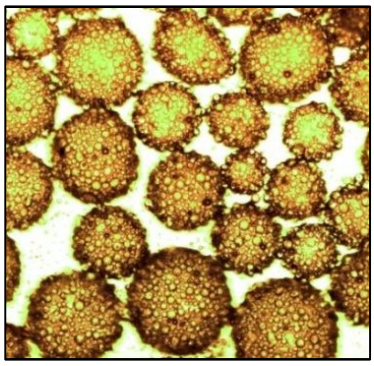

Figure 6.7: S200 silicone oil droplets stabilized by modified glass beads (22.4 µm)

6.2.3.2.5 Mixing and circulation time

The mixing and circulation times of the emulsion were evaluated using a published decolorization technique (F. Cabaret et al., 2007), which is based on an image analysis of the color of an acid-base tracer (bromocresol purple). The emulsion was prepared using silicone oil

(S200), glass microspheres, and distilled water, after which 1 mL of a 10 M NaOH solution was added. The bromocresol purple was then added to the tank during mixing. Once the mixture turned fully purple, 0.5 ml of a 12 M HCl solution was added, and the change in color to fully yellow was recorded using a Digital Handycam DCR-PC101 camera (Sony). The video was analyzed frame-by-frame using customized software. Mixing time was calculated by determining rate at which the color changed from fully purple to fully yellow (Figure 6.8). To ensure that there were no dead zones in the tank, the procedure was repeated using water. The results showed that the fluid was well mixed. Circulation time was considered to be 20% of the mixing time (t_c = 1/5 t_m) based on the assumption that the circulation time defines the time required for a fluid particle to leave and return to the impeller zone (E. L. Paul et al., 2004).

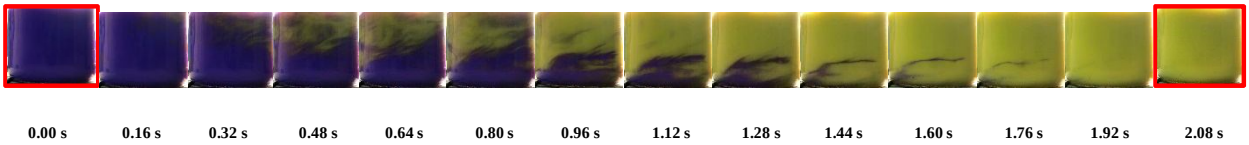

Figure 6.8: Typical color change during the mixing of a solid-stabilized emulsion

6.2.4 Results and discussion

6.2.4.1 Effect of emulsification time and coverage potential on the emulsification process

The effect of emulsification time and coverage potential on the effectively covered interface is represented on Figure 6.9. Coverage potentials were obtained from particle amount in the system according equation (6.2). The effectively covered interface increased with the coverage potential. The effectively covered interface also increased over time until equilibrium was reached. This increase was much more significant at high coverage potentials (10.71 m^2, 13.39 m^2, 16.07 m^2, and 18.75 m^2) for which equilibrium was reached after 3 h of emulsification while equilibrium was reached much faster at low coverage potentials. Based on the assumption that the interface is first generated by droplet breakage, following which particles are adsorbed and droplets are stabilized, interface generation and particle adsorption should be taken into consideration.

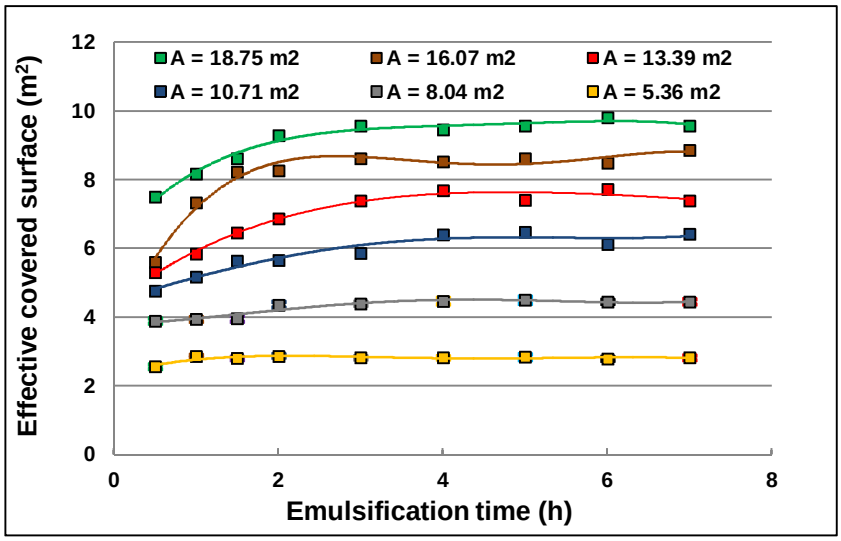

Figure 6.9: Effect of emulsification time and coverage potential on the final coverage of the interface

(A is the coverage potential obtained for different particle concentrations)

(O/W: 53%v, D_p: 22.4 µm, μ_{S1000}: 971 mPa·sec, Re = 23000)

Many studies have focused on the prediction of d_{32}. Most of the reported correlations are based on a balance between disruptive and cohesive forces and have proposed the equation shown below to calculate d_{32} (Paul E.L. et al. (2003)).

$$\left(d_{32} = \frac{6V}{A}\right) \sim C \cdot We^{-0.6} \cdots (6.5)$$

$$We = \frac{\rho_c N^2 D^3}{\sigma} \cdots (6.6)$$

$$\rho_c = \frac{m_w + m_p}{m_w/\rho_w + m_p/\rho_p} \cdots (6.7)$$

where V is the dispersed phase volume, A the dispersed phase interface, C the constant characterizing the emulsification system, We the Weber number, N the impeller speed, D the impeller diameter, σ the interfacial tension, ρ_c the continuous phase density, ρ_w the water density, ρ_p the particle density, m_w the mass of water, and m_p the mass of the particles.

Based on equation (6.5), the dependence of the interface on the properties of the continuous phase, especially density, can be expressed using the following equation:

$$A_{gen} \sim {\rho_c}^{0.6} \left(\frac{N^2 D^3}{\sigma}\right)^{0.6} \frac{6V}{C} \cdots (6.8)$$

Given similar materials and mixing conditions, the effect of the particle amount on the continuous phase density between two experiments i and j can be expressed as follows:

$$\frac{A_i}{A_j} \sim \left(\frac{\rho_{c_i}}{\rho_{c_j}}\right)^{0.6} \cdots (6.9)$$

The effect of the coverage potential ratio A_i/A_{max} (A_{max} being the largest stabilized interface corresponding to the highest particle loading) on the interface generated and final coverage interface ratios were plotted (Figure 6.10). As can be seen, the generated interface ratio increased from 85% to 100%, while changes in the effectively covered interface were closer to the changes in coverage potential, indicating that coverage potential has a greater impact on the stabilization process.

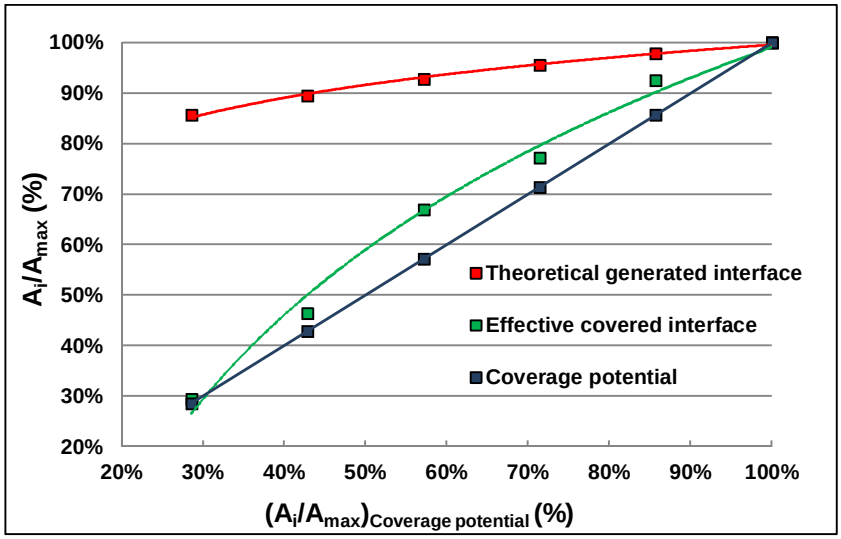

Figure 6.10: Effect of coverage potential ratio on the effectively covered interface ratio

(O/W: 53%v, D_p: 22.4 μm, μ_{S1000}: 971 mPa·sec, Re = 23000)

Droplet stabilization is affected by particle loading through the effect on particle/droplet collision frequency and collision efficiency. Many coalescence models have been proposed to describe these processes. In the case of a turbulent stirred tank, such as the one we used, it is usually

assumed that the collision mechanism is driven by the fluctuating turbulent velocity of the continuous phase. Like the coalescence approach and given an isentropic turbulent flow field (inertial regime), the particle/droplet collision frequency can be related to the energy dissipation rate (Coulaloglou C. A. and Tavlarides L. L., 1977; Lee C.-H. et al., 1987; Prince M. J. and Blanch H. W., 1990; Luo H., 1993; Colin C. et al., 2004; Carrica P. M. et al., 1999, Wang T. F. et al., 2005a, 2005b) and can be expressed using the following equation:

$$\xi\left(D_p, D_d\right) \sim \varepsilon^{1/3} \cdots (6.10)$$

The collision force can also be related to the energy dissipation rate based on the following equations proposed by V. G. Levich (1962):

$$F_c \approx \frac{\pi}{2}\rho_c \varepsilon^{2/3}\left(\frac{D_d D_p}{D_d + D_p}\right)^{8/3} \quad for \quad \left(\frac{D_d D_p}{D_d + D_p}\right) \geq \lambda \cdots (6.11)$$

or

$$F_c \approx \frac{\pi}{4}\rho_c^2 \frac{\varepsilon\left(\frac{D_d D_p}{D_d + D_p}\right)^4}{\mu} \quad for \quad \left(\frac{D_d D_p}{D_d + D_p}\right) < \lambda \cdots (6.12)$$

where F_C is the collision force, ε the turbulent energy dissipation rate, λ the Kolmogorov length scale ($(\nu^3/\varepsilon)^{1/4}$), D_p the particle diameter, and D_d the droplet diameter.

The average energy dissipation rate can be calculated from the operating conditions using equations (6.13) and (6.14).

$$P = N_P \cdot \rho_c \cdot N^3 \cdot D^5 \cdots (6.13)$$

$$\varepsilon_{avr} = \frac{P}{m_t} = \frac{N_P \cdot \rho_c \cdot N^3 \cdot D^5}{m_t} \cdots (6.14)$$

where P is power consumption, N_P the power number ($N_P^{PBT} = 1.2$), ε_{avr} the average turbulent energy dissipation rate, and m_t the theoretical mass of the system (water, oil, and particles).

The effect of coverage potential on the Weber number and average energy dissipation can be represented as shown in Figure 6.11. The plots show that an increase in particle concentration causes a decrease in the average energy dissipation rate and an increase in the Weber number, leading to an increase in interface generation and a decrease in the stabilization rate. The addition of more particles thus does not necessarily increase stabilization efficiency, and the optimal

concentration should be determined to ensure an acceptable coverage level for a given level of interface generation.

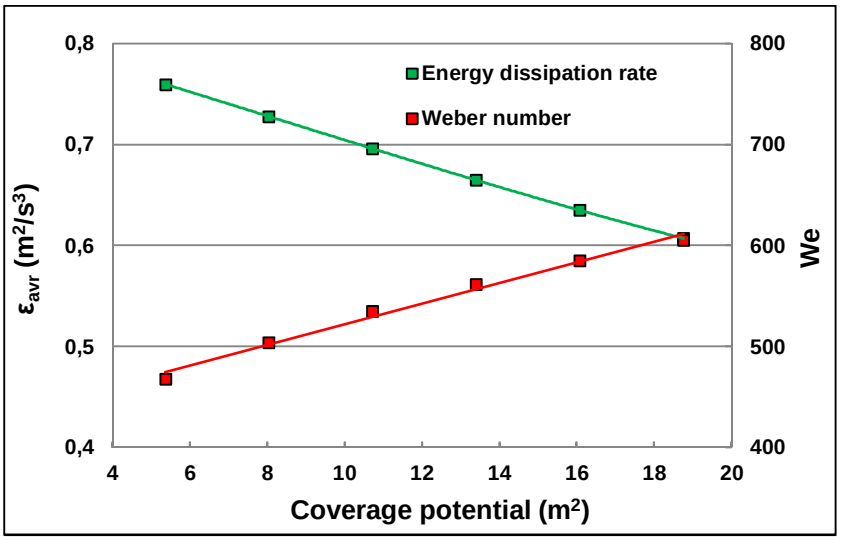

Figure 6.11: Effect of coverage potential on ε_{avr} and We

(O/W: 53%v, D_p: 22.4 μm, μ_{S1000}: 971 mPa·sec, Re = 23000)

The combined effect of the Weber number and the energy dissipation rate is shown in Figure 6.12, which also presents the effects of emulsification time and the theoretical coverage potential (particle concentration) on the effective covered interface/theoretical covered interface ratio. The results of the four emulsification time experiments showed that stabilization efficiency initially increases with the coverage potential until a maximum at approximately 10.71 m^2 is reached and then subsequently decreases. This effect can also be seen in Figure 6.13, which shows the effect on distribution width. Optimal values are thus obtained with the three intermediate coverage potentials were 10.71 m^2, 13.39 m^2, and 16.07 m^2. The initial increases in emulsification efficiency seen on Figures 6.12 and 6.13 can be attributed to increases in breakage and the coverage potential of the system. However, adding more particles resulted in a reduction in the turbulent energy dissipation rate and in stabilization efficiency.

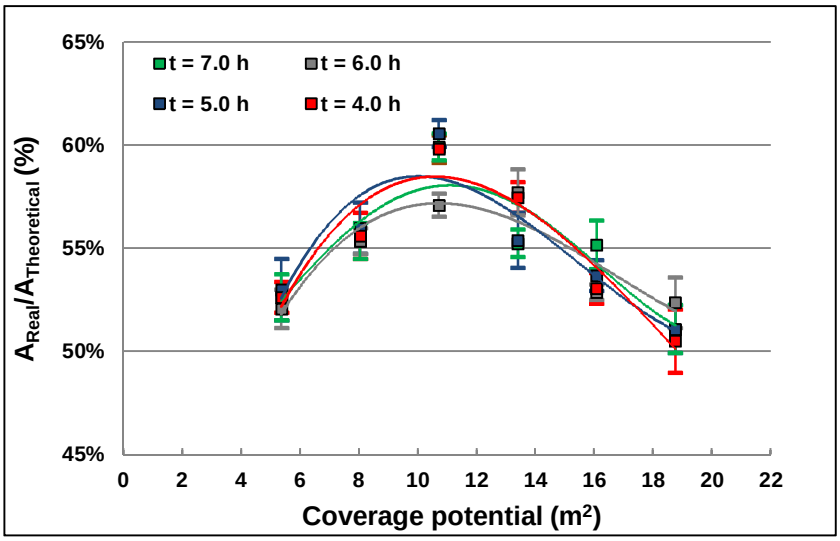

Figure 6.12: Effect of coverage potential and emulsification time on $A_{Real}/A_{Theoretical}$

(O/W: 53%v, D_p: 22.4 µm, μ_{S1000}: 971 mPa·sec, Re = 23000)

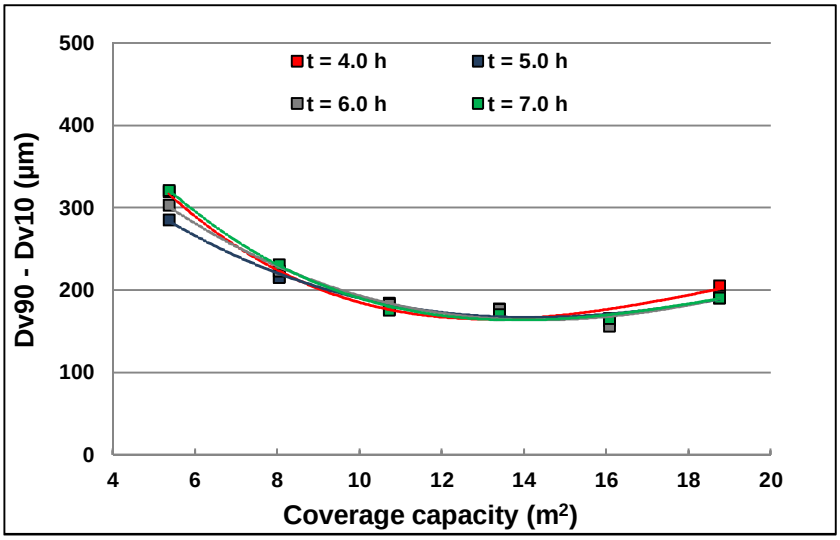

Figure 6.13: Effect of coverage potential and emulsification time on distribution width

(O/W: 53%v, D_p: 22.4 µm, μ_{S1000}: 971 mPa·sec, Re = 23000)

6.2.4.2 Effect of oil viscosity and emulsification time on the emulsification process

Figure 6.14 shows the effect of oil viscosity on the effective covered interface for different oil viscosities using the same emulsification conditions (formulation, coverage potential, and mixing intensity). The effective covered interface increased when the oil viscosity was lowered. This was caused by the breakage and stabilization processes. Decreasing the oil viscosity promoted both

interface generation and particle attachment. Calabrese et al. (1986) highlighted the effect of oil viscosity on droplet size and, as such, on the interface generated and proposed the following equations for calculating the Sauter mean diameter:

$$\frac{d_{32}}{D} = 0.053 \cdot We^{-0.6} \cdot (1 + 0.97 \cdot Vi^{0.79})^{0.6} \cdots (6.15)$$

$$Vi = \frac{\mu_d N D}{\sigma}\left(\frac{\rho_c}{\rho_d}\right)^{0.5} \cdots (6.16)$$

where μ_d is the dispersed phase dynamic viscosity and ρ_d the dispersed phase density.

The effect of the oil viscosity ratio (μ_i/μ_{min}) on the A_i/A_{max} ratio (A_{max} being the largest stabilized interface corresponding to the lowest oil viscosity μ_{min}) is shown in Figure 6.15:

$$\frac{A_i}{A_j} \sim \left(\frac{1/(1 + 0.97 \cdot Vi^{0.79})_i}{1/(1 + 0.97 \cdot Vi^{0.79})_j}\right)^{0.6} \cdots (6.17)$$

The theoretical size of the interface generated, which was calculated using equation (6.17), as well as the effective covered interface, increased when oil viscosity was reduced. However, the increase was much more significant when interface generation alone was taken into consideration, whereas the effective covered interface was less dependent on the interface generation potential. The decrease in the effective covered interface highlighted again the importance of the stabilization mechanism and coverage efficiency. Indeed, coverage efficiency depended on dispersed phase viscosity since particle/droplet contact was enhanced (easier film drainage due to droplet surface mobility) while particle adsorption was faster, which promoted stabilization. However, equilibrium was reached more slowly when oils with lower viscosities were used, especially at the lowest oil viscosity (S20). This behavior is related to the interface generation process. Oils with lower viscosities generated a larger interface ($A_{S20}/A_{S200}\approx2$ and $A_{S20}/A_{S1000}\approx3$) that had to be covered. In turn, since more particles were adsorbed, the stabilization process took longer.

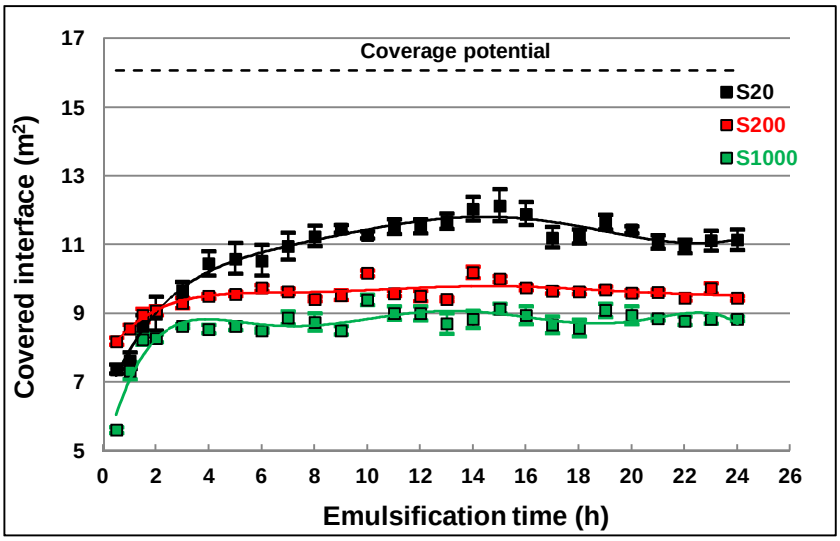

Figure 6.14: Effect of emulsification time and oil viscosity on the covered interface

(O/W: 53.5%v, D_p: 22.4 µm, Re = 23000)

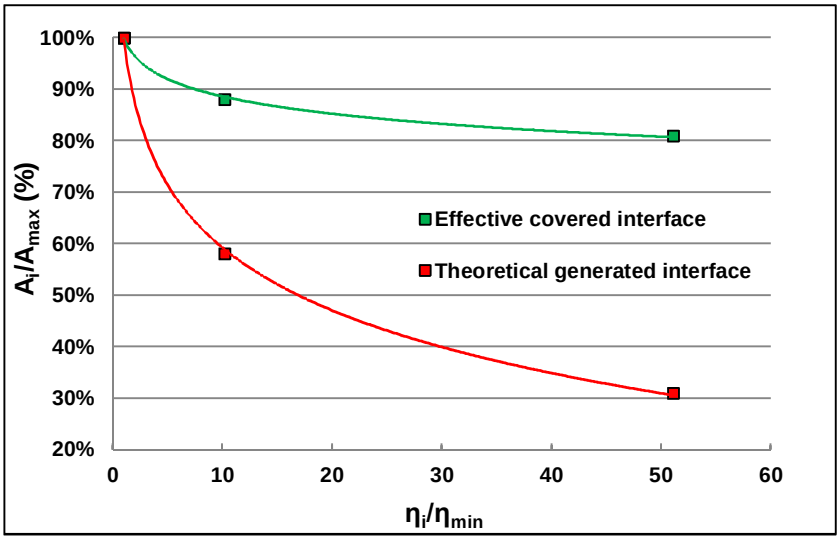

Figure 6.15: Effect of oil viscosity on the effectively covered interface ratio and the theoretical generated interface ratio

(O/W: 53.5%v, coverage potential: 16 m^2, D_p: 22.4 µm, Re = 23000)

If the less viscous oil (S20) and the most viscous one (S1000) are considered, it can be observed on Figure 6.16 that the largest d_{V10} and d_{V90} were obtained with the viscous oil S1000 which makes sense since less interface is generated and the stabilization efficiency is reduced when the oil viscosity is increased. When considering the results of the intermediate viscosity oil (S200), the largest d_{V10} and the smallest d_{V90} as well as the narrowest distribution (Figure 6.17) were

obtained. This behavior highlighted the complex interaction between the involved mechanisms during emulsification by particles, including breakage, coalescence and particles adsorption and desorption. With reduced oil viscosity, the breakage process is more significant and smaller droplets are produced. However, depending on the coverage level and the droplet/droplet collision rate, the coalescence is also promoted because the interface mobility and the non-deformability of small droplets (higher Laplace pressure). No complete explanation can be offered at the moment and further investigation is under way.

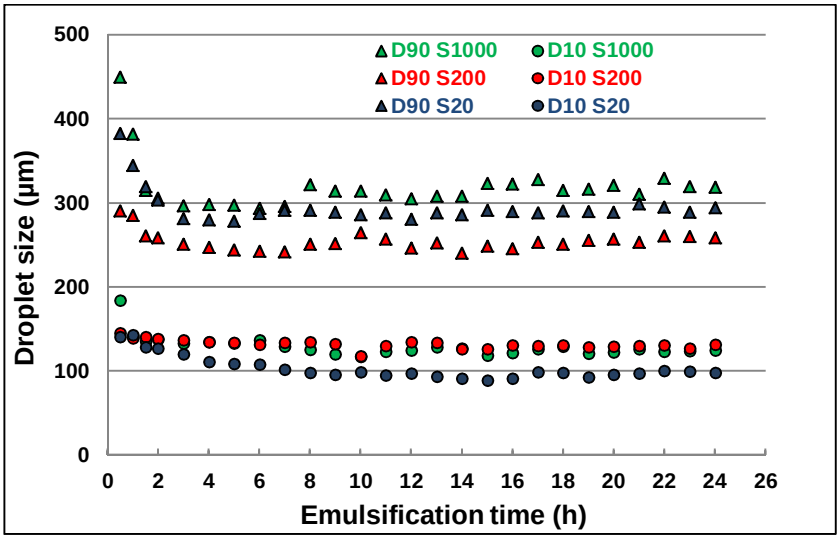

Figure 6.16: Effect of emulsification time and oil viscosity on droplet size

(O/W: 53.5%v, coverage potential: 16 m^2, D_p: 22.4 µm, Re = 23000)

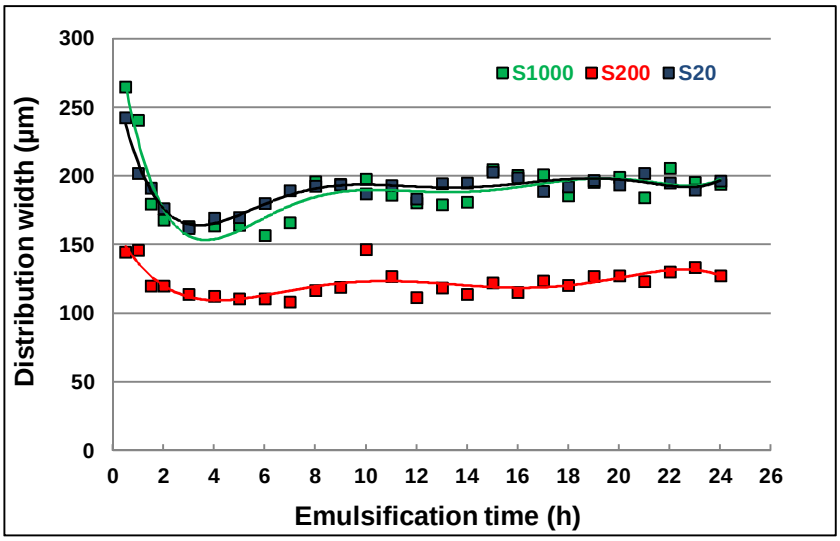

Figure 6.17: Effect of emulsification time and oil viscosity on distribution width

(O/W: 53.5%v, coverage potential: 16 m^2, D_p: 22.4 µm, Re = 23000)

6.2.4.3 Effect of Weber number and emulsification time on the emulsification process

Figure 6.18 illustrates the combined effect of emulsification time and the Weber number on the effective covered interface. Weber numbers are related to the impeller speed through equation (6.6). The plots shows the change in effective covered interface over 7 h of mixing at different Weber number. The covered interface increased over time until it reached equilibrium. Equilibrium was reached more quickly at higher impeller speeds, indicating that the stabilization process can be accelerated by increasing the energy level. However, Figure 6.18 also shows that the largest covered interface was obtained with an intermediate Weber number (We = 394.43). The generation of a smaller interface by increasing the impeller speed was unexpected. However, increasing the impeller speed increased the particle/drop collision force even more, making droplet interface deformation more significant, which in turn increased the film drainage time (Chesters A. K., 1991).

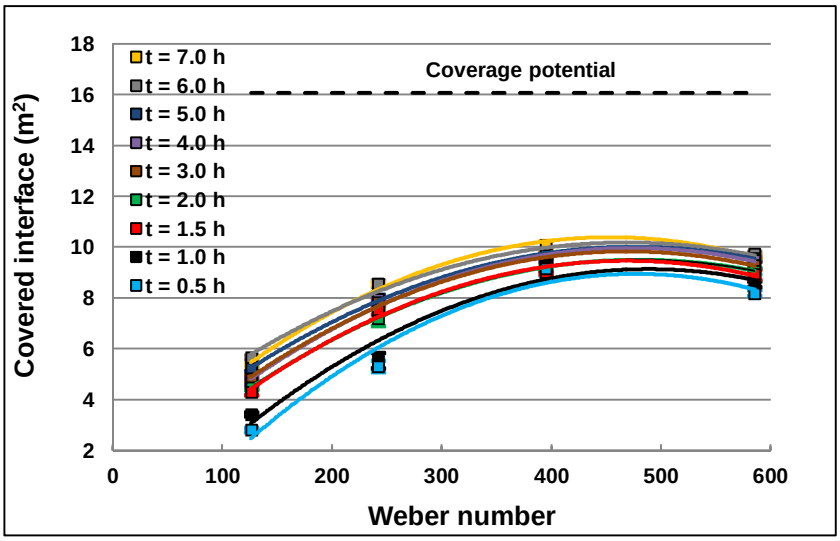

Figure 6.18: Effect of emulsification time and Weber number on the covered surface

(O/W: 53.5%v, D_p: 22.4 µm, μ_{S200}: 194 mPa·sec)

Increasing the impeller speed, represented by the Weber number, also reduced the circulation time (Figure 6.19), returning the droplets more quickly to the high shear zone of the impeller where the particles can be sheared off from the interface, thus reducing stabilization efficiency. As such, beyond a given impeller speed, particle adsorption time has to be short enough to allow the particles to attach with sufficient strength in order to counteract the detachment forces.

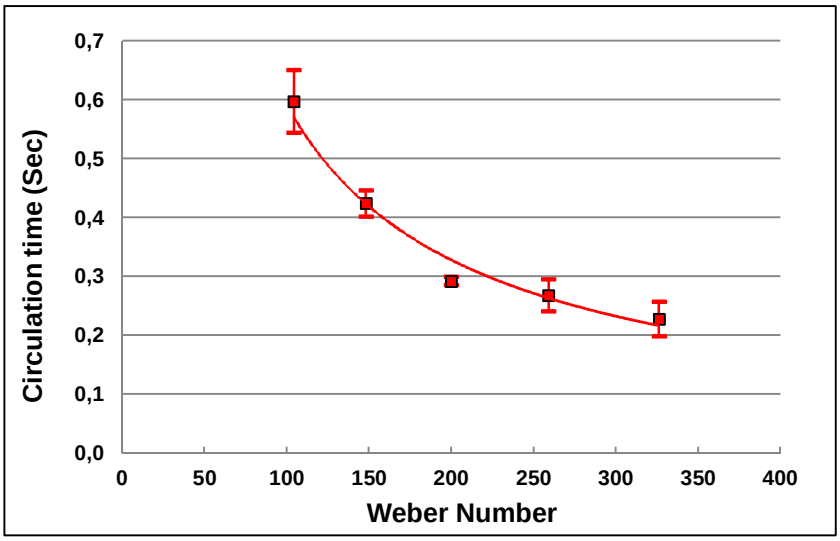

Figure 6.19: Effect of Weber number on circulation time

(O/W: 53.5%v, μ_{S200}: 194 mPa·sec)

6.2.4.4 Effect of oil viscosity and Weber number on the emulsification process

The combined effect of oil viscosity and Weber number (Weber number ~ impeller speed^2) on the covered surface is shown in Figure 6.20. The covered surface decreased with an increase in oil viscosity, as shown in Figure 6.13. However, the Weber number provided a different perspective on the energy level effect. With viscous oils, the maximum value of the covered interface was obtained at an intermediate Weber number (We ≈ 200). This behavior was analogous to the behavior illustrated in Figure 6.17 at different operating conditions (oil viscosity, particle concentration and impeller speed). The optimal value of the Weber number depended on the combined effect of the impeller speed on the particle/droplet collision force and the circulation time. However, this effect was only observed with the most viscous oils (S500, S1000, and S5000), indicating that there is a strong interaction between oil viscosity and impeller speed. When the viscosity of the oil was increased, larger droplets were produced with a lower Laplace pressure making the droplet deformation more significant during particle/droplet collision and resulting in slower film drainage. Film drainage was also hindered because the interface was less mobile when more viscous oils were used. On the other hand, increasing the impeller speed reduced the circulation time, allowing the droplets to return more quickly to the impeller zone. Particle adsorption was slower and, as such particle detachment was more pronounced with higher viscosity oils, which would explain the shape of the plots in Figure 6.20.

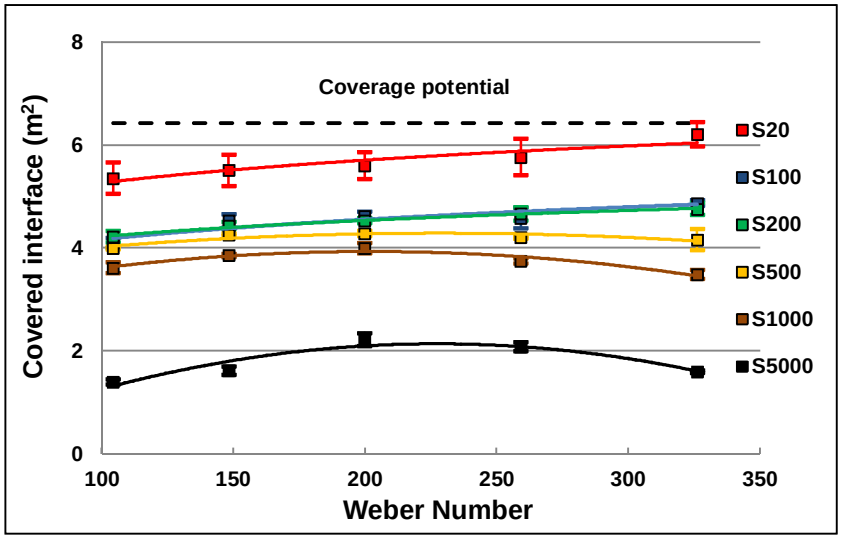

Figure 6.20: Effect of oil viscosity and Weber number on the covered interface

(O/W: 53.5%v, D_p: 22.4 μm)

The distribution width results tended to confirm the proposed mechanism for explaining the effect of oil viscosity. Figure 6.21 shows that the smallest distribution widths were obtained with intermediate viscosity oils (S100 and S200), as can also be seen on Figure 6.15 for different operating conditions. This behavior is also related to equilibrium between interface generation, stabilization and coalescence processes.

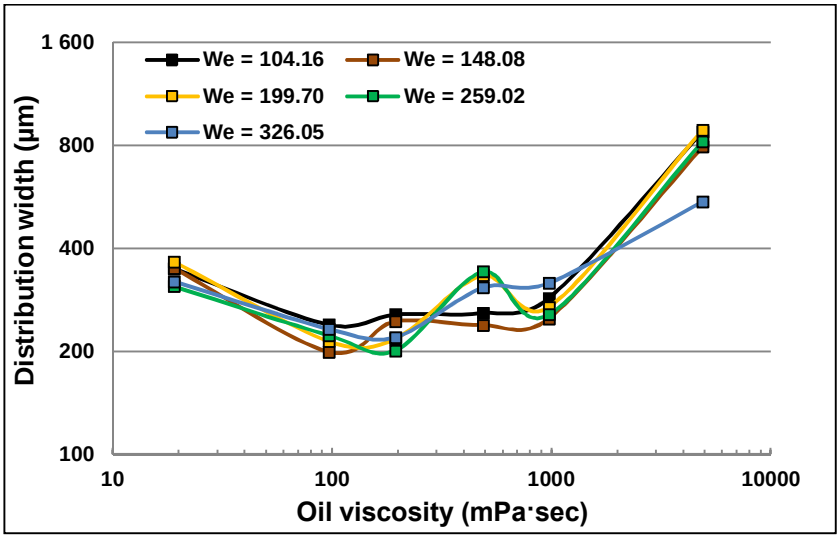

Figure 6.21: Effect of oil viscosity and Weber number on the distribution width

(O/W: 53%v, coverage potential: 6.43 m^2, D_p: 22.4 µm)

6.2.5 Conclusions

The effects of emulsification time and impeller speed on the stabilization of Pickering emulsions were investigated from a process design perspective. Concentrated emulsions (53%v) were prepared using a standard mixing configuration. Emulsification experiments were performed in an unbaffled 1-L tank using an off-centered pitched-blade turbine in order to study the effects of particle concentration, oil viscosity, impeller speed and emulsification time. Emulsion efficiency was quantified by droplet size distribution measurements using a Mastersizer 3000 (Malvern). Mixing and circulation times were evaluated using a decolorization technique.

It was assumed that the interface is first generated during the emulsification process through droplet breakage in the impeller zone, that the droplets are then covered and stabilized by the adsorption of particles at the interface, and that partially covered and uncovered droplets

subsequently coalesce. These processes are repeated throughout the emulsification operation until a droplet size distribution equilibrium is reached.

We showed that the equilibrium time could be increased by increasing the surface of the interface and/or by reducing the frequency of particle/droplet collisions. We also showed that optimal conditions have to be determined given that two processes (droplet breakage and droplet coverage) are involved. Facilitating the generation of the interface reduced droplet stabilization efficiency as well as the interface generation efficiency is affected if coverage is promoted. Stabilization efficiency increased with particle concentration due to the increase in both breakage and the coverage potential. However, stabilization efficiency decreased when the particle concentration exceeded a certain limit. This occurred due a decrease in the turbulent energy dissipation rate driving the particle/droplet collision force and hence the particle attachment process. Depending on the oil viscosity, increasing the impeller speed increased the effectively covered interface due to the increase in the interface generation capacity of the system. However, beyond an intermediate Weber number value, the effectively covered interface decreased due to the slowing of film drainage during particle/droplet collisions, which was due to droplet deformation caused by the increase in the collision force. This was more marked with the lower Laplace pressure of large droplets when high viscosity oils were used (low interface generation capacity). Film drainage during collision was also affected by oil viscosity through the effect of viscosity on interface mobility. High viscosity oils reduced film drainage, thus hindering collision and adsorption. The use of high viscosity oils also resulted in less efficient adsorption because the increase in adsorption time compared to circulation time made the particles more sensitive to shearing off in the impeller zone. However, an unexpected effect of oil viscosity was observed with the distribution width in that the narrowest distribution width was obtained with intermediate viscosity oils, which was the result of a combination of the effects of breakage, coalescence, and particle adsorption.

In summary, the stabilization of emulsions by particles is controlled by the interface generation mechanism, which is in turn controlled by the Weber number in the impeller zone and the particle adsorption mechanism, which is notably affected by the energy dissipation rate and circulation time.

6.2.6 Acknowledgments

The authors gratefully acknowledge financial support from the Natural Sciences and Engineering Research Council of Canada and TOTAL.

CHAPITRE 7. ARTICLE 5: A SEMI-EMPIRICAL APPROACH FOR PREDICTING THE MEAN SIZE OF SOLID-STABILIZED EMULSIONS

7.1 Présentation du cinquième article

Soumis dans : AIChE Journal

Auteurs : Èmir Tsabet, Louis Fradette

Dans cet article une approche semi-empirique a été adoptée pour déduire le diamètre moyen d'émulsions de Pickering produites dans une cuve agitée. Le dispositif consiste en une turbine à pales inclinées décentrée dans une cuve sans chicanes. Des émulsions concentrées ont ainsi été préparées en utilisant des huiles silicones comme phases dispersées et des microbilles de verre comme agent stabilisant. Le model proposé est basé sur la comparaison de la capacité du système à générer de l'interface à sa capacité à la couvrir par des particules afin de déduire l'interface théoriquement couverte par des particules. La deuxième étape consiste à déduire ensuite l'interface réellement couverte par des particules en et en déduire l'interface théorique couverte par taille finale a les effets des conditions opératoires sur les performances d'émulsification par des particules solides ont été étudiés. Un dispositif de mélange en cuve agitée a été utilisé, incluant une turbine à pales inclinées décentrée dans un bécher d'un litre sans chicanes. Les résultats ont révélé une forte interaction entre les paramètres affectant l'hydrodynamique du système soulignant ainsi la nécessité de définir des conditions optimales pour obtenir la plus petite taille de gouttes avec la plus étroite distribution possible. Cette interaction est notamment due à la présence de deux différents processus durant l'émulsification, la génération de gouttes et leur couverture ou stabilisation. Il a ainsi été observé que l'augmentation du niveau d'énergie favorisait la generation d'interface mais, au-delà d'une certaine limite, pouvait réduire l'efficacité de stabilisation. De même, il a été trouvé que celle-ci pouvait également être réduite par l'augmentation de la quantité de particules. Globalement, il a été établi que les conditions optimales d'émulsification dépendaient du niveau de cisaillement, du taux de dissipation de l'énergie cinétique turbulente et du temps de circulation.

7.2 A semi-empirical approach for predicting the mean size of solid-stabilized emulsions

7.2.1 Summary

The final mean droplet size of concentrated solid-stabilized emulsions was predicted using a semi-empirical approach. The first step was to estimate the coverage and interface generation potentials. The coverage potential was predicted from the properties of the particles while the interface generation potential was predicted from the correlation developed by R. V. Calabrese et al. (1986), which was modified to include the effect of coalescence since the effects of high oil and particle concentrations on the breakage and coalescence processes had to be taken into consideration. The second step was to compare the coverage and interface generation potentials and to deduce the theoretical stabilized interface by assuming that it is equal to the lowest potential. The last step was to determine the effectively covered interface from the theoretical stabilized interface by considering stabilization efficiencies. The stabilization efficiency was defined by analyzing the stabilization process at the droplet and the individual particle scales. At the droplet scale, assuming that emulsions are stabilized by covering the droplets with a network of particles, coverage efficiency was defined by comparing the coverage rate to the coalescence rate. At the particle scale, assuming that the droplet coverage results from the attachment of individual particles, three other efficiencies were defined from the particle attachment steps: The particle and the droplet first enter into contact during the collision step; the three-phase contact line is then formed and evolves until reaching the equilibrium position at which the attachment force should be enough strong to avoid detachment. This approach generated size predictions that were in good agreement with the experimental results for a broad range of viscosities at different impeller speeds and particle concentrations. This led to highlight the impact of operating conditions on the emulsification process. However, more experimental results are required to assess the effects of all the relevant parameters. We show that it is possible to link emulsification systems to different geometries by taking the mechanisms driving the emulsification process into consideration suggesting new avenues for scaling up emulsification processes.

7.2.2 Introduction

Emulsification is a common industrial process used to produce stable liquid-liquid dispersions. Depending on the application, different properties are taken into consideration to characterize these complex systems. Nevertheless, the main objective of most processes is to obtain an emulsion with the smallest droplets, the narrowest size distribution, and the longest life time. This is why most studies have focused on characterizing size distribution and developing models and correlations to predict size distributions. Two main approaches have been used. The goal of the first approach, which is empirical or semi-empirical in nature, is to develop a correlation that predicts the characteristic size of emulsions (d_{32}, d_{43}, d_{max}, d_{10}, $d_{90,}$ etc.) from experimental results and from physical properties based on a balance between energies, stresses, and forces that promote or prevent droplet generation. This approach has notably been used by H.T. Chen et al. (1967), D.E. Brown et al. (1970), J.W. Van Heuven et al. (1971), C.A. Coulaloglou et al. (1976), and R.V. Calabrese et al. (1986) to link the Sauter mean diameter to the Weber number using the following general formula:

$$D_{32} \sim We^{-0.6} \cdots (7.1)$$

However, the application of this formula is generally limited to specific conditions and cannot necessarily be applied to other conditions.

The second approach is based on modeling the relevant mechanisms driving the emulsification process (droplet generation, droplet stabilization, and droplet coalescence). Since surfactant-stabilized emulsions are stabilized by reducing the interfacial tension, only two aspects are taken into consideration to model the emulsification process, including solving a population balance formula that takes the breakage and coalescence rates into consideration. This approach was initially developed by K.J. Valentas et al. (1966) to quantify droplet size distributions during the emulsification process and is similar to a mass balance in a controlled volume. It uses an accumulation term of the number of droplets of a given class size (i), a convective term, a production term, and a sink term:

$$\frac{\partial n_{d_i}}{\partial t} + \nabla \cdot \left(\overline{U} n_{d_i}\right) - \dot{B}_{d_i} + \dot{D}_{d_i} = 0 \cdots (7.2)$$

where n_{di} is the number of class i droplets, $\bar{U}$ is the mean flow velocity, B_{di} is the birth rate of class i droplets, and D_{di} is the death rate of class i droplets.

The class i birth and death rates are calculated by taking the coalescence and breakage rates into consideration. The droplet breakage rate is modeled by defining a breakup frequency and a daughter size distribution. Y. Liao and D. Lucas (2009) reviewed the most common breakup frequency models in a turbulent regime that are based on the following assumptions for estimating the mean droplet size at a given equilibrium:

a) The turbulent kinetic energy of a fluid particle exceeds a critical value,
b) The velocity fluctuation around the particle surface is greater than a critical value,
c) The turbulent kinetic energy of the hitting eddy is greater than a critical value, and
d) The inertial force of the hitting eddy is greater than the interfacial force of the smallest daughter particle.

Critical values were defined by considering forces, stresses or energies promoting the breakage and those preventing it.

On the other hand, Y. Liao and D. Lucas (2009) reviewed three approaches in the literature to define the daughter size distribution:

a) The statistical model that considers the daughter size distribution as a random variable with a probability density following a normal, beta, or uniform distribution function,
b) The phenomenological model that is derived from physical considerations and that classifies daughter size distributions into Bell-shaped, U-shaped, and the M-shape forms, and
c) The empirical model that is based on experimental observations.

The coalescence rate is generally quantified by defining a coalescence frequency based on an empirical approach (H. Wright et al., 1994; M. Konno et al., 1988) or on physical considerations, where the coalescence frequency is defined as the product of the droplet collision frequency and the coalescence efficiency:

$$\Gamma(d, \acute{d}) = \lambda(d, \acute{d}) \cdot \xi(d, \acute{d}) \cdots (7.3)$$

where Γ (d, d´) is the coalescence frequency, λ (d, d´) is the coalescence efficiency, and ξ (d, d´) is the collision frequency.

Different models of the collision frequency in turbulent regimes that take turbulence fluctuations into consideration have been published (C.A. Coulaloglou and L.L. Tavlarides, 1977; C.-H. Lee et al., 1987; M.J. Prince and H.W. Blanch, 1990; H. Luo, 1993; C. Colin et al., 2004; P.M. Carrica et al., 1999; T.F. Wang et al., 2005a, 2005b). The film drainage model, which takes the squeezed film flow between droplets during collision into consideration, is the approach most commonly used to determine coalescence efficiency (M.J. Prince and H.W. Blanch, 1990; A.K. Chesters, 1991; C. Tsouris et al., 1994).

Once the breakage and coalescence rates have been defined, which is not a straightforward operation, the population balance formula is solved using numerical methods, and the instantaneous droplet size distribution is estimated. However, solving these formulas is very complex because of their non-linearity and the interactions between their different terms, which involve many simplification assumptions. In addition, if solid-stabilized emulsions are considered, additional complexities are added by introducing the stabilization rate associated with the formation of the particle network around the droplets. In the population balance formula, this new term will affect both the breakage and the coalescence rates as well as the particle effect on stabilized droplet behavior (creaming, settling, coagulation) and on the hydrodynamics of the system. As such, empirical or semi-empirical approaches appear to be the best choice if a less costly solution is required.

In the present work, a semi-empirical approach was used to predict the mean droplet size of a concentrated solid-stabilized emulsion (silicone oil in water stabilized by glass beads) from the process conditions. It was assumed that droplets are first generated and that the particles then start to be adsorbed and the droplets stabilized. The Calabrese correlation, which takes interfacial and viscous effects on droplet cohesive energy into consideration, was adapted to describe the coalescence rate and the particle effect. Our goal was to compare the coverage potential to the interface generation potential in order to determine the mechanism controlling the stabilization process. Different efficiencies based on physical considerations were introduced to describe particle/droplet interactions during particle/droplet collisions, particle adsorption at the interface, and particle desorption from the interface.

7.2.3 Emulsification setup

Emulsions were prepared with a standard configuration using an unbaffled 1 L beaker to ensure a simple flow field and to generate a controlled turbulence level. An off-centered, pitched-blade impeller was used to avoid vortex formation (Figure 7.1). In terms of mixing performances, this system is equivalent to a centered impeller with baffles for the considered regimes (Nishikawa M. K. et al., 1979; Novak V. P. et al., 1982; King R. et al., 1985; Karcz J. et al., 2004, 2005; Montante G. A. et al., 2006). Concentrated emulsions (O/W: 53%v) were produced using silicone oils (Clearco) as the dispersed phase (Table 7.1), distilled water as the continuous phase, and modified soda lime glass beads (Potters Industries) as the stabilizer (Table 7.2). The water was mixed at a given impeller speed, and the particles were added and were mixed for 10 minutes to homogenize the dispersion and break up aggregates. The oil was then gently added, and samples were taken at different times (Figure 7.2).

Tableau 7.1: Physical properties of silicone oils

Silicone Oils	Density (kg/m^3)	Dynamic Viscosity (mPa·sec)	Interfacial Tension (N/m)
S10	935	9.35	4.2E-02
S20	950	19.00	4.2E-02
S50	960	48.00	4.2E-02
S100	966	96.60	4.2E-02
S200	968	193.60	4.2E-02
S500	971	485.50	4.2E-02
S1000	971	971.00	4.2E-02
S5000	975	4875.00	4.2E-02

Tableau 7.2: Physical properties of particles

Particles	Type	Density (kg/m^3)	D_{32} (μm)	Contact Angle
Spheriglass 3000E	Modified glass beads	2520	22.4	93° ± 3°

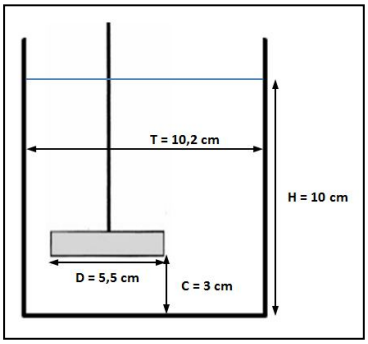

Figure 7.1: Emulsification setup

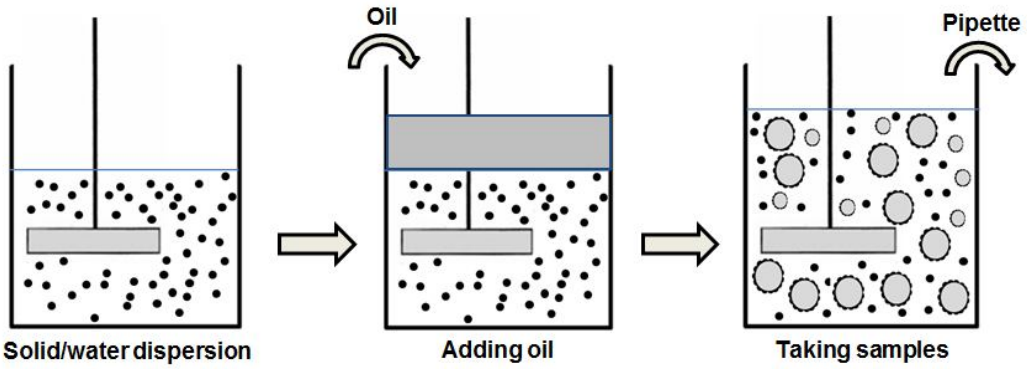

Figure 7.2: Emulsification procedure

It was assumed that droplets follow a flow loop in the tank (Figure 7.3). They are first generated in the impeller zone (breakage in the high shear zone) and are then stabilized by particle adsorption at the interface at a given rate based on the properties of the particle and the hydrodynamics of the system. Depending on the particle concentration, a limited coalescence zone is considered where uncovered and partially covered droplets coalesce. In this region, it was assumed that coalescence is not affected by the degree of adsorption of the particles and that the droplets are stable if they are fully covered irrespective of the particle attachment force at the interface. However, in the breakage zone, it was assumed that the particle attachment force plays a more significant role. If the hydrodynamic force is higher than the particle attachment force, particles can be sheared off from the interface, and the droplets can be destabilized by breakage. These processes are repeated during emulsification until the equilibrium size distribution is reached.

To assess the final size distribution, two possibilities were taken into consideration. In the first case, once the interface has been generated, if there are enough particles to cover the interface,

the final size distribution will depend on the capacity of the system to generate an interface. However, if there are not enough particles to cover the interface, the droplets will coalesce until the coverage capacity of the system is reached, and the final size distribution will depend on the coverage potential. In addition, since the droplet volume increases when particles are adsorbed, the swelling effect also has to be taken into consideration when assessing the final droplet size distribution.

However, this analysis does not take the particle attachment process, which is affected by the properties of the particle and the hydrodynamics of the system, into consideration. These aspects were assessed by studying different efficiencies associated to the particle attachment steps.

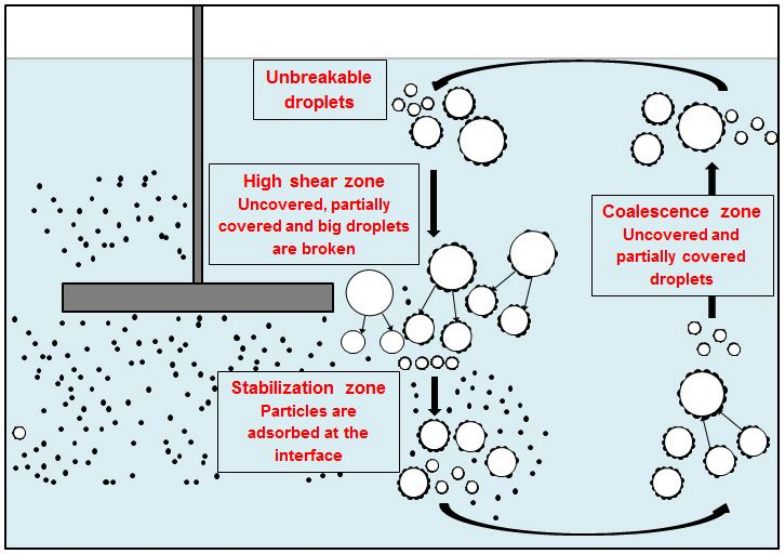

Figure 7.3: Typical representation of involved mechanisms during emulsification

7.2.4 Modelling approach

7.2.4.1 Apparent droplet size

The Sauter mean diameter (d_{32}) was measured using a Mastersizer 3000 (Malvern) and was used to determine the effectively covered interface. To estimate the final apparent droplet size, the swelling effect (S. Levine et al., 1991) of particle adsorption and the contribution of non-adsorbed part of adsorbed particles were taken into consideration. Following a geometrical analysis and using a Taylor development, S. Levine et al. (1991) obtained the following formula to describe the droplet swelling effect:

$$\left(\frac{R_{dII}}{R_{dI}}\right)^3 = 1 + N_{p/d}\left(R_p/4R_{dI}\right)\cdot\left(R_p/R_{dI}\right)^2 \cdot\left[(2+\cos\theta_{ow})\cdot(1-\cos\theta_{ow})^2 - \left(9R_p/4R_{dI}\right)\sin^2\theta_{ow} + \cdots\right]\cdots(7.4)$$

where R_{dI} is the droplet radius before particle adsorption, R_{dII} is the droplet radius after particle adsorption, R_p is the particle radius, θ_{ow} is the contact angle, and $N_{p/d}$ is the number of adsorbed particles per droplet.

In addition, the following formula was proposed to include the contribution of the non-adsorbed part of adsorbed particles in the apparent droplet diameter:

$$D_{apparent} = 2R_{dII} + \left(2R_p - h_{ads}\right)\cdots(7.5)$$

where h_{ads} is the adsorbed height of the particle.

7.2.4.2 Droplet coverage rate

As noted above, particle adsorption at the droplet interface causes swelling, which is a function of the adsorbed volume and the number of adsorbed particles. The adsorbed volume is a function of particle size and particle affinity with both phases while the second aspect depends on the number of particles required to stabilize the droplet. Much research has been devoted to this aspect, and it has been shown that the required coverage level is mainly a function of particle interactions and dynamics at the interface. On the one hand, while it has been suggested that droplets should be completely covered by at least one particle layer to ensure emulsion stability (N. Yan et al., 1994, 1995), other investigators have shown that it is not necessary to cover the entire droplet surface to stabilize it (S. Levine et al., 1989; B.R. Midmore, 1998; B.P. Binks et al., 2001; R. Vignati et al., 2003; S. Tarimala et al., 2004) because of the strong interactions between the particles and/or the particle dynamic at the interface.

We used silicone oils as a dispersed phase and glass beads as a stabilizer, and observed that the stabilized droplets were fully covered (Figure 7.4), suggesting that droplets have to be fully covered to be stabilized.

We defined the coverage rate based on the solution of the Fejes problem (L. Fejes Toth, 1953) for a sphere. L. Fejes Toth studied the arrangements of N equal sized spheres on a spherical surface and found that the coverage rate can reach $\pi/(2\sqrt{3})=0.9069$ with a hexagonal close-packed

configuration for an infinite radius of the covered sphere. We thus used this rate since the droplet radius was more than ten times larger than the particle radius.

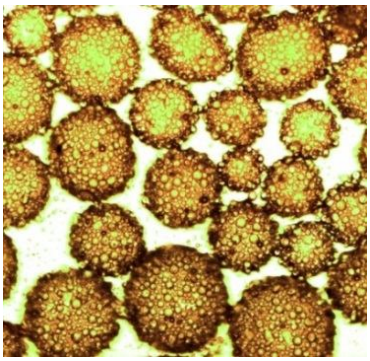

Figure 7.4: S200 silicone oil droplets stabilized by modified glass beads (22.4 µm)

7.2.4.3 Effectively covered interface

We estimated the effectively covered interface from the measured Sauter diameter since the overall oil volume, the number of particles covering a single droplet (based on coverage rate), and the particle adsorption level were known. The only unknown was the number of stabilized droplets because of the swelling effect. The following steps were used to estimate the effectively covered interface (Figure 7.5):

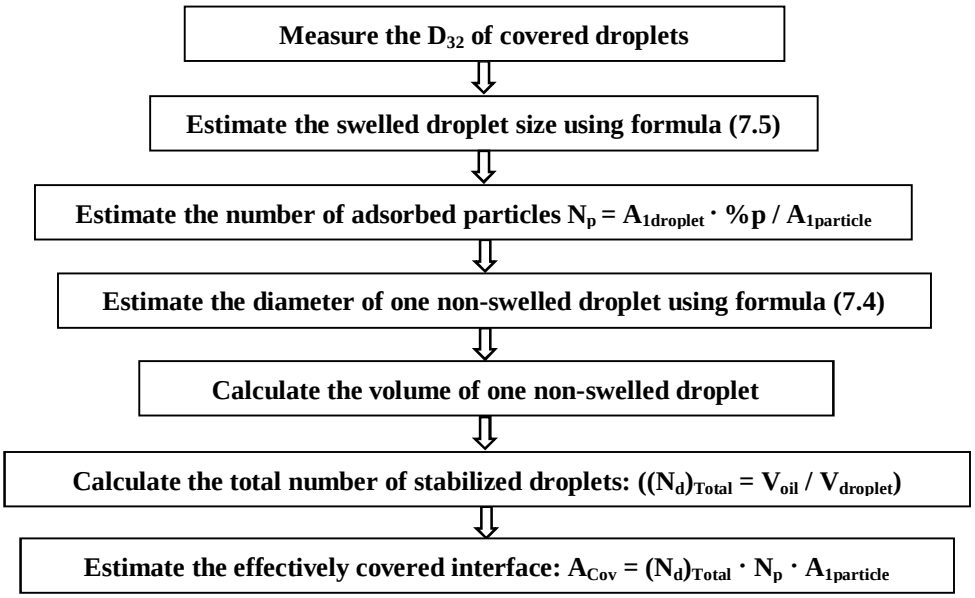

Figure 7.5: Calculation procedure of the effectively covered interface

7.2.4.4 Final droplet size based on the coverage potential

If the coverage potential is lower than the interface generated, the droplets coalesce until the coverage capacity of the system is reached. The final theoretical droplet size is thus a function of the coverage potential, irrespective of the interface generation potential of the system. As such, particle size, wettability, and amount as well as the coverage rate and the volume of the dispersed phase have to be known or calculated. The coverage potential was estimated from the properties of the particles (amount, size, and wettability) using the following formula for spherical particles:

$$A_{cov} = A_{cov/1p} \cdot \left(N_p\right)_{total} = \pi\left(R_p \sin\theta_{ow}\right)^2 \cdot \left(N_p\right)_{total} \cdots (7.6)$$

However, two iteration loops were required to estimate the swelled droplet diameter. The first loop was required to determine the non-swelled droplet size at which all the particles are adsorbed, while the second loop was required to estimate the swelled droplet diameter and the number of adsorbed particles per droplet. The steps are described on Figure 7.6.

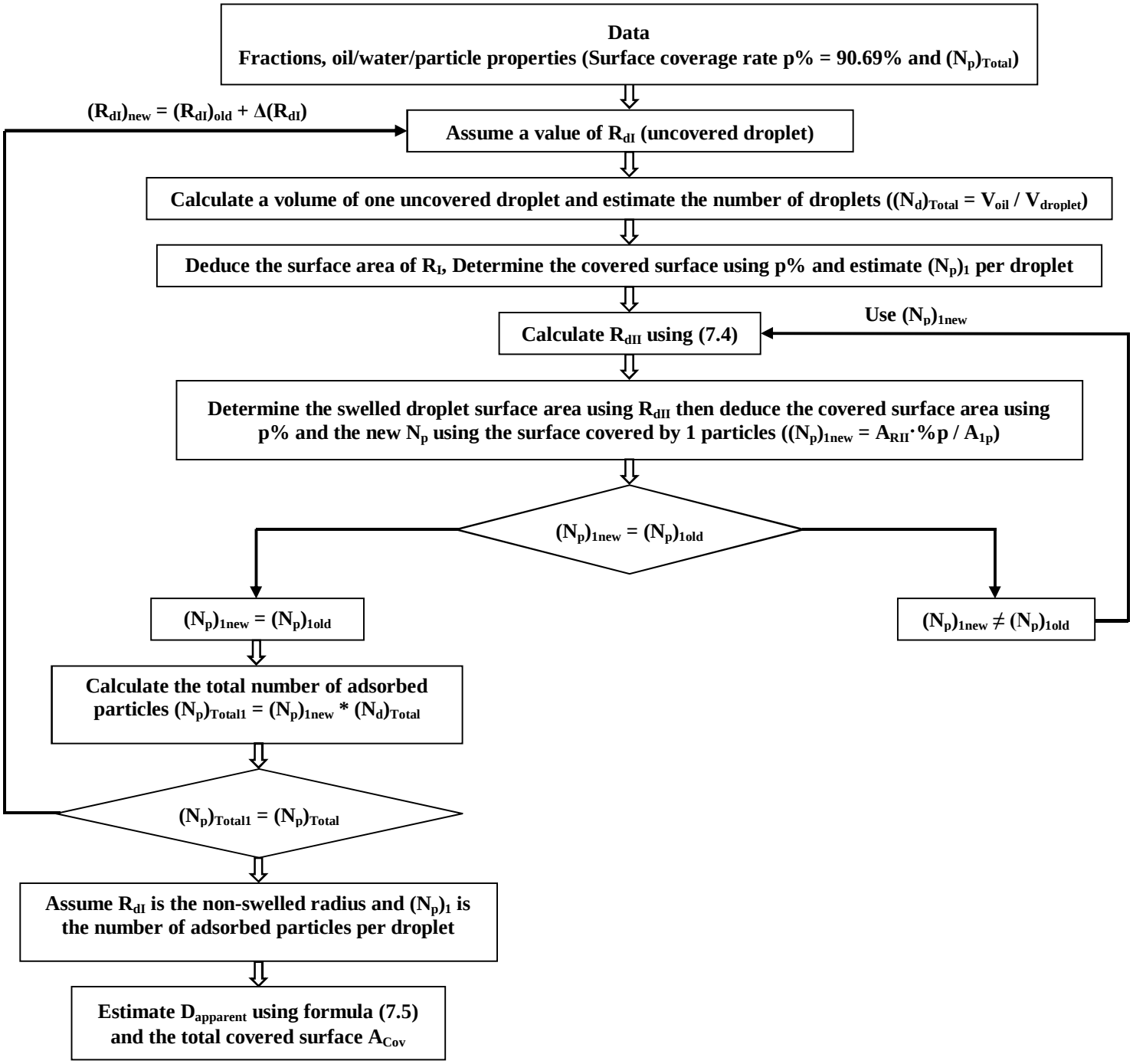

Figure 7.6: Calculation procedure of the final covered interface based on the coverage potential

7.2.4.5 Final droplet size based on the interface generation potential

When the coverage potential is higher than the interface generated, the final theoretical droplet size is mainly a function of the interface generation potential. However, since this potential is

driven by the properties of the continuous phase, the final theoretical droplet size is also a function of the number of particles. As such, the interface generated is determined based on the emulsification conditions. Many correlations have been published for determining the Sauter mean diameter in emulsification systems. However, most do not take the viscosity of the dispersed phase fraction into consideration. Table 7.3 summarizes the results of some of these studies.

Tableau 7.3: Correlations giving the average droplet size in a mixing tank (E.L. Paul et al., 2003)

Authors	**Correlation ($\frac{D_{32}}{D_i}$)**	**η_d (cP)**	**γ (dyn/cm)**	**D (cm)**	**ϕ_d**	**N (RPS)**	**Impeller Type**
Brown et al. (1970)	$0.051(1 + 3.14\phi)We^{-0,6}$	0.59 – 3.30	1.9-50.0	10.0	0.05-0.3	4.2-7.5	6-blades RT
Van Heuven et al. (1971)	$0.047(1 + 2.5\phi)We^{-0,6}$	-	8.5-48.5	3.75-40	0.04-0.35	-	6-blades RT
Coulaloglou et al. (1976)	$0.081(1 + 4.47\phi)We^{-0.6}$	1.3	43	10.0	0.025-0.15	3.2-5.2	6-blades RT
Calabrese et al. (1986)	$0.053We^{-0.6}(1 + 0.97Vi^{0.79})^{0.6}$	0.81 – 459	0.21-47	7.1-15.6	<0.002	1.4-4.7	6-blades RT
Calabrese et al. (1986)	$0.054(1 + 3\phi)We^{-0.6}\left(1 + 4.42(1 - 2.5\phi)Vi\left(\frac{D_{32}}{D_i}\right)^{0.33}\right)^{0.6}$	0.81 – 459	0.21-47	7.1-15.6	<0.3	1.4-4.7	6-blades RT

We used the Calabrese correlation (R.V. Calabrese et al., 1986) because it takes the effect of the dispersed phase viscosity on the final Sauter mean diameter into consideration. R.V. Calabrese et al. (1986) studied the emulsification of silicone oils in a tank with four baffles using a Rushton turbine (radial flow impeller). Depending on the dispersed phase viscosity and dispersed phase fraction, different expressions were proposed.

For diluted systems ($\Phi \leq 0.002$) with low to moderate oil viscosities ($\mu_d \leq 500$ cP), the Sauter mean diameter is calculated using formulas (7.7) and (7.8):

$$\frac{D_{32}}{D_i} = 0.053 \cdot We^{-0.6} \cdot (1 + 0.97 \cdot Vi^{0.79})^{0.6} \cdots (7.7)$$

$$We = \frac{\rho_c N_i^2 D_i^3}{\gamma}, Vi = \frac{\eta_d N_i D_i}{\gamma}\left(\frac{\rho_c}{\rho_d}\right)^{0.5} \cdots (7.8)$$

For more viscous dispersed phases, the Sauter mean diameter is calculated using formulas (7.9) and (7.10):

$$\frac{D_{32}}{D_i} = 2.1 \cdot Re_c^{-3/4} \cdot \left(\frac{\eta_d}{\eta_c}\right)^{3/8} \cdots (7.9)$$

$$Re_c = \frac{\rho_c N_i^2 D_i^3}{\eta_c} \cdots (7.10)$$

For more concentrated systems $\Phi \leq 0.2$, the Sauter mean droplet diameter is calculated using formula (7.11):

$$\frac{D_{32}}{D_i} = 0.054 \cdot We^{-0.6} \cdot (1 + 3\phi_{Oil}) \cdot \left(1 + 4.42(1 - 2.5\phi_{Oil}) \cdot Vi \cdot \left(\frac{D_{32}}{D_i}\right)^{1/3}\right)^{0.6} \cdots (7.11)$$

However, this formula was not experimentally validated with the viscous dispersed phase and underestimated droplet size at high holdups, as reported by A.W. Pacek et al. (1999), who attributed this effect to the fact that the dispersed phase fraction is only taken into consideration for evaluating the turbulent energy dissipation rate, which causes droplet breakage, and does not take the coalescence mechanism into consideration, limiting its use to cases where Vi→0, which gave the following form:

$$\frac{D_{32}}{D_i} = 0.054 \cdot We^{-0.6} \cdot (1 + 3\phi_{Oil}) \cdots (7.12)$$

The linear dependence of the Sauter mean droplet diameter on the dispersed phase holdup has notably been calculated by most investigators (Table 7.3) using the following formula proposed by M.S. Doulah (1975):

$$(D_{32})_{Concentrated} = \left(1 + C_\phi \cdot \phi_{Oil}\right) \cdot (D_{32})_{Diluted} \cdots (7.13)$$

We used the following formula, which was derived from formulas (7.7) and (7.13), in our study:

$$\frac{D_{32}}{D_i} = A \cdot \left(1 + C_\phi \cdot \phi_{Oil}\right) \cdot We^{-0.6} \cdot (1 + B \cdot Vi^{0.79})^{0.6} \cdots (7.14)$$

However, the linear form of the dispersed phase fraction could not predict droplet size for high holdups ($\Phi > 0.2$), as reported by D.E. Brown et al. (1970) for $\Phi_d = 0.4$ and Y. Mlynek et al. (1972) for $\Phi_d = 0.34$, making the use of the linear form or a constant C_Φ questionable at these dispersed phase fraction levels. We decided to keep the linear form and to define C_Φ as a function of the operating conditions in order to reflect their effects on the coalescence process. As such, given the swelling effect and the contribution of the particles to droplet size, the final apparent droplet size and the stabilized interface were estimated using the following steps (Figure 7.7):

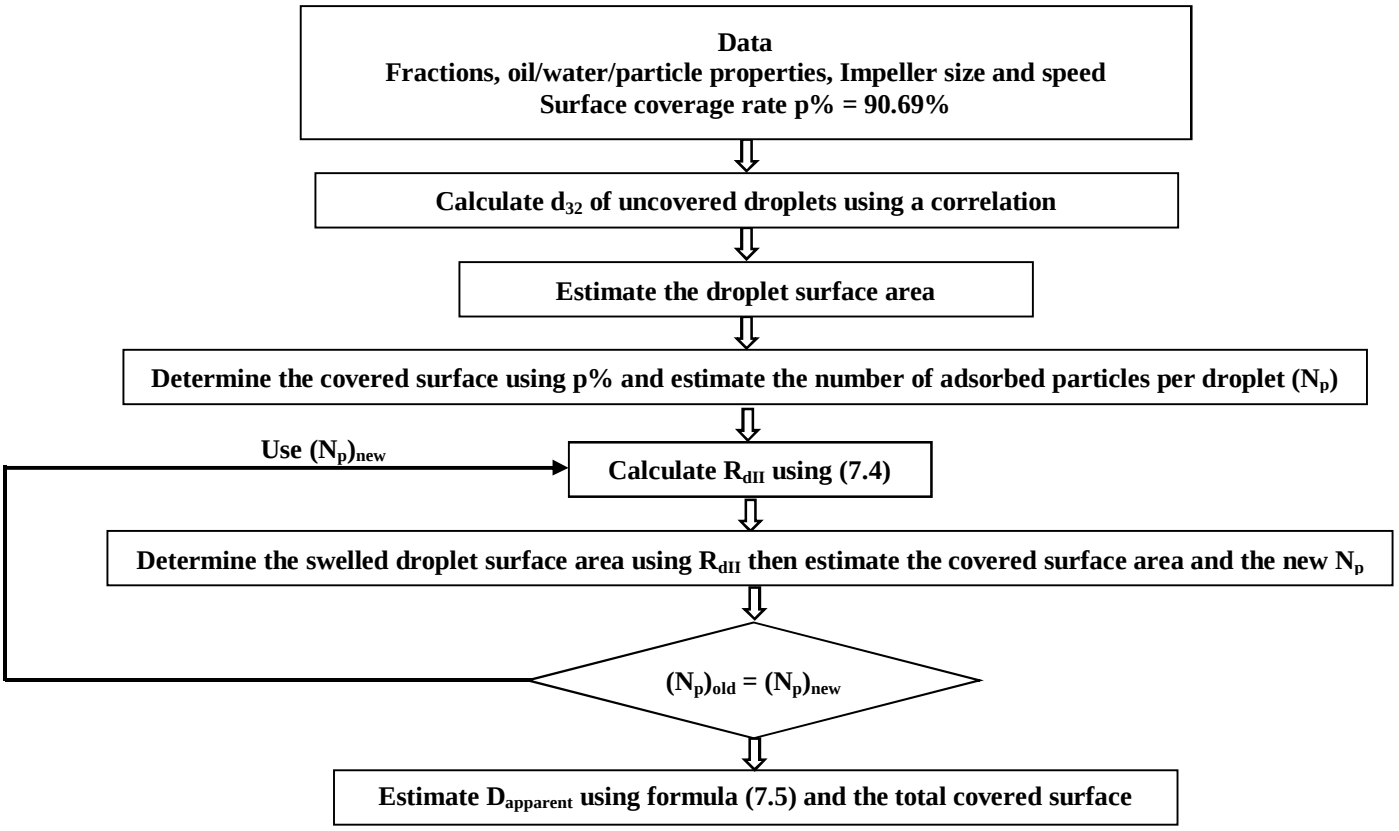

Figure 7.7: Calculation procedure of the final covered interface based on the interface generation potential

7.2.4.6 Stabilization efficiency

As mentioned previously, the interface is generated in the high shear zone by breakage, and the particles are then adsorbed at a given rate to the droplet interface, where uncovered and partially covered droplets coalesce. When the droplets return to the impeller zone, particles are prone to shearing off from the covered droplets. As such, four stabilization conditions are required for given coverage and interface generation potentials, three of which are a function of the adsorption of individual particles at the interface:

1) Particle-droplet contact has to occur during collision.
2) The three-phase contact (TPC) line has to be formed when the particles touch the droplets.
3) The particles have to be strongly adsorbed to the interface to avoid being sheared off in the impeller zone.

The fourth condition is related to ability of the system to cover droplets and prevent coalescence.

4) The coverage rate has to be higher than the coalescence rate to reach a given emulsion size.

Based on these conditions, four efficiencies can be used to estimate the final droplet size and the final covered interface. Particle/droplet collision efficiency is a function of the film drainage process, initial attachment efficiency is a function of the formation of the TPC line, particle attachment efficiency defines the ability of the particles to remain attached at the interface when covered droplets pass through the high shear zone and, lastly, droplet coverage efficiency defines the ability of the system to prevent droplet coalescence by particle coverage:

$$A_{Eff} = A_{Th} \times (E_{Col} \times E_{TPCL} \times E_{Att} \times E_{Cov}) \cdots (7.15)$$

where A_{Eff} is the effectively covered interface, A_{Th} is the theoretical covered interface, E_{Col} is the particle/droplet collision efficiency, E_{TPCL} is the TPC line formation efficiency, E_{Att} is the particle attachment efficiency, and E_{Cov} is the droplet coverage efficiency.

7.2.4.6.1 Particle/droplet collision efficiency

Collision efficiency can be defined as the probability that the particle touches the droplet surface during collision through continuous film rupture. Collision efficiency has been widely studied. The most common approach is based on the film drainage model (Y. Liao et al., 2010). Coalescence efficiency or, in the present study, collision efficiency, was assessed by defining a contact time and a drainage time and by considering that both are random variables. Based on the probabilistic approach used by S.L. Ross (1971) to define coalescence efficiency, C.A. Coulaloglou (1975) proposed the following simplified formula:

$$E_{Col} \approx exp\left(-C_1 \frac{t_d}{t_c}\right) \cdots (7.16)$$

where t_c is the contact time, t_d is the drainage time, and C_1 is the constant.

Numerous studies have been devoted to defining contact time. The approach developed by V.G. Levich (1962) for turbulent regimes is based on a dimensional analysis by which contact time can be estimated using the following formula:

$$t_c \approx C_2 \frac{\left(D_d + D_p\right)^{2/3}}{\varepsilon_t^{1/3}} \cdots (7.17)$$

Other studies have focused on drainage time, which is defined as the time required to break the film between the particles after collision. These studies have reported that drainage time is closely related to the deformability and surface mobility of the colliding particles (A.K. Chesters, 1991). S.A.K. Jeelani and S. Hartland (1994) developed a formula including interface mobility effects. They assumed a constant contact area between the particle and the film, a symmetrical flow about the vertical axis of the particle, a tangential flow to the surface of the sphere (Figure 7.8), a zero velocity at the particle boundary, and a w_d at the droplet interface:

$$t_d = \frac{3\pi\eta_c R_f^4}{4h_{cr}^2 F_{Col}[1 + (3\eta_c l_{circ}/2h_i\eta_d)]} \cdots (7.18)$$

where F_{Col} is the collision force, R_f is the radius of the film, η_c is the viscosity of the continuous phase, η_d is the viscosity of the droplet, h_i is the initial film thickness, h_{cr} is the critical film thickness, and l_{circ} is the circulation length (the distance between the droplet interface and the zero velocity into the droplet).

A. Vrij and J. Overbeek (1968) proposed the following formula to estimate the thickness of the critical film:

$$h_{cr} = 0.267\left[\frac{A_f A_H^2}{6\pi\gamma\Delta p}\right]^{1/7} \cdots (7.19)$$

where γ is the interfacial tension, A_f is the surface area of the film (assuming $h \ll R_p$ and $h \ll R_d$: $A_f = A_{fp} = A_{fd}$), A_H is the Hamaker constant ($A_H \approx 10^{-20}$ J (typical value)), and Δp is the excess pressure in the film (assumed to be equal to the Laplace pressure for small droplets (S.A.K. Jeelani et al., 1994).

Assuming that the collision force is balanced by the droplet Laplace pressure:

$$F_{Col} = \Delta p A_f = \frac{2\gamma}{R_d} A_f \Longrightarrow A_f = \frac{F_{Col} R_d}{2\gamma} \cdots (7.20)$$

and assuming a spherical deformation and a very small film thickness:

$$R_f = R_p \sin\left[\cos^{-1}\left(1 - \frac{A_f}{2\pi R_p^2}\right)\right] \cdots (7.21)$$

the collision force was estimated by V.G. Levich (1962) using the following formulas:

$$F_{Col} \approx C_3 \frac{\pi}{2} \rho_c \varepsilon_t^{2/3} \left(\frac{D_d D_p}{D_d + D_p} \right)^{8/3} \; for \left(\frac{D_d D_p}{D_d + D_p} \right) \geq \lambda \cdots (7.22)$$

or

$$F_{Col} \approx C_4 \frac{\pi}{4} \rho_c^2 \frac{\varepsilon_t \left(\frac{D_d D_p}{D_d + D_p} \right)^4}{\mu} \; for \left(\frac{D_d D_p}{D_d + D_p} \right) < \lambda \cdots (7.23)$$

where F_{Col} is the collision force, ε_t is the turbulent energy dissipation rate, λ is the Kolmogorov length scale ($(\nu^3/\varepsilon_t)^{1/4}$), D_p is the particle diameter, and D_d is the droplet diameter.

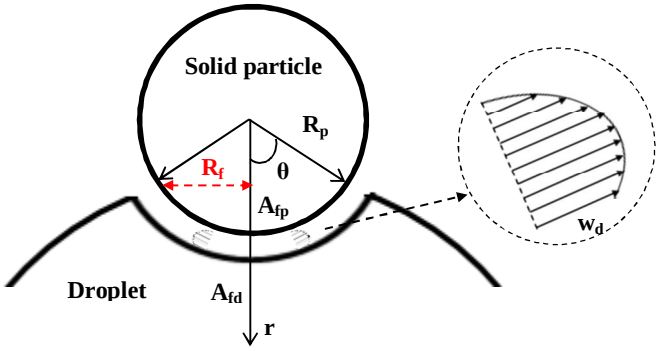

Figure 7.8: Typical representation of droplet deformation and film drainage during particle/droplet collision

7.2.4.6.2 Three-phase contact line expansion efficiency

The TPC line is formed immediately after film rupture. Driven by a difference in interfacial energies, a minimal attachment level has to be achieved quickly enough to allow TPC line expansion and avoid particle detachment. A. Sharma and E. Ruckenstein (1990) developed formula (7.24) to equate critical film thickness with the critical TPC line radius and the equilibrium contact angle using a thermodynamic approach based on the balance of the free energy of the film before rupture and after the formation of the TPC contact line:

$$\frac{2h_{cr}}{R_{cr} \sin \theta_e} = 1 + \left(\frac{1 - \cos \theta_e}{\sin \theta_e} \right)^2 exp \left(\frac{-2h_{cr}}{R_{cr} \sin \theta_e} \right) \cdots (7.24)$$

where θ_e is the equilibrium contact angle, R_{cr} is the critical TPC line radius, and h_{cr} is the critical film thickness.

On the other hand, two approaches are generally used to describe TPC line expansion. The first is based on a molecular kinetic theory that defines TPC line expansion velocity as a function of the displacement of individual molecules and hydrodynamic theory that takes viscous effects into consideration. C.M. Phan et al. (2003) proposed the following formula to estimate TPC line expansion velocity:

$$V_{TPC} = \frac{dR_{TPC}}{dt} = \frac{\gamma_{ow}}{9ln(R_m/L_m)\eta}[\theta_e^3 - \theta^3(t)] \cdots (7.25)$$

where R_{TPC}, is the TPC line radius, $\theta(t)$ is the dynamic contact angle, R_m is the macroscopic characteristic length (≈ particle radius), L_m is the molecular characteristic length (≈ 0.1 nm), and η is the dynamic viscosity.

Formula (7.25) shows that TPC line velocity decreases with the dynamic contact angle until it reaches zero at the equilibrium contact angle. Assuming a zero dynamic contact angle at t = 0, it is possible to estimate TPC line velocity at each time point by decomposing changes in the dynamic contact angle into different steps:

$$V_{TPC}(t_{i+1} = t_i + \Delta t) = \frac{\gamma_{ow}}{9ln(R_m/L_m)\eta}[\theta_e^3 - (\theta_{i+1} = \theta_i + \Delta\theta)^3] \cdots (7.26)$$

$$\Delta\theta = \frac{\theta_e - \theta_0}{N_\theta} \cdots (7.27)$$

where N_θ is the dynamic contact angle step number and θ_0 is the initial dynamic contact angle (t=0).

Assuming that the droplet size is much larger than the particle size, the TPC line radius can be related to the particle radius (Figure 7.9) using the following formula:

$$R_{TPC}(t_{i+1}) = R_p \sin\theta_{i+1} \cdots (7.28)$$

and time evolution can be estimated from the following formula:

$$t_{i+1} = \frac{R_{TPC}(t_{i+1}) - R_{TPC}(t_i)}{V_{TPC}(t_i)} + t_i \cdots (7.29)$$

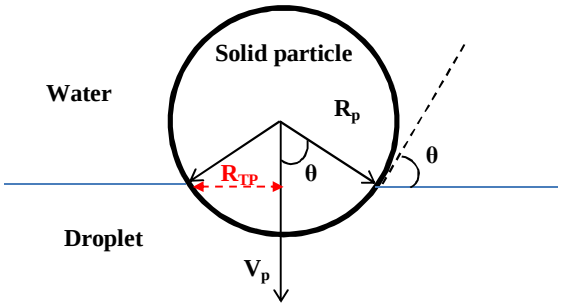

Figure 7.9: Typical representation of an adsorbed particle on a planar interface

As mentioned previously, to obtain TPC line expansion, a minimal TPC line radius has to be reached during particle-droplet contact. We used an approach similar to the one used for particle/bubble interactions in the flotation process model (H.J. Schulze et al., 1993) where TPC line expansion efficiency is defined by comparing the contact time (formula (7.17)) to the time required to reach the critical line radius, which is estimated using formula (7.24):

$$E_{TPC_{cr}} = 1 - exp\left(-t_c / t_{TPC_{cr}}\right) \cdots (7.30)$$

Like bubble/particle line expansion, the TPC line radius obtained after a given collision time was much higher than the critical TPC line radius, indicating that TPC line expansion is possible in most cases and that TPC line expansion efficiency is very close to unity.

7.2.4.6.3 Particle attachment efficiency

Attachment efficiency, which is a function of attachment and detachment forces, was defined in order to describe the stability of particles at the interface. However, given that the highest probability of detachment occurs in the impeller zone, force balances in this zone must be taken into consideration. Attachment efficiency has been studied using the flotation process model and is defined using the following formula (H.J. Schulze et al., 1993):

$$E_{Att} = 1 - exp[1 - C_{Att}(F_{Att}/F_{Det})] \cdots (7.31)$$

A.D. Scheludko et al. (1975) proposed the following formula for estimating the maximum attachment force of a spherical particle at a liquid interface:

$$F_{Att} = 2\pi\gamma_{ow}R_p\left(\cos\left(\frac{\theta}{2}\right)\right)^2 \cdots (7.32)$$

Attached particles are also subject to detachment forces mainly resulting from system hydrodynamics, the Laplace pressure droplet effect and, in some cases, particle weight. H.J. Schulze et al. (1993) notably suggested that these forces are responsible for particle detachment in flotation processes.

Hydrodynamic forces can be represented as the product of particle mass and particle acceleration (a_t) caused by the external flow field (H.J. Schulze et al. (1993)):

$$F_{Hyd} = \frac{4}{3}\pi R_p^3 \rho_p a_t \cdots (7.33)$$

while acceleration in a turbulent flow field is represented by:

$$a_t = \frac{1.9\varepsilon_t^{2/3}}{\left(R_d + R_p\right)^{1/3}} \cdots (7.34)$$

the associated Laplace pressure force by:

$$F_{Lap} = A_p \Delta p = \left(\pi R_p^2 \sin^2 \theta_{ow}\right)\left(\frac{2\gamma_{ow}}{R_d}\right) \cdots (7.35)$$

and the gravity force by:

$$F_g = \frac{4}{3}\pi R_p^3 \rho_p g \cdots (7.36)$$

which gives the detachment force:

$$F_{Det} = F_{Hyd} + F_{Lap} + F_g \cdots (7.37)$$

In a mixing tank system, it can be assumed that the highest probability of detachment occurs in the impeller zone where there is a higher dissipation energy rate ($\varepsilon_{Max} \approx (40\text{-}120)\cdot\varepsilon_{Average}$ (G. Zhou and S. Kresta**, (**1996)). On the other hand, assuming that the particle adsorbs to the droplet interface immediately after droplet generation in the impeller zone, the attachment force can be estimated by considering TPC line expansion from initial particle adsorption until the particle returns to the impeller zone which, in turn, is a function of circulation time (D.E. Leng and R.V. Calabrese, 2004). This can be expressed using the following formula:

$$t_{circ} = \frac{V_{tank}}{N_q \cdot D_i^3 \cdot N_i} \cdots (7.38)$$

where t_{circ} is the mean circulation time, N_q is the flow number (≈ 0.85 for a PBT), N_i is the impeller speed, D_i is the impeller diameter, and V_{tank} is the tank volume.

The dynamic contact angle and the corresponding TPC line radius can be estimated from formulas (7.26), (7.27), (7.28), and (7.29) by assuming that the adsorption time is equal to the calculated circulation time, which is calculated using formula (7.38). The forces calculated using formulas (7.32) and (7.37) can then be used to estimate attachment efficiency.

7.2.4.6.4 Droplet coverage efficiency

Droplet coverage efficiency refers to the ability of the system to cover the droplets generated in the coalescence zone (far from the impeller zone). We assumed that, for a given particle concentration and energy level, a given interface will be stabilized. We then defined three different efficiencies in order to take the ability of individual particles to adsorb to and stay attached to the interface into consideration. We now present a more global view using the following condition:

$$Stabilization\ rate\ > Coalescence\ rate \cdots (7.39)$$

If it is assumed that Np particles are required to fully cover a droplet of a given size and stabilize it, the condition then becomes:

$$Adsorption\ rate\ of\ N_p\ particles > Coalescence\ rate \cdots (7.40)$$

Particle adsorption and droplet coalescence rates can then be estimated based on collision frequency and contact efficiency (particle/droplet collision) or coalescence efficiency (droplet/droplet collision). Assuming that randomly distributed particles and droplets are moved by an isotropic turbulent flow with the velocity of equal size eddies, the following formulas, which are based on the formulas proposed by C.A. Coulaloglou and L.L. Tavlarides (1977), C.-H. Lee et al. (1987), M.J. Prince and H.W. Blanch (1990), and H. Luo (1993) can be used to estimate particle/droplet and droplet/droplet collision frequencies:

$$Freq_{Col_{Np/d}} = \left(C_5\left(D_p^2 + D_d^2\right).\left(D_p^{2/3} + D_d^{2/3}\right)^{1/2}\varepsilon_t^{1/3}.V_{tank}.N_d.N_{p/Total}\right)/N_{p/d} \cdots (7.41)$$

$$Freq_{Col_{d/d}} = C_6.D_d^{7/3}.\varepsilon_t^{1/3}.V_{tank}.N_d^2/(1+\phi_{Oil}) \cdots (7.42)$$

where C is an adjustable constant, E_t is the turbulent energy dissipation rate, D_p is the mean diameter of the particles, D_d is the mean diameter of the droplets, N_d is the droplet number density, $N_{p/Total}$ is the total particle number density, $N_{p/d}$ is the number of particles required to cover one droplet, and V_{tank} is the tank volume.

Droplet coalescence efficiency is defined using a formula similar to formula (7.16). A.K. Chesters (1991) proposed the following formulas to estimate the drainage time for inertial collisions of deformable droplets (parallel film model, Figure 7.10), with partially mobile interfaces and contact times:

$$t_d = \frac{\pi \cdot \eta_d \cdot F_{Col}^{1/2}}{2 \cdot (2\pi\gamma_{ow}/R_d)^{3/2}} \left(\frac{1}{h_f} - \frac{1}{h_i}\right) \cdots (7.43)$$

$$h_f = \left[\frac{A_H R_d}{16\pi\gamma_{ow}}\right]^{1/3} \cdots (7.44)$$

$$t_c = \left(\left(\frac{4\rho_d}{3\rho_c} + 1\right)\rho_c \left(\frac{R_d^3}{2\gamma_{ow}}\right)\right)^{1/2} \cdots (7.45)$$

where A_H is the Hamaker constant ($A_H \approx 10^{-20}$ J (typical value)), h_i is the initial film thickness, h_f is the final film thickness, H_d is the dispersed phase dynamic viscosity, F_{Col} is the droplet/droplet collision force, γ_{ow} is the interfacial tension, and R_d is the droplet radius.

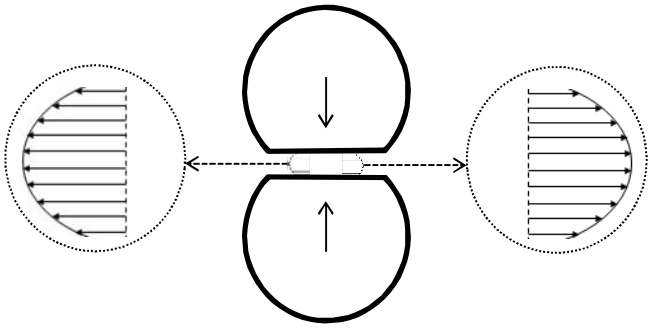

Figure 7.10: Typical representation of droplet deformation during collision based on the parallel film model

Droplet coverage efficiency can thus be estimated using the following formula:

$$E_{Cov} = exp\left(-\frac{Freq_{Col_{d/d}} E_{Coalescence}}{Freq_{Col_{Np/d}}}\right) \cdots (7.46)$$

7.2.4.7 Emulsification performance calculation

Emulsification performances are evaluated based on droplet size calculations, energy consumption, and the time required to reach equilibrium. As mentioned previously, it was assumed that droplets are generated and are then stabilized, which involves two general conditions. In the first case, if the interface generation potential is higher than the coverage potential of the system, the droplets will be partially covered and will coalesce until the coverage potential of the system is reached (limited coalescence process). The final mean diameter will thus depend on the coverage potential. In the second case, there are at least enough particles to cover the interface generated. The final mean diameter will thus depend on the interface generation potential of the system. However, stabilization efficiency, which involves particle/droplet collision, particle adsorption, and droplet coverage efficiency, must be taken into consideration. The following calculation procedure was used (Figure 7.11):

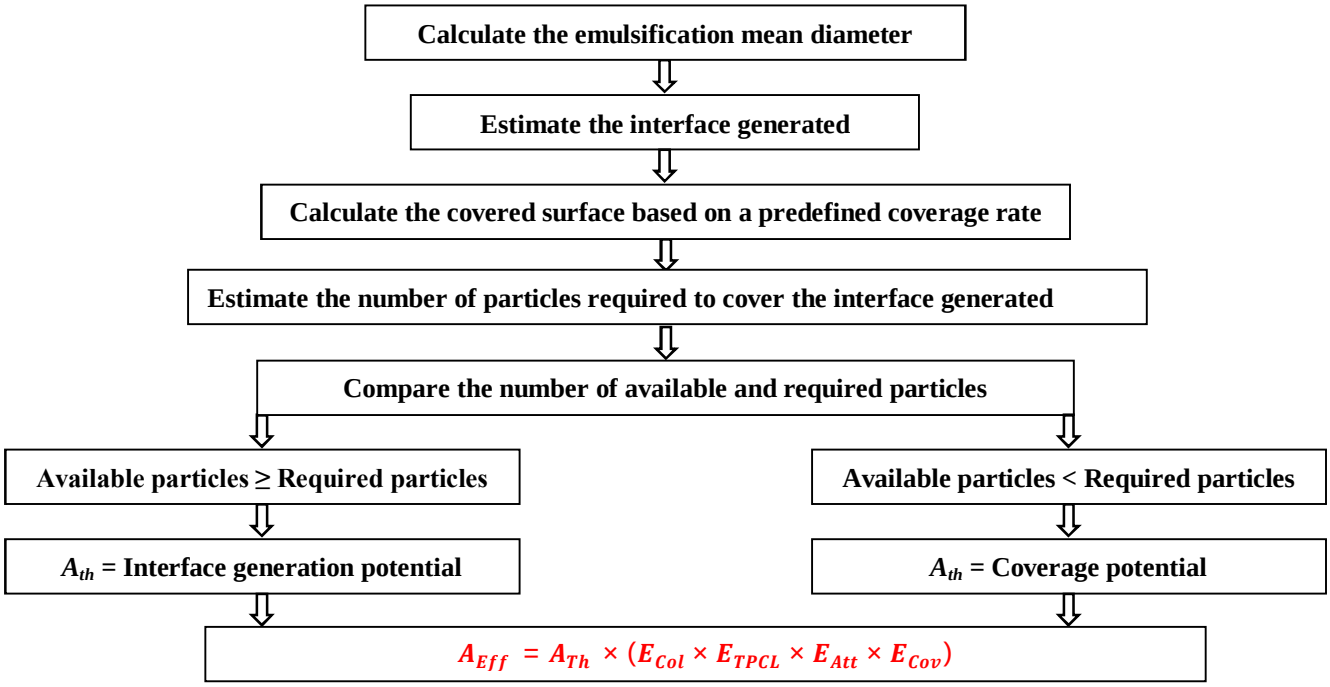

Figure 7.11: Calculation procedure of the effectively covered interface

7.2.5 Results and discussion

7.2.5.1 Interface generation potential

As mentioned above, the stabilization process is controlled by the coverage potential or by the interface generation potential. The first step was thus to estimate the two potentials and the second was to use the defined efficiencies to estimate the effectively covered interface and thus the mean droplet size.

To estimate the capacity of the system to generate an interface, the constants of formula (7.14) were adjusted for a free particle emulsification system since we were studying an entirely different system (off-centered PBT versus baffled RT). The emulsions were stabilized using a non-ionic surfactant (Tween 80 from Sigma Aldrich, γ_{ow} = 15 mN/m). Different viscosities and impeller speeds were studied, and we determined that the Sauter mean diameter could be estimated using the following formula:

$$\frac{D_{32}}{D_i} = 0.0125 \cdot (1 + (0.0106 \cdot Re_d^{0.3} \cdot Re_c^{0.4}) \cdot 3 \cdot \phi_{Oil}) \cdot We^{-0.6} \cdot (1 + 0.97 \cdot Vi^{0.79})^{0.6} \cdots (7.47)$$

As can be seen in Figure 7.12, there was good agreement between the theoretical results obtained with formula (7.47), assuming that C_Φ is a function of operating conditions, and the experimental results. This approach made it possible to use a linear form of the dispersed phase fraction and to take the tendency of the system to coalesce and turbulence damping due to the presence of the dispersed phase into consideration.

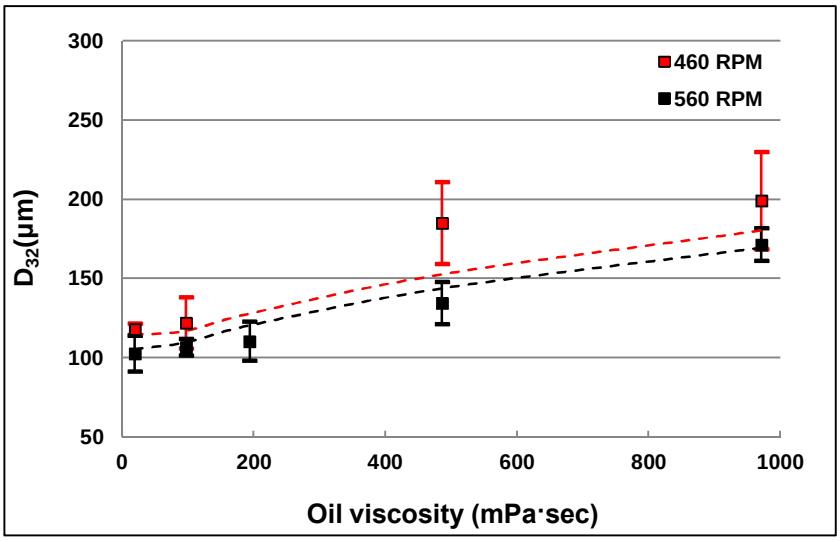

Figure 7.12: Effect of Oil viscosity and impeller speed on the Sauter diameter of a surfactant stabilized emulsion

(O/W: 53%v, Tween 80: 0.1%v)

7.2.5.2 Validating the model using solid-stabilized emulsions

The proposed form was validated using the results from solid-stabilized emulsions. Different dispersed phase viscosities, Weber numbers (We~N^2), and coverage potentials were studied, and the new model constant was deduced from the experimental results shown in Figure 7.13 and Figure 7.14 using the following formula:

$$C_{Model} = \frac{D_i}{D_{32}} \cdot We^{-0.6} \cdot (1 + 0.97 \cdot Vi^{0.79})^{0.6} \cdots (7.48)$$

Figure 7.15 and 7.16 show that the model constant follows a power law of the impeller speed while Figure 7.17 shows a power law of the viscosity of the dispersed phase. These effects were observed with four viscosities (S100, S200, S500 and S1000) at five impeller speeds (4.33, 5.17, 6.00, 6.83, and 7.67 RPS) that corresponded to five Weber numbers (104.16, 148.08, 199.70, 259.02, and 326.05) with C_1 = 0.25 and all other constants equal to unity. Based on these findings, the model coefficient can be expressed using the following formula:

$$C_{Model} = A \cdot \left(1 + B \cdot \phi_{Oil} \cdot \left(N_i^{0.7} \cdot \left(\frac{\eta_d}{\rho_d}\right)^{-0.3}\right)\right) \cdots (7.49)$$

The dependence of the model constant on impeller speed has been related to the coalescence effect. H. Wright et al. (1994) reported that increasing the impeller speed increases the droplet/droplet collision frequency and, as such, the coalescence frequency. They investigated the factors affecting the coalescence process in a baffled stirred tank using a six-blade Rushton turbine and different dispersed phase fractions (1% - 25%) to develop an empirical formula for estimating coalescence frequency:

$$Freq_{Coal} = 3.72.10^{-3} \cdot \phi_{Oil}^{1.42} \cdot N_i^{0.52} \cdot \left(v_1^{1/2} + v_2^{1/2}\right) \cdots (7.50)$$

where Φ_{Oil} is the oil volume fraction, N_i is the impeller speed, and v_i is the droplet volume.

On the other hand, formula (7.49) shows that the model constant increases if the dispersed phase viscosity is reduced, which can also be related to the coalescence mechanism, since coalescence is promoted by reducing the viscosity of the oil, which has an effect on droplet surface mobility. This effect was notably evident with the characteristic drainage time estimated by formula (7.43), which shows that drainage time increases with dispersed phase viscosity, indicating that film drainage and, as such, coalescence is hindered when viscous oils are used.

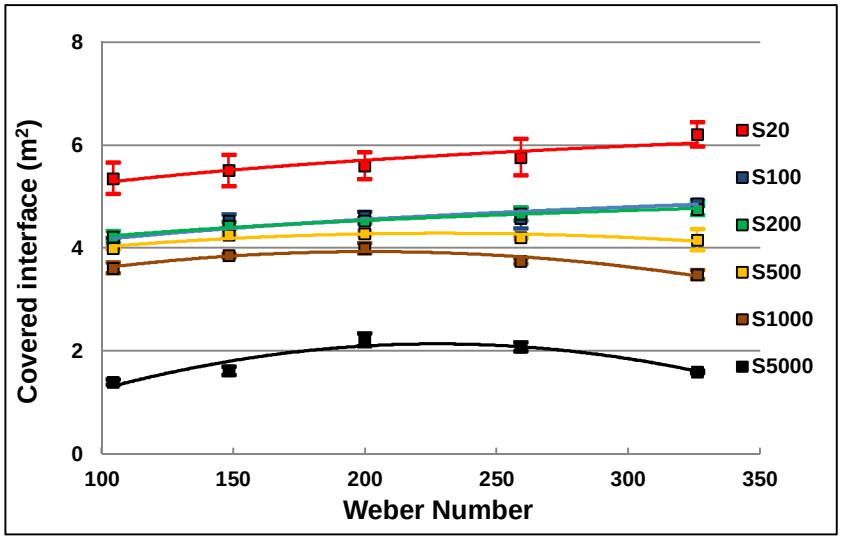

Figure 7.13: Effect of oil viscosity and Weber number on the covered surface

(O/W: 53%v, coverage potential: 6.43 m^2, D_p: 22.4 μm)

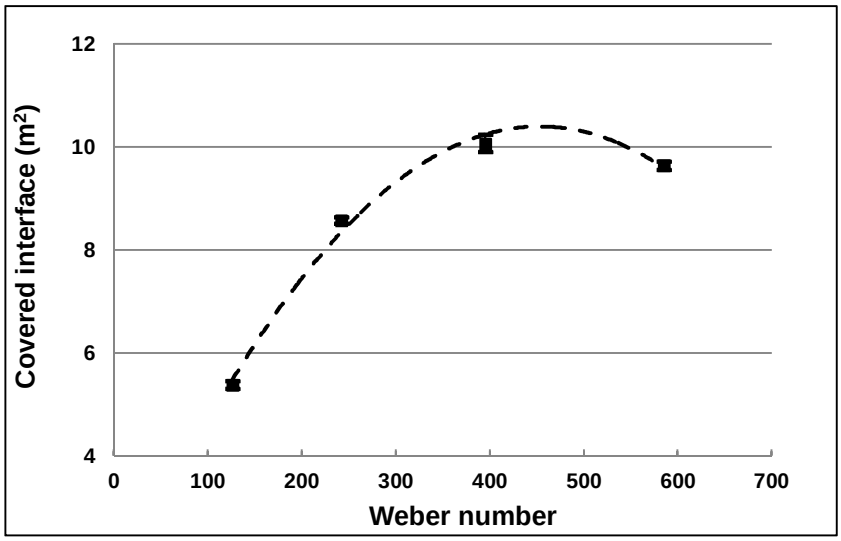

Figure 7.14: Effect of Weber number on the covered interface

(O/W: 53.5%v, coverage potential: 16 m^2, d_p: 22.4 µm, η_{S200}: 194 mPa·s)

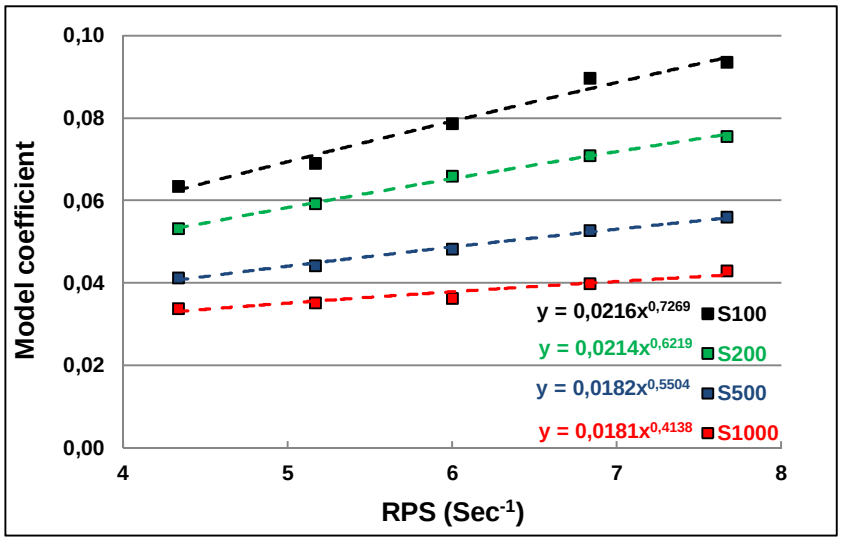

Figure 7.15: Effect of impeller speed on the new Calabrese coefficient for different viscosities

(O/W: 53%v, coverage potential: 6.43 m^2, D_p: 22.4 µm)

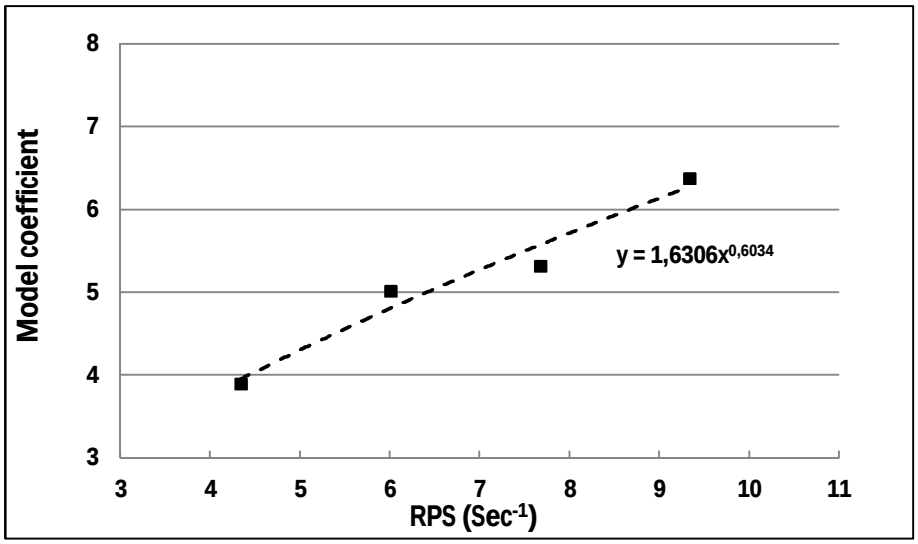

Figure 7.16: Effect of impeller speed on the new Calabrese coefficient

(O/W: 53%v, coverage potential: 16 m^2, D_p: 22.4 µm, η_{S200}: 194 mPa·s)

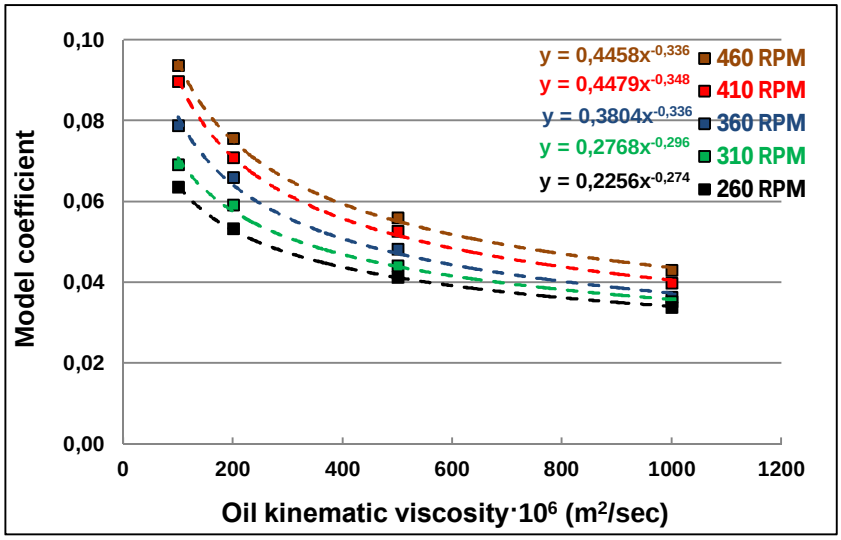

Figure 7.17: Effect of kinematic viscosity on the new Calabrese coefficient for different impeller speeds

(O/W: 53%v, coverage potential: 6.43 m^2, D_p: 22.4 µm)

The effect of the coverage potential and the properties of continuous phase were then studied using a viscous oil (S1000) and a high impeller speed (560 rpm) with different particle fractions (Figure 7.18).

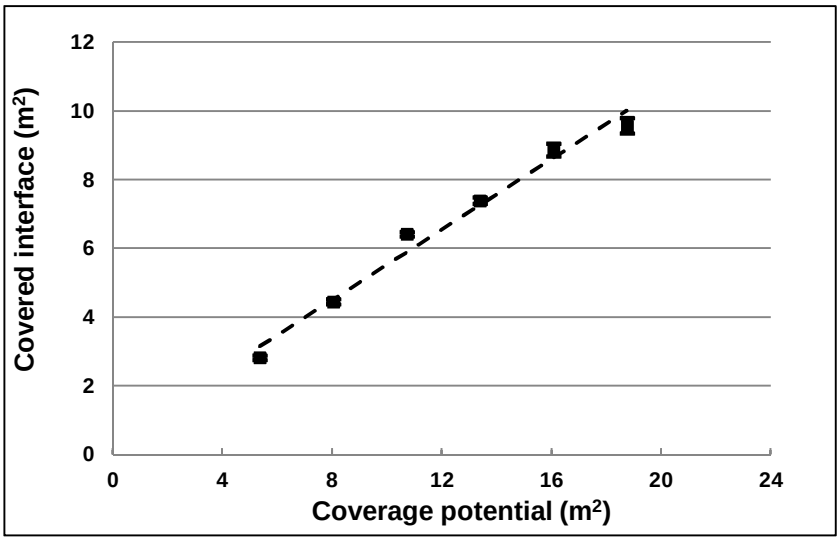

Figure 7.18: Effect of the coverage potential on the covered interface

(O/W: 53%v, d_p: 22.4 µm, η_{S1000}: 971 mPa·s, Re = 23000)

We studied the dependence of the model constant on the new parameters using Einstein's law (Einstein A. (1906)) to evaluate continuous phase viscosity and found that the model constant can be expressed by the following formula:

$$\frac{D_{32}}{D_i} = C_{Model} \cdot We^{-0.6} \cdot (1 + 0.97 \cdot Vi^{0.79})^{0.6} \cdots (7.51)$$

$$C_{Model} = 0.0125 \cdot \left(1 + \left(0.137 \cdot \left(1 + 2.5\phi_p\right)^{-4.5} \cdot Re_d^{0.3} \cdot Re_c^{0.4}\right) \cdot 3 \cdot \phi_{Oil}\right) \cdots (7.52)$$

Formulas (7.51) also encompasses the effect of the particle fraction on the film drainage process during droplet/droplet collision and hence on the droplet coalescence mechanism. Increasing the particle fraction in the continuous phase reduced coalescence efficiency since more time was required for film drainage, confirming the results reported by S.A.K. Jeelani and S. Hartland (1994) using formula (7.18).

Figures 7.19, 7.20, 7.21 and 7.22 shows good agreement between the results predicted by the model and the experimental results, for viscosities a wide range of viscosities, impeller speeds and coverage potentials obtained from particle fractions. Model predictions were notably able to reproduce the transition between the region where the emulsification is controlled by the coverage potential and the region where the emulsification is controlled by the interface generation potential (Figure 7.19). The first region, for viscosities lower than 96.60 mPa·sec,

being characterized by a relatively constant covered surface since the same amount of particles were used with all the viscosities, and the second region, for viscosities higher than 100 Cst, characterized by a decrease in the covered surface.

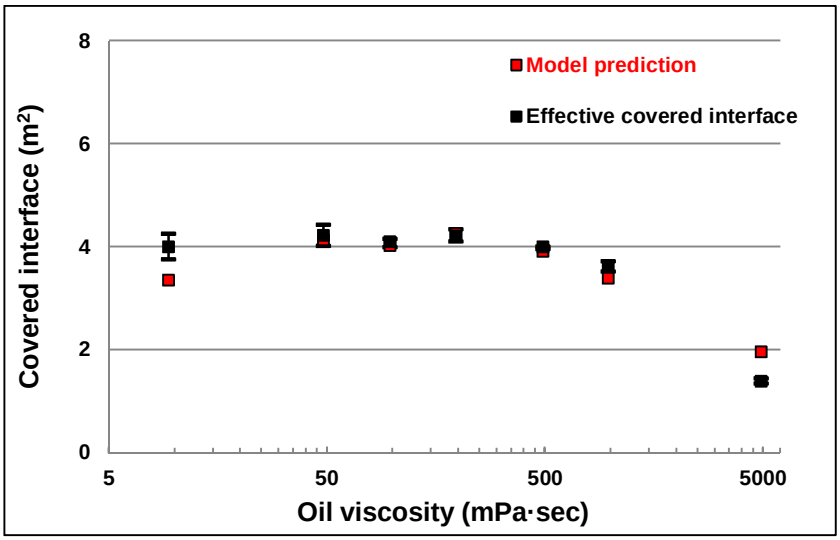

Figure 7.19: Effect of oil viscosity on the covered interface predicted by the model

(O/W: 53%v, coverage potential: 6.43 m^2, D_p: 22.4 µm, Re = 11400)

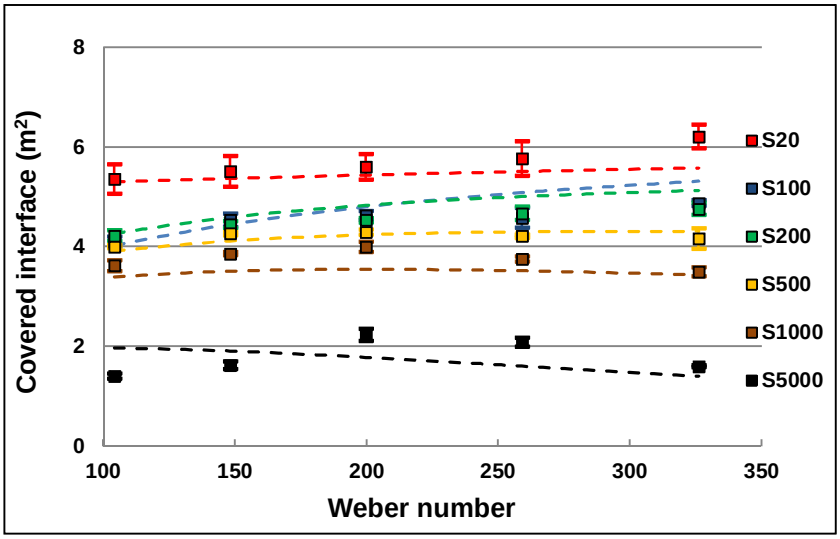

Figure 7.20: Effect of oil viscosity and Weber number on the covered interface predicted by the model

(O/W: 53%v, coverage potential: 6.43 m^2, D_p: 22.4 µm)

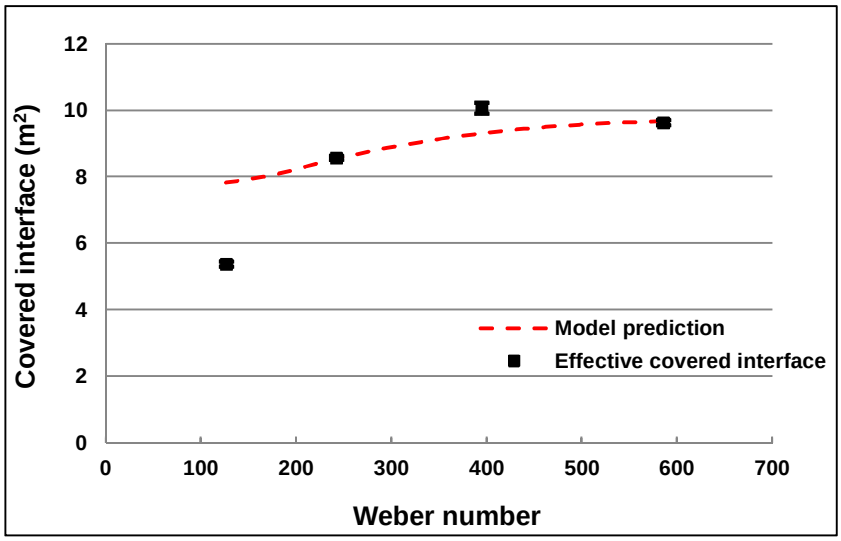

Figure 7.21: Effect of Weber number on the covered interface predicted by the model

(O/W: 53%v, coverage potential: 16 m^2, D_p: 22.4 µm, η_{S200}: 194 mPa·s)

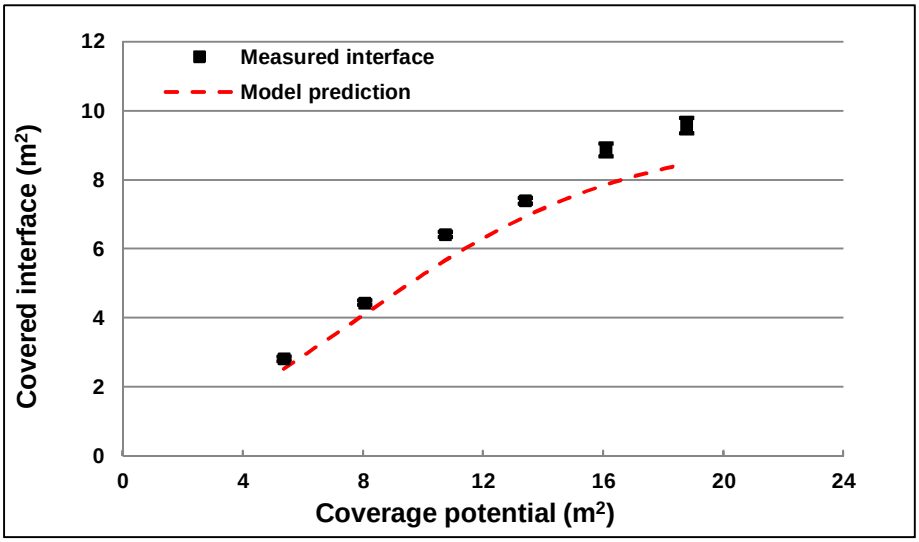

Figure 7.22: Effect of the coverage potential on the covered interface predicted by the model

(O/W: 53%v, D_p: 22.4 µm, η_{S1000}: 971 mPa·s, Re = 23000)

7.2.5.3 Effect of operating conditions on stabilization efficiency

We propose a new representation to describe the effect of coalescence on the interface generation potential of a high hold-up system and hence on the stabilized interface of solid-stabilized emulsions. Four efficiencies were investigated. Coverage efficiency, which describes the ability of the system to cover the interface generated, was determined by comparing the coalescence frequency to the particle/droplet collision frequency. Particle/droplet collision efficiency characterizes the probability of film drainage and hence contact between the particle and the droplet, TPC line expansion efficiency characterizes the probability of the formation a stable contact line around the particle after particle/droplet contact, while attachment efficiency characterizes the ability of the particle to resist detachment forces and remain adsorbed to the droplet surface.

7.2.5.3.1 Effect of impeller speed and oil viscosity

Figure 7.23 shows the effect of impeller speed and dispersed oil viscosity on particle/droplet collision efficiency. Efficiency decreased when the impeller speed and/or the oil viscosity were increased. The effect of impeller speed was essentially related to the impact on the energy dissipation rate. Increasing the impeller speed increased the energy dissipation rate and reduced the contact time defined by formula (7.17), and increased the collision force defined by formula (7.22) or (7.23). Increasing the collision force resulted in a larger droplet deformation surface. As such, more fluid had to be drained between the particle and the droplet, which increased the required drainage time defined by formula (7.18). Drainage time was also affected by the dispersed phase viscosity. By increasing the viscosity of the oil, droplet surface mobility was reduced, which in turn increased the drainage time. This effect was more significant when the impeller speed was increased since both impeller speed and oil viscosity contribute to reducing particle/droplet collision efficiency.

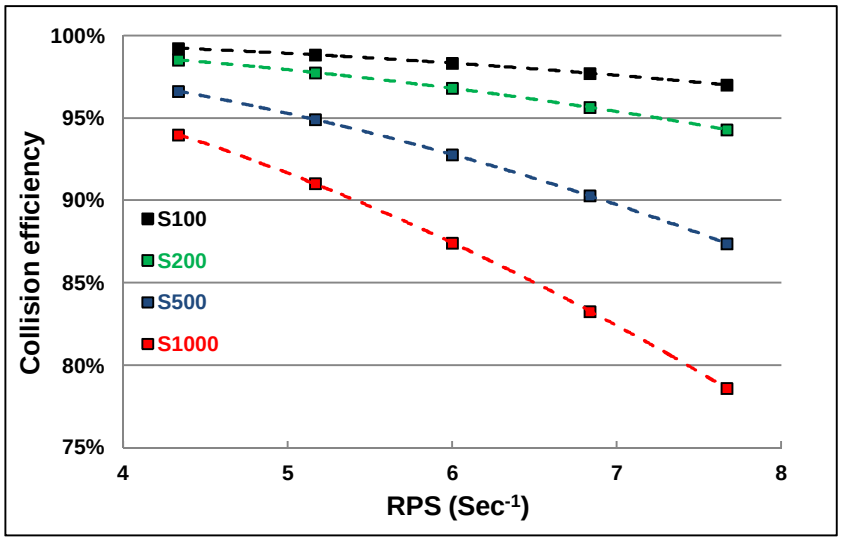

Figure 7.23: Effect of oil viscosity and impeller speed on particle/droplet collision efficiency

(O/W: 53%v, coverage potential: 6.43 m^2, D_p: 22.4 μm)

Figure 7.24 shows the effect of impeller speed and oil viscosity on droplet coverage efficiency. As can be seen, droplet coverage efficiency was equal to 100% at high oil viscosities (S500 and S1000) and decreased with lower viscosity oils (S100 and S200). This effect was mainly related to the coalescence efficiency defined by the drainage/contact time ratio. When the impeller speed was increased, the contact time was reduced since smaller droplets were generated and more energy was produced. On the other hand, drainage time was only affected by the effect of energy on droplet deformation. The increase in the droplet/droplet collision frequency with the increase in impeller speed was thus modulated by the decrease in coalescence efficiency and the increase in particle/droplet collision frequency. It can also be seen that coverage efficiency decreased with the decrease in dispersed phase viscosity, which is also related to coalescence efficiency. When the viscosity of the oil was increased, the droplet surface became less mobile and film drainage took more time, reducing coalescence efficiency and increasing coverage efficiency.

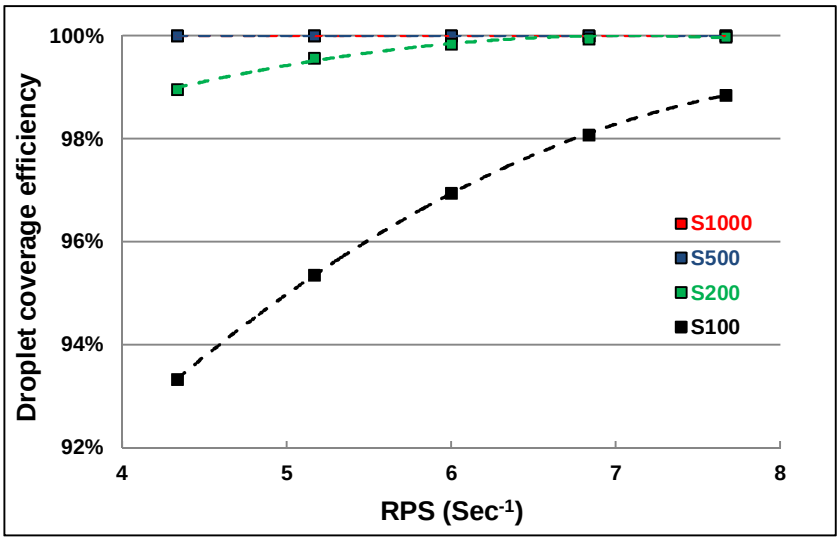

Figure 7.24: Effect of oil viscosity and impeller speed on droplet coverage efficiency

(O/W: 53%v, coverage potential: 6.43 m^2, D_p: 22.4 μm)

Figure 7.25 shows the effect of particle attachment efficiency, or the ability of the adsorbed particle to remain attached to the interface, for different oil viscosities and impeller speeds. Attachment efficiency was close to 100% in all cases. However, attachment efficiency decreased when the impeller speed was increased. Increasing the impeller speed reduced droplet circulation time, and the droplets returned more quickly to the high shear zone where inadequately adsorbed particles were sheared off. In addition, smaller droplets were generated, resulting in a higher Laplace pressure, which contributed to the detachment of the particles. On the other hand, attachment efficiency increased with oil viscosity, which was also due Laplace pressure since larger droplets were generated, resulting in a lower pressure.

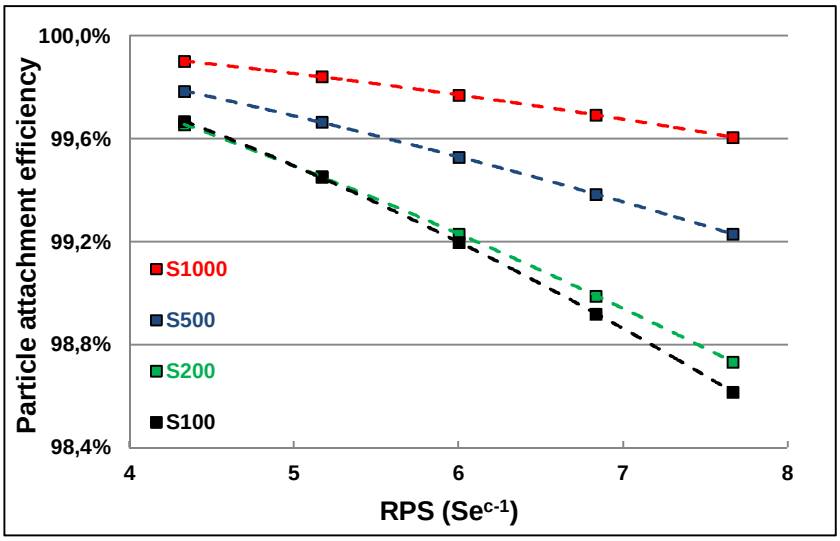

Figure 7.25: Effect of oil viscosity and impeller speed on droplet coverage efficiency

(O/W: 53%v, coverage potential: 6.43 m^2, D_p: 22.4 µm)

7.2.5.3.2 Coverage potential effect

The effect of the particle fraction on stabilization was investigated using a viscous oil (S1000) with an impeller speed of 560 rpm. As shown in Figure 7.26, the effect of the particle fraction was a function of the interface coverage potential. Coverage efficiency was equal to 100% because drainage time was very long compared to contact time due to droplet surface mobility, which resulted in very low droplet coalescence efficiency.

Figure 7.26 also shows that attachment efficiency was more sensitive to the particle fraction. Attachment efficiency was reduced from 100% at the lowest coverage capacity to approximately 74% at the highest. This was caused by the increase in droplet Laplace pressure since smaller droplets were produced when the particle fraction was increased. Adding more particles affected the properties of the continuous phase properties, increasing both the viscosity and the density. An increase in continuous phase viscosity resulted in a lower coalescence term in the Sauter mean diameter formula (Formula (7.51)) and a higher breakage capacity through the effect of continuous phase density on the Weber number.

Lastly, particle/droplet collision efficiency increased with the increase in the particle fraction. As mentioned previously, increasing the particle fraction increased the continuous phase density and the viscosity, resulting in smaller droplets with a relatively high Laplace pressure and,

consequently, less droplet deformation. If less droplet deformation occurs, less fluid is trapped between the particle and the droplet during collision, promoting film drainage. However, it should be noted that the particle fraction had a more significant effect on attachment efficiency at this viscosity (S1000).

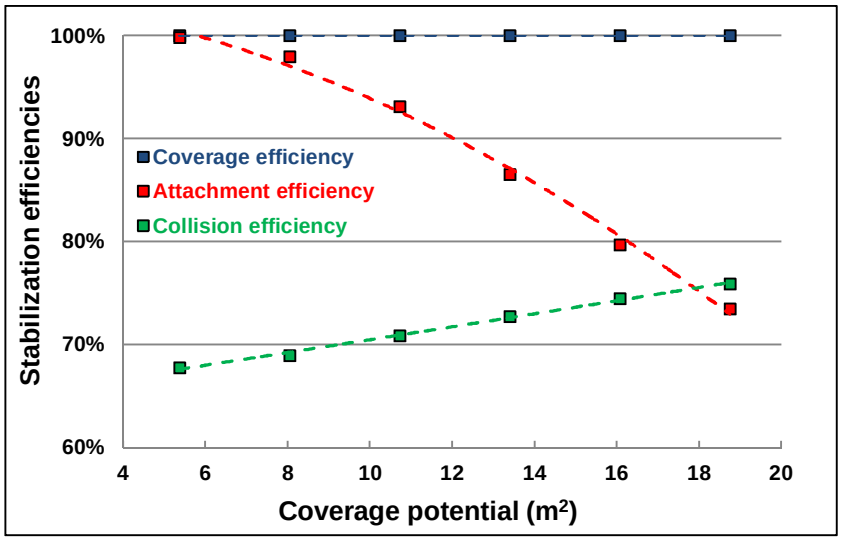

Figure 7.26: Effect of the coverage potential on stabilization efficiency

(O/W: 53%v, D_p: 22.4 µm, η_{S1000}: 971 mPa·s, Re = 23000)

7.2.6 Conclusions

A new semi-empirical approach was developed to estimate the final mean Sauter diameter of concentrated solid-stabilized emulsions prepared in a standard unbaffled tank with an off-centered PBT. The model took the droplet swelling resulting from particle adsorption at the interface into consideration. The model was used to compare the interface generation potential of the system to the coverage potential and to determine the dominant stabilization process and thus the theoretical stabilized interface.

The interface coverage potential was estimated from the properties of the particles while the interface generation potential was estimated by modifying the Calabrese correlation to take the coalescence mechanism and the effect of particles on the breakage mechanism into consideration. Four efficiencies derived from physical considerations based on four stabilization conditions were also investigated:

1) Droplet coverage efficiency: If Np particles are required to totally cover and stabilize a droplet of a given size, the collision frequency between the Np particles and the droplet should be higher than the droplet/droplet collision efficiency, meaning that the coverage rate should be higher than the coalescence rate.
2) Particle/droplet collision efficiency: The film separating the particles and the droplets during collision should be drained to allow particle/droplet contact.
3) Three-phase contact line formation efficiency: The TPC line should be formed immediately after particle/droplet contact to allow particle adsorption to continue until the equilibrium position is reached.
4) Particle attachment efficiency: The adsorbed particles should be adsorbed more strongly at the interface to avoid detachment during passage through the high shear zone.

A modified Calabrese formula was developed based on these conditions. The predictions of the formula showed good agreement with experimental results for a wide range of oil viscosities (S20 - S5000), Weber numbers (104.16 to 558.215), and coverage potentials (5.36 m^2 to 18.75 m^2). It even reproduced the observed increases and decreases in the covered interface that occurred with the various oil viscosities. The additional coalescence term showed good agreement with the dependence on the impeller speed determined using an empirical approach developed by H. Wright et al. (1994) for a geometry similar to that studied by R.V. Calabrese et al. (1986), indicating that similar mechanisms are involved in the stabilization process despite differences in geometry and conditions. This will help in the development of an approach for scaling up process operations. Lastly, the effects of the operating conditions on the proposed stabilization efficiencies were determined and the relevance of each stabilization efficiency was demonstrated.

7.2.7 Acknowledgments

The authors gratefully acknowledge financial support from the Natural Sciences and Engineering Research Council of Canada and TOTAL.

CHAPITRE 8.PROBLÉMATIQUES ASSOCIÉES À LA CONCEPTION D'UN PROCÉDÉ D'ÉMULSIFICATION PAR DES PARTICULES (APPLICATION AU TRANSPORT DES PÉTROLES LOURDS)

Cette partie est une illustration des perspectives du travail présenté dans les chapitres précédents. Il s'agit d'établir les lignes directrices pour la conception d'un procédé d'émulsification de bitume par des particules à l'échelle industrielle à des fins de transport. Les problématiques associées à cette opération sont abordées et de nouveaux axes de recherche sont ainsi définis.

En considérant à la fois les résultats obtenus précédemment et les contraintes associées au transport de pétrole par pipeline, la première étape consiste à déterminer les propriétés de l'émulsion à produire à partir des objectifs du procédé. Ensuite, la deuxième étape est de choisir le type et les propriétés des particules à utiliser. La troisième étape consiste à choisir le type d'équipement d'émulsification, à définir les conditions opératoires optimales et à établir les règles d'un scale-up pour passer de l'échelle de laboratoire à l'échelle industrielle. La dernière étape serait dédiée au dimensionnement des équipements utilisés.

8.1 Réglementation du transport de pétrole par pipelines

Actuellement, le bitume est transporté par dilution (30% de diluant et 70% de bitume) avec un brut synthétique sous l'appellation « synbit. » ou avec du naphta sous l'appellation « dilbit ». Dans certains cas, les deux produits sont utilisés et le bitume dilué porte le nom de « dilsynbit. ».

Le transport de pétrole par pipeline est contrôlé par l'Office National de l'Énergie au Canada et par le Federal Energy Regulatory Commission aux États-Unis. La densité maximale exigée par l'Office National de l'Énergie est de 940 kg/m^3, la viscosité maximale est de 350 cSt et la teneur maximale en eau et sédiments du pétrole transporté est de 0,5%v. Les propriétés des particules présentes dans le pétrole (taille, forme et densité) sont également prises en considération afin d'éviter la sédimentation, l'érosion et le bouchage des pompes et autres équipements. Globalement, les tailles observées sont de l'ordre du micron. Le niveau d'acidité du bitume dilué est également un paramètre important afin de prévenir la corrosion des pipelines. L'acidité est généralement quantifiée par le TAN (Total Acid Number) qui est une mesure de la quantité nécessaire (en milligrammes) d'hydroxyde de potassium (KOH) pour neutraliser les acides

contenus dans un gramme de pétrole. Le type d'acides organiques présents dans le bitume dilué est également pris en compte car les acides ayant un poids moléculaire élevé tels que les acides naphténiques sont relativement stables et ne posent pas de réels problèmes de corrosion dans les conditions standard. Ceci dit, en plus du contrôle du niveau d'acidité, le taux de soufre est également contrôlé. Présent à des concentrations allant de 4% à 6% massique dans les bitumes canadiens, il est particulièrement corrosif lorsqu'il est sous la forme de sulfure d'hydrogène (H_2S). La vitesse d'écoulement, la pression et la température sont également prises en considération. Les valeurs maximales observées pour chaque paramètre sont représentées sur le tableau 8.1. Ces différentes contraintes montrent la complexité de l'opération de transport des produits pétroliers et les défis technologiques à relever afin de rentabiliser l'opération et d'éviter les accidents.

Tableau 8.1: Données maximales relevées pour le transport de bitume dilué (Transportation Research Board, 2013)

Propriété	BS&W (%v)	H_2S (ppm massique)	Soufre (% massique)	Densité (kg/m^3)	TAN (mg KOH/g)	Température (°C)	Vitesse (m/sec)
Valeur maximale relevée	0,5	11,0	5,2	1115	3,75	50	2,5

8.2 Émulsification des pétroles lourds et des bitumes

8.2.1 Propriétés de l'émulsion

La mise en émulsion de pétroles lourds ou des bitumes à fait l'objet de différents travaux dont ceux de Gregoli et al. (1988), Marchal et al. (1988), Catafalmo et al. (2001), et Gingras et al. (2007). Cependant, la plupart de ces travaux ont utilisé des tensio-actifs pour la stabilisation des émulsions ce qui favorisait la génération d'interface. L'utilisation de particules solides a été considérée par Bragg et al. (2003) qui se sont intéressés aux forages pétroliers et au transport par pipeline. Cette étude a abouti à l'établissement d'un brevet. Bragg et al. (2003) recommandent de produire des émulsions contenant 30% d'eau et 70% d'huile d'une taille inférieure à 200 μm, stabilisées par des particules hydrophiles d'une taille inférieure à 10 μm dans le cas des particules sphériques ou une aire spécifique de 200 μm^2 pour les particules non sphériques. L'utilisation de coke pétrolier, de particules d'argile ou de silice est suggérée. La fraction en particules est comprise entre 0,01% et 5% en poids. Il est également recommandé de maintenir un pH entre 7,5

et 10 afin de ne pas altérer la mouillabilité des particules, mouillabilité qui pourrait être affectée par les hydrocarbures polaires présents dans le pétrole.

Sachant qu'une taille d'émulsion de 200 μm peut être obtenue en utilisant des cuves agitées ou des mélangeurs statiques, ce sont ces deux dispositifs qui seront considérés dans ce chapitre.

8.2.2 Choix des particules solides

Différents critères doivent être pris en compte pour le choix des particules. En effet, l'objectif étant de stabiliser des gouttes de bitume dans de l'eau, les particules choisies devront être relativement hydrophiles. En raison de la viscosité élevée du bitume, la taille de particules ne devra pas dépasser une certaine limite afin de favoriser son attachement à l'interface. Il devra également y avoir assez de particules pour couvrir l'interface générée. La disponibilité et le coût des particules au niveau des sites de production consitituent donc un critère important de même que la possibilité de récupération et de régénération à la fin du transport.

Différents types de particules, tels que les argiles, la silice et les minerais, sont disponibles au niveau des sites d'extraction de bitume. Dans ce travail, nous proposons l'utilisation de minerais ayant un intérêt commercial et devant être transportés des sites d'extraction vers les sites de traitement et d'exportation. Sur la base de ces considérations, les métaux lourds présents dans les sables bitumineux semblent offrir une opportunité intéressante. En effet, différents travaux ont été consacrés à l'étude des minerais extraits avec les sables bitumineux ce qui a révélé un potentiel considérable. Une étude réalisée par Whitcomb & Associates. (2005) a notamment établi qu'il va être possible d'atteindre une production d'environ 1 million tonne/an de TiO_2 et 300000 tonne/an de $ZrSiO_4$. Une attention particulière est portée aux minerais précurseurs de l'oxyde de titane, tels l'Ilménite ou l'Ilménite altérée ($FeTiO_3$ ou $Fe_2Ti_3O_9$) qui contiennent entre 60 et 65% de TiO_2, et la Leucoxene (Forme complexe de l'oxyde de titane associée à des silicates et des argiles et contenant typiquement plus de fer que d'oxyde de titane) qui en contient entre 70 et 84%. Ces deux minerais conducteurs ont une densité variant entre 3.5 g/cm^3 et 5 g/cm^3, et possèdent des propriétés magnétiques. Différents travaux ont montré que l'oxyde de titane était particulièrement présent dans la fraction solide extraite lors du traitement secondaire au niveau des centrifugeuses (Jusqu'à 14% (Alberta Chamber of Ressources, 1996)).

L'idée serait donc de transporter le bitume et les minerais d'intérêt par pipeline, ceux-ci étant adsorbés à la surface des gouttes de bitume pour les stabiliser. Il est ainsi suggéré d'utiliser les minerais précurseurs de l'oxyde de titane (Ilménite, Leucoxene, Rutile…) en raison de leur disponibilité, de leur intérêt et de leurs propriétés de surface et de leurs propriétés magnétiques permettant une éventuelle séparation de l'émulsion par l'application d'un champ magnétique. Il est cependant nécessaire de tenir compte de la densité élevée de ces minerais qui pourrait provoquer la sédimentation des gouttes.

8.2.2.1 Traitement et conditionnement des particules

Afin de mettre en œuvre un procédé de séparation, différents travaux ont d'abord été consacrés à la caractérisation des minerais constituant la fraction solide de la mousse secondaire ce qui a permis d'identifier les différentes problématiques associées à cette opération. Ainsi, il été trouvé que la plupart des minerais présents dans les déchets solides avaient des propriétés physiques très proches (Tableau 8.2) ce qui rend la séparation particulièrement compliquée.

Tableau 8.2: Composition typique des minerais lourds contenus dans la fraction solide obtenue par centrifugation au niveau d'une installation Syncrude (Oxenford et al. (2001))

Minerai	% massique
Ilménite Altérée	23.0
Leucoxene	16.6
Rutile	4.0
Ilménite	2.8
Zircon	15.2
Pyrite	4.0
Goethite	1.6
Tourmaline	16.7
Grenat	6.0
Staurolite	4.8
Sidérite	3.0
Calcite	0.6
Kyanite	0.6
Apatite	0.6
Autres: Monazite, micas…	0.5

Différentes solutions ont été proposées pour séparer ces différents minerais dont celle utilisant la technique de la flottation. Ce procédé est essentiellement basé sur les propriétés de surface des minerais. La séparation se faisant par l'introduction de bulles d'air dans le système, les particules les moins hydrophiles (non-polaires) auront tendance à s'adsorber aux surfaces des bulles pour être récupérées par la suite sous forme de mousse. Afin de favoriser la flottation de certains minerais par rapport aux autres des collecteurs sont utilisés pour modifier les propriétés de surface des minerais d'intérêt. Ces collecteurs sont des agents tensio-actifs qui modifient la mouillabilité des particules pour les rendre plus hydrophobes. Des agents moussant peuvent également être ajoutés afin de stabiliser les bulles et ainsi la mousse contenant le minerai séparé. Des régulateurs peuvent aussi être utilisés afin d'augmenter la sélectivité des collecteurs. Ces agents peuvent, soit favoriser l'adsorption du collecteur aux surfaces du minerais d'intérêt et sont appelés dans ce cas agents activateurs, soit être utilisés pour réduire l'hydrophobicité de certains minerais afin d'empêcher leur flottation augmentant ainsi la sélectivité de l'opération. La flottation a été utilisée par Oxenford et al. (2001) avec d'autres procédés pour traiter les produits solides issus des centrifugeuses. Il a été possible de séparer les minerais contenant de l'oxyde de titane de ceux contenant du Zircon avec des concentrations très acceptables. Chachula et al. (2003) ont également procédé au traitement d'un échantillon de Rutile fourni par Lakefield Research Ltd et Syncrude Canada Ltd par flottation et séparation magnétique et ont également obtenus des résultats très satisfaisants.

Plus récemment une étude conduite par Titanium corporation a abouti à la mise au point d'un procédé de séparation avec une récupération du bitume résiduel (Moran et al. (2013)). Le procédé est constitué de trois étapes, la première étant la concentration des métaux lourd via deux cellules de flottation, un solvant est ensuite ajouté afin d'éliminer le bitume mélangé aux minerais, ce solvant étant par la suite récupéré.

Ce procédé a notamment été testé au niveau d'une usine pilote et a donné des résultats très satisfaisants en termes de concentration de minerais lourd mais également en termes de qualités du bitume et du solvant récupéré. De plus, vu que le minerai n'est pas soumis à une calcination, sa susceptibilité magnétique n'est pas affectée et il est donc possible d'envisager une séparation par voie magnétique.

Titanium corporation envisage actuellement d'exploiter les minerais lourds issus de la centrifugation de la mousse de bitume dilué selon le schéma global illustré sur la figure 8.1 afin d'en extraire l'Ilménite, le Leucoxene et le Zircon dont le transport vers les sites de traitement et/ou d'exportation est prévu par voie ferroviaire.

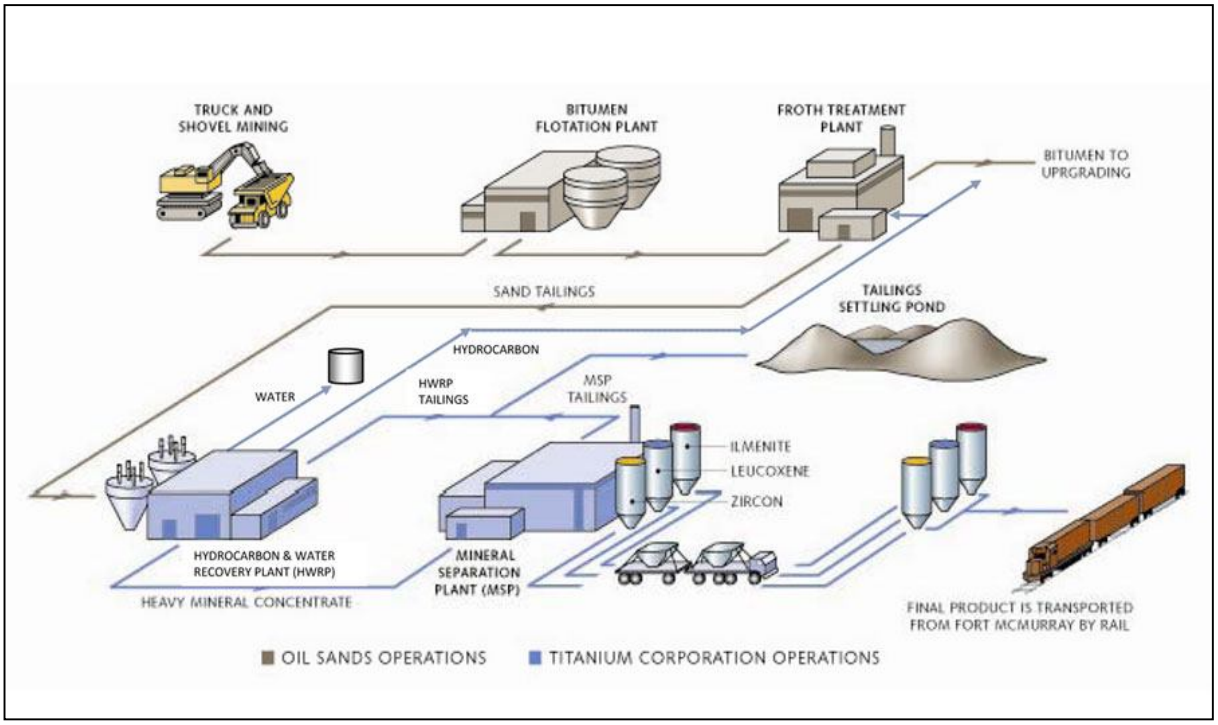

Figure 8.1: Schéma d'extraction des minerais lourds (Titanium corporation, 2010)

C'est donc dans ce contexte que nous proposons de transporter ces minerais par pipeline en utilisant ces particules pour stabiliser les émulsions de bitume. Si les propriétés des minerais le permettent, il pourrait être envisagé d'utiliser ces minerais ensemble pour la stabilisation de l'émulsion et les traiter à la fin du transport lorsqu'ils auront été séparés de l'émulsion.

8.2.2.2 Potentiel de transport des particules par émulsification

En considérant une production de 200000 barils/jour de bitume ayant une densité égale à celle de l'eau et un taux de couverture des gouttes de 90%, la quantité de particules pouvant être transportée pour différentes tailles de gouttes et tailles de particules est représentées sur la Figure 8.2. Les résultats montrent clairement qu'il est possible de transporter des quantités considérables de particules. On peut ainsi voir que cette quantité augmente avec la taille des particules mais est réduite lorsque la taille des gouttes est réduite vu que plus d'interface est générée. Cependant, il

faudrait également prendre en compte l'effet des particules adsorbées sur le comportement de l'émulsion.

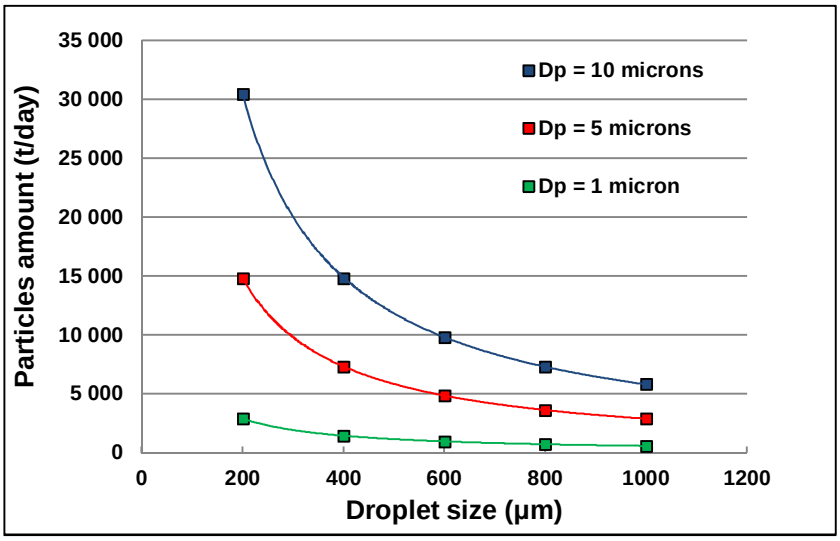

Figure 8.2: Effet de la taille de goutte et de la taille des particules sur la quantité de particules pouvant être adsorbées à la surface des gouttes

8.2.2.3 Effet des particules sur le comportement des émulsions de Pickering

L'effet des particules sur la densité apparente des gouttes est représenté sur la figure 8.3 pour une densité de particules de 5000 kg/m^3, et un taux de couverture de 90%. La densité apparente des gouttes recouvertes de particules est ainsi donnée par :

$$\rho_{Cov/d} = \frac{m_{drop} + m_{Ads/p}}{m_{drop}/\rho_{drop} + m_{Ads/p}/\rho_p} \cdots (8.1)$$

$\rho_{Cov/d}$ étant la densité apparente des gouttes, ρ_{drop} la densité de la phase dispersée, ρ_p la densité des particules, m_{drop} la masse de la goutte, et $m_{Ads/p}$ la masse des particules adsorbées.

Les résultats montrent que le rapport densité goutte / densité eau augmente avec la taille des particules et diminue avec la taille de goutte. Une augmentation de la densité apparente pourrait être problématique pour l'opération de transport vu que les gouttes seraient plus susceptibles de sédimenter, mais constituerait un avantage en termes de séparation car elle faciliterait la séparation par différence de densité.

Cette propriété pourrait donc être exploitée au niveau d'autres procédés de séparation. En effet, la plupart des procédés de séparation utilisent la différence de densité des constituants à séparer.

Dans le cas des émulsions de Pickering, les gouttes recouvertes de particules peuvent être considérées comme étant des particules solides composites dont les propriétés dépendent de celles de la phase dispersée et des particules solides utilisées comme agent stabilisant de l'émulsion. Il est donc possible de favoriser le crémage, la floculation ou la sédimentation des émulsions produites et séparer la phase dispersée par le biais des particules ou bien séparer les particules en utilisant la phase dispersée. L'efficacité de séparation dépend donc de la taille de gouttes, de leurs propriétés, des propriétés des solides adsorbés aux interfaces et de leur quantité.

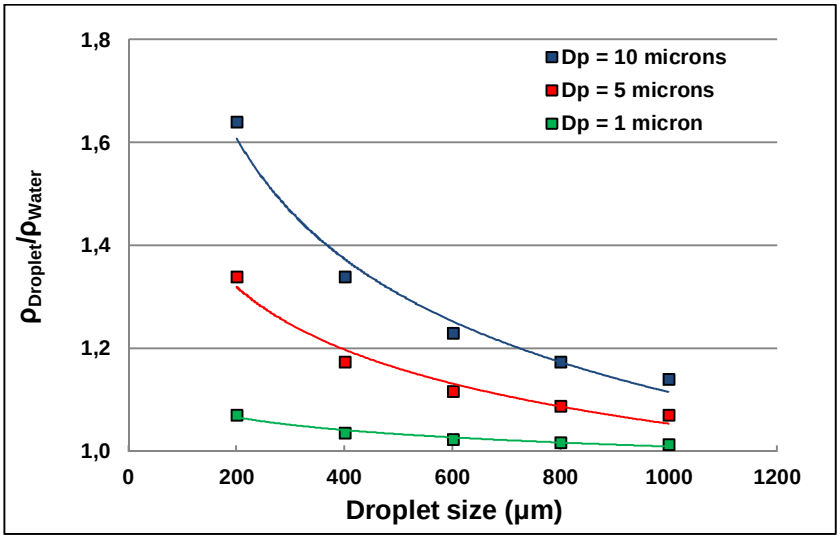

Figure 8.3: Effet de la taille de goutte et de la taille des particules sur le rapport densité apparente goutte / densité eau

8.2.3 Mise en émulsion du bitume

8.2.3.1 Émulsification dans une cuve agitée

La taille d'émulsion recherchée étant de l'ordre de 200 µm, le dispositif d'émulsification présenté aux chapitres précédents pourra donc être considéré (Figure 8.4) et le modèle présenté au chapitre 7 être utilisé pour prédire les propriétés des émulsions produites.

Afin d'évaluer l'aptitude du système à produire des émulsions ayant la taille requise nous avons considéré les résultats obtenus au chapitre 6 en utilisant des huiles silicones dont les propriétés sont décrites dans le tableau 8.3 et les particules de verre modifié présentées dans le tableau 8.4.

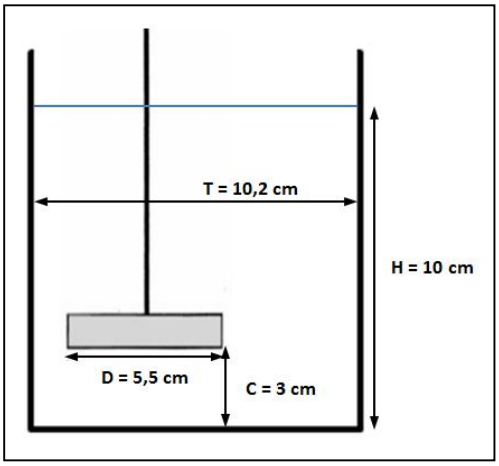

Figure 8.4: Dispositif d'émulsification

Tableau 8.3: Propriétés physiques des huiles silicones

Désignation	Densité (kg/m^3)	Viscosité (mPa·sec)	Tension interfaciale (N/m)
S20	950	19.00	4.2E-02
S100	966	96.60	4.2E-02
S200	968	193.60	4.2E-02
S500	971	485.50	4.2E-02
S1000	971	971.00	4.2E-02
S5000	975	4875.00	4.2E-02

Tableau 8.4: Physical properties of particles

Désignation	Type	Densité (kg/m^3)	D_{32} (µm)	Angle de contact
Spheriglass 3000E	Verre modifié	2520	22.4	93° ± 3°

L'effet du nombre de Weber représentant le niveau d'énergie et de la viscosité de l'huile sur la taille moyenne de goutte est représenté sur la Figure 8.5. Les résultats montrent qu'il est nécessaire d'utiliser des huiles dont la viscosité est inférieure à 1000 mPa·sec pour atteindre une taille moyenne d'émulsion inférieure à 400 µm.

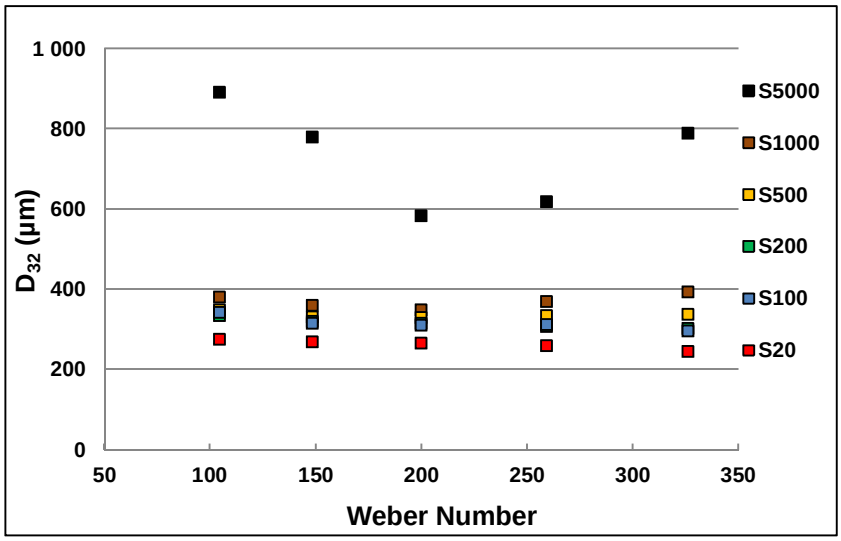

Figure 8.5: Effet du nombre de Weber et de la viscosité de l'huile sur la taille de goutte

Ces résultats mettent donc en évidence la nécessité de réduire la viscosité et/ou la tension interfaciale des bitumes dont la viscosité est supérieure à 10^5 mPa·sec à la température ambiante et la tension interfaciale entre 20 et 40 N/m. Ceci peut être réalisé en chauffant le bitume durant l'émulsification jusqu'à des températures de l'ordre de 90ºC (Figure 8.6), en diluant partiellement le bitume avec des fractions légères (Figure 8.7), ou bien en réduisant la tension interfaciale en utilisant des molécules tensio-actives afin de favoriser la génération d'interface durant l'émulsification. Cette dernière option reviendrait donc à produire des émulsions co-stabilisées par des particules et des tensio-actifs. Ces systèmes peuvent notamment être rencontrés pendant les opérations de traitement du bitume au niveau des sites d'extraction où des gouttelettes d'eau extrêmement stables se forment et posent des problèmes de séparation du bitume. Beaucoup de travaux ont été consacrés à ces systèmes mais la dynamique de stabilisation, encore mal définie, nécessite plus d'investigation.

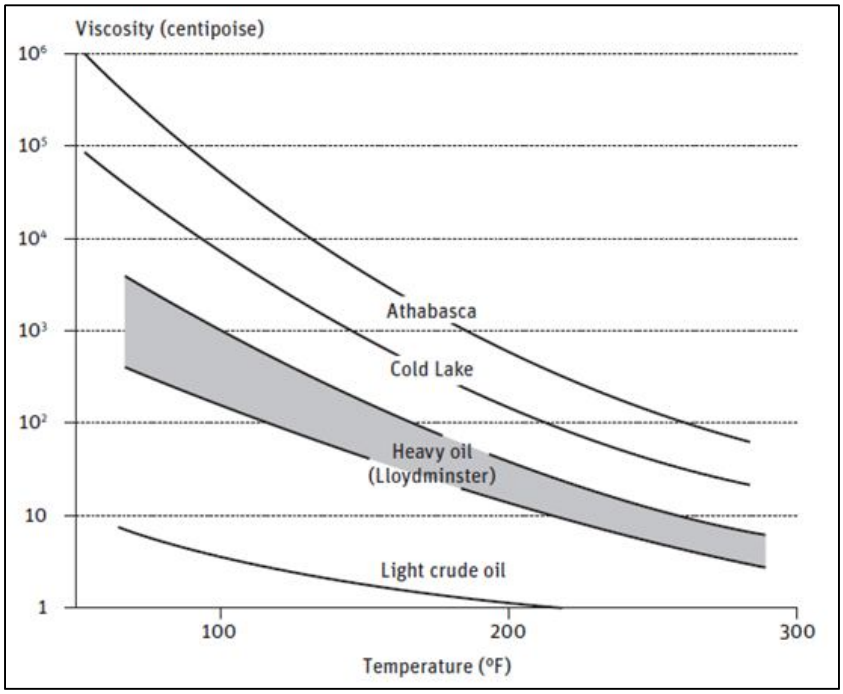

Figure 8.6: Effet de la température sur la viscosité de différents types de pétrole

(Transportation Research Board, 2013)

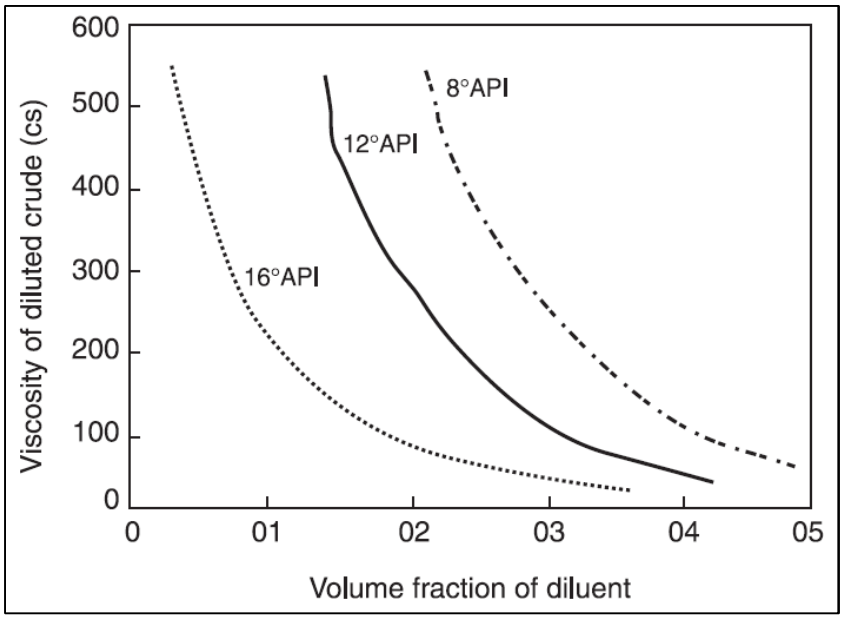

Figure 8.7: Effet de la dilution sur la viscosité de différents types de pétrole lourd

(Saniere et al. (2004))

Les futurs travaux devraient également s'orienter vers le choix du dispositif d'émulsification où d'autres géométries en cuves agitées pourraient être considérées (type et nombre d'agitateurs, chicanes…) pour essayer de produire des émulsions avec les propriétés requises pour le transport. D'autres systèmes, tels que les mélangeurs statiques, pourront également être étudiés.

8.2.3.2 Émulsification par des mélangeurs statiques

L'utilisation de mélangeurs statiques est suggérée pour un fonctionnement continu en raison de la taille relativement élevée de l'émulsion qui doit être produite (200 µm).

En effet, l'utilisation d'un système de type rotor/stator produirait des tailles beaucoup plus petites en raison du niveau de cisaillement élevé, ce qui augmenterait, d'une part, la viscosité apparente du brut d'une part, et risquerait d'endommager le produit d'autre part.

De plus, l'utilisation d'un mélangeur dynamique nécessiterait des coûts de maintenance relativement importants. Les mélangeurs statiques ont souvent été utilisés pour produire des émulsions de bitume stabilisées par des agents tensio-actifs. Gregoli et al. (1988) ont ainsi utilisé un mélangeur statique fourni par Komax pour émulsifier du pétrole visqueux alors que Marchal et al. (1988) avaient utilisé un mélangeur de type Kenics (Chemineer Ltd) pour la préparation d'émulsions concentrées à 70% de bitume avec des tailles allant de 2 à 8 µm. Il a été également proposé d'utiliser un SMX (Sulzer Chemtech) pour ce type d'émulsions (Catafalmo et al. (2001)). Globalement il est recommandé d'utiliser des mélangeurs de type Kenics, SMX, SMV, LLPD et Komax SM pour les dispersions de liquides immiscibles.

Trois critères sont généralement considérés pour le choix d'un mélangeur statique : le coût qui est relié à la complexité des éléments internes et donc à la fabrication, la chute de pression générée par l'écoulement et définie par un coefficient de frottement, et enfin l'efficacité de mélange ou de dispersion obtenue à partir du coefficient de variation défini par le rapport entre la déviation standard de la concentration et la concentration moyenne du mélange et qui doit être proche de zéro (Habituellement CoV = 0.05). À cela vient s'ajouter la distribution de taille des gouttes lorsqu'il s'agit d'une opération d'émulsification.

Dans ce même contexte, Gingras et al. (2007) ont étudié l'effet des conditions opératoires sur les performances d'emulsification en ligne de bitume (PG 64-22 de McAsphalt, Canada). Ils ont notamment considéré l'effet du débit (90 – 370 kg/h), du type de mélangeur (SMX et hélicoïdal),

de la configuration de mélange ainsi que la concentration de bitume (81% - 94%) et la température (90 - 97°C). Leurs résultats ont montré qu'il était possible d'obtenir des tailles de gouttes de l'ordre de 2 μm et que les configurations pour lesquelles la chute de pression était réduite correspondaient à celles où les mélangeurs SMX étaient insérés après les mélangeurs hélicoïdaux.

Dans le cas présent où il est question de l'émulsification de bitume dans une optique de transport, un choix de mélangeurs statiques devra d'abord être fait, ensuite une sélection de la configuration de mélange incluant le nombre de mélangeurs, leurs dimensions et leur disposition.

Globalement, tel que mentionné précédemment, deux types de mélangeurs peuvent être considérés : un mélangeur statique à géométrie complexe dont le coût est relativement élevé et engendrant une perte de charge conséquente mais ayant une efficacité élevée tel que le SMX, ou alors un mélangeur ayant une géométrie moins complexe, engendrant une perte de charge moins importante mais avec une efficacité moins élevée tel que le Kenics. À ces considérations viennent s'ajouter celles reliées aux opérations de maintenance et de nettoyage. Une étude comparative conduite par Rauline et al. (2000) ont montré qu'en termes de performances de mélange le SMX était équivalaient à 2 ou 3 Kenics. Il est ainsi recommandé d'utiliser entre 6 et 9 éléments pour un SMX avec L/D = 1 alors que 24 éléments sont requis pour un Kenics avec L/D ≈ 1.5 pour obtenir des résultats similaires avec CoV = 0.05 (Rauline D. et al (2000)). Pour l'émulsification de pétrole lourd, Gregoli et al. (1988) recommandent de ne pas dépasser 3.556 m/sec de vitesse et 4.14 bar de perte de charge à travers les mélangeurs. Théron et al (2011) ont comparé les performances d'émulsification en régime turbulent d'un SMX, d'un SMX plus et d'un SMV (Figure 8.8). Les auteurs ont ainsi quantifié la perte de charge et la taille d'émulsion pour chaque type de mélangeur et ont également étudié l'effet de la fraction volumique de la phase dispersée, le débit, la géométrie ainsi que le nombre d'éléments de mélange.

Les résultats ont montré que le SMX génère une chute de pression deux fois plus importante que celle générée par le SMX plus, alors que celle obtenue avec le SMV était légèrement inférieure à celle du SMX plus. Cependant, il a été trouvé également que le SMX produisait des tailles de gouttes plus petites et des distributions plus étroites que le SMX plus et le SMV (Tableau 8.5).

Tableau 8.5: Taille de gouttes obtenues par Théron et al. (2011) pour Φ_d=25% et V≈1.35 m/sec

Type	SMX	SMX+	SMV
D_{32} (µm)	31.8	36.5	46.5

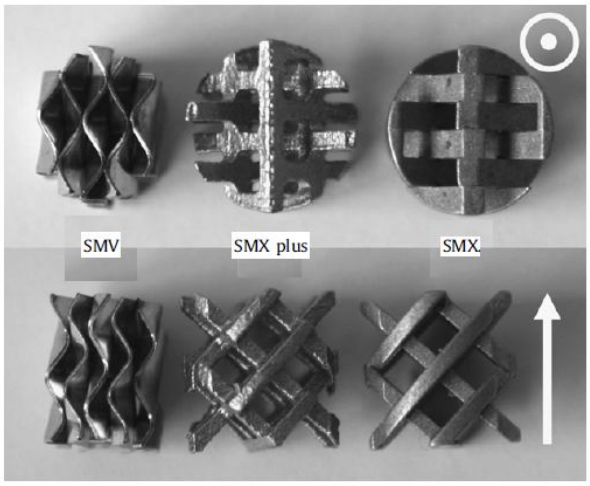

Figure 8.8: Mélangeurs statiques utilisés par Théron et al. (2011)

Il a été également observé que la fraction volumique de la phase dispersée avait peu d'effet sur la taille de goutte avec le SMX. Ce comportement a été attribué au temps de séjour relativement bas (≤ 0.1 sec). D'autre part, il a été révélé que la taille de gouttes diminuait avec le nombre d'éléments sauf au-delà de 10 éléments pour le SMX+ et le SMV où elle se maintenait à une valeur constante.

Ceci dit, une étude plus approfondie qui tient compte des contraintes associées au procédé considéré, devra être réalisée afin de choisir la configuration optimale d'émulsification. Similairement à ce qui a été réalisé dans le cas de la cuve agitée, cette étude comporterait une portion expérimentale qui pourra être réalisée sur le même dispositif utilisé par Gingras et al (2007) pour l'émulsification de bitume en ligne au niveau du laboratoire de l'URPEI (Figure 8.9). Dans cette partie, seront ainsi identifiés les mécanismes contrôlant l'émulsification par des particules solides à travers des mélangeurs statiques et seront déduits les paramètres clés de cette opération. Sur la base des résultats obtenus, sera développé ensuite un modèle permettant de prédire les propriétés des émulsions produites à partir des conditions opératoires. Finalement, il sera nécessaire d'établir les règles permettant de passer à des échelles plus grandes et être ainsi en mesure de concevoir un procédé d'émulsification à l'échelle industrielle.

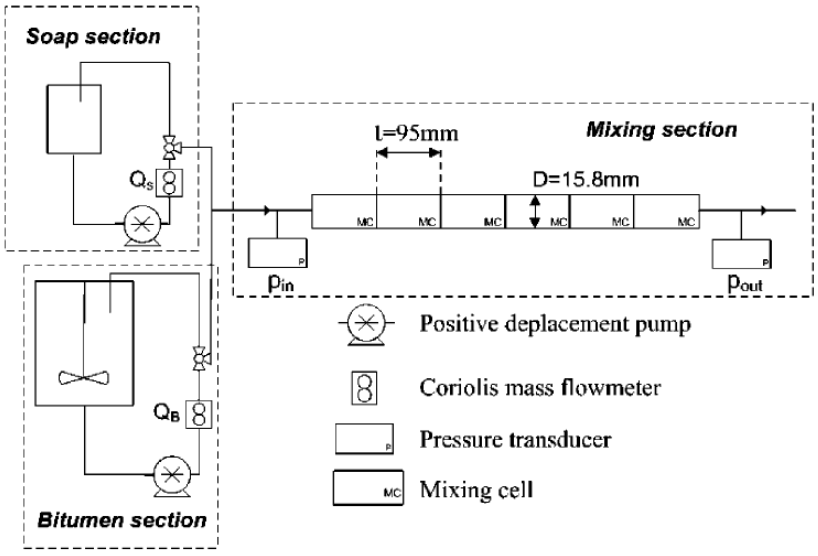

Figure 8.9: Dispositif d'emulsification de bitume en ligne utilisé par Gingras et al. (2007)

Malgré le fait que le fonctionnement d'un mélangeur statique soit différent des cuves agitées, les mêmes étapes pourront être suivies pour prédire les propriétés de l'émulsion. La première étape serait donc d'évaluer le potentiel de génération d'interface et le potentiel de couverture. La seconde étape serait de comparer les deux potentiels pour déduire l'interface théoriquement couverte. Enfin, la dernière étape consisterait à déduire l'interface réellement couverte, et donc la taille finale de l'émulsion, à travers la définition des efficacités de stabilisation.

Si le potentiel de couverture est relativement simple à calculer, le potentiel de génération d'interface est un peu plus compliqué à déduire car il faudrait disposer d'une corrélation tenant compte du type de mélangeurs choisis, de la présence de particules, de la viscosité élevée de la phase dispersée ainsi que de sa fraction.

Différents modèles sont disponibles dans la littérature. Legrand et al. (2001) ont utilisé 6 mélangeurs statiques en série de type SMX et ont considéré des fractions volumiques de la phase dispersée allant jusqu'à 25%. Considérant le mélangeur statique comme un milieu poreux, Legrand et al. (2001) ont proposé un modèle permettant de prédire la perte de charge et la taille d'émulsion à partir de la géométrie et des conditions opératoires. Ce modèle a été validé pour différents régimes (laminaire, transitoire et turbulent) avec différentes géométries (Tableau 8.6) mais n'a cependant pas pris en considération l'effet de la viscosité de la phase dispersée.

Tableau 8.6: Conditions expérimentales considérées par Legrand et al. (2001)

	Débit (m^3/sec)	Diamètre SM (m)	Tortuosité	Porosité	d_p (m)
SMX3	1.42E-06 - 8.50E-06	3.20E-03	1.5	0.77	0.75E-03
SMX4	1.42E-06 - 8.50E-06	4.80E-03	1.5	0.78	1.34E-03
SMXG10	1.42E-06 - 8.50E-06	1.00E-02	1.3	0.66	1.96E-03

Théron et al (2011) ont adopté une approche similaire à celle de Legrand et al. (2001) pour déduire le diamètre moyen de l'émulsion. Le modèle proposé n'a été validé que pour un seul rapport de viscosité et n'illustre donc pas l'effet de ce paramètre sur les performances d'émulsification.

L'effet du rapport de viscosité sur la taille d'émulsion a été pris en considération dans d'autres travaux tels que ceux de Streiff et al. (1997) réalisés avec des mélangeurs de type SMV, SMX et SMXL pour une fraction de la phase dispersée de 1% et ceux de Hirschberg et al. (2009) réalisés avec le SMX plus avec une fraction de 5%. Les modèles proposés ont été dérivés de celui proposé par Berkman et al. (1988) réalisé pour un mélangeur Kenics et validé en régime turbulent pour les conditions représentées sur le tableau 8.7. Ces modèles n'ont cependant été validés que pour de faibles concentrations de la phase dispersée.

Tableau 8.7: Conditions expérimentales considérées par Berkman et al. (1988)

Type	N_{sm}	D_{sm} (cm)	L_{sm}/D_{sm}	η_d/η_c	Φ_d	V_{sm} (m/sec)
Kenics	24	1.91	1.5	0.6 - 204	0.057% - 0.1%	0.58 – 1.05

Les effets du rapport de viscosité et de la fraction de la phase dispersée ont été considérés par Lobry et al. (2011) qui ont étudié les performances d'émulsification en régime turbulent à travers un mélangeur de type SMV. Il a ainsi été observé que la chute de pression diminuait avec la fraction volumique jusqu'au point d'inversion de phase ou celle-ci augmentait. Il a également été montré que la fraction volumique de la phase dispersée n'avait pas d'effet significatif sur la taille d'émulsion (Tableau 8.8).

Tableau 8.8: Taille de gouttes obtenues par Lobry et al. (2011)

Φ_d	10%	20%	25%	40%	60%
D_{32} (μm)	38.90	37.10	38.30	37.12	40.10

Ce résultat a suggéré que la coalescence avait peu d'effet à travers les mélangeurs statiques et que l'émulsification était principalement contrôlée par le processus de génération d'interface. Cet effet a été attribué au temps de contact très court entre les gouttes lors des collisions en raison du niveau élevé de turbulence, ce qui réduit l'efficacité de collision et donc celle de coalescence.

Ces travaux illustrent la difficulté associée au choix du modèle à utiliser dans le cas de l'émulsification du bitume par des particules pour son transport où il est question d'une phase dispersée très visqueuse et très concentrées en présence de particules solides. Néanmoins, les résultats obtenus par Lobry et al. (2011) laisseraient penser qu'il serait possible d'utiliser les modèles proposés pour les fractions relativement faibles dans notre cas et qu'il faudrait juste y inclure l'effet des particules solides et de la phase dispersée sur le niveau de turbulence. Les modèles de Berkman et al. (1988) pour le Kenics, de Streiff et al. (1997) pour le SMV, le SMX et le SMXL et de Hirschberg, et al (2009) pour le SMX plus, semblent être les mieux adaptés pour le cas considéré. De même que pour les tailles de gouttes considérés, et tel qu'il a été mentionné précédemment, il serait avantageux d'utiliser des mélangeurs statiques ayant une géométrie relativement complexe tel que le SMX plus et le SMV qui sont plus efficaces que les mélangeurs hélicoïdaux et ont l'avantage de générer une chute de pression moins importante que le SMX.

Après avoir obtenu l'interface théoriquement couverte à partir des potentiels de couverture te de génération d'interface, l'étape suivante consisterait à déterminer l'efficacité de stabilisation à partir des quatre conditions d'attachement définies dans le chapitre 7 :

1) La particule doit entrer en contact avec la goutte lors de la collision.
2) La ligne de contact des trois phases doit se former après le contact.
3) La force d'attachement de la particule doit être assez importante pour éviter le détachement.
4) La fréquence de stabilisation doit être plus importante que la fréquence de coalescence.

Sur la base de ces quatre conditions pourront ensuite être définies les quatre efficacités à partir desquelles est obtenue l'efficacité globale de stabilisation :

$$A_{Eff} = A_{Th} \times (E_{Col} \times E_{TPCL} \times E_{Att} \times E_{Cov}) \cdots (8.2)$$

Dépendant essentiellement du taux de dissipation de l'énergie cinétique dans le système, les expressions de ces efficacités seront les mêmes que celles considérées pour le cas de la cuve

agitées. Certains ajustements devront cependant être effectués pour prendre en compte la géométrie du système et le fait que ce soit un procédé continu.

8.2.3.3 Le scale-up de l'opération d'émulsification

L'objectif du scale-up est de reproduire le procédé à une échelle plus grande en gardant les mêmes performances. Cette opération peut s'avérer être très complexe lorsque différents phénomènes sont mis en jeu. Une compréhension des mécanismes contrôlant le procédé est donc indispensable. Dans le cas d'une émulsification standard en cuve agitée, où il est question de rupture et de coalescence, il est souvent recommandé de maintenir un taux de dissipation d'énergie constant (P/V) pour les systèmes peu ou non coalescents et un temps de circulation constant pour les systèmes très coalescents. Il est également recommandé de maintenir une certaine similarité géométrique pour le premier cas et d'utiliser, pour les systèmes coalescents, plus d'agitateurs avec éventuellement une plus grande taille (Paul et al. (2004)). Ceci dit, il a été observé que cette approche n'était valable, dans le meilleur des cas, que pour un scale-up d'environ cents fois le volume initial, et que des ajustements devaient être effectués pour des scale-up plus importants.

Dans le cas de l'émulsification par des particules la complexité de l'opération de scale-up est accentuée par la présence de particules et le mode de stabilisation de l'émulsion. En effet, en plus des mécanismes de génération d'interface et de coalescence, il est nécessaire de considérer la suspension des particules solides et leur adsorption à la surface des gouttes produites. Dans le cas présent, il est possible de commencer l'analyse en nous basant sur le modèle proposé au chapitre 7 pour une configuration en cuve agitée (Figure 8.4). La première étape du modèle est de déterminer le potentiel de génération d'interface, ensuite de le comparer au potentiel de couverture pour déduire l'interface théoriquement couverte, et finalement de définir les différentes efficacités de stabilisation pour déduire l'interface réellement couverte par des particules. Sur la base de cette approche, deux régimes d'émulsification ont été définis. Le premier régime concerne le cas où le système contient assez de particules pour couvrir l'interface générée. Dans ce premier cas, une corrélation a été proposée pour prédire la taille d'émulsion, et donc l'interface générée, à partir des conditions opératoires :

$$\frac{D_{32}}{D_i} = C_{Model} \cdot We^{-0.6} \cdot \left(1 + 0.97 \cdot Vi^{0.79}\right)^{0.6} \cdots (8.3)$$

$$C_{Model} = 0.0125 \cdot \left(1 + \left(0.137 \cdot \left(1 + 2.5\phi_p\right)^{-4.5} \cdot Re_d^{0.3} \cdot Re_c^{0.4}\right) \cdot 3 \cdot \phi_{Oil}\right) \cdots (8.4)$$

$$We = \frac{\rho_c N_i^2 D_i^3}{\gamma_{ow}} \cdots (8.5)$$

$$Vi = \frac{\eta_d N_i D_i}{\gamma_{ow}} \left(\frac{\rho_c}{\rho_d}\right)^{0.5} \cdots (8.6)$$

$$Re_c = \frac{\rho_c N_i D_i^2}{\eta_c} \cdots (8.7)$$

$$Re_d = \frac{\rho_d N_i D_i^2}{\eta_d} \cdots (8.8)$$

La taille de l'émulsion est fonction de différents groupes adimensionnels avec différents exposants : Le nombre de Weber, le nombre de viscosité, les nombre de Reynolds, et les fractions volumiques de la phase dispersée liquide et des particules solides.

Dans le deuxième cas, l'émulsification est contrôlée par le potentiel de couverture à travers le phénomène de coalescence limitée (Arditty et al. (2003)), l'interface théoriquement couverte est donnée par :

$$A_{cov} = A_{cov/1p} \cdot \left(N_p\right)_{total} \cdots (8.9)$$

A_{cov} étant l'interface théoriquement couverte, $A_{cov/1p}$ l'interface couverte par une particule, et $(N_p)_{total}$ le nombre total de particules.

Une fois le régime d'émulsification établi, la surface réellement couverte est déterminée en utilisant les efficacités de stabilisation dont les expressions sont essentiellement des fonctions du taux de dissipation de l'énergie cinétique turbulente, du temps de circulation, de la taille de goutte générée et des propriétés des phases (densités, viscosités, taille et mouillabilité des particules…).

Cette analyse préliminaire nous permet déjà de voir que dans le cas où l'émulsification est contrôlée par le potentiel de génération d'interface, les conditions opératoires interviennent à travers différents paramètres : le nombre de Weber ($\sim N^2 \cdot D^3$), le nombre de viscosité ($\sim N \cdot D$), les nombres de Reynolds ($\sim N \cdot D^2$), le niveau de puissance ($\sim N^3 \cdot D^5$), ainsi que le temps de circulation ($\sim N^{-1} \cdot D^{-3}$).

Dans le deuxième cas, les propriétés de l'émulsion sont beaucoup plus affectées par le niveau de puissance ($\sim N^3 \cdot D^5$) et le temps de circulation ($\sim N^{-1} \cdot D^{-3}$). Les autres paramètres interviennent indirectement à travers la taille de goutte au niveau des efficacités de stabilisation.

Ce constat nous permet donc de privilégier le cas où l'émulsification est contrôlée par le potentiel de couverture. La mise à l'échelle se ferait donc en considérant le taux de dissipation de l'énergie cinétique turbulente et le temps de circulation. La taille de goutte pouvant être ajustée à travers les fractions volumiques de la phase dispersée et des particules et les propriétés des phases. Cependant, il est important de mentionner qu'il pourrait être nécessaire de reproduire la même distribution d'énergie dans la cuve pour que le résultat de la mise à l'échelle soit le même.

Cette approche pourrait être considérée dans le cas des mélangeurs statiques une fois que le modèle proposé au chapitre 7 aura été adapté à cette configuration d'émulsification.

8.2.4 Déstabilisation de l'émulsion et séparation des phases

Il a été suggéré dans ce travail d'utiliser des particules d'Ilménite et/ou de Leucoxene pour la stabilisation de l'émulsion. Ce choix a été dicté par les propriétés physiques de ces particules, et notamment leurs propriétés électriques et magnétiques. L'idée serait donc d'utiliser un champ magnétique pour détacher les particules des interfaces et ensuite exploiter leur densité élevée pour les séparer de la phase aqueuse ou éventuellement mettre en place un procédé de flottation. Une étape de traitement doit également être envisagée pour mettre aux normes d'exploitation le bitume et les particules solides. Dans cette partie seront ainsi définies les lignes directrices permettant la conception d'un procédé de déstabilisation des émulsions de bitume.

Considéré comme étant des matériaux paramagnétiques et conducteurs, il est possible d'envisager la séparation des particules d'Ilménite et/ou de Leucoxene de l'interface par l'application d'un champ magnétique ou électrique afin de générer une force supérieure à la force capillaire responsable de l'attachement des particules aux interfaces. Scheludko et al. (1975) ont proposé l'expression ci-dessous pour estimer la force maximale d'attachement pour des particules sphériques:

$$F_{Att} = 2\pi\gamma_{ow} R_p \left(\cos\left(\frac{\theta}{2}\right)\right)^2 \cdots (8.10)$$

La Figure 8.10 illustre l'effet de la tension interfaciale et de la taille de particules sur ces forces d'attachement en considérant un angle de 90°.

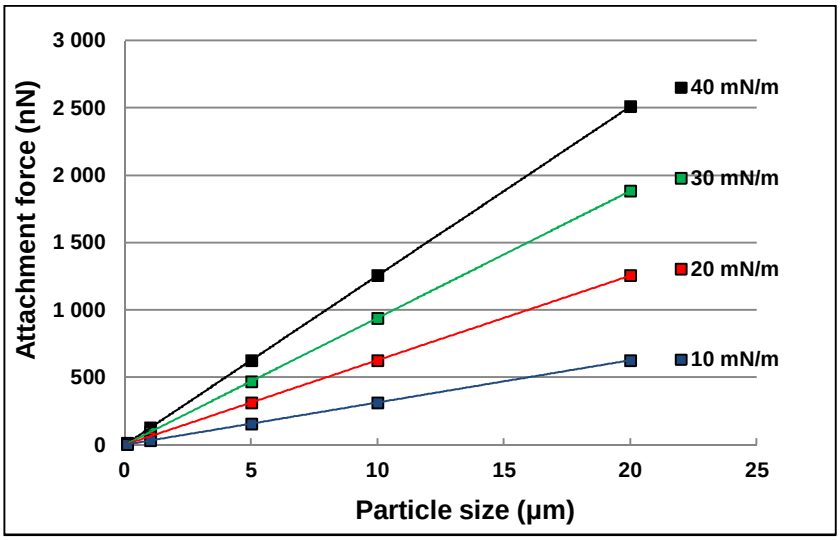

Figure 8.10: Effet de la tension interfaciale et de la taille de particule sur la force d'attachement maximale des particules à l'interface

La séparation par champ magnétique est déjà présente dans l'industrie minière où différentes technologies ont été développées, dont celle des séparateurs humides à haute intensité magnétique (Wet high-intensity magnetic separators, WHIMS machines) et des séparateurs à haut gradient magnétique (High gradient magnetic separation, HGMS machines). Ces deux technologies ont été décrites par Wills (2006) et ont notamment été considérées pour le cas de l'Ilménite dans différents travaux (Dobbins et al. (2007), Da-he (2000 et 2004), Yu-Feng et al. (2010), Chen et al. (2013), et Lu-zheng et al. (2013)). Dobbins et al. (2007) ont ainsi présenté les avantages des séparateurs humides à haute intensité magnétique qui augmentent l'efficacité de séparation de l'Ilménite. Une autre technologie exploitant à la fois la différence de densité et les propriétés magnétiques du minerai d'intérêt a également été développée. Il s'agit des hydrocyclones magnétiques qui ont fait l'objet de différents travaux. Premaratne et al. (2003 a et b) ont ainsi considéré ce dispositif pour séparer l'Ilménite des sables de plage du Sri Lanka. Ils ont appliqué, dans un premier temps, des champs magnétiques de différentes intensités (schéma décrit sur la Figure 8.11) en utilisant un aimant permanent et ensuite un séparateur magnétique isodynamique Cook (Frantz isodynamic magnetic separator) sur un échantillon contenant 80% de minerais lourds dont environ 70% d'Ilménite et 8% de Rutile avec une taille de particules

inférieure à 355 μm. Leurs résultats ont montré que l'Ilménite et la Pseudorutile se trouvent particulièrement concentrés dans les concentrés 2, 3 et 4 alors que le concentré 1 contient de la Magnétite et de l'Ilménite et que le résidu final contient du Zircon et de l'Ilménite. Les résultats ont ainsi révéler qu'un champ magnétique de 0.5 Tesla était suffisant pour séparer les minerais contenant du Titane. Les auteurs ont également démontré que l'augmentation de l'intensité du champ produit améliorait le rendement de l'opération de séparation.

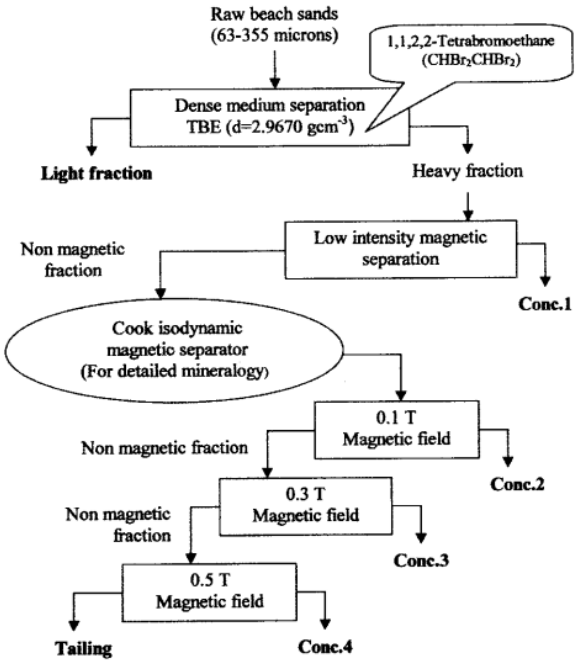

Figure 8.11: Schéma de la procédure de séparation utilisée par Premaratne et al. (2003)

Dans un second travail Premaratne et al. (2003b) ont évalué l'efficacité de séparation à travers un hydrocyclone magnétique qui consiste en un hydrocyclone classique auquel a été ajouté un aimant permanent (néodyme-fer-bore) selon le schéma illustré sur la Figure 8.12. Les résultats ont révélé que, comparativement aux hydrocyclones classiques, l'efficacité de séparation était améliorée de 5% avec les hydrocyclones magnétiques.

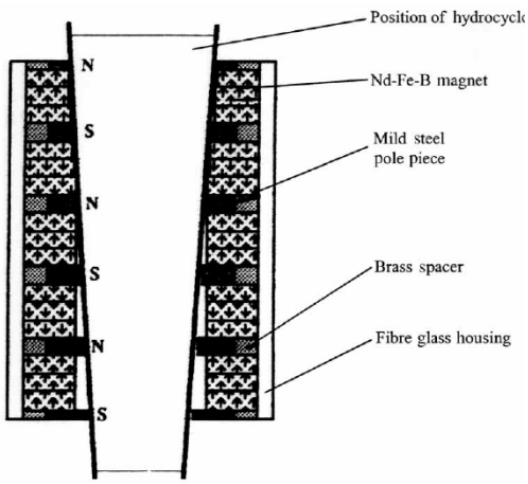

Figure 8.12: Schéma de l'hydrocyclone magnétique utilisé par Premaratne et al. (2003)

Les forces mises en jeu dans un tel dispositif sont la force centrifuge, la force de trainée et la force magnétique donnée par :

$$F_{Magn} = \mu_0 \chi V_p H \nabla H \cdots (8.11)$$

μ_0 étant la permittivité du vide en $kg \cdot m/s^2A^2$, χ la susceptibilité magnétique volumique, V_p le volume de la particule et H l'intensité du champ magnétique en A/m.

À travers ces différentes techniques il est donc possible de concevoir un dispositif pouvant déstabiliser l'émulsion en générant une force magnétique supérieure à la force d'attachement des particules et de séparer ainsi la phase huileuse de l'eau. Une étape de traitement des deux phases devra cependant être envisagée afin de satisfaire aux normes d'exploitation de l'eau et du bitume.

CHAPITRE 9. DISCUSSION GENERALE

Le remplacement des molécules tensio-actives par des particules solides à l'échelle industrielle présente de nouvelles opportunités et un certain nombre d'avantages dont celui de permettre la déstabilisation des émulsions à travers le contrôle des propriétés des particules.

Ainsi, s'inscrivant dans une optique de développement d'un procédé d'émulsification par des particules, le présent travail a pour principal objectif d'identifier les mécanismes mis en jeu durant la stabilisation de l'émulsion et de définir les conditions opératoires optimales (formulation et paramètres procédés) d'un tel procédé avec comme hypothèse de recherche qu'il est tout à fait possible d'utiliser des particules solides pour la stabilisation d'émulsion à l'échelle industrielle.

Ayant fait l'objet d'une multitude de travaux depuis les années quatre-vingts, différents effets associés à ces systèmes ont été révélés, allant des mécanismes d'adsorption des particules aux interfaces fluides jusqu'au comportement des émulsions (type, stabilité, taille…).

À l'échelle particulaire, les interactions impliquées lors de l'approche, de l'attachement de la particule et entre les particules adsorbées à l'interface ont été donc identifiées et dans certains cas quantifiées, incluant notamment les forces de van der Waals, les forces de la double couche électrique, les forces d'hydratation, les forces hydrophobiques et les forces capillaires. Parallèlement, à l'échelle de l'émulsion, différentes études ont été conduites pour identifier les paramètres affectant le comportement des émulsions de Pickering (Type, stabilité, taille, rhéologie). Les résultats ont ainsi révélé que le type d'émulsion dépendait de l'affinité des particules avec les deux phases, des proportions de ces deux phases et de la procédure de dispersion des particules. Quant à la stabilité, il a été observé qu'elle était directement liée à la compacité du réseau de particules adsorbées à l'interface. Elle est ainsi très liée à la mouillabilité des particules, à leur taille et forme ainsi qu'à leur quantité. Reflétant le niveau de stabilité des émulsions, il a été trouvé que la taille de celle-ci dépendait des mêmes paramètres affectant sa stabilité.

La rhéologie de ces systèmes n'a cependant été abordée que récemment mais il a pu être établi que, dans la plupart des cas, ces systèmes présentaient un comportement rhéofluidifiant avec une

contrainte seuil suivant le modèle de Herschel-Bulkeley. Des effets viscoélastiques et/ou thixotropes ont également été observés. L'ensemble de ces effets a ainsi été résumé dans le premier article.

Ceci dit, bien que beaucoup d'effets aient fait l'objet d'études, les données disponibles dans la littérature ne permettent pas encore la conception d'un procédé d'émulsification avec des particules et que l'effet de différents paramètres doit être approfondi, tel que celui de la viscosité qui constitue, dans la plupart des cas, la contrainte du procédé.

À cet effet, le problème a été abordé dans ce travail en considérant deux échelles. L'échelle de la particule où l'objectif est de favoriser la collision particule/goutte et l'adsorption des particules aux interfaces et l'échelle de la goutte où l'objectif est de favoriser la génération d'interface et sa couverture.

Le second article a ainsi été consacré à l'étude de l'échelle de la particule. Dans cette première partie expérimentale, les interactions mises en jeu lors de l'approche d'une particule de verre ou de polyéthylène (65 μm) et de son adsorption à une interface eau/huile silicone ont été quantifiées en utilisant la technique de la sonde colloïdale. L'étude de l'effet des propriétés des phases a permis de mettre en évidence les dynamiques impliquées pendant ces deux étapes. Il a ainsi pu être observé que l'approche et l'adsorption étaient favorisées par la réduction de la taille de la particule, la réduction de la viscosité ou par l'utilisation de particules ayant une meilleure affinité avec la phase huileuse. L'étape de l'approche a été associée à un processus de drainage de film alors que l'adsorption a été reliée à une montée capillaire.

Les articles 3 et 4 ont par ailleurs été consacrés à l'étude de l'échelle de la goutte ou un dispositif expérimental d'émulsification a été mis en place. Ce dispositif consistait en une cuve d'un litre dans laquelle a été disposée une turbine à pales inclinées qui a été décentrée pour éviter la formation de vortex. Des émulsions concentrées huile/eau (53%v) ont été préparées en utilisant des huiles silicones et des particules de verre. Les émulsions produites ont été caractérisées par des mesures de distribution de taille en utilisant un Mastersizer 3000 de Malvern, des techniques de visualisation et des mesures de temps de mélange et de circulation en utilisant la technique de la décolorisation.

Les résultats obtenus dans l'article 3 ont confirmé les effets observés à l'échelle de la particule et ont montré qu'il est possible de réduire l'effet de l'augmentation de la viscosité de l'huile en

réduisant la taille des particules ou en utilisant des particules ayant une hydrophobicité intermédiaire ce qui, notamment, favorise le drainage du film et l'adsorption des particules.

Les conditions opératoires (temps et niveau d'énergie) ont été abordées dans l'article 4 et il a été révélé que la stabilisation des huiles les moins visqueuses prenait plus de temps en raison de l'augmentation de la quantité d'interface générée. Un effet intéressant a été également observé lors de l'étude de l'effet couplé de la viscosité de l'huile et du niveau énergétique. Il a ainsi été mis en évidence que l'augmentation de la capacité du système à générer de l'interface, à travers l'augmentation du niveau d'énergie, pouvait réduire l'efficacité d'adsorption des particules et donc l'efficacité de stabilisation. Cet effet étant particulièrement significatif avec les huiles les plus visqueuses où la taille de goutte et le temps d'adsorption sont plus importants, ce qui réduit l'efficacité de drainage du film en raison de la déformabilité des gouttes et l'efficacité d'adsorption suite au détachement des particules n'ayant pas atteint leur position d'équilibre à l'interface.

Il a été également établi qu'une quantité optimale de particules doit être considérée afin de couvrir l'interface générée sans réduire le taux de dissipation de l'énergie cinétique turbulente contrôlant notamment la force de collision entre les particules et les gouttes.

Sur la base des résultats obtenus, une procédure permettant l'estimation de la taille moyenne de l'émulsion à partir des propriétés du système et des conditions opératoires a été proposée dans l'article 5.

Considérant l'effet de gonflage de goutte résultant de l'adsorption des particules, cette approche semi empirique consiste à déduire tout d'abord un diamètre théorique de goutte en comparant la capacité du système à générer de l'interface à sa capacité de couverture.

Ainsi, si la quantité de particules disponible est suffisante à couvrir l'interface produite, l'émulsification est contrôlée par le potentiel de génération d'interface. Sinon, elle est contrôlée par le potentiel de couverture à travers le processus de coalescence limitée.

La capacité de couverture a été déduite à partir des propriétés des particules alors que la capacité de génération d'interface a été obtenue à partir des propriétés des phases et l'hydrodynamique du système. Cette dernière capacité a notamment été obtenue en modifiant la corrélation proposée par Calabrese R. V. et al. (1986) pour tenir compte de la présence de particules, de l'effet de la coalescence et de la géométrie du système.

La seconde étape a consisté à déduire la taille réelle en introduisant plusieurs efficacités associées aux étapes de la stabilisation. Une efficacité de couverture a ainsi été définie en comparant les taux de couverture des gouttes et la fréquence de coalescence, une efficacité de contact ou de collision en comparant le temps de drainage du film séparant la particule et la goutte et le temps de contact, une efficacité de formation de la ligne de contact des trois phases après la collision, de même qu'une efficacité d'attachement comparant les forces d'attachement et de détachement a été introduite.

Cette approche a abouti à la définition d'une version modifiée de la corrélation de Calabrese R. V. et al. (1986) qui a notamment donné des résultats très satisfaisants pour une large gamme de viscosités (19 mPa·sec - 4875 mPa·sec), de nombres de Weber (104.16 - 326.05) et de capacités de couverture (5.36 m^2 - 18.75 m^2). Cette corrélation a également reproduit les effets résultant de la compétition des mécanismes de génération d'interface et de stabilisation de même que l'effet de la coalescence. La transition entre le régime d'émulsification contrôlé par le potentiel de couverture et celui contrôlé par le potentiel de de génération d'interface, a également été reproduite.

Finalement, considérant les propriétés d'émulsion observées, une solution a été proposée pour le transport des pétroles lourds de l'ouest canadien vers les sites de raffinage et d'exportation. En effet, le transport de ce pétrole lourd et visqueux pose de sérieux problèmes aux industriels qui utilisent actuellement la dilution pour réduire la viscosité du bitume et permettre son pompage. Nous proposons de remplacer cette technique par l'émulsification par des particules solides.

Il est ainsi suggéré d'utiliser les particules d'Ilménite et/ou de Leucoxene (minerais contenant de l'oxyde de titane) pour la stabilisation d'émulsions de pétrole lourd dans l'eau afin de réduire sa viscosité apparente et de permettre son transport par pipeline.

Présents à des proportions relativement élevées dans la fraction solide issue des unités de centrifugation (traitement secondaire des sables bitumineux), cette approche permettrait de transporter également ces minerais en même temps que le bitume vers les sites de traitement et d'exportation et se substituerait au transport par voie ferroviaire. Ces minerais ont été choisis en raison de leur intérêt commercial, de leur disponibilité au niveau des sites d'extraction de bitume, mais également en raison de leurs propriétés physiques et plus particulièrement leurs propriétés

magnétiques qui permettraient la déstabilisation de l'émulsion par l'application d'un champ magnétique.

Cette approche soulève cependant différentes problématiques tel que le choix du dispositif adéquat, les conditions optimales d'émulsification, l'effet des particules sur les propriétés de l'émulsion produite et finalement le scale-up. Aussi et pour parvenir à la conception d'un tel procédé d'émulsification à l'échelle industrielle, ces aspects devront être abordés dans les projets futurs.

CHAPITRE 10. CONCLUSION ET RECOMMANDATIONS

Le principal objectif de ce travail de thèse consiste à identifier les mécanismes mis en jeu durant la stabilisation d'émulsion par des particules solides et de définir les conditions optimales (formulation et paramètres procédés) d'un tel procédé. Pour atteindre cet objectif, trois objectifs spécifiques ont été considérés et cinq articles sont présentés.

La stabilisation de la plupart des émulsions à l'échelle industrielle est réalisée par des molécules tensioactives dont la demande ne cesse d'augmenter tout autant que les coûts de production.

Ainsi, dans l'actuel contexte économique et écologique, il est devenu nécessaire de trouver une solution alternative à l'utilisation des tensioactifs et c'est par conséquent, dans ce contexte, que l'utilisation des particules solides est suggérée pour la stabilisation des émulsions.

Ce choix s'appuie notamment sur les résultats disponibles dans la littérature et résumés dans l'article 1. Il a ainsi été trouvé qu'il était possible de stabiliser différents types d'émulsions simples ou multiples en utilisant différents types de particules. Une longue stabilité de ces systèmes a également été observée, stabilité qu'il est possible d'interrompre dans plusieurs cas par centrifugation, par séparation magnétique ou en modifiant la mouillabilité des particules.

Ceci dit et afin de concevoir un tel procédé une analyse plus poussée est nécessaire. À cet effet, deux échelles ont été considérées. L'échelle de la particule où il est question d'interactions entre une particule solide et une interface liquide/liquide. Cette échelle a ainsi été étudiée en identifiant ces différentes interactions et en déterminant les paramètres les affectant. Les résultats, présentés dans l'article 2 et notamment obtenus grâce à la technique de la sonde colloïdale, montrent que, pour favoriser l'attachement de particule, il est nécessaire d'accélérer le drainage du film séparant la particule et l'interface lors de la collision et de maximiser la force capillaire afin d'éviter le détachement.

La deuxième partie a ensuite été consacrée à l'échelle de la goutte en utilisant un dispositif d'émulsification en cuve agitée. L'effet des propriétés des phases, présenté dans l'article 3, a d'abord été considéré. Le lien entre l'échelle de la particule et celui de la goutte a ainsi été établi montrant que la stabilisation est améliorée en favorisant le drainage de film et en maximisant la force d'attachement des particules. Il a également été trouvé que la stabilisation peut être

améliorée dans le cas des viscosités élevées en réduisant la taille des particules ou en utilisant des particules ayant une meilleure affinité avec la phase dispersée. Deux régimes d'émulsification ont également été identifiés. Le premier étant contrôlé par le potentiel de couverture et le second par le potentiel de génération d'interface. L'effet des conditions opératoires, présenté dans l'article 4, a ensuite été étudié. Il a été ainsi trouvé qu'il est nécessaire de considérer l'interaction entre le niveau d'énergie, la viscosité de la phase dispersée et la quantité de particules afin de définir les conditions optimales favorisant à la fois la génération d'interface et sa stabilisation.

La troisième partie a été consacrée au développement d'un modèle permettant de prédire les propriétés des émulsions produites à partir des conditions du système. La procédure a consisté d'abord à comparer le potentiel de couverture avec celui de la génération d'interface afin de déduire l'interface théoriquement couverte et ensuite à déduire celle réellement couverte en tenant compte des efficacités de stabilisation.

Cette approche semi-empirique, décrite dans l'article 5, a permis d'obtenir des tailles moyennes de gouttes très proches des données expérimentales validant ainsi l'analyse proposée.

Ce travail de thèse a ainsi permis de mettre en évidence les principaux paramètres contrôlant le processus de stabilisation des émulsions de Pickering. Il a été également possible de révéler de nouveaux effets reflétant la nécessité de trouver un compromis entre la génération d'interface et sa stabilisation pour la conception d'un procédé d'émulsification par des particules. Les résultats obtenus ont de même permis le développement d'une procédure pour prédire les propriétés d'émulsions à partir des propriétés du système et des conditions opératoires.

Une dernière partie a été consacrée à l'application des émulsions de Pickering pour le transport des pétroles lourds de l'ouest canadien vers les sites de raffinage et d'exportation. L'objectif étant de réduire la viscosité apparente du bitume en le dispersant sous forme de gouttelettes dans une phase aqueuse afin de permettre son pompage à travers des pipelines, il a ainsi été proposé de stabiliser les émulsions en utilisant des minerais ayant un intérêt commercial et donc, de transporter donc le bitume et ces minerais d'intérêt par pipeline.

Les lignes directrices d'un tel projet d'émulsification ont été établies sur la base des résultats obtenus dans cette thèse. Les principaux défis à relever ont été également mis en évidence et dont la plupart vont pouvoir être considérés pour dans le cadre d'autres projets de conception de procédés d'émulsification par des particules.

Le premier axe de recherche qui pourrait être développé concerne le type d'équipement qu'il faudra utiliser pour ce type d'opération. En effet, ayant utilisé une turbine à pâles inclinées décentrée dans une cuve sans chicanes, ce travail devra être étendu à d'autres configurations en cuve agitées en considérant d'autres types d'agitateurs, le nombre d'agitateurs et leur position, la présence de chicanes…etc.

D'autres dispositifs de mélange, tels que les mélangeurs statiques qui offrent beaucoup d'avantages par rapport aux cuves agitées, devront également faire l'objet d'études. Une fois qu'une configuration optimale, favorisant à la fois la génération d'interface et sa stabilisation, aura été définie, une mise à l'échelle sera nécessaire pour passer de l'échelle du laboratoire à l'échelle industrielle. Pour réaliser cette étape il est nécessaire que les mécanismes contrôlant le procédé soient bien identifiés et que les effets de la mise à l'échelle sur ces mécanismes soient étudiés. Finalement, le modèle proposé dans ce travail, pour prédire les propriétés de l'émulsion, pourra être adapté pour tenir compte de la configuration d'émulsification qui aura été choisie et des contraintes de la mise en échelle et, par conséquent, simplifier la conception de ces procédés à l'échelle industrielle

Le deuxième axe de recherche porterait sur l'effet des particules sur le comportement de l'émulsion. En effet, selon les propriétés des particules, l'émulsion produite pouvait sédimenter, crémer ou floculer ce qui affecterait le procédé d'émulsification ainsi que le transport par pipeline.

Cet aspect pourrait cependant être exploité au niveau des procédés de séparation dont la plupart sont basés sur la différence de densité entre les éléments à séparer. C'est d'ailleurs ce même principe qui est utilisé au niveau des procédés de séparation de minerais par flottation où la flottabilité des bulles d'air est exploitée pour séparer les minerais hydrophobes des minerais hydrophiles. Les émulsions de Pickering pourraient donc être exploitées dans ce même contexte.

Le troisième axe de recherche concernerait les émulsions co-stabilisées par des particules et des agents tensio-actifs. Ces systèmes sont notamment rencontrés durant le traitement des bitumes et plus particulièrement lors de la séparation du bitume de l'eau. Durant cette opération des gouttes d'eau se forment et sont stabilisées par des particules solides (argiles, produits de corrosion…) et des surfactants naturels (asphaltènes). Dans certains cas se forment également des émulsions multiples huile/eau/huile très stables.

La compréhension de la dynamique de stabilisation de ces systèmes est donc indispensable pour pouvoir séparer l’eau du bitume.

BIBLIOGRAPHIE

Abismail, B., Canselier, J. P., Wilhelm, A. M., Delmas, H., & Gourdon, C. (1999). Emulsification by ultrasound: drop size distribution and stability. Ultrasonics Sonochemistry, 6(1-2), 75-83.

Alberta Chamber of Resources, (1996). The Future of the Oil Sands Heavy Mineral Production. Executive Summary, Mineral Developments Agreement, Co-product study,

Arditty, S., Whitby, C. P., Binks, B. P., Schmitt, V., & Leal-Calderon, F. (2003). Some general features of limited coalescence in solid-stabilized emulsions. European Physical Journal E. 12(2), 355-355.

Aston, D. E., & Berg, J. C. (2001). Quantitative analysis of fluid interface-atomic force microscopy. Journal of Colloid & Interface Science, 235(1), 162-169.

Aveyard, R., Binks, B. P., & Clint, J. H. (2003). Emulsions stabilised solely by colloidal particles. Advances in Colloid and Interface Science 100. 503-546.

Aveyard, R., Binks, B. P., & Clint, J. H. (2003). Emulsions stabilised solely by colloidal particles. Advances in Colloid and Interface Science, 100. 503-546.

Aveyard, R., Binks, B. P., Clint, J. H., Fletcher, P. D. I., Horozov, T. S., Neumann, B., & Burgess, A. N. (2002). Measurement of long-range repulsive forces between charged particles at an oil-water interface. Physical Review Letters, 88(24), 1-4.

Aveyard, R., Clint, J. H., & Nees, D. (2000). Small solid particles and liquid lenses at fluid/fluid interfaces. Colloid and Polymer Science, 278(2), 155-163.

Aveyard, R., Clint, J. H., Nees, D., & Paunov, V. N. (2000a). Compression and structure of monolayers of charged latex particles at air/water and octane/water interfaces. Langmuir, 16(4), 1969-1979.

Aveyard, R., Clint, J. H., Nees, D., & Quirke, N. (2000b). Structure and collapse of particle monolayers under lateral pressure at the octane/aqueous surfactant solution interface. Langmuir, 16(23), 8820-8828.

Bazhlekov, I. B., Chesters, A. K., & van de Vosse, F. N. (2000a). The effect of the dispersed to continuous-phase viscosity ratio on film drainage between interacting drops. International Journal of Multiphase Flow, 26(3), 445-466.

Bazhlekov, I. B., van de Vosse,, F. N., & Chesters, A. K. (2000b). Drainage and rupture of a Newtonian film between two power-law liquid drops interacting under a constant force. Journal of Non-Newtonian Fluid Mechanics, 93(2-3), 181-201.

Berkman, P. D., & Calabrese, R. V., (1988), Dispersion of viscous liquids by turbulent flow in a static mixer. AIChE Journal 34(4), 602–609.

Biggs, S. (1996). Non-equilibrium interaction forces between adsorbed polymer layers. Journal of the Chemical Society-Faraday Transactions, 92(15), 2783-2789.

Biggs, S., & Proud, A. D. (1997). Forces between silica surfaces in aqueous solutions of a weak polyelectrolyte. Langmuir, 13(26), 7202-7210.

Binks, B. P. (2002). Particles as surfactants: similarities and differences, Current Opinion in Colloid & Interface Science, 7(1-2), 21-41.

Binks, B. P. (2007). Colloidal particles at liquid interfaces. Physical Chemistry Chemical Physics, 9(48), 6298-6299.

Binks, B. P., & Clint, J. H. (2002). Solid wettability from surface energy components: Relevance to Pickering emulsions. Langmuir, 18(4), 1270-1273.

Binks, B. P., Clint, J. H., & Whitby, C. P. (2005). Rheological behavior of water-in-oil emulsions stabilized by hydrophobic bentonite particles. Langmuir, 21(12), 5307-5316.

Binks, B. P., Dyab, A. K. F., & Fletcher, P. D. I. (2003). Novel emulsions of ionic liquids stabilised solely by silica nanoparticles. The Royal Society of Chemistry, 20, 2540-2541.

Binks, B. P., Dyab, A. K. F., & Fletcher, P. D. I. (2007). Contact angles in relation to emulsions stabilised solely by silica nanoparticles including systems containing room temperature ionic liquids. Physical Chemistry Chemical Physics, 9(48), 6391-6397.

Binks, B. P., & Fletcher, P. D. I. (2001). Particles adsorbed at the oil-water interface: A theoretical comparison between spheres of uniform wettability and "Janus" particles. Langmuir, 17(16), 4708-4710.

Binks, B. P., Isa, L., & Tyowua, A. T. (2013). Direct Measurement of Contact Angles of Silica Particles in Relation to Double Inversion of Pickering Emulsions. Langmuir, 29(16), 4923-4927.

Binks, B. P., & Kirkland, M. (2002). Interfacial structure of solid-stabilised emulsions studied by scanning electron microscopy. Physical Chemistry Chemical Physics, 4(15), 3727-3733.

Binks, B. P., Liu, W. H., & Rodrigues, J. A. (2008). Novel stabilization of emulsions via the heteroaggregation of nanoparticles. Langmuir, 24(9), 4443-4446.

Binks, B. P., & Lumsdon, S. O. (1999). Stability of oil-in-water emulsions stabilised by silica particles. Physical Chemistry Chemical Physics, 1(12), 3007-3016.

Binks, B. P., & Lumsdon, S. O. (2000). Catastrophic phase inversion of water-in-oil emulsions stabilized by hydrophobic silica. Langmuir, 16(6), 2539-2547.

Binks, B. P., & Lumsdon, S. O. (2000a). Effects of oil type and aqueous phase composition on oil-water mixtures containing particles of intermediate hydrophobicity. Physical Chemistry Chemical Physics, 2(13), 2959-2967.

Binks, B. P., & Lumsdon, S. O. (2000b). Influence of particle wettability on the type and stability of surfactant-free emulsions. Langmuir, 16(23), 8622-8631.

Binks, B. P., & Lumsdon, S. O. (2000c). Transitional phase inversion of solid-stabilized emulsions using particle mixtures. Langmuir, 16(8), 3748-3756.

Binks, B. P., & Lumsdon, S. O. (2001). Pickering emulsions stabilized by monodisperse latex particles: Effects of particle size. Langmuir, 17(15), 4540-4547.

Binks, B. P., Meunier, J., & Langevin, D. (1989). Characteristic Sizes, Film Rigidity and Interfacial-Tensions in Microemulsion Systems. Progress in Colloid & Polymer Science, 79, 208-213.

Binks, B. P., Murakami, R., Armes, S. P., & Fujii, S. (2005). Temperature-induced inversion of nanoparticle-stabilized emulsions. Angewandte Chemie-International Edition, 44(30), 4795-4798.

Binks, B. P., Murakami, R., Armes, S. P., & Fujii, S. (2006). Effects of pH and salt concentration on oil-in-water emulsions stabilized solely by nanocomposite microgel particles. Langmuir, 22(5), 2050-2057.

Binks, B. P., Murakami, R., Armes, S. P., Fujii, S., & Schmid, A. (2007). pH-responsive aqueous foams stabilized by ionizable latex particles. Langmuir, 23(17), 8691-8694.

Binks, B. P., Philip, J., & Rodrigues, J. A. (2005). Inversion of silica-stabilized emulsions induced by particle concentration. Langmuir, 21(8), 3296-3302.

Binks, B. P., & Rocher, A. (2009). Effects of temperature on water-in-oil emulsions stabilised solely by wax microparticles. Journal of Colloid & Interface Science, 335(1), 94-104.

Binks, B. P., & Rodrigues, B. A. (2009). Influence of surfactant structure on the double inversion of emulsions in the presence of nanoparticles. Colloids and Surfaces A: Physicochemical and Engineering Aspects, 345(1-3), 195-201.

Binks, B. P., & Rodrigues, J. A. (2003). Types of phase inversion of silica particle stabilized emulsions containing triglyceride oil. Langmuir, 19(12), 4905-4912.

Binks, B. P., & Rodrigues, J. A. (2007). Enhanced stabilization of emulsions due to surfactant-induced nanoparticle flocculation. Langmuir, 23(14), 7436-7439.

Binks, B. P., & Whitby, C. P. (2004). Silica particle-stabilized emulsions of silicone oil and water: Aspects of emulsification. Langmuir, 20(4), 1130-1137.

Binks, B. P., & Whitby, C. P. (2005). Nanoparticle silica-stabilised oil-in-water emulsions: improving emulsion stability. Colloids and Surfaces A: Physicochemical and Engineering Aspects, 253(1-3), 105-115.

Bonaccurso, E., Kappl, M., & Butt, H. J. (2002). Hydrodynamic force measurements: Boundary slip of water on hydrophilic surfaces and electrokinetic effects. Physical Review Letters, 88(7),

Bowen, W. R., & Jenner, F. (1995). Dynamic Ultrafiltration Model for Charged Colloidal Dispersions - a Wigner-Seitz Cell Approach. Chemical Engineering Science, 50(11), 1707-1736.

Bragg, J. R., & Varadaraj, R. (2006). Solids-stabilized oil-in-water emulsion and a method for preparing same. US Patent No 7.121.339 B2.

Braisch, B., Kohler, K., Schuchmann, H. P., & Wolf, B. (2009). Preparation and Flow Behaviour of Oil-In-Water Emulsions Stabilised by Hydrophilic Silica Particles. Chemical Engineering & Technology, 32(7), 1107-1112.

Brugger, B., Rosen, B. A., & Richtering, W. (2008). Microgels as Stimuli-Responsive Stabilizers for Emulsions. Langmuir, 24(21), 12202-12208.

Bulatovic, S. & De Silvio, E. (2000). Process development for impurity removal from tin gravity concentrate. Minerals Engineering, 13(8), 871-879.

Butt, H. J. (1991). Measuring Electrostatic, van der Waals, and Hydration Forces in Electrolyte-Solutions with an Atomic Force Microscope. Biophysical Journal, 60(6), 1438-1444.

Butt, H. J., Cappella, B., & Kappl, M. (2005). Force measurements with the atomic force microscope: Technique, interpretation and applications. Surface Science Reports, 59(1-6), 1-152.

Cabaret, F., Bonnot, S., Fradette, L., & Tanguy, P. A. (2007). Mixing time analysis using colorimetric methods and image processing. Industrial & Engineering Chemistry Research, 46(14), 5032-5042.

Calabrese, R.V., Wang, C. Y., & Bryner, N. P. (1986). Drop Breakup in Turbulent Stirred-Tank Contactors Part III: Correlations for Mean Size and Drop Size Distribution. AIChE Journal, 32(4), 677-681.

Carrica, P. M., Drew, D., Bonetto, F., & Lahey, R. T. (1999). A polydisperse model for bubbly two-phase flow around surface ship. International Journal of Multiphase Flow, 25(2), 257-305.

Catafalmo, V.; Shiveley, T. M.; Blum, G. L.; Lipic, P. M.; Desmarais, T. A. (2001). Apparatus & process for in-line preparation of HIPEs. Patent WO0127165.

Chachula, F., & Liu, Q., (2003), Upgrading a rutile concentrate produced from Athabasca oil sands tailings. Fuel, 82 (8), 929-942.

Chan, D. Y. C., & Horn, G. R. (1985). The Drainage of Thin Liquid Films between Solid Surfaces. Journal of Chemical Physics, 83(10), 5311-5324.

Chen, H. T., & Middleman, S., (1967), Drop size distribution in agitated liquid–liquid Systems". AIChE Journal 13(5), 989-995.

Chen, L., Xu, G., Huang, J., & Wen, S. (2013). Centrifugal high gradient magnetic separation of fine Ilmenite. Advanced Materials Research, 634. 3304-3307.

Chesters, A. K., (1991), The Modeling of Coalescence Processes in Fluid Liquid Dispersions: A Review of Current Understanding. Chemical Engineering Research & Design, 69(4), 259-270.

Colin, C., & Riou, X., (2004), Turbulence and shear-induced coalescence in gas–liquid pipe flows. Fifth International Conference on Multiphase Flow, ICMF'04. Yokohama, Japan,

Corrsin, S. (1964), The isotropic turbulent mixer: II, Arbitrary Schmidt number. AIChE Journal, 10(6), 870-877.

Coulaloglou, C. A. (1975). Dispersed phase interactions in an agitated flow vessel, PhD Dissertation, Illinois Institute of Technology, Chicago,

Coulaloglou, C. A., & Tavlarides L. L. (1976). Drop size distribution and coalescence frequencies of liquid–liquid dispersions in flow vessels. AIChE Journal, 22(2), 289-297.

Coulaloglou, C. A., & Tavlarides L. L. (1977). Description of interaction processes in agitated liquid–liquid dispersions. Chemical Engineering Science, 32(11), 1289-1297.

Craig, V. S. J., Neto, C., & Williams, D. R. M. (2001). Shear-dependent boundary slip in an aqueous Newtonian liquid. Physical Review Letters, 87(5), 1-4.

Cui, Z., Liu, Q., & Etsell, T. H. (2002) Magnetic properties of Ilmenite, hematite and oil sand minerals after roasting. Minerals Engineering, 15(12), 1121-1129

Cui, Z. G., Shia, K.-Z., Cuia, Y.-Z, & Binks, B. P. (2008). Double phase inversion of emulsions stabilized by a mixture of $CaCO_3$ nanoparticles and sodium dodecyl sulphate. Colloids and Surfaces A: Physicochemical and Engineering Aspects, 329(1-2), 67-74.

Da-he, X. (2000). Research and commercialisation of treatment of fine Ilmenite with SLON magnetic separators. Magnetic and Electrical Separation, 10(2), 121-130.

Da-he, X. (2004), SLON Magnetic Separators Applied in the Ilmenite Processing Industry. Physical Separation in Science and Engineering, 13(3), 119 - 126.

Dai, L. L., Tarimala, S., Wu, C. Y., Guttula, S., & Wu, J. (2008). The structure and dynamics of microparticles at Pickering emulsion interfaces. Scanning, 30(2), 87-95.

Danov, K. D., & Kralchevsky, P. A. (2006). Electric forces induced by a charged colloid particle attached to the water-nonpolar fluid interface. Journal of Colloid & Interface Science, 298(1), 213-231.

Danov, K. D., Kralchevsky, P. A., & Boneva, M. P. (2004). Electrodipping force acting on solid particles at a fluid interface. Langmuir, 20(15), 6139-6151.

Das, P. K., Legrand, J., Morançaisa, P., & Carnellea, G. (2005). Drop breakage model in static mixers at low and intermediate Reynolds number. Chemical Engineering Science, 60(1), 231-238.

Derkach, S. R. (2009). Rheology of emulsions. Advances in Colloid and Interface Science, 151(1-2), 1-23.

Ding, A. L., Binks, B. P., & Goedel, W. A. (2005). Influence of particle hydrophobicity on particle-assisted wetting. Langmuir, 21(4), 1371-1376.

Dobbins, M., Domenico J. & Dunn P. (2007). A discussion of Magnetic Separation Techniques for Concentring Ilmenite and Chromite Ores. 6th International Heavy Minerals Conference, The Southern African Institute of Mining and Metallurgy.

Drelich, J., Nalaskowski, J., Gosiewska, A., Beach, E., & Miller, J. D. (2000). Long-range attractive forces and energy barriers in de-inking flotation: AFM studies of interactions between polyethylene and toner. Journal of Adhesion Science and Technology, 14(14), 1829-1843.

Drummond, C. J., Georgaklis, G., & Chan, D. Y. C. (1996). Fluorocarbons: Surface free energies and van der Waals interaction. Langmuir, 12(11), 2617-2621.

Ducker, W. A., Senden, T. J., & Pashley, R. M. (1992). Measurement of Forces in Liquids Using a Force Microscope. Langmuir, 8(7), 1831-1836.

Ducker, W. A., Xu, Z. G., & Israelachvili, J. N. (1994). Measurements of Hydrophobic and Dlvo Forces in Bubble-Surface Interactions in Aqueous-Solutions. Langmuir, 10(9), 3279-3289.

Dudasova, D., Simon, S., Hemmingsen, P. V., & Sjoblom, J. (2008). Study of asphaltenes adsorption onto different minerals and clays, Part 1. Experimental adsorption with UV depletion detection. Colloids and Surfaces A: Physicochemical and Engineering Aspects, 317(1-3), 1-9.

Dudasova, D., Flaten, G. R., Sjoblom, J., & Oye, G. (2009). Study of asphaltenes adsorption onto different minerals and clays Part 2. Particle characterization and suspension stability. Colloids and Surfaces A: Physicochemical and Engineering Aspects, 335(1-3), 62-72.

Eichenlaub, S., Chan, C., & Beaudoin, S. P. (2002). Hamaker constants in integrated circuit metallization. Journal of Colloid & Interface Science, 248(2), 389-397.

Einstein, A., (1906), A new determination of molecular dimensions. Annalen der Physik, 19. 289-306.

Fa, K. Q., Nguyen, A. V., & Miller, J. D. (2005). Hydrophobic attraction as revealed by AFM force measurements and molecular dynamics simulation. Journal of Physical Chemistry B. 109(27), 13112-13118.

Fejes, T. L. (1953). Lagerungen in der Ebene auf der Kugel und im Raum. Berlin, Springer.

Fielden, M. L., Hayes, R. A., & Ralston, J. (1996). Surface and capillary forces affecting air bubble-particle interactions in aqueous electrolyte. Langmuir, 12(15), 3721-3727.

Fournier, C. O., Fradette, L., & Tanguy, P. A. (2009). Effect of dispersed phase viscosity on solid-stabilized emulsions. Chemical Engineering Research & Design, 87(4A), 499-506.

Frelichowska, J., Bolzinger, M. A., & Chevalier, Y. (2009). Pickering emulsions with bare silica. Colloids and Surfaces A: Physicochemical and Engineering Aspects, 343(1-3), 70-74.

Fujii, S., Armes, S. P., Binks, B. P., & Murakami, R. (2006). Stimulus-responsive particulate emulsifiers based on lightly cross-linked poly(4-vinylpyridine)-silica nanocomposite microgels. Langmuir, 22(16), 6818-6825.

Gafanova, O. V., & Yarranton, W. (2001). The stabilization of water in hydrocarbon emulsions by asphaltenes and resins. Journal of Colloid & Interface Science, 241, 469-478.

Giesbers, M., Kleijn, J. M., & Stuart, M. A. C. (2002). The electrical double layer on gold probed by electrokinetic and surface force measurements. Journal of Colloid & Interface Science, 248(1), 88-95.

Gillies, G., & Prestidge, C. A. (2004). Interaction forces, deformation and nano-rheology of emulsion droplets as determined by colloid probe AFM. Advances in Colloid and Interface Science, 108, 197-205.

Gillies, G., Kappl, M., & Butt, H. J. (2005a). Surface and capillary forces encountered by zinc sulfide-microspheres in aqueous electrolyte. Langmuir, 21(13), 5882-5886.

Gillies, G., & Prestidge, C. A. (2005b). Colloid probe AFM investigation of the influence of cross-linking on the interaction behavior and nano-rheology of colloidal droplets. Langmuir, 21(26), 12342-12347.

Gingras J.-P, Fradette, L., Tanguy, P., & Bousquet, J. (2007). Inline Bitumen Emulsification Using Static Mixers. Industrial and Engineering Chemistry Research, 46(8), 2618-2627.

Golemanov, K., Tcholakova, S., Kralchevsky, P. A., Ananthapadmanabhan, K. P., & Lips, A. (2006). Latex-particle-stabilized emulsions of anti-Bancroft type. Langmuir, 22(11), 4968-4977.

Grace, H. P. (1982). Dispersion phenomena in high viscosity immiscible fluid systems and application of static mixers as dispersion devices in such systems. Chemical Engineering Communication, 14, 225.

Gregoli, A. A., Hamshar, J. A., Olah, A. M., Riley, C. J., & Rimmer, D. P. (1988). Preparation of stable crude oil transport emulsions. US Patent No 4.725.287.

Gu, G. X., Zhou, Z., Xu, Z. H., & Masliyah, J. H. (2003). Role of fine kaolinite clay in toluene-diluted bitumen/water emulsion. Colloids and Surfaces A: Physicochemical and Engineering Aspects, 215(1-3), 141-153.

Hadamard, J. S. (1911). Mouvement permanent lent d'une sphère liquide et visqueuse dans un liquide visqueux. Compte Rendu, 152-1735.

Hannisdal, A., Ese, M. H., Hemmingsen, P. V., & Sjoblom, J. (2006). Particle-stabilized emulsions: Effect of heavy crude oil components pre-adsorbed onto stabilizing solids. Colloids and Surfaces A: Physicochemical and Engineering Aspects, 276(1-3), 45-58.

He, Y. Q., Wu, F., Sun, X. Y., Li, R. Q., Guo, Y. Q., Li, C. B., Gao, J. P. (2013). Factors that Affect Pickering Emulsions Stabilized by Graphene Oxide. Applied Materials & Interfaces, 5(11), 4843-4855.

Hey, M. J., & Kingston, J. G. (2006). Maximum stability of a single spherical particle attached to an emulsion drop. Journal of Colloid & Interface Science, 298(1), 497-499.

Hillier, A. C., Kim, S., & Bard, A. J. (1996). Measurement of double-layer forces at the electrode/electrolyte interface using the atomic force microscope: Potential and anion dependent interactions. Journal of Physical Chemistry, 100(48), 18808-18817.

Hiraiwa, D., Yoshimura, T., & Esumi, K. (2006). Interaction forces between poly (amidoamine) (PAMAM) dendrimers adsorbed on gold surfaces. Journal of Colloid & Interface Science, 298(2), 982-986.

Hirose, Y., Kumara, S., & Kato, T. (2008). Adsorption Dynamics in Pickering Emulsions. Progress of Theoretical Physics Supplement, 175, 81-92.

Horozov, T. S., Aveyard, R., Binks, B. P., & Clint, J. H. (2005). Structure and stability of silica particle monolayers at horizontal and vertical octane-water interfaces. Langmuir, 21(16), 7405-7412.

Horozov, T. S., Aveyard, R., Clint, J. H., & Binks, B. P. (2003). Order-disorder transition in monolayers of modified monodisperse silica particles at the octane-water interface. Langmuir, 19(7), 2822-2829.

Horozov, T. S., Binks, B. P., & Gottschalk-Gaudig, T. (2007). Effect of electrolyte in silicone oil-in-water emulsions stabilised by fumed silica particles. Physical Chemistry Chemical Physics, 9(48), 6398-6404.

Hirschberg, S., Koubek, R., Moser, F., & Schock, J. (2009). An improvement of the Sulzer SMX static mixer significantly reducing the pressure drop. Chemical Engineering Research and Design, 87(4), 524-532.

Hu, K., Fan, F. R. F., Bard, A. J., & Hillier, A. C. (1997). Direct measurement of diffuse double-layer forces at the semiconductor/electrolyte interface using an atomic force microscope. Journal of Physical Chemistry B, 101(41), 8298-8303.

Hurd, A. J. (1985). The electrostatic interaction between interfacial colloidal particles. Journal of Physics A: Mathematical and General, 18(16), 1055-1060.

Hutter, J. L., & Bechhoefer, J. (1993). Calibration of Atomic-Force Microscope Tips. Review of Scientific Instruments, 64(7), 1868-1873.

Hwang, K., Singh, P., & Aubry, N. (2010). Destabilization of Pickering emulsions using external electric fields. Electrophoresis, 31(5), 850-859.

Israelachvili, J. N., & Pashley, R. M., (1984), Molecular Layering of Water in Thin Films between Mica Surfaces and its Relation to Hydration Forces. Journal of Colloid & Interface Science, 101(2), 511-523.

Jeelani, S. A. K., & Hartland, S. (1994). Effect of Interfacial Mobility on Thin-Film Drainage. Journal of Colloid & Interface Science, 164(2), 296-308.

Jeelani, S. A. K., & Hartland, S. (1998). Effect of surface mobility on collision of spherical drops. Journal of Colloid & Interface Science, 206(1), 83-93.

Joseph, D. D., Wang, J., Bai, R., Yang, B. H., & Hu, H. H. (2003). Particle motion in a liquid film rimming the inside of a partially filled rotating cylinder. Journal of Fluid Mechanics, 496, 139-163.

Kanda, Y., Nakamura, T., & Higashitani, K. (1998). AFM studies of interaction forces between surfaces in alcohol-water solutions. Colloids and Surfaces A: Physicochemical and Engineering Aspects, 139(1), 55-62.

Karaman, M. E., Pashley, R. M., Waite, T. D., Hatch, S. J., & Bustamante, H. (1997). A comparison of the interaction forces between model alumina surfaces and their colloidal properties. Colloids and Surfaces A: Physicochemical and Engineering Aspects, 129. 239-255.

Karcz, J., & Szoplik, J. (2004). An Effect of the Eccentric Position of the Propeller Agitator on the Mixing Time. Chemical Papers, 58, 9-14.

Karcz, J., Cudak, M., & Szoplik, J. (2005). Stirring of a Liquid in a Stirred Tank with an Eccentrically Located Impeller. Chemical Engineering Science, 60, 2369-2380.

Kekicheff, P., Marcelja, S., Senden, T. J., & Shubin, V. E. (1993). Charge Reversal Seen in Electrical Double-Layer Interaction of Surfaces Immersed in 2:1 Calcium Electrolyte. Journal of Chemical Physics, 99(8), 6098-6113.

King, R., & Muskett, M. J. (1985). Fluid loading and power measurements on an eccentrically mounted pitched blade impeller. Proceedings of the 5th European Conference on Mixing, Wurzburg, West Germany, June 10–12, 285-301.

Kloet, J. V., Schramm, L. L., & Shelfantook, B. (2001), The influence of bituminous froth components on water-in-oil emulsion stability as determined by the micropipette technique. Colloids and Surfaces A: Physicochemical and Engineering Aspects, 192(1), 15 -24.

Komura, S., Hirose, Y., & Nonomura, Y. (2006). Adsorption of colloidal particles to curved interfaces. Journal of Chemical Physics, 124(24),

Konno, M., Muto, T., & Saito, S. (1988). Coalescence of dispersed drops in an agitated tank. Journal of Chemical Engineering of Japan, 21(4), 335-338.

Kruglyakov, P. M., & Nushtayeva, A. V. (2004). Phase inversion in emulsions stabilised by solid particles. Advances in Colloid and Interface Science, 108. 151-158.

Larson, I., Chan, D. Y. C., Drummond, C. J., & Grieser, F. (1997). Use of atomic force microscopy force measurements to monitor citrate displacement by amines on gold in aqueous solution. Langmuir, 13(9), 2429-2431.

Larson, I., Drummond, C. J., Chan, D. Y. C., & Grieser, F. (1995). Direct Force Measurements between Dissimilar Metal-Oxides. Journal of Physical Chemistry, 99(7), 2114-2118.

Lee, C.–H., Erickson, L. E., & Glasgow, L. A. (1987). Bubble breakup and coalescence in turbulent gas–liquid dispersions. Chemical Engineering Communications, 59(1-6), 65-84.

Legrand, J., Morançais P. & Carnelle G. (2001). Liquid– Liquid Dispersion in an SMX-SULZER Static Mixer, Chemical Engineering Research and Design, 79 (8), 949-956.

Lehle, H., Noruzifar, E., & Oettel, M. (2008). Ellipsoidal particles at fluid interfaces. European Physical Journal, 26(1-2), 151-160.

Leng, D. E., & Calabrese, R. V. (2004). Handbook of industrial mixing: Immiscible Liquid–Liquid Systems. Edited by Paul E. L., Atiemo-Obeng V. A., & Kresta S. M., John Wiley & Sons, 639-746.

Levich, V. G. (1962). Physicochemical hydrodynamics. Englewood Cliffs N. J., Prentice-Hall,

Levine, S., & Bowen, B. D. (1991). Capillary Interaction of Spherical-Particles Adsorbed on the Surface of an Oil-Water Droplet Stabilized by the Particles 1. Colloids and Surfaces, 59, 377-386.

Levine, S., & Bowen, B. D. (1992). Capillary Interaction of Spherical-Particles Adsorbed on the Surface of an Oil-Water Droplet Stabilized by the Particles 2. Colloids and Surfaces, 65 (4), 273-286.

Levine, S., & Bowen, B. D. (1993). Capillary Interaction of Spherical-Particles Adsorbed on the Surface of an Oil-Water Droplet Stabilized by the Particles 3. Colloids and Surfaces A: Physicochemical and Engineering Aspects, 70(1), 33-45.

Levine, S., Bowen, B. D., & Partridge, S. J. (1989a). Stabilization of Emulsions by Fine Particles 1. Partitioning of Particles between Continuous Phase and Oil-Water Interface. Colloids & Surfaces, 38(4), 325-343.

Levine, S., Bowen, B. D., & Partridge, S. J. (1989b). Stabilization of Emulsions by Fine Particles 2. Capillary and van der Waals Forces between Particles. Colloids & Surfaces, 38(4), 345-364.

Liang, Y., Hilal, N., Langston, P., & Starov, V. (2007). Interaction forces between colloidal particles in liquid: Theory and experiment. Advances in Colloid and Interface Science, 134(35), 151-166.

Liao, Y. X., & Lucas, D. (2009). A literature review of theoretical models for drop and bubble breakup in turbulent dispersions. Chemical Engineering Science, 64(15), 3389-3406.

Liao, Y. X., & Lucas, D. (2010). A literature review on mechanisms and models for the coalescence process of fluid particles. Chemical Engineering Science, 65(10), 2851-2864.

Lifshitz, E. M.. (1956). The theory of attractive forces between solids. Journal of Experimental and Theoretical Physics, 2(1), 73-83.

Liu, J., Zhou, Z., Xu, Z., & Masliyah, J. (2002). Bitumen-clay interactions in aqueous media studied by zeta potential distribution measurement. Journal of Colloid & Interface Science, 252(2), 409-418.

Liu, J. J., Zhang, L. Y., Xu, Z. H., & Masliyah, J. (2006). Colloidal interactions between asphaltene surfaces in aqueous solutions. Langmuir, 22(4), 1485-1492.

Lobry, E., Theron, F., Gourdon, C., Le Sauze, N., Xuereb, C., & Lasuye, T. (2011). Turbulent liquid–liquid dispersion in SMV static mixer at high dispersed phase concentration. Chemical Engineering Science, 66. 5762–5774.

Loudet, J. C., Alsayed, A. M., Zhang, J., & Yodh, A. G. (2005). Capillary interactions between anisotropic colloidal particles. Physical Review Letters, 94(1),

Loudet, J. C., Yodh, A. G., & Pouligny, B. (2006). Wetting and contact lines of micrometer-sized ellipsoids. Physical Review Letters, 97(1), 1-4.

Luo, H. (1993). Coalescence, breakup and liquid circulation in bubble column reactors. PhD, Dissertation, the Norwegian Institute of Technology, Trondheim.

Lu-Zheng, C., Guo-Dong, X., & Jian-Xiong, H. (2013). Principle of cyclic centrifugal high gradient magnetic separation and pilot-scale test for fine Ilmenite. Journal of Kunming University of Science and Technology, 38(1), 28-31.

Madivala, B., Vandebril, S., Fransaer, J., & Vermant, J. (2009). Exploiting particle shape in solid stabilized emulsions. Soft Matter, 5(8), 1717-1727.

Marchal, J. L., Yeadon, G., Lepert, A., Mourand, J., Rauline, A. J. M., Lapie, T., & Marchal, J. **(**1988). Paving. Patent EP283247-A2.

Masliyah, J. H., Pal, R., & Yan, Y. (1996). Rheology of oil in water emulsions in the presence of fine solids. XIIth International Congress on Rheology, Proceedings, 618-619.

McLachlan, A. D. (1963). Proceedings of the Royal Society of London A. 202-224.

McLean, S. C., Lioe, H., Meagher, L., Craig, V. S. J., & Gee, M. L. (2005). Atomic force microscopy study of the interaction between adsorbed poly(ethylene oxide) layers: Effects of surface modification and approach velocity. Langmuir, 21(6), 2199-2208.

Melle, S., Lask, M., & Fuller, G. G. (2005). Pickering emulsions with controllable stability. Langmuir, 21(6),

Midmore, B. R. (1998). Preparation of a novel silica-stabilized oil/water emulsion. Colloids and Surfaces A: Physicochemical and Engineering Aspects, 132 (2-3), 257-265.

Mills, P., & Snabre, P. (1994). Settling of a Suspension of Hard-Spheres. Europhysics Letters, 25(9), 651-656.

Messick, M. A., (1982), Pipeline transportation of heavy crude oil. US Patent 4.343.323.

Montante, G., Bakker, A., Paglianti, A. & Magelli, F. (2006). Effect of the Shaft Eccentricity on the Hydrodynamics of Unbaffled Stirred Tanks. Chemical Engineering Science, 61, 2807–2814.

Moran, K., Doiron J., Hill, A., & Sishtla C. (2013). Production of Heavy Minerals Concentrate and Bitumen from Oil Sands Froth Treatment Tailings. The Canadian Journal of Chemical Engineering, 91(8), 1383-1394.

Morançais, P., Hirech, K., Carnelle, G., & Legrand J. (1999). Friction Factor in Static Mixer and Determination of Geometric Parameters of SMX Sulzer Mixers. Chemical Engineering Communications, 171. 77 - 93.

Mulvaney, P., Perera, J. M., Biggs, S., Grieser, F., & Stevens, G. W. (1996). The direct measurement of the forces of interaction between a colloid particle and an oil droplet. Journal of Colloid & Interface Science, 183(2), 614-616.

Nikolaides, M. G., Bausch, A. R., Hsu, M. F., Dinsmore, A. D., Brenner, M. P., Weitz, D. A., & Gay, C. (2002). Electric-field-induced capillary attraction between like-charged particles at liquid interfaces. Nature, 420(6913), 299-301.

Novak, V., Ditl P., & Rieger, F. (1982). Mixing in unbaffled vessels the influence of an eccentric impeller position on power consumption and surface aeration. Proceedings of the 4th European Conference on Mixing, Noordwijkerhout, Netherlands, April 27–29, 1982, 57-70.

Nishikawa, M., Ashiwake, K., Hashimoto, N., & Nagata, S. (1979). Agitation Power and Mixing Time in off-Centering Mixing. International Journal of Chemical Engineering, 19, 153–159.

Nudurupati, S., Janjua, M., Singh, P., & Aubry, N. (2010). Effect of parameters on redistribution and removal of particles from drop surfaces. Soft Matter, 6(6), 1157-1169.

Oxenford, J., Coward, J., & Bulatovic, S. (2001). Heavy Minerals from Albert's Oil Sands, CIM AGM, Quebec City, April 30 - May 2, 2001.

Pal, R. (1996). Effect of droplet size on the rheology of emulsions. AIChE Journal, 42(11), 3181-3190.

Pal, R. (2000). Shear viscosity behavior of emulsions of two immiscible liquids. Journal of Colloid & Interface Science, 225(2), 359-366.

Perry, R. H. and Green, D. W. (2008). Perry's Chemical Engineers' Handbook, 8th edition, McGraw-Hill,

Phan, C. M., Nguyen, A. V., & Evans, G. M. (2003). Assessment of hydrodynamic and molecular-kinetic models applied to the motion of the dewetting contact line between a small bubble and a solid surface. Langmuir, 19(17), 6796-6801.

PhanThien, N., & Pham, D. C. (1997). Differential multiphase models for polydispersed suspensions and particulate solids. Journal of Non-Newtonian Fluid Mechanics, 72(2-3), 305-318.

Pichot, R., Spyropoulos, F., & Norton, I. T. (2009). Mixed-emulsifier stabilised emulsions: Investigation of the effect of monoolein and hydrophilic silica particle mixtures on the stability against coalescence. Journal of Colloid & Interface Science, 329(2), 284-291.

Pickering, S. U., (1907), Emulsions, J. Chem, Soc,, 91. 2001-2021.

Premaratne, W., & Rowson, N. (2003a). Development of a magnetic hydrocyclone separation for the recovery of titanium from beach sands. Physical Separation in Science and Engineering, v 12(4), 215-222.

Premaratne, W., & Rowson, N. (2003b). The processing of beach sand from Sri Lanka for the recovery of titanium using magnetic separation. Physical Separation in Science and Engineering, 12(1), 13-22.

Preuss, M., & Butt, H. J. (1998). Direct measurement of particle-bubble interactions in aqueous electrolyte: Dependence on surfactant. Langmuir, 14(12), 3164-3174.

Preuss, M., & Butt, H. J. (1999). Direct measurement of forces between particles and bubbles. International Journal of Mineral Processing, 56(1-4), 99-115.

Prince, M. J., & Blanch, H. W. (1990). Bubble Coalescence and Break-up in Air-Sparged Bubble-Columns. AIChE Journal, 36(10), 1485-1499.

Princen, H. M., (1969), Equilibrium Shape of Interfaces, Drops and Bubbles, Rigid and Deformable Particles at Interfaces. Surface and Colloid Science, 2, 1-84.

Ramsden, W. *(*1903). Separation of solids in the surface-layers of solutions and suspensions. Proceedings of the Royal Society of London, 72. 156-164.

Rapacchietta, A. V., & Neumann, A. W. (1977). Force and Free Energy Analyses of Small Particles at Fluid Interfaces: II. Spheres. Journal of Colloid & Interface Science,, 59(3), 555-567.

Rauline, D., Le Blévec, J.-M, Bousquet, J., & Tanguy, P. A. (2000). A Comparative Assessment of the Performance of the Kenics and SMX Static Mixers, Chemical Engineering Research & Design, 78 (3), 389-396.

Ross, S. L. (1971). Measurements and models of the dispersed phase mixing process. PhD Dissertation, the University of Michigan, Ann Arbor,

RuizGarcia, J., Gamez Corrales, R., & Ivlev, B. I. (1997). Foam and cluster structure formation by latex particles at the air/water interface. Physica A. 236(1-2), 97-104.

Rybczynski, W. (1911). Bulletin International de l'Académie des Sciences de Cracovie A, 1(40).

Saadatmand, M. and Yarranton, H. W. (2008). Rag Layers in Oil Sand Froths. Industrial & Engineering Chemistry Research, 47, 8828-8839.

Sacanna, S., Kegel, W. K., & Philipse, A. P. (2007). Thermodynamically stable Pickering emulsions. Physical Review Letters, 98(15), 1-4.

Scheludko, A. D., and Nikolov, A. D. (1975). Measurement of surface tension by pulling a sphere from a liquid. Colloid and Polymer Science, 253(5), 396-403.

Schulze,, H. J., and Stockelhuber, W. (1993). Coagulation and Flocculation: Flotation as a hetero-coagulation process: Possibilities of calculating the probability of flotation. Edited by Dobias B. and Stechemesser H., 455-515.

Senden, T. J., Drummond, C. J., & Kekicheff, P. (1994). Atomic-Force Microscopy - Imaging with Electrical Double-Layer Interactions. Langmuir, 10(2), 358-362.

Sharma, A., & Ruckenstein, E. (1990). Energetic Criteria for the Breakup of Liquid-Films on Nonwetting Solid-Surfaces. Journal of Colloid & Interface Science, 137(2), 433-445.

Simon, S., Theiler, S., Knudsen, A., Oye, G., & Sjoblom, J. (2010). Rheological Properties of Particle-Stabilized Emulsions. Journal of Dispersion Science and Technology, 31(5), 632-640.

Singh, P., & Joseph, D. D. (2005). Fluid dynamics of floating particles. Journal of Fluid Mechanics, 530. 31-80.

Sprow, F. B. (1967a). Distribution of drop sizes produced in turbulent liquid–liquid dispersion. Chemical Engineering Science, 22(3), 435-442.

Sprow, F. B. (1967b). Drop size distributions in strongly coalescing liquid–liquid systems. AIChE Journal, 13(5), 995-998.

Stamatoudis, M., & Tavlarides, L. L. (1985). Effect of Continuous-Phase Viscosity on the Drop Sizes of Liquid-Liquid Dispersions in Agitated Vessels. Industrial & Engineering Chemistry Processing, 24(4), 1175-1181.

Stamou, D., Duschl, C., & Johannsmann, D. (2000). Long-range attraction between colloidal spheres at the air-water interface: The consequence of an irregular meniscus. Physical Review E, 62(4), 5263-5272.

Stiernstedt, J., Nordgren, N., Wagberg, L., Brumer, H., Gray, D. G., & Rutland, M. W. (2006). Friction and forces between cellulose model surfaces: A comparison. Journal of Colloid & Interface Science, 303(1), 117-123.

Stiller, S., Gers-Barlag, H., Lergenmueller, M., Pflucker, F., Schulz, J., Wittern, K. P., & Daniels, R. (2004). Investigation of the stability in emulsions stabilized with different surface modified titanium dioxides. Colloids and Surfaces A: Physicochemical and Engineering Aspects, 232(2-3), 261-267.

Streiff, F.A., Jaffer, S., & Schneider, G. (1999). The design and application of static mixer technology. 3rd International Symposium on Mixing in Industrial Processes, Osaka, Japan, 107-114.

Streiff, F.A., Mathys, P., & Fisher, T.U. (1997). New fundamentals for liquid-liquid dispersion using static mixers. 9th European Conference of Mixing (Paris, France), Récents Progrès en Génie des Procédés, Lavoisier, Tec Doc, 11(51), 307–314

Tambe, D. E., & Sharma, M. M. (1994). The Effect of Colloidal Particles on Fluid-Fluid Interfacial Properties and Emulsion Stability. Advances in Colloid and Interface Science, 52, 1-63.

Tarimala, S., & Dai, L. L. (2004a). Structure of microparticles in solid-stabilized emulsions. Langmuir, 20(9), 3492-3494.

Tarimala, S., Ranabothu, S. R., Vernetti, J. P., & Dai, L. L. (2004b). Mobility and in situ aggregation of charged microparticles at oil-water interfaces. Langmuir, 20(13), 5171-5173.

Tarimala, S., Wu, C. Y., & Dai, L. L. (2006). Dynamics and collapse of two-dimensional colloidal lattices. Langmuir, 22(18), 7458-7461.

Taylor, G. I. (1932). The viscosity of a fluid containing small drops of another fluid. Proceeding of the Royal Society of London, 138-141.

Théron, F., & Le Sauze, N. (2011). Comparison between three static mixers for emulsification in turbulent flow. International Journal of Multiphase Flow, 37(5), 488–500

Toikka, G., Hayes, R. A., & Ralston, J. (1998). Surface forces between zinc sulfide and silica in aqueous electrolyte. Colloids and Surfaces A: Physicochemical and Engineering Aspects, 141(1), 3-8.

Torres, L. G., Iturbe, R., Snowden, M. J., Chowdhry, B. Z., & Leharne, S. A. (2007). Preparation of o/w emulsions stabilized by solid particles and their characterization by oscillatory rheology. Colloids and Surfaces A: Physicochemical and Engineering Aspects, 302(1-3), 439-448.

Transparency Market Research (2012-07-10), Surfactants Market By Product Types, Substrates, Geography & Applications – Global Industry Trends And Forecasts To 2017.

Transportation Research Board (2013). Effects of Diluted Bitumen on Crude Oil Transmission Pipelines, Special report 311.

Tsouris, C., & Tavlarides, L. L. (1994). Breakage and Coalescence Models for Drops in Turbulent Dispersions. AIChE Journal, 40(3), 395-406.

Tsuji, S., & Kawaguchi, H. (2008). Thermo-sensitive Pickering emulsion stabilized by poly(N-isopropylacrylamide)-carrying particles. Langmuir, 24(7), 3300-3305.

Tyrrell, J. W. G., & Attard, P. (2002). Atomic force microscope images of nanobubbles on a hydrophobic surface and corresponding force-separation data. Langmuir, 18(1), 160-167.

Valentas, K. J., Bilous, L., & Amundson A. R. (1966). Analysis of Breakage in Dispersed Phase Systems. Industrial & engineering chemistry fundamentals, 5(2), 271-279.

Valle-Delgado, J. J., Molina-Bolivar, J. A., Galisteo-Gonzalez, F., Galvez-Ruiz, M. J., Feiler, A., & Rutland, M. W. (2005). Hydration forces between silica surfaces: Experimental data and predictions from different theories. Journal of Chemical Physics, 123(3), 1-4.

Van Heuven, J. W., & Beek, W. J. (1971). Power input, drop size and minimum stirrer speed for liquid-liquid dispersions in stirred vessels. Proceeding in International Solvent Extraction Conference, The Hague, the Netherlands, 1, 70-81.

Vermeulen, T., Williams, G. M., & Langlois, G. E. (1955). Interfacial area in liquid–liquid and gas–liquid agitation. Chemical Engineering Progress, 51, 85-95.

Veeramasuneni, S., Yalamanchili, M. R., & Miller, J. D. (1998). Interactions between dissimilar surfaces in high ionic strength solutions as determined by atomic force microscopy. Colloids and Surfaces A: Physicochemical and Engineering Aspects, 131(1-3), 77-87.

Vignati, E., Piazza, R., & Lockhart, T. P. (2003). Pickering emulsions: Interfacial tension, colloidal layer morphology, and trapped-particle motion. Langmuir, 19(17), 6650-6656.

Vinogradova, O. I. (1995). Drainage of a Thin Liquid-Film Confined between Hydrophobic Surfaces. Langmuir, 11(6), 2213-2220.

Vrij, A., & Overbeek, J. (1968). Rupture of thin liquid films due to spontaneous fluctuations in thickness. Journal of American Chemical Society, 90(12), 3074-3078.

Wang, S. Q., Liu, J. J., Zhang, L. Y., Xu, Z. H., & Masliyah, J. (2009). Colloidal Interactions between Asphaltene Surfaces in Toluene. Energy & Fuels, 23(1), 862-869.

Wang, T. F., Wang, J. F., & Jin, Y. (2005a). Population balance model for gas-liquid flows: Influence of bubble coalescence and breakup models. Industrial & Engineering Chemistry Research, 44(19), 7540-7549.

Wang, T. F., Wang, J. F., & Jin, Y. (2005b). Theoretical prediction of flow regime transition in bubble columns by the population balance model. Chemical Engineering Science, 60(22), 6199-6209.

Wang, W. X., Zhou, Z., Nandakumar, K., Xu, Z. H., & Masliyah, J. H. (2004). Effect of charged colloidal particles on adsorption of surfactants at oil-water interface. Journal of Colloid & Interface Science, 274(2), 625-630.

Wang, X., & Alvarado, V. (2008), Effect of Salinity and pH on Pickering Emulsion Stability. Proceedings - SPE Annual Technical Conference and Exhibition, 4. 2676-2692.

Wang, Z., Wang, S. C., Schroeder, V., & Schubert, H. (2000). Effect of continuous phase viscosity on membrane emulsification. Chinese Journal of Chemical Engineering, 8(2), 108-112.

Whitby, C. P., Fornasiero, D., & Ralston, J. (2010). Structure of oil-in-water emulsions stabilised by silica and hydrophobised titania particles. Journal of Colloid & Interface Science, 342(1), 205-209.

Whitcomb & Associates (2005). Prefeasibility study: Oils sands heavy minerals project, Retrieved March 30. 2007. from http://www,titaniumcorporation,com/s/Library,asp,

Williams, D. F., & Berg, J. C. (1992). The Aggregation of Colloidal Particles at the Air-Water-Interface. Journal of Colloid & Interface Science, 152(1), 218-229.

Wills, B. A. (2006). Mineral processing technology: an introduction to the practical aspects of ore treatment and mineral recovery (6th ed.). Amsterdam, Boston, London : Elsevier/BH, 2006.

Wright, H., & Ramkrishna, D. (1994). Factors Affecting Coalescence Frequency of Droplets in a Stirred Liquid-Liquid Dispersion. AIChE Journal, 40(5), 767-776.

Yan, N. X., Gray, M. R., & Masliyah, J. H. (2001). On water-in-oil emulsions stabilized by fine solids. Colloids and Surfaces A: Physicochemical and Engineering Aspects, 193(1-3), 97-107.

Yan, N. X., Kurbis, C., & Masliyah, J. H. (1997). Continuous demulsification of solids-stabilized oil-in-water emulsions by the addition of fresh oil, Industrial & Engineering Chemistry Research, 36(7), 2634-2640.

Yan, N. X., Maham, Y., Masliyah, J. H., Gray, M. R., & Mather, A. E. (2000). Measurement of contact angles for fumed silica nanospheres using enthalpy of immersion data. Journal of Colloid & Interface Science, 228(1), 1-6.

Yan, N. X., & Masliyah, J. H. (1994). Adsorption and Desorption of Clay Particles at the Oil-Water Interface. Journal of Colloid & Interface Science, 168(2), 386-392.

Yan, N. X., & Masliyah, J. H. (1995a). Characterization and Demulsification of Solids-Stabilized Oil-in-Water Emulsions ,1. Partitioning of Clay Particles and Preparation of Emulsions. Colloids and Surfaces A: Physicochemical and Engineering Aspects, 96(3), 229-242.

Yan, N. X., & Masliyah, J. H. (1995b). Characterization and Demulsification of Solids-Stabilized Oil-in-Water Emulsions ,2. Demulsification by the Addition of Fresh Oil. Colloids and Surfaces A: Physicochemical and Engineering Aspects, 96(3), 243-252.

Yan, N. X., & Masliyah, J. H. (1996). Demulsification of solids-stabilized oil-in-water emulsions. Colloids and Surfaces A: Physicochemical and Engineering Aspects, 117(1-2), 15-25.

Yan, N. X., & Masliyah, J. H. (1996). Effect of pH on adsorption and desorption of clay particles at oil-water interface. Journal of Colloid & Interface Science, 181(1), 20-27.

Yan, N. X., & Masliyah, J. H. (1997). Creaming behavior of solids-stabilized oil-in-water emulsions. Industrial & Engineering Chemistry Research, 36(4), 1122-1129.

Yan, Y. H., & Masliyah, J. H. (1993a). Effect of Oil Viscosity on the Rheology of Oil-in-Water Emulsions with Added Solids. Canadian Journal of Chemical Engineering, 71(6), 852-858.

Yan, Y. H., & Masliyah, J. H. (1993b). Solids-Stabilized Oil-in-Water Emulsions - Scavenging of Emulsion Droplets by Fresh Oil Addition. Colloids and Surfaces A: Physicochemical and Engineering Aspects, 75, 123-132.

Yang, F., Liu, S. Y., Xu, J., Lan, Q., Wei, F., & Sun, D. J. (2006). Pickering emulsions stabilized solely by layered double hydroxides particles: The effect of salt on emulsion formation and stability. Journal of Colloid & Interface Science, 302(1), 159-169.

Yang, F., Niu, Q., Lan, Q., & Sun, D. J. (2007). Effect of dispersion pH on the formation and stability of Pickering emulsions stabilized by layered double hydroxides particles. Journal of Colloid & Interface Science, 306(2), 285-295.

Yarranton, H. W., Hussein, H. & Masliyah, J. H. (2000). Water in hydrocarbon emulsions stabilized by asphaltenes at low concentrations. Journal Colloids and Surfaces, 228, 52-63.

Yu-Feng, G., Dan, H., Tao, J., Guan-Zhou, Q., & Shuishi, L. (2010). Study on preparation of titanium-rich material from Ilmenite by reduction-magnetic separation, TMS Annual Meeting, 1, 587-596.

Zhou, G. & Kresta, S. (1996). Impact of tank geometry on the maximum turbulence energy dissipation rate for impellers. AIChE Journal, 42(9), 2476 -2490.

Zhou, J., Qiao, X. Y., Binks, B. P., Sun, K., Bai, M. W., Li, Y. L., & Liu, Y. (2011). Magnetic Pickering Emulsions Stabilized by Fe_3O_4 Nanoparticles. Langmuir, 27(7), 3308-3316.

Zhou, Z. A., Hussein, H., Xu, Z. H., Czarnecki, J., & Masliyah, J. H. (1998). Interaction of ionic species and fine solids with a low energy hydrophobic surface from contact angle measurement. Journal of Colloid & Interface Science, 204(2), 342-349.